EFFECT OF CONCRETE STRENGTH ON THE PERFORMANCE OF FRP WRAPPED RC COLUMN UNDER COMBINED AXIAL-FLEXURE LOADING

TECHNICAL REPORT

Prepared by

Omar Chaallal, Ph.D., P.E., and

Mohsen A. Shahawy, Ph.D., P.E.

Structural Research Center

Florida Department of Transportation

Tallahassee, Florida 32310

March 2000

ABSTRACT

Reinforced concrete beam-columns (RCBC) in need of strengthening and repair are very common. The use of FRP wrapping as a rehabilitation and retrofitting technique can present real advantages with regards to durability, maintenance costs, serviceability, and ultimate strength. Recently, the FDOT has undertaken an experimental investigation on the behavior of RCBC wrapped with CFRP. The RCBC were then made of 3 ksi concrete. This study is a continuity of that investigation and considers RCBC made of high-strength concrete of 6 ksi and above

The main objectives of this study are as follows: (i) Investigate the behavior of carbon-wrapped rectangular high-strength concrete beam-columns when subjected to eccentric loadings; and (ii) Evaluate the effect of concrete strength on the behavior of RCBC, (iii) Provide guidelines for the design of carbon-wrapped rectangular high-strength concrete beam-columns subjected to a combined axial force-flexural moment.

Six series are performed in this study. Each series is made of a high-strength RC column without carbon fiber reinforced plastic (CFRP) jacket as a control specimen and two RC columns retrofitted with CFRP jacket. The six series correspond to the following load eccentricities 0" (i.e., concentric loading), 3" (5.5 mm), 6" (15 mm), 12" (300 mm), 16" (400 mm), and pure bending (i.e., an eccentricity approaching infinity). The test specimens, which have: corbels at the ends, have an 8" x 14" (200 x 350 mm) rectangular cross section and a total length of 140" (3500 mm). The length between corbels is 7' (2100 mm). The target concrete strength of concrete was 6,000 psi.

The CFRP jacketing slightly improved the uniaxial capacity of the beam-columns; the maximum gain achieved was around 10%. This is substantially lower than the gain achieved in normal strength concrete (NSC) specimens. However, it enhanced significantly the flexural capacity of the beam-columns where a gain of more than 45 % was observed, compared to 54 % in NSC. Under combined loading conditions, that gain reached 61 %, compared to 70% in NSC. While the source of increase in pure flexure was mainly attributed to the longitudinal weaves of the CFRP, fabric, the contribution of the transverse weaves within the compression controlled zone increased with increasing axial load to become predominant in pure compression. Finally, within the conditions and the limits of this study, the proposed design procedure based on the stress of confined concrete in the compression zone compared reasonably well with experimental results. The confined stress was calculated using the bi-linear stress-strain model developed specifically for FRP wrapped circular columns in conjunction with an effective confinement ratio that takes into account the rectangular shape of the beam-columns. However, the experimental stress-strain model for rectangular specimens wrapped with FRP material should improve the response prediction.

ABSTRACT

LIST OF FIGURES

ECCENTRICITY = 6"

ECCENTRICITY = 12"

ECCENTRICITY = 16"

PURE BENDING

LIST OF TABLES

APPENDICES

CHAPTER 1

INTRODUCTION

This chapter introduces the report. It states the problem and spells the objectives of the study. It also presents the outline of the present report.

1.1 Problem Statement

Reinforced concrete beam-columns (RCBC) in need of strengthening and repair are very common. The use of fiber reinforced plastic (FRP) wrapping technique can be very efficient and cost-effective. No research has been reported dealing with rectangular RCBC retrofitted with composite wrapping and subjected to a combined axial compression - bending moment condition. However, recently the FDOT initiated *an* extensive investigation on the behavior of RCBC wrapped with carbon fiber reinforced plastic (CFRP) made with a 3000 psi normal strength concrete (NSC) (Chaallal and Shahawy 1999). The present study is a continuity of that investigation and considers RCBC made of high-strength concrete (HSC).

1.2 Research Objectives

This project is intended to examine several aspects in the use of fiber reinforced plastic (FRP) laminates for strengthening rectangular RC columns subjected to combined axial compression and bending moment conditions.

The objectives of this study are as follows

1. Design and carry out an experimental study on the behavior of rectangular high-strength RC columns confined with externally bonded CFRP laminates.
2. Investigate the behavior of carbon-wrapped rectangular high-strength concrete beam - columns when subjected to eccentric loading.
3. Evaluate the effect of concrete strength on the behavior of RC beam-columns. 4. Provide guidelines for the design of carbon-wrapped rectangular high-strength concrete beam-columns subjected to a combined axial force-flexural moment.

1.3 Report Outline

This report consists of two parts:

- *Part I : Test program and procedure, is* contained in chapter 2. The latter describes the specimens, the materials, as well as the instrumentation used and presents the testing procedure and the experimental program.

  Part II : Presentation and analysis of the results, is covered by chapter 3 (Presentation of the results) and chapter 4 (Analysis of the results).

Chapter 5 summarizes the conclusions and discusses various recommendations.

PART I

TEST PROGRAM AND PROCEDURE

CHAPTER 2

EXPERIMENTAL PROGRAM

This chapter presents the experimental program. It gives details of the specimens, the material used, the instrumentation as well as the testing procedures.

2.1 Description of Specimens

The test specimens (see Fig. 2.1) have an 8" x 14" (200 x 350 mm) rectangular cross section and a total length of 140" (3500 mm). The length between corbels is T (2100 mm). Note, however; that for pure flexure and pure compression conditions, four specimens each (one control and three wrapped) were cast as simple rectangular beams (total length = 140" for pure flexure and 84" for pure compression) with no corbels. The total length of each corbel is 28" (700 mm), with a total height also of 28". Steel reinforcement details of the specimens are presented in Figure 2.1. Primary internal reinforcement consists of 2 layers of grade 60 #6 (~ = 19 mm) bars, the first layer having d', 2" (50 mm), while the second layer has d = 12" (300 mm). Shear stirrups, consisting of grade 60 closed #3 (~ = 9.5 m) bars, are spaced evenly though the effective length at a spacing of 4" (100 mm).

2.2 Materials

Concrete was delivered by the same supplier with a specified compression strength of 6000 psi (42 MPa), thereby simulating a moderately high strength concrete. The concrete mix design used is presented in Table 2.1, see also Appendix A. The strengths achieved' in used is presented in Table 2. l , see also Appendix A. The strengths achieved in the different pours are presented in Table 2.2. As can be seen in this table, the average compressive strength achieved is around 8800 psi (61 MPa).

In the specimens receiving carbon lamination, two layers of the standard CFRP system are applied. The standard system consists of a bi-directional weave with 6 to 7 yarns per inch in each direction and per layer. Adhesive used for this project is an Aerospace-grade Amine based epoxy. The basic properties of CFRP and adhesive are presented in Table 2.3

2.3 Instrumentation

All specimens were instrumented using strain gages in the longitudinal, and some of them were instrumented by strain gages in the transverse direction, glued either on a concrete surface or on CFRP outer layer. A schematic view of the location of gages is presented in Fig. 2.3. During the test, the applied load as well as the displacements at different points along the length between corbels were monitored throughout the test. A view of test apparatus and setup is presented in Fig. 2.2.

2.4 Testing Procedure and Program

Six series of at least three tests are performed in this study. Each series is made of a RC column without CFRP jacket as a control specimen and a RC column retrofitted with CFRP jacket. The six series correspond to the following load eccentricities 0" (i.e., concentric loading), 3" (5.5 mm), 6" (15 mm), 12" (300 mm), 16" (400 mm), and pure bending (i.e., an eccentricity approaching infinity). A typical view of a specimen during the test is shown in Fig. 2.4.

The test program of the different series is presented in Table 2.4. Note that the specimens were labeled BC-XLY-EZ:

Where: X, Y, and Z are all numeric values:

BC stands for "Beam- Column" project.

XLY stands for "X" number of carbon "L"ayers with a concrete strength of "Y"ksi.

EZ stands for "E"ccentricity of "Z" inches.

2.5 Load Capacity Prediction of Specimens

2.5.1 Specimens With No Wrap

In the general case where columns are subjected to a combined axial compression bending moment, the nominal load capacity varies- as the applied moment (that is, the load eccentricity) varies. Although it is possible to derive equations to evaluate the strength of columns subjected to combined bending and axial loads, the equations are tedious to use. For this reason; interaction diagrams for columns are generally computed by assuming a. series of strain distributions, each corresponding to a particular point on the interaction diagram, and computing the corresponding values of P and M (see Fig. 2.3).

(i) With reference to Fig. 2:3 the nominal concentric load capacity, P", of a RC column is given by ACI Code as follows:

$$P_{,,} = 0.85\ f\ (A_g - Asc) + AJy \qquad (2.1)$$

where f $_c$ = compression strength of concrete; A_b = total gross area of concrete section; A_s, = total steel area (A,, = A, + A'S), and fy = yield stress of steel reinforcement.

Noting that:

f_y = 60 ksi .

A_{st} = 1.76 in.^{z} (4#6)

f e = 6,000 psi

A_9 = 112 in.2

and using Eq. (2.1), the nominal concentric load P_n follows:

$P_n = 0.85 \times 6{,}000\ (1.2 - 1.76) + (1.76 \times 60{,}000)$

$P_n = 562{,}224 + 105{,}600$

$P_n = 387$ kips

Therefore, with reference to Fig. 2.3, point A is given by:

$P_n = 668$ kips and $M_n = 0$

(ii) The balanced point C can be calculated as follows with reference to strain distributions:

$$d \;= 12\,\text{in}.$$

$$c_b = \frac{\varepsilon_{cu} \times d}{\varepsilon_{cu} + \varepsilon_y} = 7.2$$

$$\varepsilon_s' = \frac{0.003\,(7.2 - 2)}{7.2} = 0.00215 > \varepsilon_y \Rightarrow\ f_s' = f_y = 60\,\text{ksi}$$

$$M_{nb} = 0.85\,f_c'\,ba\,(\bar{y} - \frac{a}{2}) + A_s' f_y\,(\bar{y} - d') + A_s f_y\,(d - \bar{y})$$

with $\bar{y} = h/2 = 7"$, it follows:

$P_{nb} = 250$ kip, $M_{nb} = 1512$ kip-in, and $e_b = 6.0"$

(iii) Similarly, other points either controlled by compression (i.e., corresponding to $c > c_b$ or by flexure (i.e., $c < c_b$) can be determined to complete the theoretical design interaction diagram (see Fig: 4.8). In this study the interaction diagram was generated using a specially developed spread sheet (Excel), as presented in Appendix B.

Table 2.1 - Concrete Mix Design (per cubic yard)

Water	300 Lbs	(136 kg)
Cement	750 Lbs	(340 kg)
Coarse aggregate [(1)]	1680 Lbs	(762 kg)
Fine aggregate	1274 Lbs	(578 kg)
W/C Ratio	0.40	

Note : [(1)] 3/4" maximum aggregate size, river rock

Table 2.2 - Concrete Average Strength of Different Pours

Pour No.	Test No.	Maximum Load (Kips)	Compressive Strength ksi (MPa)	Average ksi (MPa)
1	1	230	8.14 (56.1)	
	2	241	8.52 (58.7)	9.07 (62.5)
	3	299	10.57 (72.9)	
2	1	258	9.12 (62.8)	
	2	232	8.21 (56.6)	8.50 (58.6)
	3	231	8.17 (56.3)	
			Overall Average	8.78 (60.5)

Note : There was a third pour from which only one control specimen was tested with results similar to pour 1.

Table 2.3 - Material Properties of Carbon Wraps

DESCRIPTION-	MANUFACTURER'S DATA[1] -	FDOT'S SUGGESTED VALUES FOR DRY COMPOSITE[2]
Tensile Strength	530 ksi (3.65 GPa)	124 ksi (0.85 GPa)
Tensile Modulus of Elasticity	33500 ksi (231 GPa)	10,000 ksi (68.9 GPa)
Ultimate Tensile Elongation	1.4%	1.2
Filament Diameter	7 gm .	7 [,m
Filaments/yarn	12000	12000
Thickness of layer		0.02 in. (0.5 mm)

(1) Reported for the carbon fabric only (11 yarns/inch, 70 x 10-Sin'/yarn, unidirectional)

(2) Apparent values based on 6.7 yarns/in. in average and 0.02 in. thickness/layer.

Table 2.4 - Test Program

SERIES	SPECIMEN NO.	CRFP LAYERS	ECCENTRIBITY (INCH.)	COMMENTS
1	BC-OL6-EO BC-2L6-E0-1 BC-2L6-EO-2	0 2 Layers 2 Layers	0 0 0	No corbels (84") in all the series
2	BC-01,3-E3 BC-2L6-E3-1 BC-2L6-E3-2	0 2 Layers 2 Layers	3 3 3	
3	BC-OL3-E6 BC-2L6-E6-1 BC-2L6-E6-2	0 2 Layers 2 Layers	6 6 6	
4	BC-OL3-E12 BC-2L6-El2-1 BC-2L6-E12-2	0 2 Layers 2 Layers	12 12 12	
5	BC-OL3E-E16 BC-2L6-16-1 BC-2L6-16-2	0 2 Layers 2 Layers	16 16 16	
6	BC-013-FL BC-2L6-FL-1 BC-2L6-FL-2 BC-2L6-FL-3	0 2 Layers 2 Layers 2 Layers	PB(`) PB(') PBM PB(°	No corbels-(84") in a11 the series

Note: (') PB = Pure Bending

PART II

PRESENTATION AND ANALYSIS OF THE RESULTS.

CHAPTER 3

PRESENTATION OF THE RESULTS

This chapter presents the experimental results of all the series mainly in terms of load or moment versus midspan deflections, secondary moments and strain distribution.

The maximum experimental values obtained from tests for all series are summarized in Table 3.1. The table gives the maximum axial load, as well as the primary, secondary, and total moments attained, the maximum deflection at midspan, the maximum tensile, compressive and transverse (when available) strains, the maximum curvature and curvature ductility at midspan and the modes of failure. Some of the experimental values were not reported in the table due to malfunction of some of the instruments during testing.

3.1 Series One: Concentric Load

The results of specimens tested with concentric loads (that is specimens labeled BC-OL6E0 and BC-2L6EO) are presented in Fig. 3.1 to Fig. 3.5. Note that Figure 3.1 and Figure 3.2 showing respectively the curves of the load versus deflection at different locations. along the beam-column and the secondary moment versus midspan deflection are not displayed due to malfunction of the instrumentation. It must also be noted that due to the limitation of the test rig capacity and the achieved compressive strength well above the targeted strength, it was impossible to drive the specimens of this series to rupture in pure compression. Therefore, at around maximum rig capacity (800 kips) two concentrated equal loads (See Fig. 2.2c) were applied at midspan to generate flexure in addition to compression. In so doing, a point is defined in the interaction diagram close to the point sought by this series and which corresponds to $M_{,,}$ = 0 and $P_{,,} = P_{man}$

Fig. 3.3 presents the strain distribution across the beam-column depth at midspan, for different loading levels. It is seen that in all specimens, the strain distribution across the beam-column depth at midspan was fairly uniform. The observed strain gradients across the section are due to secondary moments and to the applied concentrated lateral loads (flexure) particularly at higher loadings. The maximum strain reached in control specimen approached 1000,uc, whereas that of wrapped specimen was around 1400με.

The longitudinal compressive strain distributions along beam-column length for different loading levels (Fig. 3.4) for specimens BC-OL6EO and BC-2L6EO are not displayed due to malfunction of the strain gauges.

Fig. 3.5 presents the load versus transverse surface strain at midspan for specimens BC-0L6EO and specimen BC-2L6EO. It is observed that in control specimen with no corbels (Fig. 3.5a) the transverse strains at the different sides of the beam-column were quite different and depended on the magnitude of the axial compressive strain. However, the curves of load versus transverse strain captured by bottom and West gauges, and similarly for top and East gauges, were very similar. The strains were higher in the 14 inch-bottom side which were more compressed. It attained 300με at maximum load. The opposite 14 inch-side experienced a maximum strain slightly less than 220/.e at maximum compressive load. The transverse strains at the 8 inch-sides were also around 300ge and 220/-tc. The wrapped specimens with no corbels experienced transverse strains that were quite different from one side to another. The maximum transverse train ranged from 150,uc to 420gE (see Figs. 3.5b to d).

3.2 Series 2: 3-inch Eccentricity

The results of specimens tested with 3-inch eccentric compressive load (that is specimens labeled BC-0L6E3 and BC-2L6E3) are presented in Fig. 3.6 to Fig. 3.9. Figure 3.6 presents the primary, the secondary and the total moment versus the midspan deflection. Note that the moment and deflexion reached by Specimen BC-2L6-E3-1 (Fig. 3.6b) are small compared to specimens 2 and 3. This is due to premature failure. It is seen that the secondary moment increased almost linearly to reach 14.8% and 18.8% of the total moment at ultimate load for BC-OL6E3 and BC-2L6E3 specimens, respectively.

The strain distribution across the beam-column depth at midspan for selected total applied moments up to ultimate are displayed in Fig. 3.7. It is seen that the compressive strain attained 3139$\mu\epsilon$ for specimen BC-OL6E3 and 4242$\mu\epsilon$ for BC-2L6E3. As can be seen, the gauge readings in Specimen BC-2L6E3-1 (Fig. 3.7b) were note correct and should therefore not be considered for analysis.

The longitudinal tension and compressive strain distributions along beam length for different loading levels are presented in Fig. 3.8. It is observed that the strains are fairly uniform particularly in the zone between corbels and for low to moderate loadings.

Fig. 3.9 presents the applied total moment versus the transverse surface strain around the midspan section of specimens BC-OL6E3 and BC-2L6E3. In the control, specimen the maximum transverse strain was achieved in the 8-inch East side (compression face) and was around 642$\mu\epsilon$ (see also Table 3.1). Similarly, in the wrapped specimen, it was around 1320$\mu\epsilon$ at the same face. In the 8-inch tension face (West side), no transverse strain was observed.

The transverse strain in top and bottom sides (14-inch faces) of BC-OL6-E3 Specimen attained 160$\mu\epsilon$ and 105$\mu\epsilon$, that is an average strain of 133$\mu\epsilon$. The corresponding values attained in BC-2L6-E3 specimens were 200$\mu\epsilon$ and 170$\mu\epsilon$, that is an average transverse strain of 185$\mu\epsilon$. Note that the strain gauges were glued at face centers, which were in compression (see strain distribution across depth, Fig. 3.7).

3:3 Series 3: 6-inch Eccentricity

The results of specimens tested with 6-inch eccentric compressive load (that is specimens labeled BC-0L6E6 and BC-2L6E6) are presented in Fig. 3.10 to Fig. 3.13. Figure 3.10 presents the primary, the secondary and the total moment versus the midspan deflection. It is seen that the secondary moment increased almost linearly to reach 13.8 and 15.3 % of the total moment at ultimate load for specimens BC-OL6E6 and BC-21,6E6, respectively.

The strain distributions across the beam-column depth at midspan for selected total applied moments are displayed in Fig. 3.11. It is seen that compressive strain attained 3746με for specimen BC-OL6E6 and 7444με for specimens BC-21,6E6. Note that the neutral axis of unwrapped specimen was around 7 inches compared to 6 inches (from compression face) for wrapped specimen.

The longitudinal tension and compressive strain distributions along beam-column length for different loading levels are presented in Fig. 3.12. It is observed that the compression strains as well as tension strains in the central zone away from corbels, are fairly uniform particularly for low to moderate loading. The non-uniformity of strains in tension face in unwrapped specimen is due to cracking.

Fig. 3.13 presents the applied total moment versus the transverse surface strain around the midspan section of specimens BC-OL6E6 and BC -2L6E6. It is observed that the East side, that is the 8-inch compression face experienced the highest transverse strain (maximum strain around 952με for unwrapped and 2038με for wrapped), whereas in the 8-inch tension face (west side) no transverse strain was-observed.

The transverse strains in top and bottom sides (14-inch face) were small, less than 200με. Note that the strain gauges were glued at the centers of the specimen faces, which were close to neutral axis but in tension (see strain distribution across the depth, Fig. 3.11).

3.4 Series 4: 12-inch Eccentricity

The results of specimens tested under 12-inch eccentric compressive load (that is specimens labeled BC-OL6El2 and BC-2L6E12) are presented in Fig. 3.14 to Fig. 3.17. Fig. 3.14 presents the primary, the secondary and the total applied moment versus the midspan deflection. It is seen that the secondary moment increased almost linearly to reach 14.2% and 12.9% of the total moment at ultimate load for BC-OL6E12, and BC-2L6E12, respectively.

The strain distributions across the beam-column depth at midspan for selected total applied moments are displayed in Fig. 3.15. It is seen that the compressive strain attained 4327με (see also Table 3.1) for specimen BC-OL6E12 and 5346με for BC-2L6E12 (see also Table 3.1). Note that the neutral axis of the unwrapped specimen was around 3.6 in. (from compression face) compared to around 5 in. for the wrapped specimens.

The longitudinal compressive and tensile strain distribution along the column--beam length for different loading levels are presented in Fig. 3.16. It is observed that the strains are fairly uniform along the beam-column, particularly in the central zone and for low to moderate loads. The non-uniformity of strains in tension face of unwrapped specimen is due to cracking.

Fig. 3.17 presents the applied total moment versus the transverse surface strain around the midspan section of specimens BC-OL6E12 and BC-2L6E12. Again, it is observed that the East side, that is the 8-inch compression face experienced the highest transverse strain (maximum strain around 518με for unwrapped and 906με for wrapped specimens), whereas in the 8-inch tension face (West side), no transverse strain was observed. Practically no transverse strains were read in top and bottom sides (14-inch faces) as the location of the strain gauges was close to that of the neutral axis.

3.5 Series 5: 16-inch Eccentricity

The results of specimens tested under 16-inch eccentric compressive load (that is specimens labeled BC-0L6E16 and BC-2L6E16) are presented in Fig. 3.18 to Fig. 3.21. Figure 3.18 presents the primary, the secondary and the total applied moment versus the midspan deflection. It is seen that the secondary moment increased almost linearly to reach 10.7 % and 10.3 % of the total applied moment at ultimate load for BC-OL3El6 and BC-2L6E16, respectively.

The strain distributions across the beam-column depth at midspan for selected total applied moments are displayed in Fig. 3.19. It is seen that the maximum compressive strain attained 1913ME for specimen BC-OL6E16 and 3234/IE for BC-2L6E16. Note that the neutral axis of unwrapped specimen was around 2.0 inches from compression face compared to 5.0 inches for wrapped specimens.

The longitudinal compressive strain distributions along beam length for different loading levels are presented in Fig. 3.20. his observed that the strains are fairly uniform, particularly at the central zone and for low to moderate loads. Obviously at a higher applied load, cracks develop, which explains some of the high strain readings.

Fig. 3.21 presents the applied total moment versus the transverse surface strain around the midspan section of specimens BC-OL6E16 and BC-2L6El6. It is observed in both wrapped ans unwrapped specimen that the East side, that is the 8-inch compression face, experienced the highest. transverse strain (around 430,uE for unwrapped and 866ME for wrapped), whereas in the 8-inch tension face (West side), no transverse strain is observed. The transverse strains in top and bottom sides (14-inch faces) were practically equal to zero, the location of the surface strain gauges being below the neutral axis (that is in tension zone, see strain distribution across the depth, Fig. 3.19).

3.6 Series 6: Pure Flexure

The results of specimens tested in four-point flexure with no axial load (that is specimens labeled BC-OL6-FL, BC-2L6-FLl; BC-2L6-FL2 and BC-2L6-FL3) are presented in Fig. 3.22 to Fig. 3.24. Note that all the specimens in this series were simple rectangular beams with no corbels spanning 132º (total length= 140").

Fig. 3.22 presents the applied moment versus the midspan deflection. It is seen that the moment corresponding to first cracking is 140 kip-in for unwrapped and around 260 kip-in for wrapped specimens, whereas the moment at yield of steel is respectively around 540 kip-in and 800 kip-in. It is seen that the post yielding moment-deflection curve of the wrapped specimens is consistently linear.

The strain distribution across the beam depth at midspan for selected applied moments are displayed in Fig. 3.23. It is seen that the compressive strain attained 3055με in BC-OL6-FL, and 2558με in BC-2L6-FL. The neutral axis at yielding of steel is seen to be equal to 2.4 inches from compression face for BC-OL6-FL, whereas it is around 4.0 inches for BC-2L6-FL.

Fig. 3.24 shows the applied moment versus the longitudinal strains at 'different locations of inidspan section. The cracking and the yielding moment can clearly be identified in these curves. Fig. 3.25 presents the curves of the applied moment versus the transverse strain on the compression face of midspan section. It is observed that the transverse train attained 656με for the unwrapped specimen and over 440με in wrapped specimens.

Table 3.1 Maximum Experimental Results ($f'c = 8.8$ ksi)

Specimen	Pmax	Moment			Midspan	Microstrain (Max)			n.a depth	Curvature					Failure mode
		primary	secondary	total	Deflection	compression	tension	Transverse	at yield	maximum	conf/unconf	yield	ductility	conf/unconf	
	kip	kip.in	kip.in	kip.in	in.										
(1)	(2)	(3)	(4)	(5)	(6)	(7)	(8)	(9)	(10)	(11)	(12)	(13)	(14)	(15)	(16)
BC-0L6-E0	985 (a)	-	-	-	-	-	-	-	NA	-	-	na	na	-	Bursting of concrete at left end, breakage of stirrups, buckling of steel (see note b)
BC-2L6-E0-1	1100 (a)	-	-	-	-	-	-	-	NA	-	-	na	na	-	Failure by splitting and bursting at top and bottom (see note b)
BC-2L6-E0-2	1100 (a)	-	-	-	-	-	-	-	NA	-	-	na	na	-	Failure by bursting at right end (see note b)
BC-2L6-E0-3	1100 (a)	-	-	-	-	-	-	-	NA	-	-	na	na	-	Failure by bursting at right end (see note b)
BC-0L6-E3	500	1501	262	1763	0,523	-3139	2599	642	11	410		2000	0,20		Crushing of concrete in compression at end
BC-2L6-E3-1	365	1098	143	1241	0,391	-2228	2824	1320	7	361	0,88	400	0,90	4,40	Bursting of concrete at a corner in compression, premature failure
BC-2L6-E3-2	625	1874	433	2307	0,692	-4242	1496	1172	10	410	1,14	1000	0,41	0,45	Tension fracture of frp followed by bursting in compression
BC-0L6-E6	236	1415	226	1641	0,957	-3746	5515	952	7	662		400	1,65		Crushing of concrete in compression after yielding of steel
BC-2L6-E6-1	309	1854	328	2182	1,062	-7444	6397	1093	5,5	989	1,49	308	3,21	1,94	Tension fracture of frp at midspan and then bursting of concrete at a corner in compression
BC-2L6-E6-2	312	1873	339	2211	1,085	-6190	5928	2038	6	866	0,88	333	2,60	0,81	Tension fracture of frp at midspan and then bursting of concrete at a corner in compression
BC-0L6-E12	82	987	164	1151	1,991	-4327	24885	518	3,5	2087		235	8,87		Crushing of concrete in compression after yielding of steel
BC-2L6-E12-1	123	1470	193	1663	1,574	-3989	11085	401	5	1077	0,52	286	3,77	0,42	Tension fracture of frp at midspan and then bursting of concrete at a corner in compression
BC-2L6-E12-2	135	1618	240	1858	1,779	-5346	9264	906	4	1044	0,97	250	4,17	1,11	Tension fracture of frp at midspan and then bursting of concrete at a corner in compression
BC-0L6-E16	61	981	117	1098	1,9	-1913	12971	433	2	1063		200	5,32		Crushing of concrete in compression after wide cracks in tension zone
BC-2L6-E16-1	96	1539	177	1716	1,84	-3234	8133	743	5	812	0,76	286	2,84	0,53	Tension rupture of CFRP in tension at 22in. Left of midspan
BC-2L6-E16-2	93	1481	161	1642	1,74	-2082	6841	866	5	637	0,78	286	2,23	0,78	Tension rupture of CFRP in tension at 8in. Left of midspan
BC-0L6-FL	0	838	0	838	2,33	-3055	20315	656	2,3	1669		206	8,10		Crushing of concrete in compression after yielding of steel
BC-2L6-FL-1	0	1140	0	1140	1,19	-2095	8087	360	3,2	727	0,44	227	3,20	0,40	Tension failure at bottom near midspan and buckling at compression face
BC-2L6-FL-2	0	1217	0	1217	1,41	-2558	11500	440	3,2	1004	0,60	227	4,42	0,55	Tension failure at bottom near midspan and buckling at compression face
BC-2L6-FL-3	0	1054	0	1054	0,99	-1807	7362	343	3	655	0,39	222	2,95	0,36	Tension failure at bottom near midspan and buckling at compression face

Note (a): Extrapolated from P-M interaction diagram because no values available in pure compression due to limitation of testing frame

Note (b): Failure mode due to a compression force of around 800 kips and then four-point flexure of around 260 kip-in.

CHAPTER 4

ANALYSIS AND DISCUSSION

This chapter analyzes and discusses the experimental results in terms of the moment versus midspan deflection, the strain distribution, curvature and ductility.

4.1 Overall Behavior

The maximum experimental values obtained form tests for all series were summarized in Table 3.1.

It is observed that the maximum tensile strain in specimens subjected to eccentric loadings varied from 2599με to 24885με in unwrapped specimens and from 1496/-Lc to 11500Qϵ in wrapped specimens. In NSC, these values were from 791 to 28000με and from 1418με to 12590με , respectively. The maximum strain corresponding to breakage of the CFRP fabric was around 1.11% and was achieved in the specimen with 12" eccentricity. In NSC it was around 1.25 % and was achieved in pure flexure. These values are slightly below the maximum elongation provided by the manufacturer (see Table 2.3). The maximum transverse strain at midspan for wrapped specimens varied from 360 to 1782gE, which is below the range (1630με – 5600με) achieved in NSC wrapped specimens. In unwrapped specimens it varied from 298 to 952με. No transverse strains were recorded in NSC unwrapped specimens. In specimens subjected to eccentric loads, the maximum deflection at midspan corresponding to maximum load varied from 0.52 to 2.33 in compared to 0.83 to 1.69 inches in NSC for control and from 0.39 to 1.84 inches compared to 0.79 to 1.63 inches in NSC for wrapped specimens. This was in line with the maximum curvature at midspan, which varied from 410 x 10^{-6} to 2087 x 10^{-6} in.⁻' (249 x 10^{-6} to 2290 x 10^{-6} for NSC) for control and from 361 x 10^{-6} to 1077 X10^{-6} iri' (390 x 10^{-6} to 1192 x 10' in' for NSC) for wrapped specimens. The curvature ductility, defined here as the ratio of the curvature at maximum load and the curvature at yield, varied from 0.20 to 8.87 and from 0.41 to 4.17 for unwrapped and wrapped specimens, respectively. In NSC, these values were from 0.25 to 10.88 and from 0.61.to 4.17, respectively. The ultimate curvature usually used for ductility calculation, was not considered here because some of strain gauges broke during the failure stage and therefore the strains could not be reasonably compared.

The maximum moment capacity in pure flexure achieved by the wrapped specimens was 1217 kip-in, that is 45% increase with respect to unwrapped specimens. In NSC, 59% increase was achieved. The maximum secondary moment due to the so-called P-Delta effect varied from 10.6% to 14.8 % for unwrapped and from 9.8% to 18.7% for wrapped specimens, with respect to the total applied moment. In NSC, it varied from 7.9 to 12.2% for unwrapped and from 9.2 to 21 % for wrapped specimens. Typical views of the. Beam columns after tests are presented in Fig. 4.1. It was observed that generally the wrapped specimens subjected to an axial load in addition to flexure ruptured by tension fracture of CFRP fabric in the tension face accompanied by bursting of corners at the compressive face (see Fig. 4.1). The wrapped specimen under pure flexure failed by rupture of the CFRP wrap at the tension face near the midspan and buckling at the compression face.

In the following sections the behavior of wrapped specimens will be presented, analyzed and compared to control specimens mainly in terms of the applied moment versus the midspan deflection, the longitudinal strain distribution at midspan, the maximum transverse strain behavior at midspan and the ductility enhancement achieved by the CFRP wrapping. Design considerations and interaction diagrams of CFRP wrapped beam-columns will also be discussed.

4.2 Applied Moment versus Midspan Deflection Behavior

Representative curves of applied total moment versus midspan deflection are presented in Fig. 4.2. Typically and similarly to normal strength concrete beam-columns, the unwrapped specimens featured a higher initial slope compared to wrapped specimens. However, this is reversed as the load progressed, the lower the eccentricity the higher the applied moment at which the reversal occurred. This is attributed to the fact that at the initial stage of loading the outer CFRP shells, which possess a lower modulus of elasticity than that of steel, were engaged before the longitudinal steel reinforcement in wrapped specimens, compared to control specimens where the steel contributed earlier. For flexure controlled conditions, the strengthened beam-columns exhibited a higher flexural stiffness compared to control specimens. This. difference in stiffness increased with increasing eccentricity. This can be attributed to the fact that as the eccentricity increased, the control specimens featured more cracks which obviously affected the flexural stiffness, compared to wrapped specimens where the effect of concrete cracking was minimal.

The total moment corresponding to first cracking varied from 150 kip-in to 3.00 kipin for unwrapped specimens. The theoretical value as per the ACI code, is equal to 187 kipin. The cracked moment was not apparent from the curves of wrapped specimens, although a slight change in the slope at roughly 260 kip-in was noticed in some specimens controlled by flexure (Fig. 4.2d and e).

Yielding of steel, which is characterized by the change of the post-crack slope, is clearly apparent in wrapped specimens although, more evident in control specimens. However, in wrapped specimens yielding generally occurred at a higher applied moment and a higher midspan deflection than in control specimens (see Fig. 4.2). This is attributed to the retention of composite action in the tension face which lowered the neutral axis and to the confining effect which allowed the concrete in compression to achieve a higher strain (see strain distributions in Fig. 4.4). This resulted in a higher curvature and hence' a greater displacement at yielding of steel. The branch corresponding to post yielding of steel is seen to be quasi-linear ascending in wrapped and perfectly plastic in control specimens. In wrapped specimens under pure bending, the slope of this branch is about 40% that of the preyielding branch. This value was about 30% for normal strength concrete. However, this value is expected to increase with the modulus of elasticity and the number of layers of the FRP wrap.

Generally, wrapped specimens achieved higher moment capacities than control specimens, although the difference in moment capacities generally decreased as the axial load increased. This feature can also be seen from the experimental interaction diagrams presented later in Fig. 4.8. The wrapped beam-columns also exhibited large deflections beyond yielding stress of steel. However, given the applied moment, they showed reduced deflections and thereby increased serviceability.

The effect of the load eccentricity on the behavior of wrapped specimens is seen in Fig. 4.3, which presents the curves of applied moment versus mid-span deflection of specimens with eccentricities of 3" (75 mm), 6" (150 mm), 12" (300 mm), 16" (400mm) and infinity (pure flexure). The following observations can be reported. Note that similar observations were drawn from results on normal strength concrete beam-columns.

(a) The flexural stiffness, characterized by the slope of the curve after first cracking, increased as the eccentricity decreased. The stiffness enhancement was due to axially applied load. This enhancement was more effective when the location of applied load was closer to the center of the specimen cross section.

(b) Given the applied moment, the specimens with lower eccentricities featured less displacement.

(c) The lower the eccentricity, the higher the moment and the corresponding displacement at which yielding of steel occurred.

4.3 Strain Distribution at Midspan Section

The strain distributions across the beam-column depth at midspan for selected total applied moments are displayed in Fig. 4.4. The strain distribution is seen to be essentially linear up to rupture for both wrapped and unwrapped specimens. The increase in the compressive strain due to the confinement effect varied from 23 % to 98 % in the specimens subjected to eccentric loadings, compared to 50% to 166% for NSC. Given the eccentricity, the neutral axis depth from compression face of wrapped specimens was similar to that of corresponding control specimens, whereas in NSC beam-columns it was smaller. Also, the neutral axis depth decreased as the eccentricity increased.

The superior maximum compressive strain achieved by wrapped compared to unwrapped specimens, is clear from the figures. This is attributed to the confinement effect of the CFRP jacket in the compression zone. As the eccentricity increased the maximum tensile strain also increased thereby engaging more efficiently the CFRP weaves in the longitudinal direction. This efficiency is optimized in pure flexure where rupture occurred by failure of the CFRP material at a tensile strain approaching 11500$\mu\epsilon$.

4.4 Curvature and Ductility

Fig. 4.5 presents the behavior of the maximum curvature and the curvature ductility with increasing axial load in specimens under combined conditions. As expected the: maximum curvature as well as the ductility decreased as the axial load increased for both wrapped and unwrapped specimens. The curvature and the ductility achieved by the wrapped specimens were generally superior to those of corresponding control specimens for higher axial loads. This enhancement in deformation capabilities was attributed to the confinement provided by the CFRP jacket, which resulted in higher stain capacities.

4.5 Transverse Strain at Midspan

Fig. 4.6 shows typical curves representing the applied total moment versus he transverse surface strain around the midspan section of wrapped specimens where readings were available. It is observed that the transverse strain is present in the compression zone from the early stage of loading. The confinement provided by the wrap, which is directly related to the transverse strain (the higher the transverse strain, the greater the confining pressure), was engaged earlier in the loading for specimens with the smallest eccentricities (eccentricity = 3 in). This is due to the fact that these beam-columns have a greater cross-section area under compression since their neutral axis is deeper and are obviously subjected to a higher applied load for a given moment.

The 8-inch compression face experienced the highest transverse strain, whereas in the 8-inch tension face, no transverse strain was observed. It was also noted that the transverse strain increased as the compressive longitudinal strain increased (see Fig. 4.4, strain distribution across the midspan depth). The large transverse strains developed at the compression face after the confinement is engaged indicate significant expansion of the cover concrete. The strains increased as the displacement increased even though the applied load was essentially constant.

Note that the transverse strains in the 14-inch faces were not monitored in this investigation. However, results on NSC beam-columns showed that the magnitude of the transverse strains depends whether the center of the faces is in tension or in compression. It was also observed that the higher the compressive strain in the center of the face, the greater the transverse strain. Therefore, when the longitudinal strains were tensile, the transverse strains were equal to zero.

4.6 Interaction diagram 4.6.1 Design philosophy

One way of calculating the capacity of RC beam-columns wrapped with FRP and subjected to a combined axial force-bending moment, is by considering the improved ultimate compressive strain to calculate the ultimate stress of confined concrete in compression using a reliable stress-strain model. This way of doing has already been used by other researchers to calculate the moment capacity of wrapped sections with conjunction of the hander stress-strain model (hander et al. 1988) for confined concrete (e.g. Xiao et al. 1996). It has also been used successfully by the authors for normal strength concrete beam-columns (Chaallal and Shahawy, 1999) using the new model developed by Mirmiran and Shahawy (1997) and presented below.

4.6.2 Stress-Strain Model

In this study the analytical bilinear stress-strain model (see Fig. 4.7) developed specially for RC circular columns wrapped with FRP jackets (Mirmiran and Shahawy 1997) is used to calculate the compressive strength of confined concrete, whereas the maximum strain is taken as 0.005 as confirmed by the experimental data obtained in this study. According to the model, the confined strength of concrete, f_{cc} , can be computed from:

$$f_{cc} = f_c + 3.38\ f_r^{0.7} \tag{4.1}$$

where f, is the compressive strength of unconfined concrete and f_r is the confinement pressure. It must be noted that recent experimental studies (e.g. Harries et al. 1996) showed that the stress-strain curve describing FRP jacketed RC columns are also bilinear and very similar in shape to circular columns.

The model expressed by Eq. (4.1) was derived on the basis of experiments performed on circular columns. However, while all of the section is fully confined in a circular column, considerable dilation of the section is required before the flat sides of the wraps are engaged in the -confinement of a rectangular column. Due to the relatively small strain capacity of the CFRP fabric, the wrap will typically rupture at its corners before the sides of the wrap can develop any significant confinement. This type of failure has been observed in many of the tested specimens as will be reported later. In addition and contrary to a circular column, the lateral confining pressure differs in the two axes- in a rectangular column. Clearly, this should be reflected in the calculation of the confining pressure in the interim of reliable experimentally - based models for rectangular columns.

One way of adjusting the confining pressure is by using an effective confinement ratio based on the shape of the section and defined as the area of effectively confined concrete over the gross-sectional area (see Fig. 4.8). For a rectangular column the lateral confining stresses induced by the jacket in the x and y directions, $f_{r,x}$ and $f_{r,y,}$ are:

$$f_{r,x} - P_{j,X} k_e f_i \tag{4.2}$$

$$f_{r,y} - p_{i,y} k_e f_i \tag{4.3}$$

where k_e is the effective confinement ratio given by:

$$k_e = A_e / A_{cc} \tag{4.4}$$

where A_e and A_CC are respectively the effectively confined and concrete core areas, given by (see Fig. 4.8 for definitions):

$$A_e = t_x t_v - ((w_X^2 + w_r^2)/3) - A_s \tag{4.5}$$

and

$$A_{cc} = A_c - A_s \tag{4.6}$$

with $w_{,,} = t_X$ -2r and $w_{,,} = t_y$ -2r . The section area ratios of FRP wraps $p_{j,X}$ and $p_{;,y}$ are given by:

$$p_{j,X} = 2\ t.\ /\ t_X \qquad (4.7)$$

$$p_{J.Y} = 2\ t_j\ / \qquad (4.8)$$

where t_j_is the thickness of the wrap. The average jacket stress f_j when the peak axial load is attained can be calculated as:

$$f; = E_j\ \varepsilon_{j,experimental} \qquad (4.9)$$

where E_i and $\varepsilon_{j,experimental}$ are the modulus of elasticity of FRP wrap (see Table 2.3) and the average experimental transverse strain, the maximum of which was found to be 0.002 for HSC and 0.003 for NSC. Recent studies (Restrepol and DeVino 1996) reported values of ε_i of the order of 0.005.

4.6.3 Interaction Diagram

The points defining the experimental maximum values of axial compression and corresponding maximum bending moment are plotted in Fig. 4.9 in terms of the ratios $P_{,,}/P_O$ and $M_n/M_{,,}$ for both wrapped and unwrapped specimens. The resulting interaction diagrams are compared in Fig. 4.10 with the corresponding theoretical interaction diagrams. The theoretical values are based on a concrete compressive strength of 8.8 ksi (see Table 2.2). Note that $P_{,,}$ and M_O are the experimental axial force and corresponding bending moment capacity. The theoretical values of wrapped beam-columns were calculated as for control specimens but with maximum stress and ultimate strain pertaining to confined concrete and calculated using the model described above. The ultimate strain of the CFRP fabric was taken as E = 12000,uE, as confirmed by

HSC. Finally, interaction diagrams calculated using net area of carbon fibers (i.e. modulus of elasticity and equivalent thickness of carbon fibers) are compared in Fig. 4.12 to those: computed using dry composite area (i.e. apparent values of modulus of elasticity and thickness).

An easy to use and self explanatory spread sheet tool has been developed in this study, which displays the equations used as well as the procedure to derive the theoretical interaction diagram using the philosophy outlined above. This tool is illustrated in Appendix B. A diskette is also provided at the end of this report and address unwrapped as well as wrapped beam-columns.

With reference to Fig. 4.9 to Fig. 4.12, the following observations can be made: (a) For control specimens the experimental and theoretical results were very close (see Fig. 4.10).

(b) For wrapped specimens, the experimental results compared reasonably well with the theoretical values (see Fig. 4.10 and Fig. 4.11). Therefore, within the conditions and the limits of this study, the proposed design procedure seems adequate.

(c) In wrapped specimens, the point corresponding to the experimental balanced condition moved slightly upwards with respect to that of unwrapped specimens (see Fig. 4.9).

(d) The CFRP jacketing improved the uniaxial capacity of the HSC beam-columns; the maximum gain achieved was around 10% compared to 30% for NSC. However, it. enhanced significantly the flexural capacity of the beam-columns since a gain of more than 45% and 61% was observed under pure flexure and under combined conditions, respectively. In NSC, these values were respectively 54% and 74%.

. (e) The highest increase in flexural capacity was achieved near the balanced condition for both NSC and HSC specimens.

(f) Below the balanced point, the rate of increase in the moment capacity was higher in HSC than in NSC specimens (see Fig. 4.10).

(g) It is seen from Fig. 4.12 that the interaction diagrams predicted using either, the net area of carbon fibers or the apparent values of dry composite are identical. Therefore both approaches are valid for design.

CHAPTER 5

CONCLUSIONS AND RECOMMENDATIONS

This chapter presents the conclusions reached in this study. It also provides some recommendations for further studies.

5.1 Conclusions

The results of an experimental investigation on the performance of reinforced high-strength (HS) concrete rectangular beam- columns strengthened with externally applied bi-directional carbon fiber reinforced plastic material were presented. Results showed that the strength capacity of beam-columns improved significantly as a result of the combined action of the longitudinal and the transverse weaves of the bi-directional composite fabric. The longitudinal CFRP elements contributed mostly to flexural capacity, whereas the transverse elements enhanced the compressive capacity of the compression zone through confinement action. A design procedure of such elements was also proposed in form of an easy to use spead sheet (Excel).

The following conclusions can be drawn from the study:

1. The CFRP jacketing slightly improved the uniaxial capacity of the beam-columns; the maximum gain achieved was around 10%. This is very low compared to NSC (30%). However, it enhanced significantly the flexural capacity of the beam-columns where a maximum gain of more than 45 % was observed in pure flexure. This is slightly below the 54% increase observed in' normal strength concrete. Under combined conditions, that gain reached 61 % in HSC beam-columns compared to 70 % in NSC beam-columns. While the source of increase in pure flexure was mainly attributed to the longitudinal weaves of the

CFRP fabric, the contribution of the transverse weaves within the compression controlled zone increased with increasing axial load to become predominant in pure compression.

2. The increase in the compressive strain due to the confinement effect varied from 23 % to 177 %. This is similar to the behavior of NSC beam-columns where the increase was in the range [50-166 %].

3. Given the axial load, the curvature and the ductility achieved by the wrapped specimens were consistently superior to those of corresponding control specimens. This feature was more pronounced for lower axial loads.

4. Yielding of steel in wrapped specimens generally occurred at a higher applied moment and a higher midspan deflection than in control specimens.

5. The transverse confinement was engaged in the compression zone from the early stage of loading.

6. Finally, within the conditions and the limits of this study, the proposed design procedure based on the stress of confined concrete in the compression zone compared reasonably well with experimental results. The confined stress was calculated using the bilinear stress-strain model developed specifically for FRP wrapped columns in conjunction with an effective confinement ratio that takes into account the rectangular shape of the beam-columns.

5.2 Recommendations

The procedure used to derive the interaction diagrams was based on the stress-strain model based on experiments on wrapped cylindrical specimens. Therefore, the experimental stress-strain behavior of rectangular specimens wrapped with FRP material and subjected to an axial load should be determined. In particular, the following parameters are of interest: the aspect ratio, the radius of the section corner and the concrete strength.

ACKNOWLEDGEMENTS

This research work was performed in the Structures Research Center, FDOT, Tallahassee, Florida. The authors would like to acknowledge the assistance from the staff of the Structures Research Center and in particular Adnan Al-Saad, P.E., and Tom Beitelman, P.E. The conclusions and recommendations presented in this paper are those of the authors and not necessarily the Florida Department of Transportation.

REFERENCES

Ahmad, S.H., and Shah, S.P. (1982a). *"Complete triaxial stress-strain curves* for . *concrete"* Proceedings, ASCE, v. 108, ST4, 728-742.

Ahmad; S. H. and Shah, S.P. (1982b). *'Stress-strain curves of concrete confined by spiral reinforcemen'ACI* Journal, 79(6), 484-490.

Ahmad, S.J., Khaloo, A.R. and Irshaid, A. (1991). *"Behavior of concrete spirally confined by fiberglass filaments ".* Mag. of Concrete Research, 43 (156), 143-148.

Balmer, G. G. (1949). *'Shearing Strength of Concrete under High Triaxial Stress". U.S.* Bureau of Reclamation, Structural Research Laboratory, Report No. SP-23, Denver; CO.

Bavarian, B., Shively, R., Ehrgott, R., and DiJulio, R., (1996), *'External Support* of *Concrete Structures Using Composite Materials,* "Proceedings of the First International Using Composites in Infrastructure, ICCI `96, H. Saadatmanesh and M. R. Ehsani, Editors, Tucson, Arizona, pp. 917-928.

Benzoni, G., Priestely, M.J.N., and Seible, F., (1997), *"Seismic Performance of a Full Scale Bridge Column - As Built and As Repaired,"* Recent Advances in Bridge Engineering: Advanced Rehabilitation, Durable Materials, Nondestructive Evaluation and Management, Urs Meier and Raimondo Betti, Editors, Proceedings of the U.S./Canada/Europe Workshop on Bridge Engineering, Zurich 14-15, July, pp. 75-82.

Cabrera, S. (1996). *"Shear strength and seismic performance of concrete-filled FRP tubes".* MS thesis, University of Central Florida, Orlando, FL.

Chaallal, O., Shahawy, M. (1999). *"Performance of FRP Wrapped Reinforced Concrete Column Under Combined Axial-Flexural Loading",*, ASCE Structural Engineering Journal, Under press.

Chai, Y.H., Priestly, M.J.N., and Seible, F. (1991). *"Seismic retrofit of circular bridge columns for enhanced flexural performance".* ACI Struct. J., 88 (5), 572-584.

Chinn, J., and Zimmerman, R.M. (1965). *"Behavior of plain concrete under various triaxial compression loading conditions".* Technical Report No. WLTR-64-163, Air Force Weapons Laboratory, NM.

Considère, A. (1903). *"Résistance à la compression du beton armé et du beton fretté".* Génie Civil.

El Echary, H., (1997). *"Length effect on concrete-filled FRP tubes using acoustic emission".* MS thesis, University of Central Florida, Orlando, FL.

Fardis, M.N., and Khalili, H.H. (1982). *"FRP-encased concrete as a structural material".* Mag. of Concrete Research., 34 (121), 191-201.

Fardis, M.N., and Khalili, H.H. (1981). *"Concrete encased in fiberglass-reinforced plastic".* ACI J., 78 (6), 440-446.

Gardner, N.J., and Jacobson, E.R. (1967). *"Structural behavior of concrete filled steel tubes".* ACI J., 64 (7), 404-413.

Harmon, T.G., Gould, P.L., Wang, E. and Ramakrishnan, S., (1998), *"Behavior of Confined Concrete Under Cyclic Loading,"* Proceedings of the Second International on Composites in Infrastructures, ICCI'98, H. Saadatmanesh and M.R. Ehsani, Editors, Tucson, Arizona, pp. 398-409.

Haroun, M.A., Feng, M.Q., Bhatia, H., Sultant, M., Hoshijima, T., Kobatake, Y., (1997), *"Testing Bridge Columns Enhanced by Fiber Composite Jackets,"* Recent Advances in Bridge Engineering: Advanced Rehabilitation, Durable Materials, Nondestructive Evaluation and Management, Urs Meier and Raimondo Better, Editors, pp. 143-141.

Harries, K.A., Kestner, J., Pessiki, S., Sause, R., and Ricles, J., (1998), "*Axial Behavior of Reinforced Concrete Columns Retrofit with FRPC Jackets*," Proceedings of the First International Using Composites in Infrastructure, ICCI '98, H. Saadatmanesh and M. R. Ehsani, Editors, Tucson, Arizona, pp. 411-425.

Hosotani, M., Kawashima, K. and Hoshikima, J., (1997), "*A study on Confinement Effect of Concrete Cylinders by Carbon Fiber Sheets*," Non metallic (FRP) Reinforcement for Concrete Structures, Proceedings of the Third International Symposium, Vol. 1, Sapporo, Japan, pp. 209-216.

Iyengar, K.T.S.R., Desayi, R., and Reddy, K.N. (1970). *"Stress-strain characteristics of concrete confined in steel binders".* Magazine of Concrete Research (London), 22 (72), 173-184.

Kanatharana, J. and Lu, L.-W., (1998), *"Strength and Ductility of Concrete Columns Reinforced with FRP Tubes,"* Proceedings of the Second International on Composites in Infrastructure, ICCI '98, H. Saadatmanesh and M. R. Ehsani, Editors, Tucson, Arizona, pp. 370-384.

Kataoka, T. et al. (1997), "*Ductility of Retrofitted RC Columns with Continuous Fiber Sheets*," Non metallic (FRP) Reinforcement for Concrete Structures, Proceedings of the Third International Symposium, Vol. 1, Sapporo, Japan, pp.547-554.

Katsumata, H., et al., (1998), *"A Study with Carbon Fiber for Earthquake-Resistant Capacity of Existing Reinforced Concrete Column,"* Proceedings of the Ninth Conference on Earthquake Engineering, Tokyo, Japan, Vol 7, pp. 517-522.

Katsumata, H., and Kobatake, Y., (1997), "*Retrofit of Existing Reinforced Concrete Columns Using Carbon Fibers,*" Non metallic (FRP) Reinforcement for Concrete Structures, Proceedings of the Second International Symposium, Vol. 1, Sapporo, Japan, pp. 555-570.

Klöppel, Von K., and Goder, W. (1957). *"Traglastversuche mit ausbetonierten Stahlrören und Aufstellyung einer Bemessungsformel".* Der Stahlbau (Berlin), 26 (1).

Knowles, B.R., and Park, R., (1970), *"Axial Load Design for Concrete Filled Steel Tubes,"* Journal of the Structural Division, Proceedings of the American Society of Civil Engineers, Vol. 96, ST10, pp. 2125-2153.

Kono, S. Inazumi, M. and Kaku, T., (1998), "*Evaluation of Confining Effects of CRFP Sheets on Reinforced Concrete members*," Proceedings of the Second International on Composites in Infrastructure, ICCI '98, H. Saadatmanesh and M. R. Ehsani, Editors, Tucson, Arizona, pp. 343-355.

Lavergne, S., Labossiere, P., (1997), "*Experimental Study of Concrete Columns Confined by a Composite Jackets Under Combined Axial and Flexural Load,*" Annual Congress of the CSCE, Vol. 6, Edited by K. W. Neale, P. Labossiere et G. McClure, Sherbrooke, Quebec, pp. 11-20.

Mander, J.B., Priestely, M.J.N., and Park, R., (1984), "*Seismic Design of Bridge Piers,*" Research Report No. 84-2, University of Canterbury, New Zealand.

Mander, J.B., Priestley, M.J.N., and Park, R., (1988), "*Theoretical Stress-Strain Model for Confined Concrete,,*" Journal of Structural Engineering, ASCE, Vol. 114, No. 8, pp. 1804-1826.

Mirmiran, A., Kargahi, M., Samaan, M., and Shahawy, M.., (1996), "*Composite FRP - Concrete Column with Bi-Directional External Reinforcement,*" Proceedings of the First International Conference on Composites in Infrastructure, ICCI '96, H. Saadatmenash and M.R. Ehsani, Editors, Tucson, Arizona, pp. 903-916.

Mirmiran, A., and Shahawy, M., (1997), "*Behavior of Concrete Columns Confined with Fiber Composites*", Journal of Structural Engineering, ASCE, Vol. 123, pp. 583-590.

Miyaushi, K., Nishibayashi, S. and Inoue, S., (1997), "*Estimation of Strengthening Effects with Carbon Fiber Sheet for Concrete column,*" Non metallic (FRP) Reinforcement for Concrete Structures, Proceedings of the Third International Symposium, Vol. 1, Sapporo, Japan, pp.217-232.

Monti, G., and Spoelstra, M.R. (1997). *"Fiber-section analysis of RC bridge piers retrofitted with FRP jackets".* Proc. Structures Congress XV Building to Last, ASCE, Portland, OR., 884-888.

Nagasaka, T., Okamoto, T. and Tanigaki, M. (1997), *"Shear Strengthening effectiveness of Aramid Fiber Tapes on Existing R/C Columns,"* Non metallic (FRP) Reinforcement for Concrete Structures, Proceedings of the Third International Symposium, Vol. 1, Sapporo, Japan, pp. 539-546.

Nanni, A., and Bradford, N.M. (1995). *"FRP jacketed concrete under uniaxial compression".* Constr. & Bldg. Mater., 9 (2), 115-124.

Nanni, A., and Norris, M. (1995). *"FRP jacketed concrete under flexure and combined flexure-compression".* Constr. & Bldg. Mater., 9 (5), 273-281.

Newman, R., and Newman, J.B. (1971). *"Failure theories and design criteria for plain concrete".* Proc. Int. Civil Engr. Mater. Conf. on Struct., Solid Mech. And Engr. Design, Wiley Interscience, New York, NY, 936, 936-995.

Pantazopoulou, S.J. (1995). *"Role of expansion on mechanical behavior of concrete".* J. Struct. Engr., ASCE, 121 (12), 1795-1805.

Park, R., Priestley, M.J.N., Gill, W., (1982), *"Ductility of Square-Confined Concrete Columns,"* Journal of Structural Engineering, ASCE, 108(ST4), 929-950.

Picher, F., Rochetter, P. and Labossie re, p. (1996), *"Confinement of Concrete Cylinders with CFRP,"* Proceedings of the First International Conference on Composites in Infrastructure, ICCI '96, Edited by Saadatmanesh and Ehsani, Tucson, Arizona, pp. 829-841.

Pico, O. (1997). *"Confinement effectiveness of square FRP tubes in hybrid columns".* MS thesis, University of Central Florida, Orlando, FL.

Popovics, S., *(1973), "Numerical Approach to the Complete Stress-Strain Curves for Concrete,"* Cement and Concrete Research, Vol. 3, No. 5, pp. 583-599.

Priestley, M.J.N., Seible, F., and Alvi, G.M., *(1996), "Seismic Design and Retrofit of Bridges,"* John Wiley and Sons, Inc., p. 686.

Priestley, M.J.N., Seible, F., Fyfe, E., (1992), "*Column Seismic Retrofit Using Fiberglass/Epoxy Jackets,"* First Internaitonal Conference, Advanced Composite Materials for Bridges and Structures. K. W. Neale et P. Labossiere, Editors, pp. 287-298.

Priestley, M.J.N., (1991), *"Seismic Assessment of Exsting Concrete Bridges,"* In Seismic Assessment and Retrofit of Bridges, University of California, San Diego, Structural Systems Research Project Report No. SSRP 91-03, July 1991, pp. 84-149.

Priestley, M.J.N., (1991), *"Design of Retrofit Measure for Concrete Bridges,"* In Seismic Assessment and Retrofit of Bridges, University of California, San Diego, Structural Systems Research Report No. SSRP 91-03, July 1991, pp. 197-250.

Prion, H.G.L., and Boehme, J. (1994). *"Beam-column behavior of steel tubes filled with high strength concrete".* Canadian J. Civil Engr., 21 (2), 207-218.

Restrepol, III. I., and DeVino, B., (1996), *"Enhancement of the Axial Load Carrying Capacity of Reinforced Concrete Columns by Means of Fiberglass-Epoxy Jackets,"* Advanced Composite Materials in Bridges and Structures, Second International Conference, Canadian Society of Engineering, M.M. El-Badry, Editor, pp. 547-553.

Richart, F.E., Brandtzaeg, A., and Brown, R.L., *(1928), "Study of the Failure of Concrete under Combined Compressive Stresses,"* Bulletin 185, University of Illinois Engineering Experiment Station, Urbana, IL.

Richart, F.E., Brandtzaeg, A., and Brown, R.L. (1929). *"Failure of Plain and Spirally Reinforced Concrete in Compression".* Engineering Experiment Station Bulletin No. 190., University of Illinois, Urbana, IL.

Saadatmanesh M., Ehsani, M.R., Limin Jin, (1996), *"Behavior of Concrete Retrofitted with Fiber Composite Straps Under Cyclic Loading".* Fiber Composites Infrastructure. Proceedings of the First International Conference on Composites in Infrastructures, ICCI '96, H. Saadatmanesh and M.R. Ehsani, Editors, Tucson, Arizona, U.S.A., pp. 842-856.

Saadatmanesh, H., Ehsani, M.R. and Li, M.W. (1994). *"Strength and Ductility of Concrete Columns Externally Reinforced with Fiber Composite Straps".* ACI Struct. J., 91 (4), 434-447.

Saatcioglu, M., Razvi, S.R. (1992), *"Strength and Ductility of Confined Concrete,"* Journal of Structural Engineering, 118(6), 1590-1607.

Samaan, M., Mirmiran, A., and Shahawy, M., (1998), "*Modeling of Concrete Confined by Fiber Composites*", J. Struct. Engrg., ASCE (in Press).

Scherer, M.E. (1996). *"Design optimization and behavior of concrete-filled FRP tubes".* MS thesis, University of Central Florida, Orlando, FL.

Scott, B.D., Park, R., and Priestley, M.J.N., *(1982), "Stress-Strain Behavior of Concrete Confined by Overlapping Hopps at Low and High Strain Rates,"* ACI Structural Journal, Vol. 79, No. 1, pp. 13-27.

Seible, F., (1997), *"Bridge Pier Rehabilitation with Continuous Carbon Fiber Wraps,"* Recent Advances in Bridge Engineering: Advanced Rehabilitation, Durable Materials, Nondestructive Evaluation and Management, Urs Meier and Raimondo Betti, Editors, Proceedings of the U.S./Canada/Europe Workshop on Bridge Engineering, Zurich 14-15, July, pp 59-66.

Sheikh, S. A., (1982), *"A Comparative Study of Confinement Models,"* American Concrete Institute Journal, 79(4), 296-306.

Sheikh, S.A., and Uzumeri, S.M., *(1980), "Strength and Ductility of Tied Concrete Columns,"* Journal of Structural Division, ASCE, Vol. 106, No. 5, pp. 1079-1102.

Sheikh, S.A., and Yeh, C. (1986). *"Flexural behavior of confined concrete columns".* ACI J., 83 (3), 389-404.

Sheikh, S.A., and Yeh, C. (1992). *"Analytical moment-curvature relations for tied concrete columns".* J. Of Struct. Engr., ASCE, 118 (2), 529-544.

Sîrbu, G. and al. (1997), *"Seismic Resistance of Reinforced Concrete Pier with Carbon Fiber Sheet Retrofitting,"* Non metallic (FRP) Reinforcement for Concrete Structures, Proceedings of the Third International Symposium, Vol. 1, Sapporo, Japan, pp.571-578.

Watanabe, K., and al. (1997), "*Confinement Effect of FRP Sheet on Strength and Ductility of Concrete Cylinders Under Uniaxial Compression*," Non metallic (FRP) Reinforcement for Concrete Structures, Proceedings of the Third International Symposium, Vol. 1, Sapporo, Japan, pp.233-238.

Xiao, Y., Martin, G.R., Yin, Z., Ma, R., (1996), *"Seismic Retrofit of Existing Reinforced Concrete Bridge Columns Using a Prefabricated Composite Wrapping System."* Proceedings of the First International Conference on Composites in Infrastructure, ICCI '96, H. Saadatmanesh and M.R. Ehsani, Editors, Tucson, Arizona, U.S.A., pp. 903-916.

Ziara, M.M., Haldane, D., and Kuttab, A.S. (1995). *"Flexural behavior of beams with confinement".* ACI Struct. J., 92 (1), 103-1.

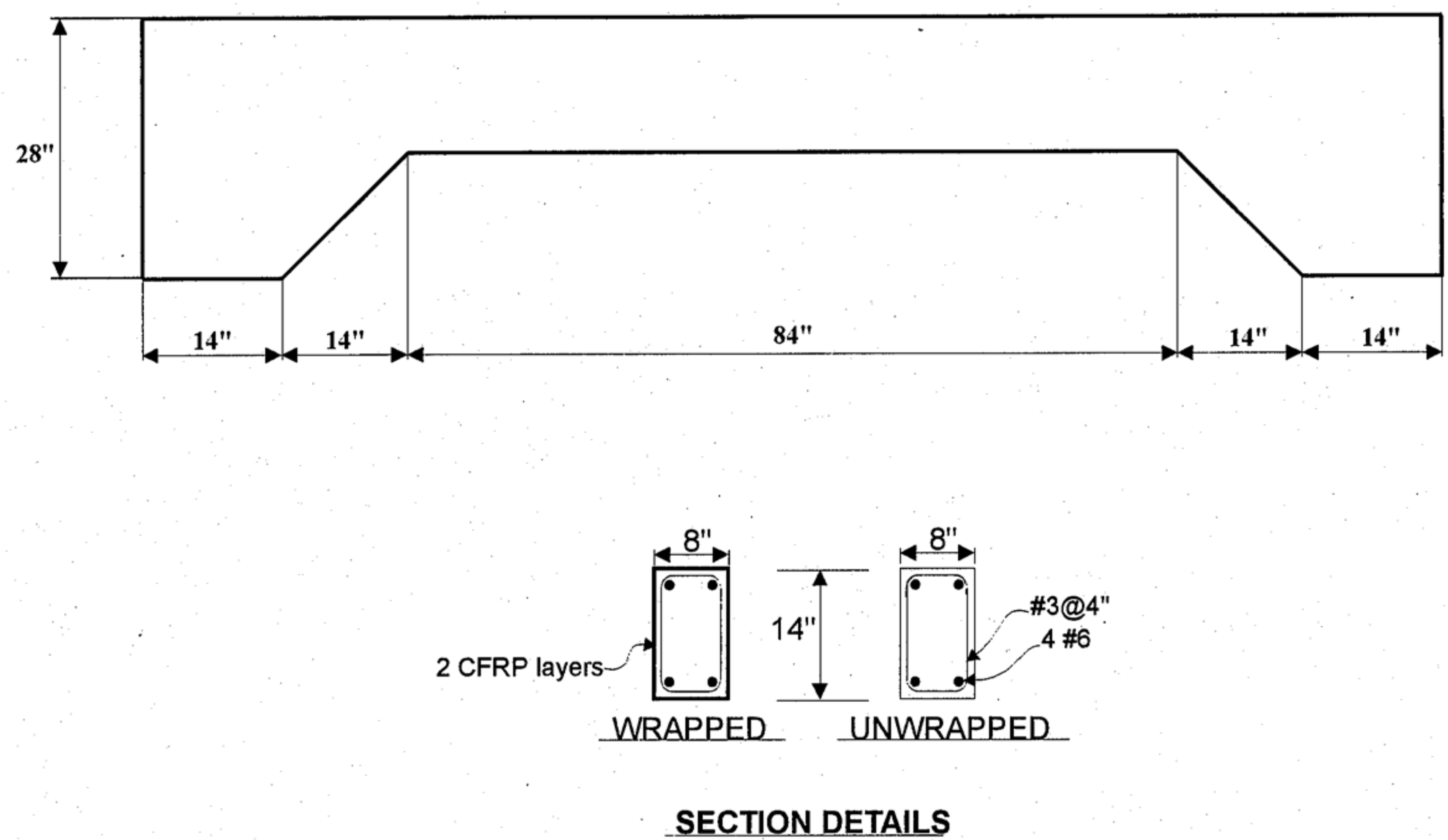

Fig. 2.1(a) Details of Specimen with Corbels

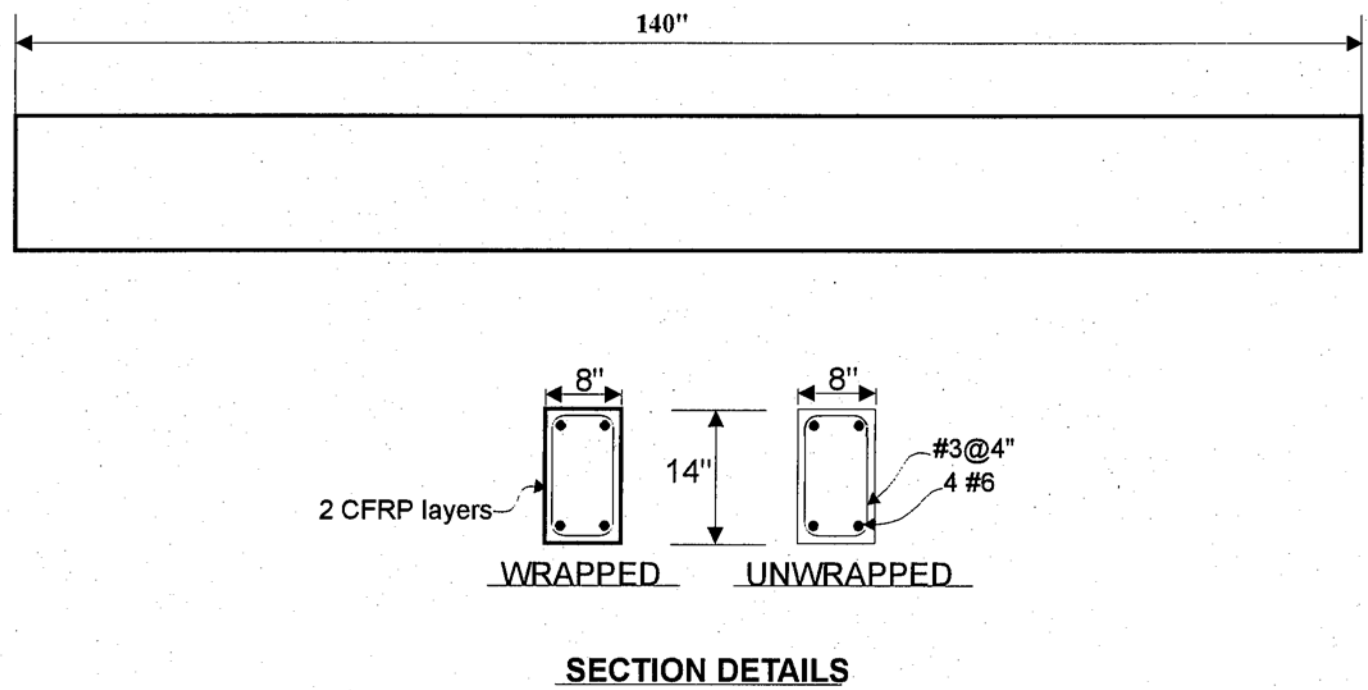

Figure 2.1 (b) Details of Specimen Without Corbels For Flexure

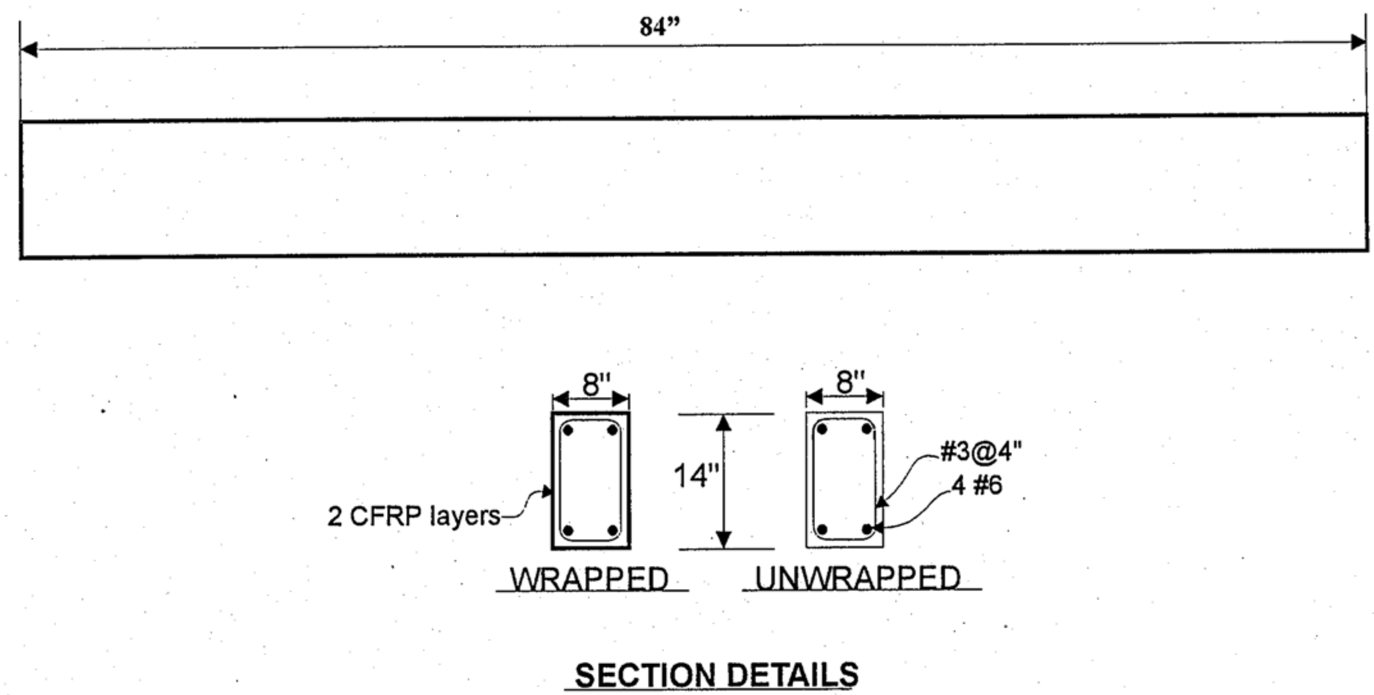

Figure 2.1(c) Details of Specimen Without Corbels For Pure Compression

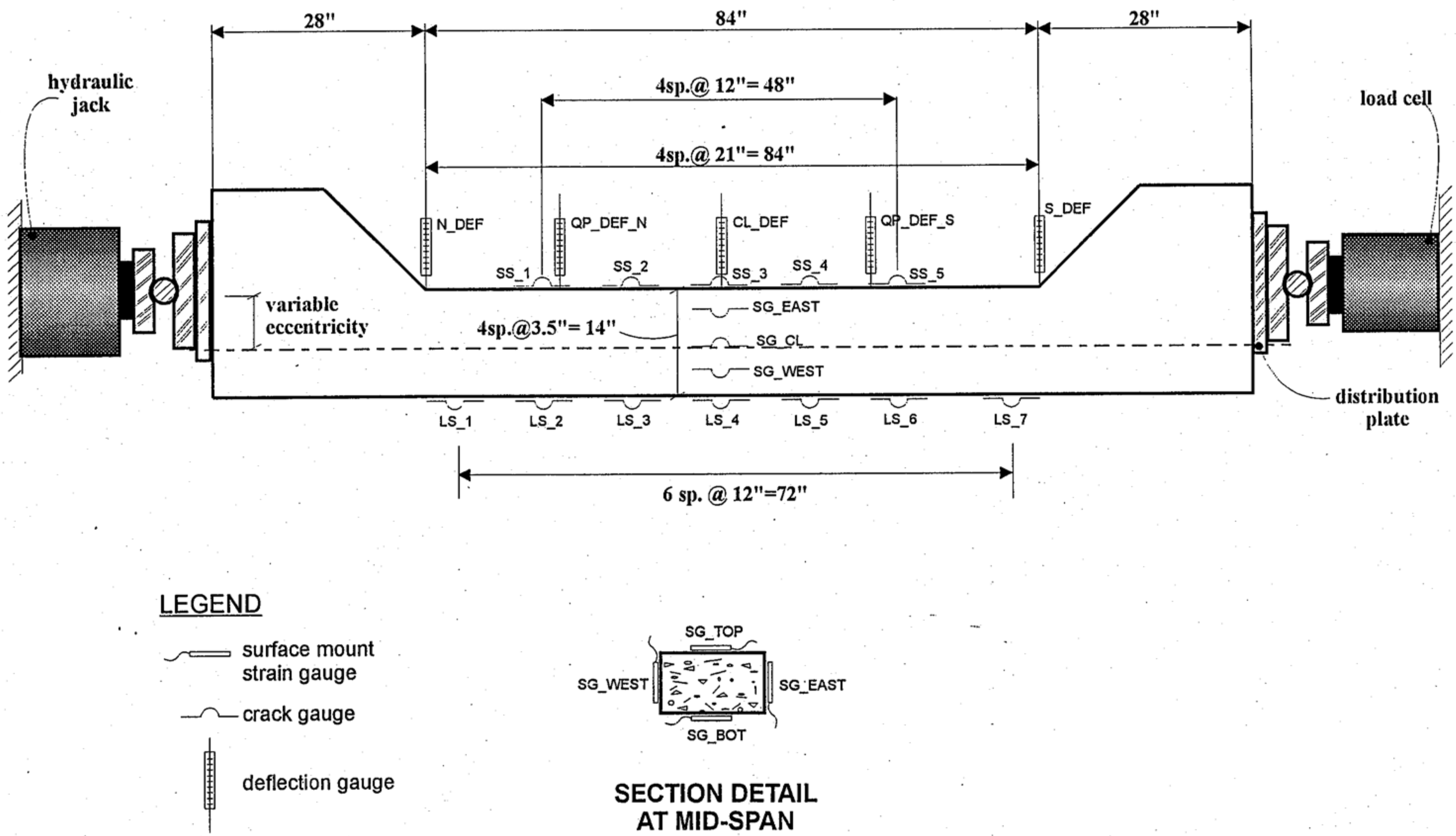

Fig.2.2(a) Instrumentation Detail of Specimen With Corbels

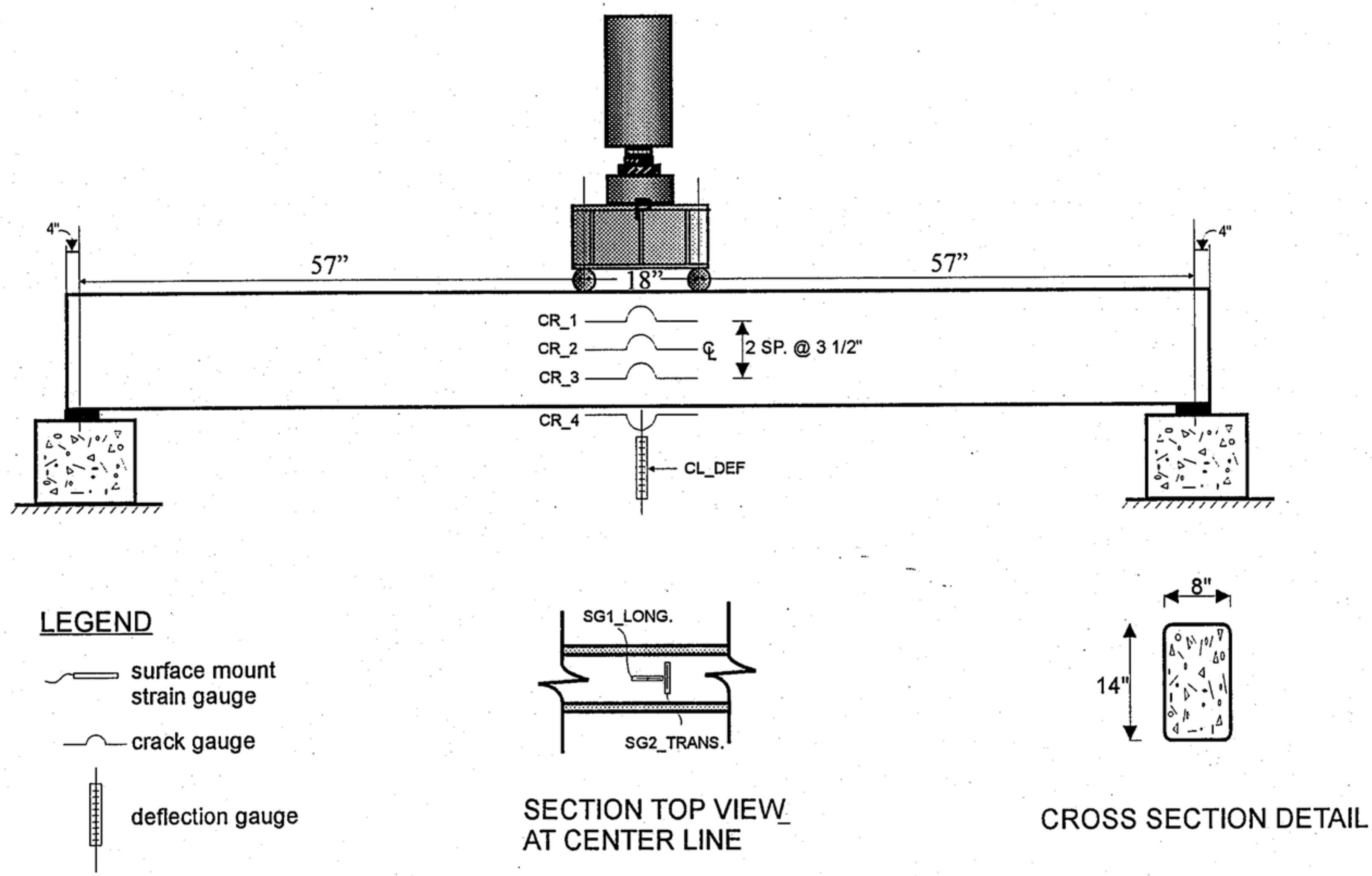

Figure 2.2(b) Instrumentation Detail of Specimen Without Corbels For Pure Flexure

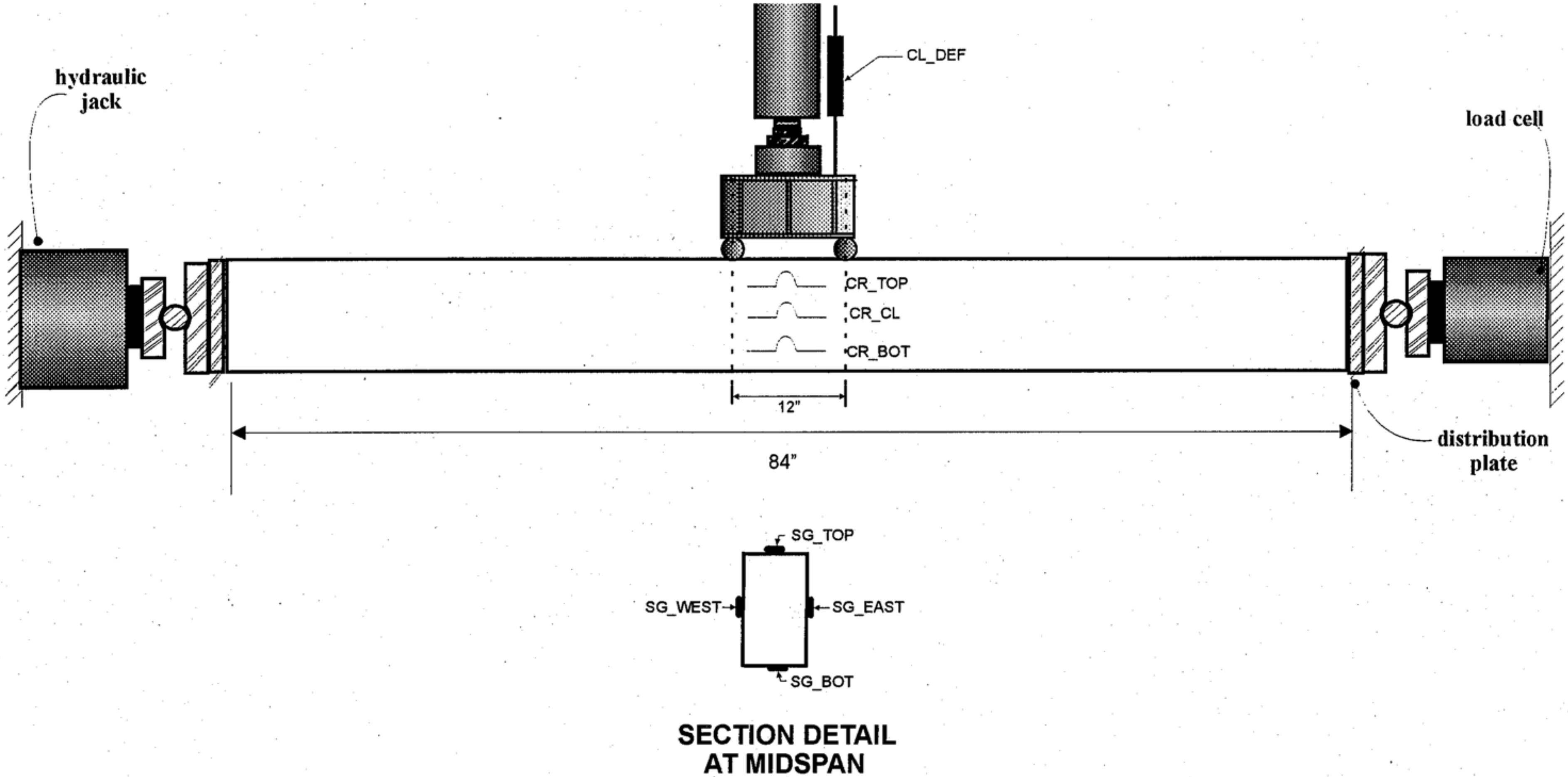

Figure 2.2(c) Instrumentation Detail of Specimen Without Corbels For Pure Compression

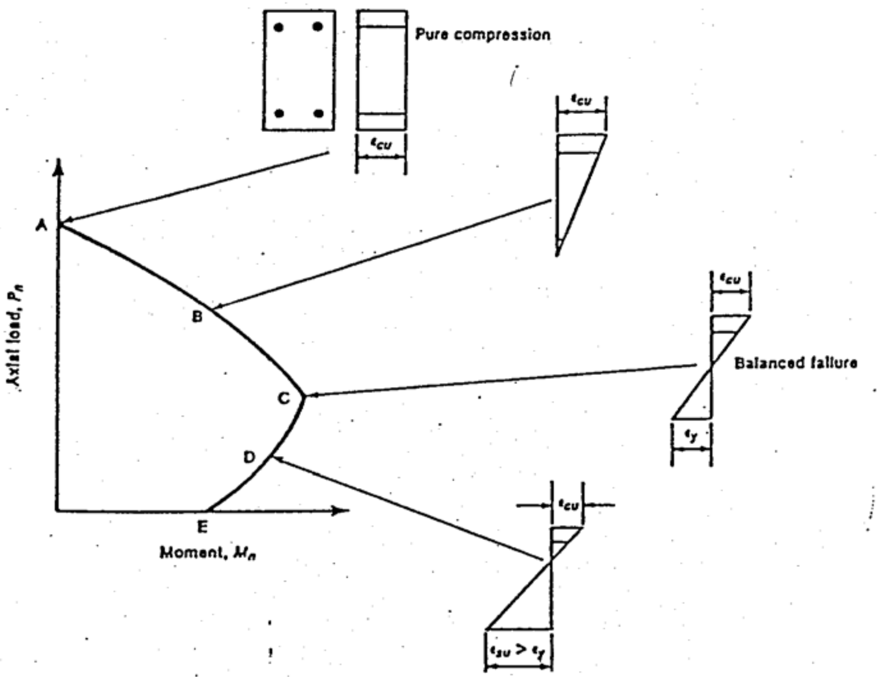

Fig. 2.3 Strain Distributions Corresponding to Points on Interaction Diagram

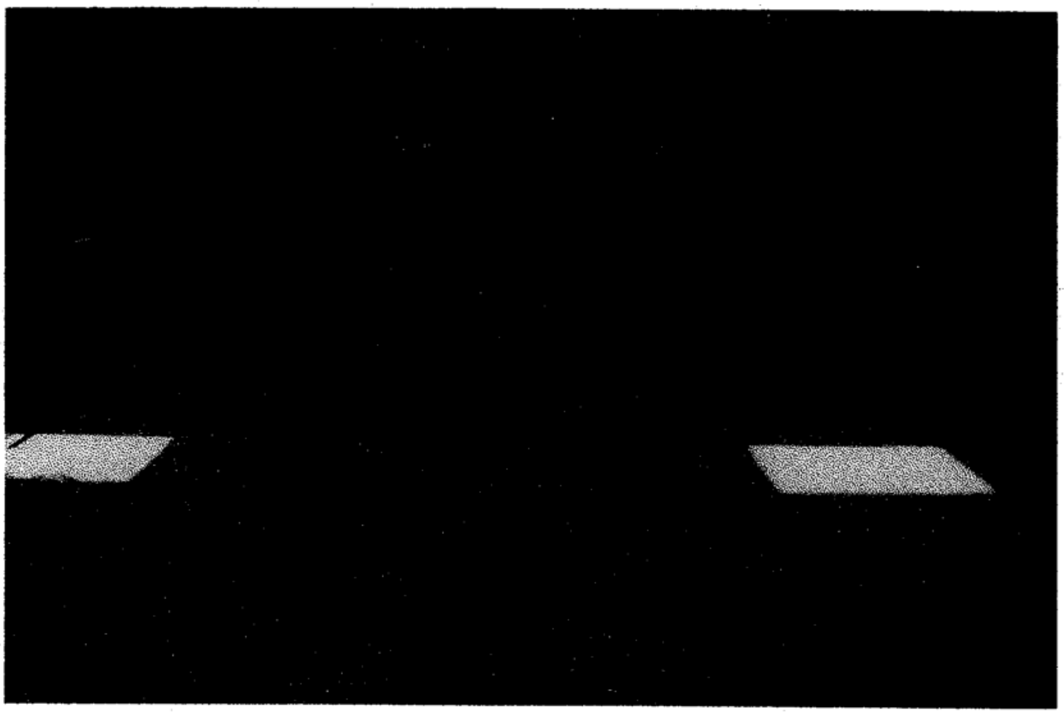

Fig. 2.4 – Typical view of a specimen during the test

Fig. 3.1a, b, c, &d - Moment vs. Deflection Along Beam Length

Specimen # BC-0L6-E0

Not Available

No Deflection Gauges were Placed on Tested Specimens

Fig 3.2a, b, c & d - Applied Moment vs. Center line Deflection

Specimen # BC-0L6-E0

Not Available

Secondary Moment Depends on center line Deflection

Fig. 3.3a - Center Line Strain Distribution

Specimen # BC-0L6-E0 (No Corbels)

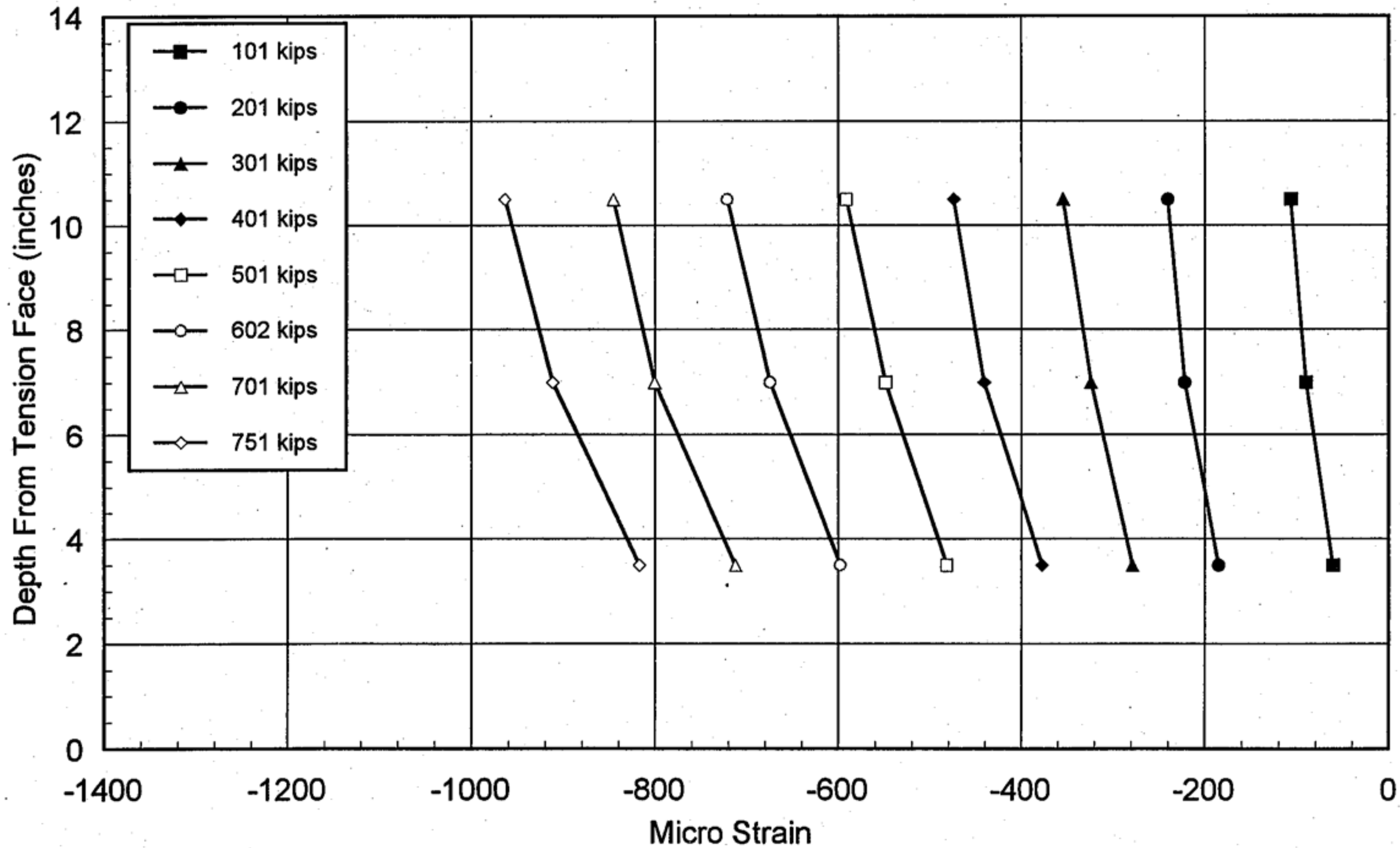

Fig. 3.3b - Center Line Strain Distribution

Specimen # BC-2L6-E0-1 (No Corbels)

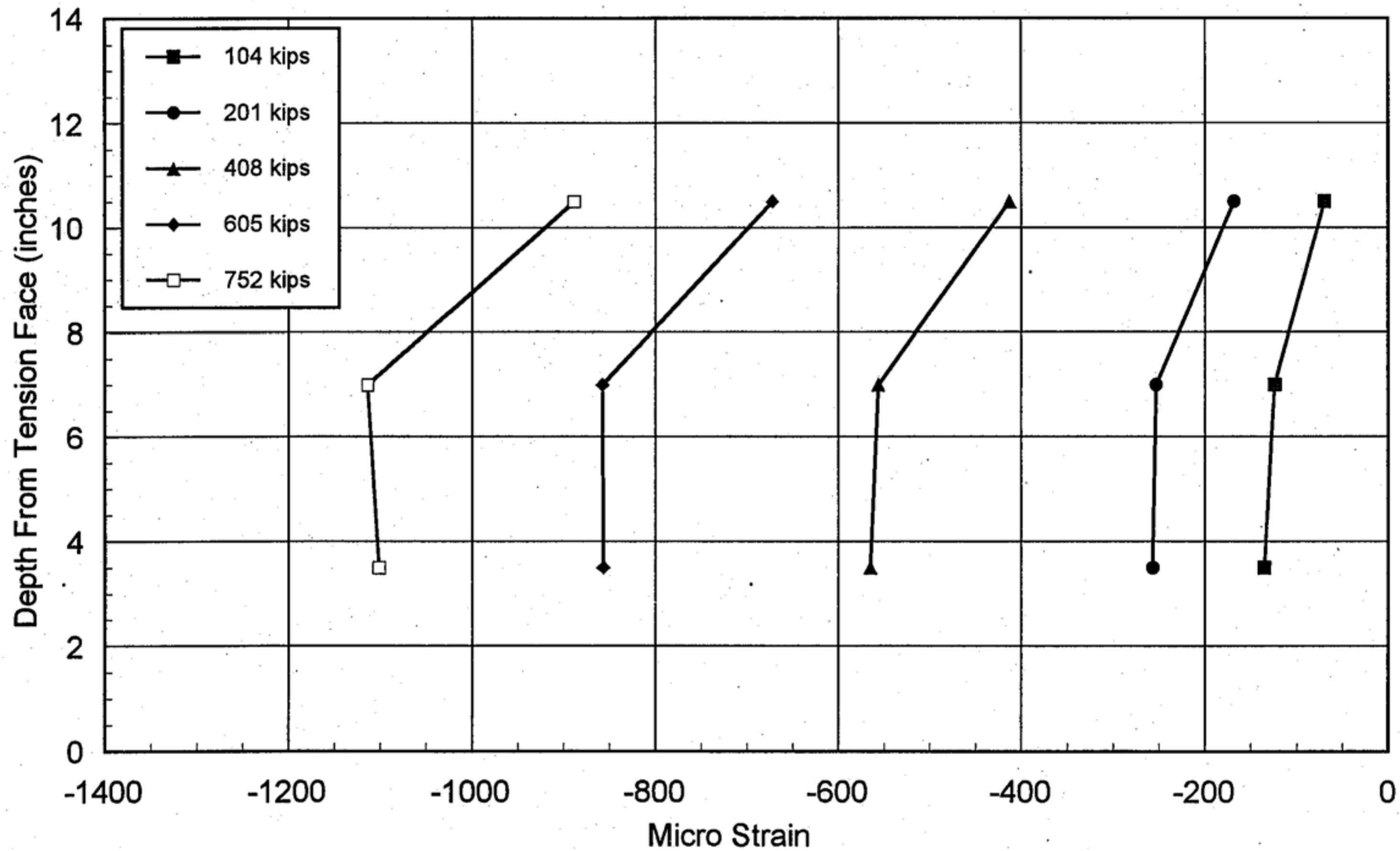

Fig. 3.3c - Center Line Strain Distribution

Specimen # BC-2L6-E0-2 (No Corbels)

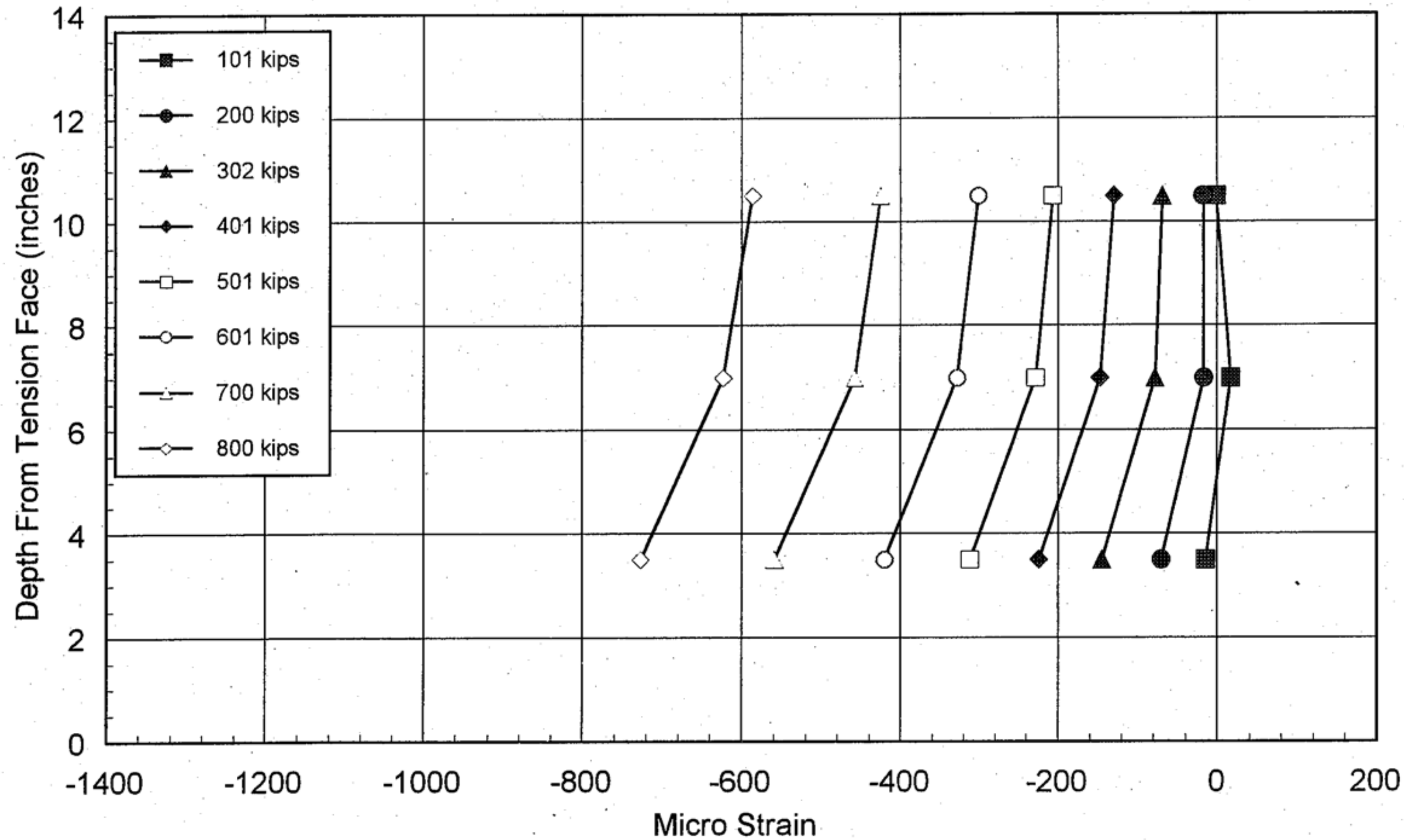

Fig. 3.3d - Center Line Strain Distribution

Specimen # BC-2L6-E0-3 (No Corbels)

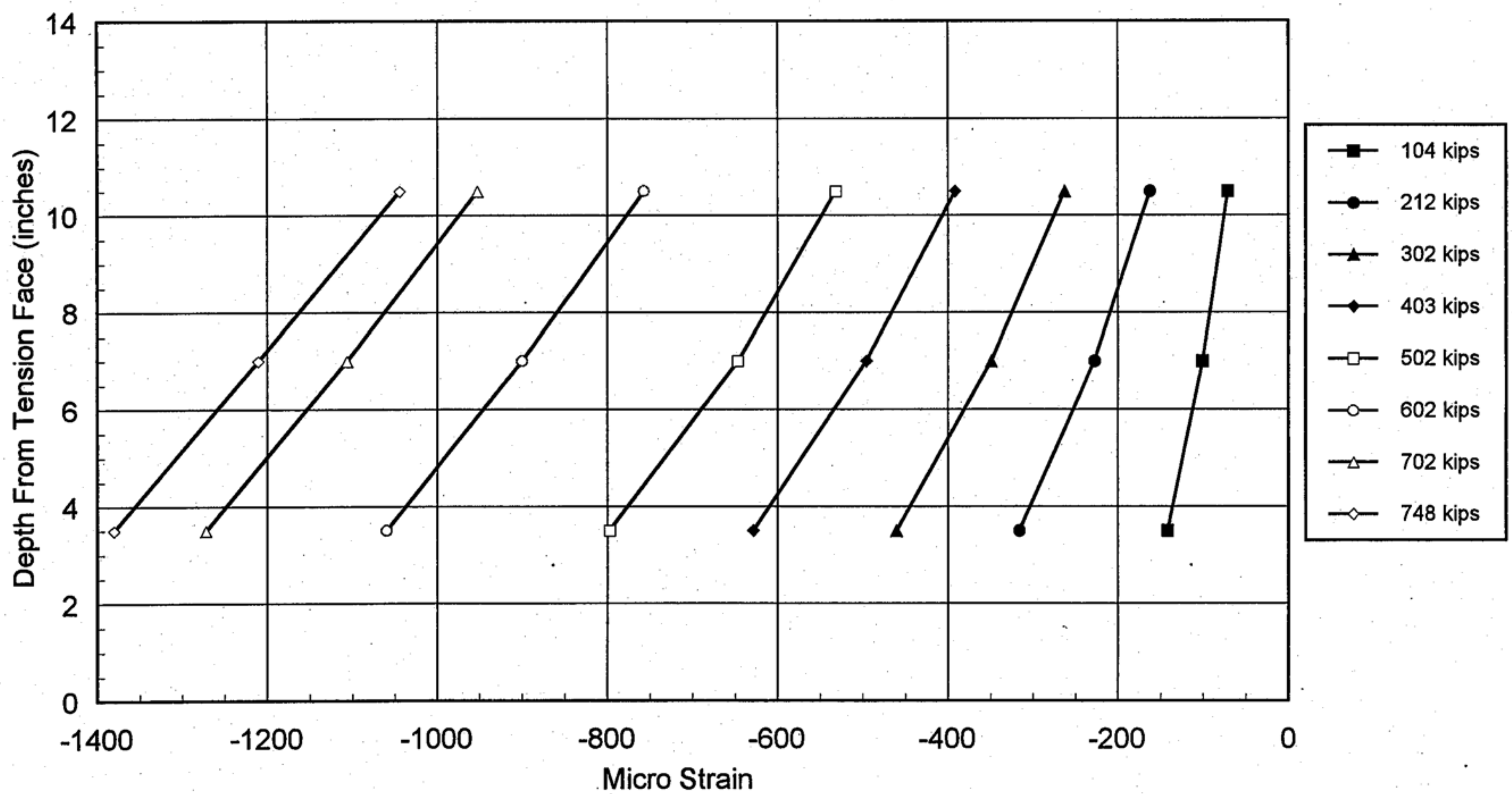

Fig. 3.4a, b, c, & d - Longitudinal Tension Strain Distribution Along Beam Length

Specimen # BC-0L6-E0

Not Available

No Strain Gauges were Placed Along Tension Length

Fig. 3.4a, b, c, & d - Longitudinal Compressive Strain Distribution Along Beam Length

Specimen # BC-0L6-E0

Not Available

No Strain Gauges were Placed Along Compression Length

Fig. 3.5a - Load vs.Transverse Strain At midspan

Specimen # BC-0L6-E0 (No Corbels)

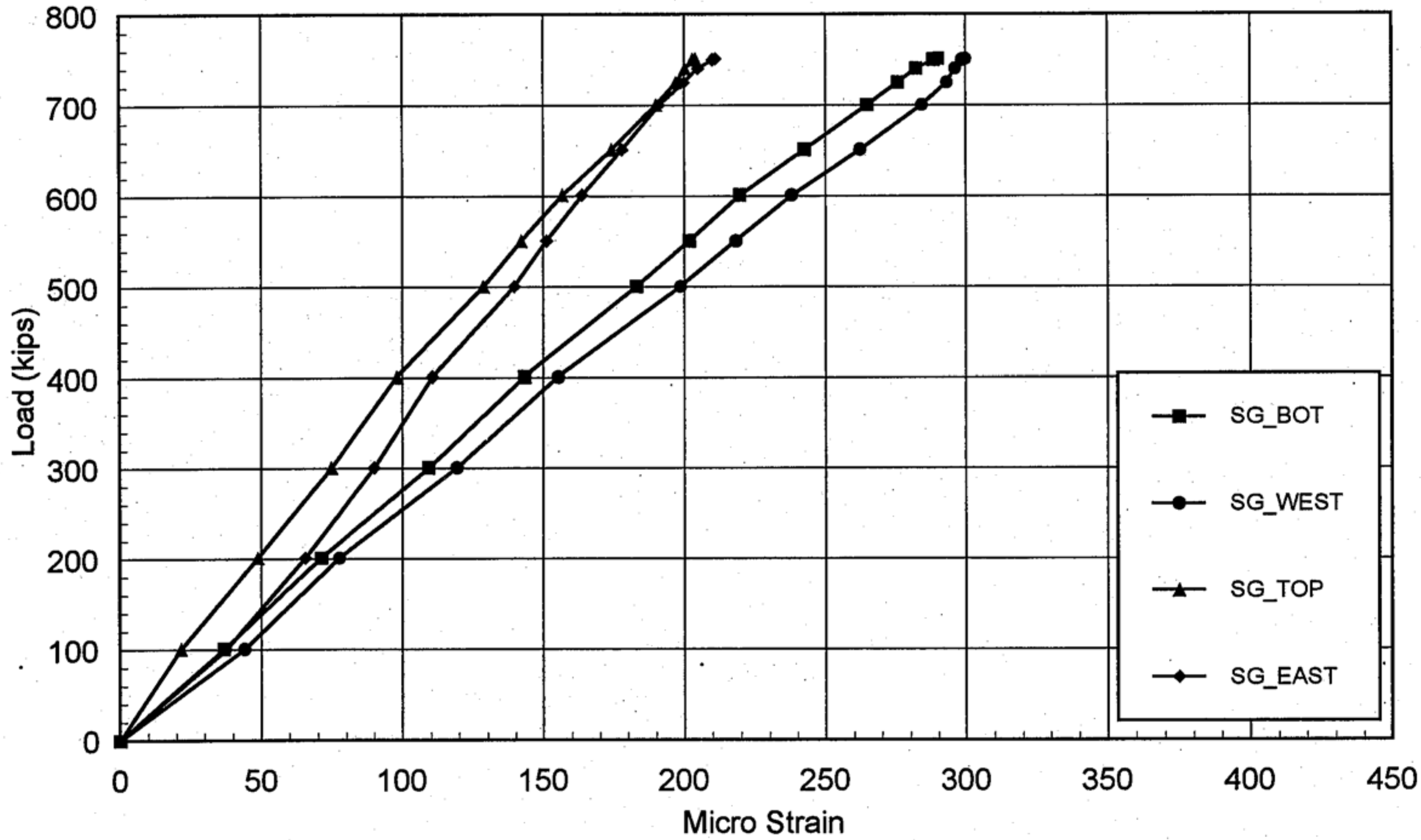

Fig. 3.5b - Load vs.Transverse Strain At Midspan

Specimen # BC-2L6-E0-1 (No Corbels)

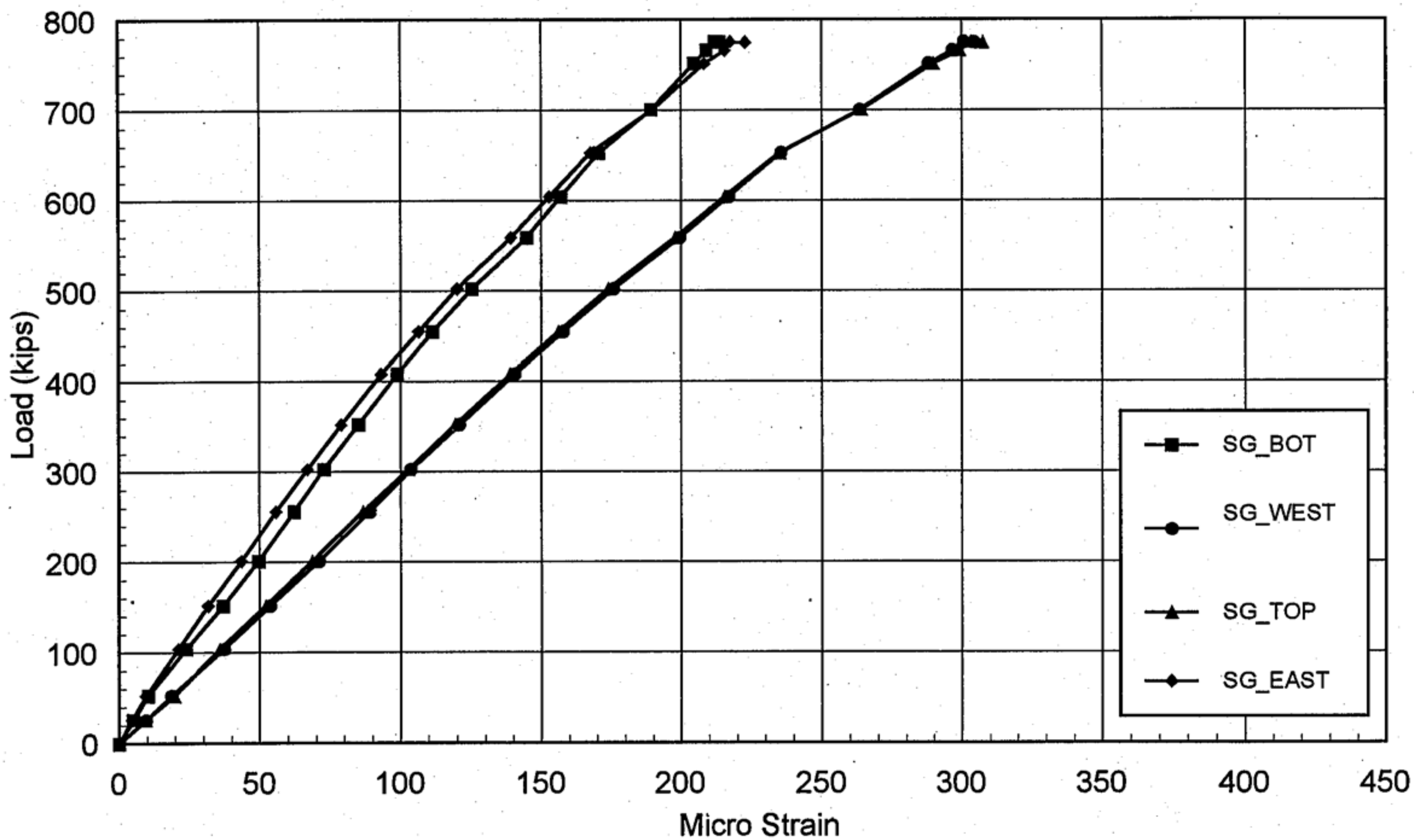

Fig. 3.5c - Load vs.Transverse Strain At Midspan

Specimen # BC-2L6-E0-2 (No Corbels)

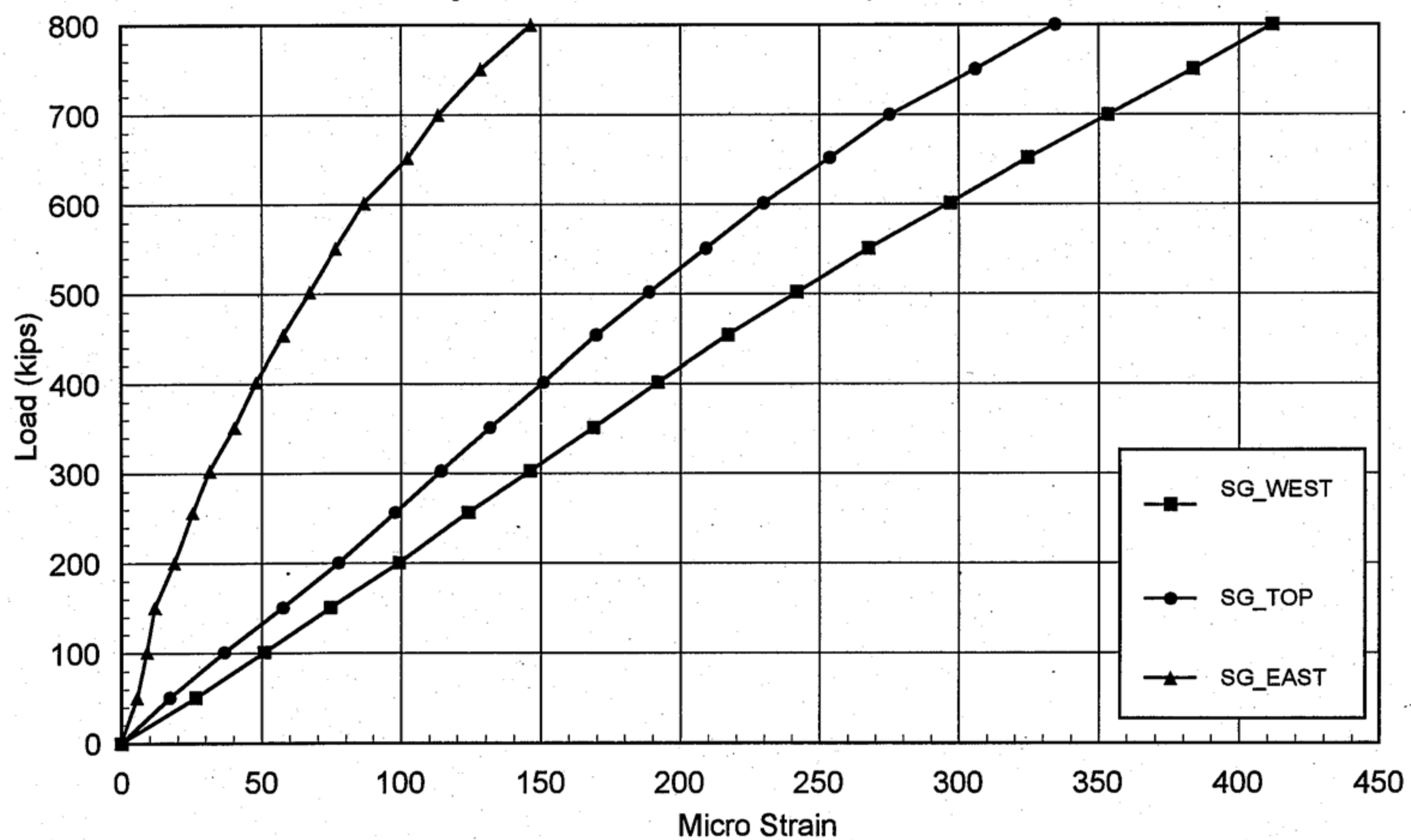

Fig. 3.5d - Load vs.Transverse Strain At Midspan

Specimen # BC-2L6-E0-3 (No Corbels)

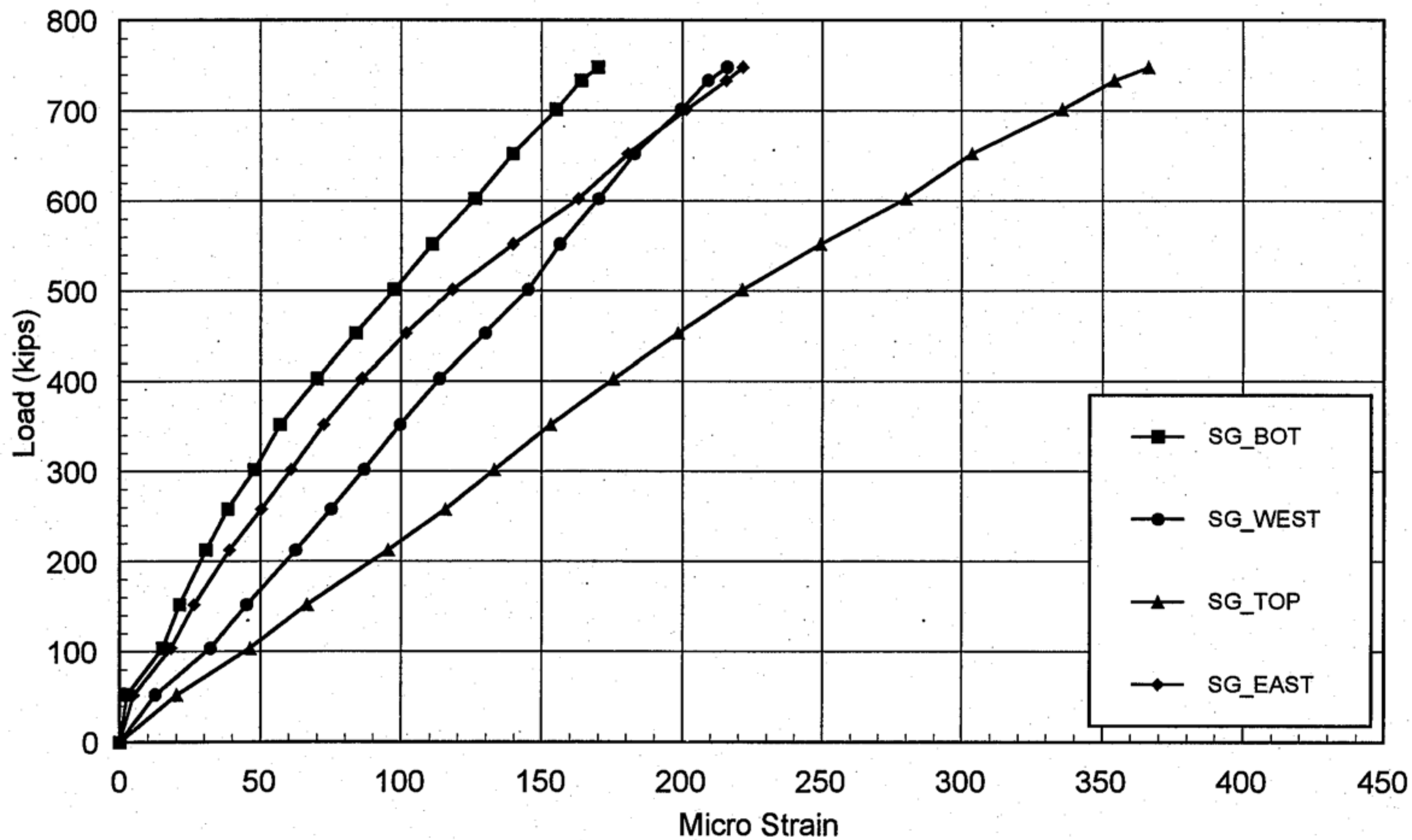

Fig 3.6a - Applied Moment vs. Center line Deflection

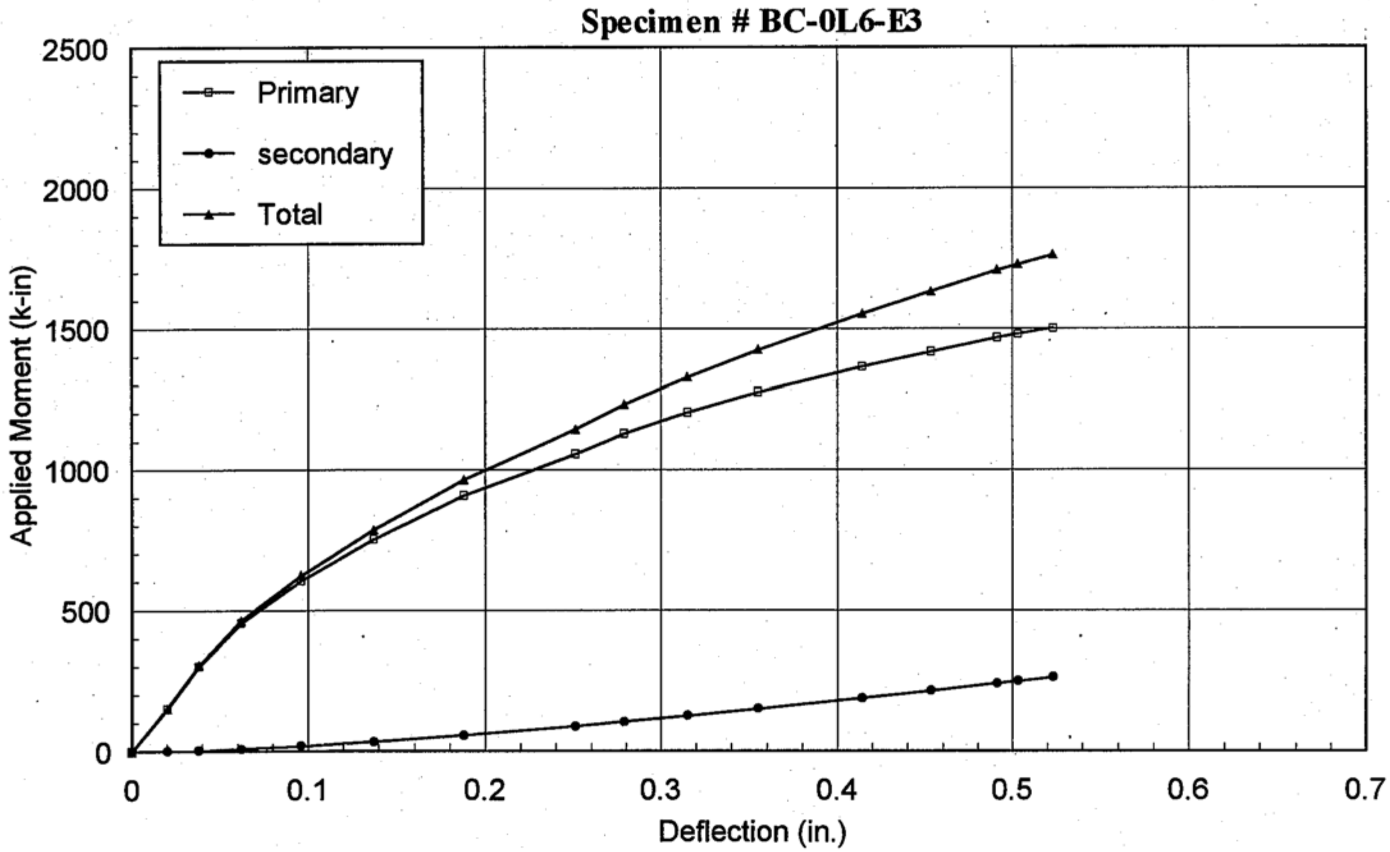

Fig 3.6b - Applied Moment vs. Center line Deflection

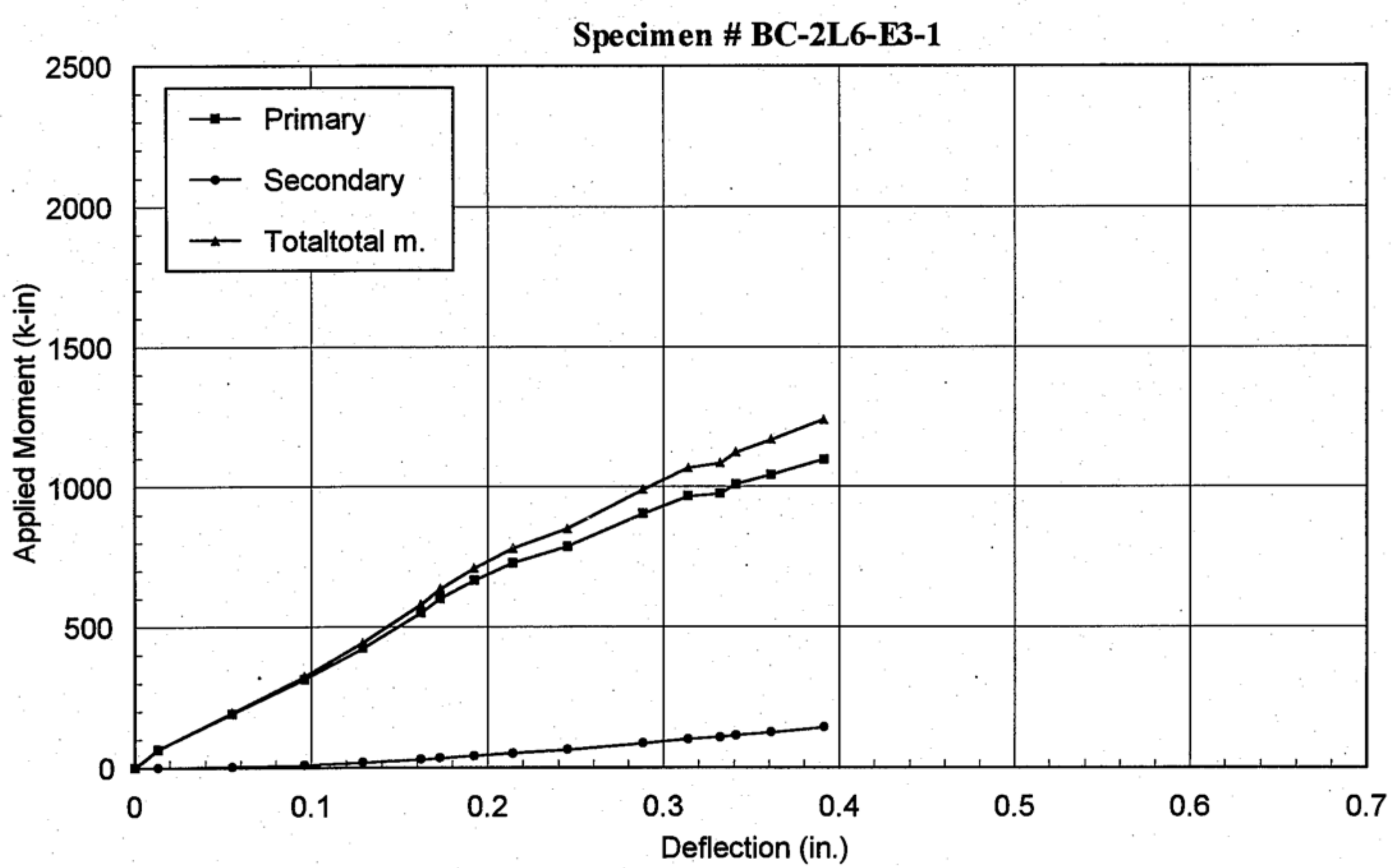

Fig 3.6c - Applied Moment vs. Center line Deflection

Specimen # BC-2L6-E3-2

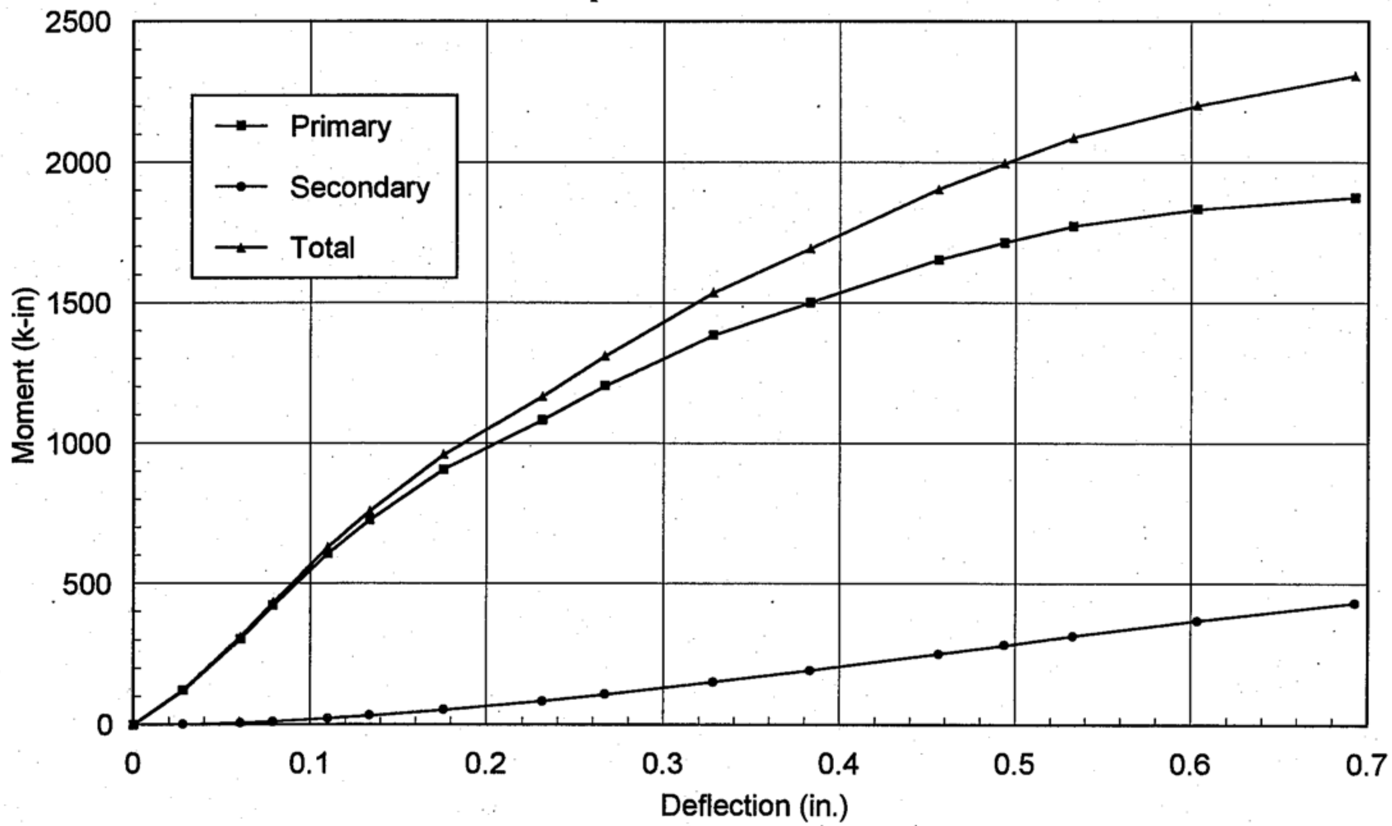

Fig. 3.7a - Centerline Strain Distribution

Specimen # BC-0L6-E3

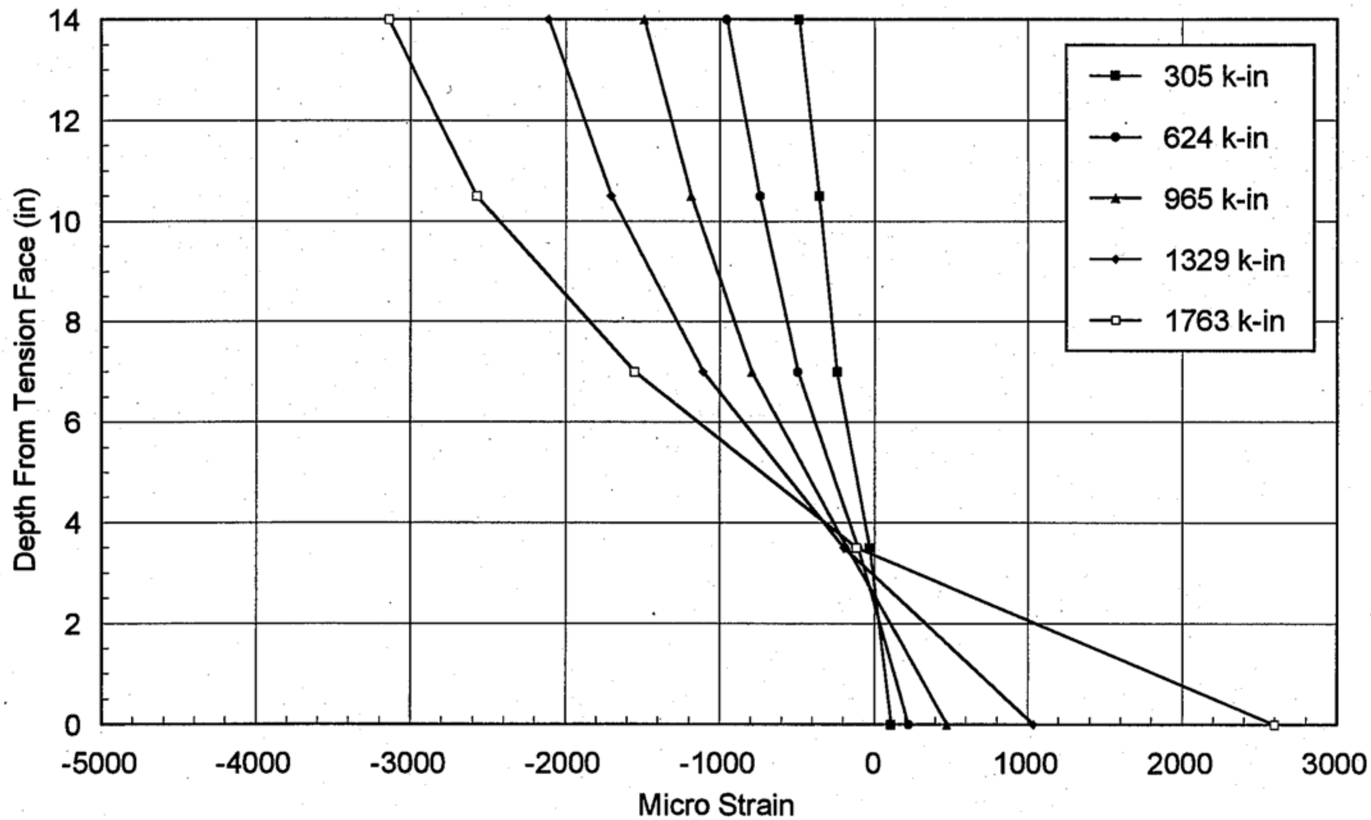

Fig. 3.7b - Centerline Strain Distribution

Specimen # BC-2L6-E3-1

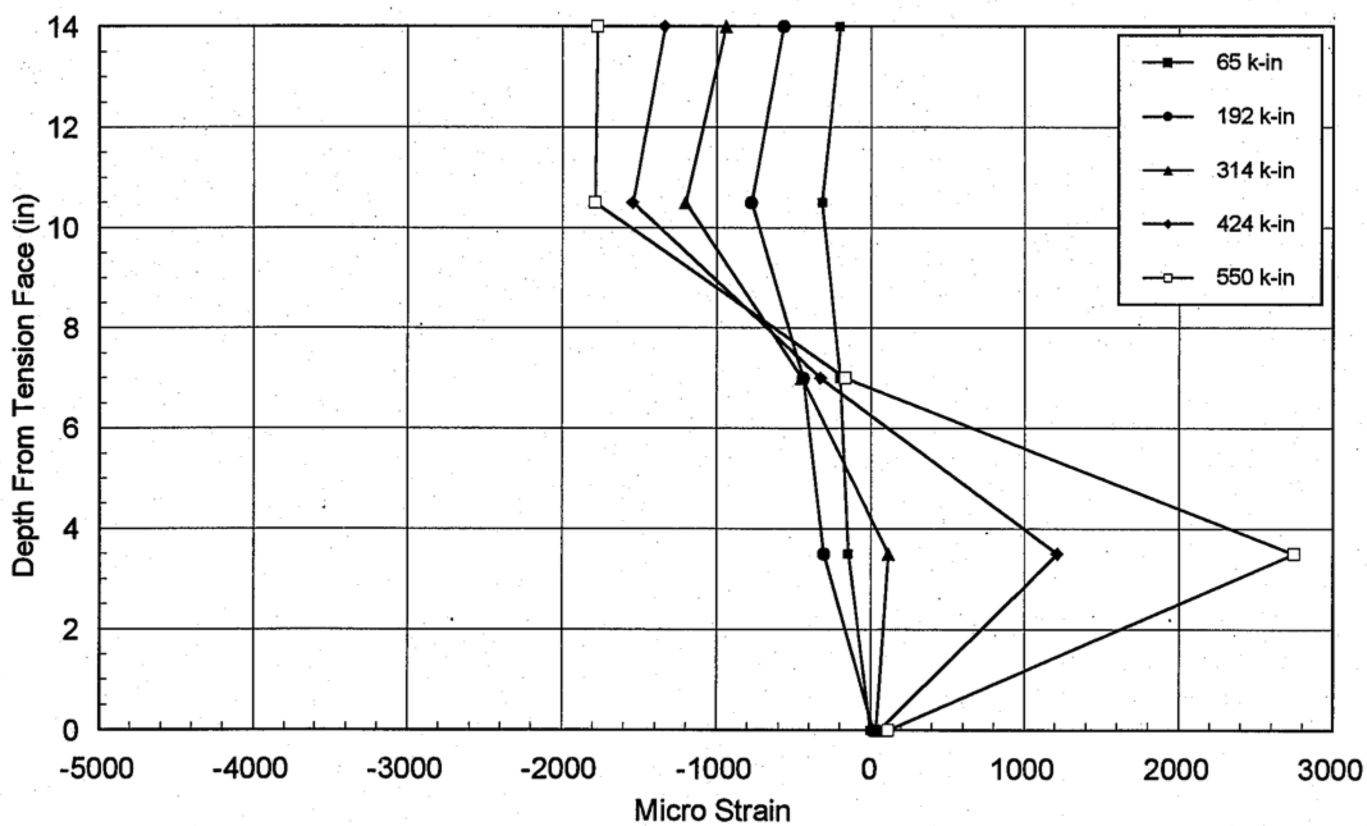

Fig. 3.7c - Centerline Strain Distribution

Specimen # BC-2L6-E3-2

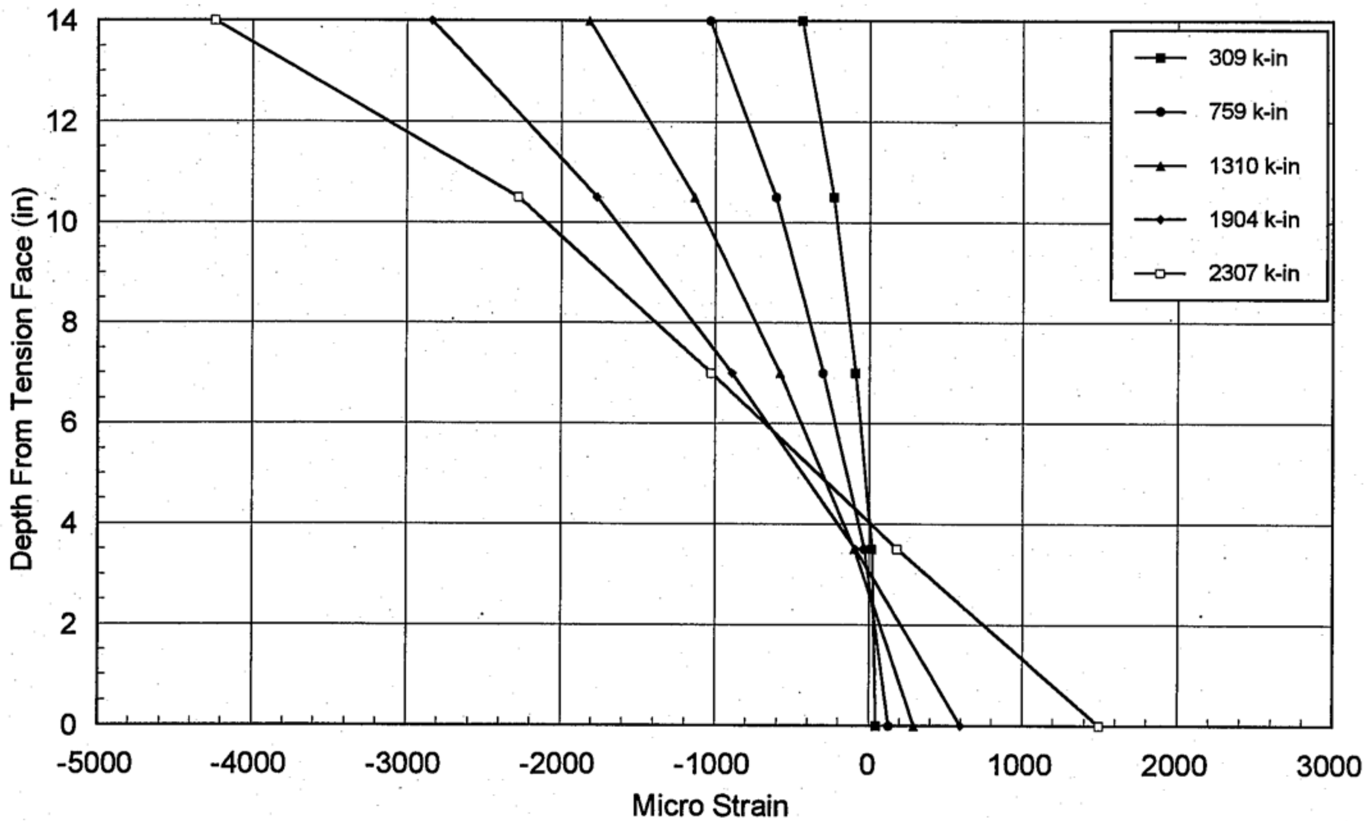

Fig. 3.8a - Longitudinal Tension Strain Distribution Along Beam Length

Specimen # BC-0L6-E3

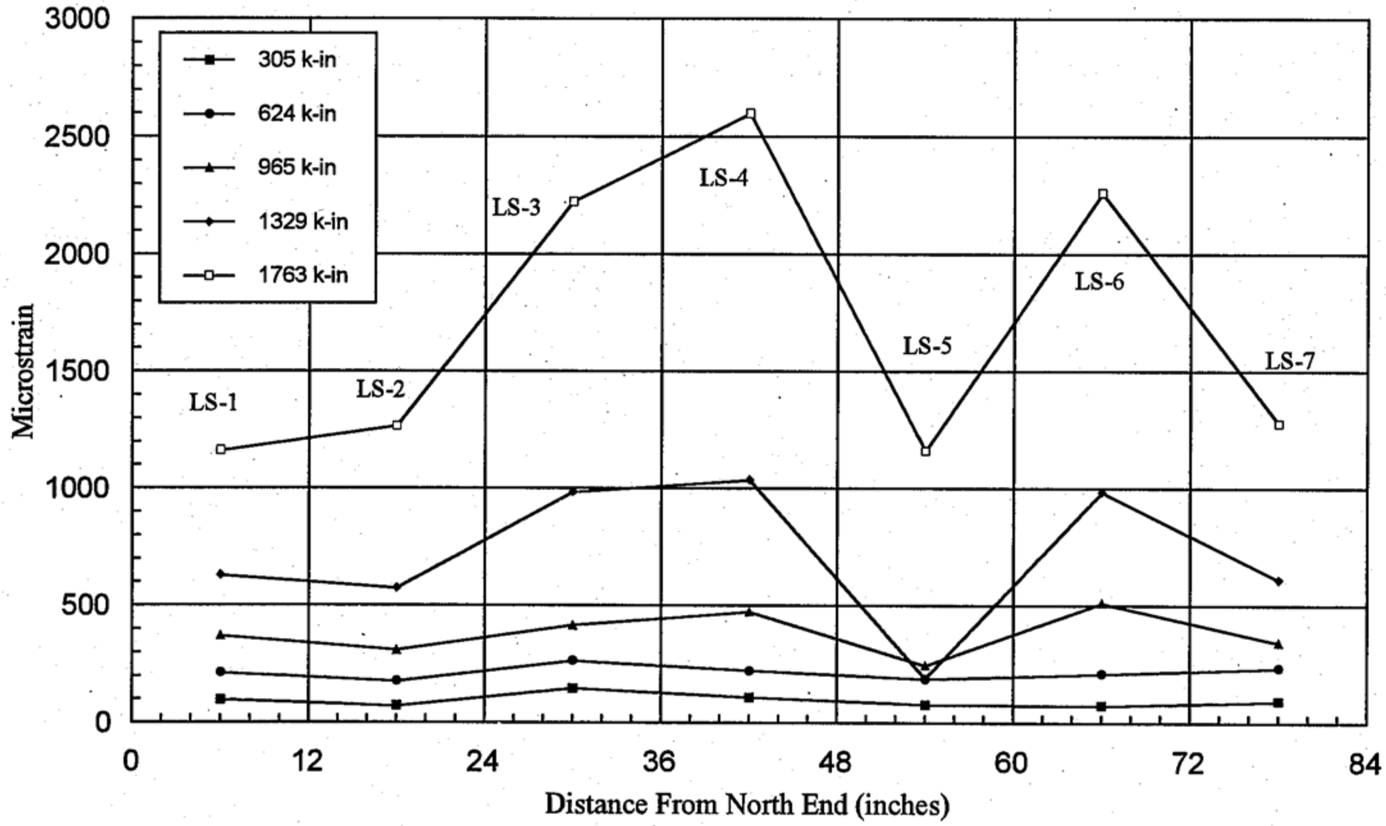

Fig. 3.8a - Longitudinal Compressive Strain Distribution Along Beam Length

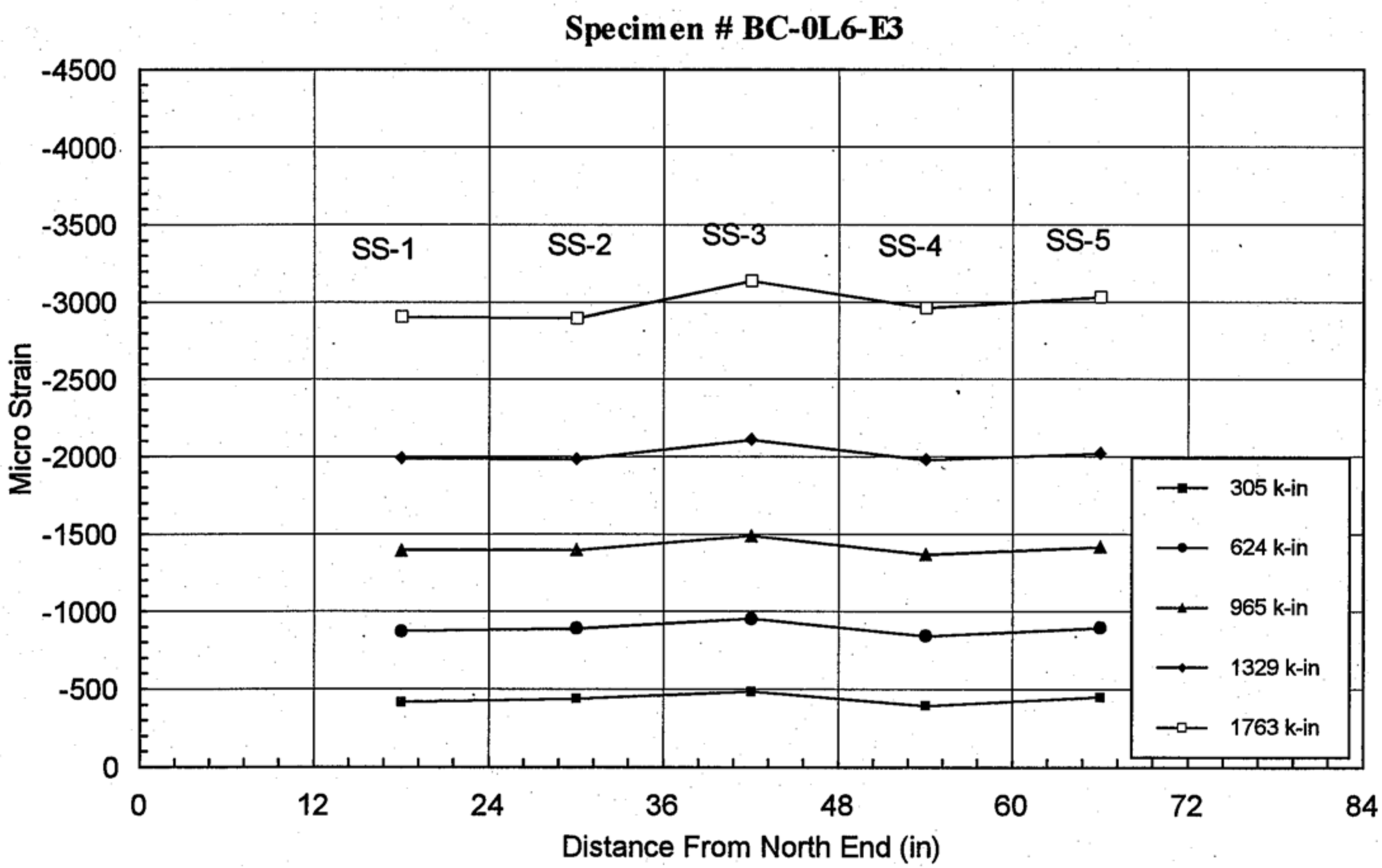

Fig. 3.8b - Longitudinal Tension Strain Distribution Along Beam Length

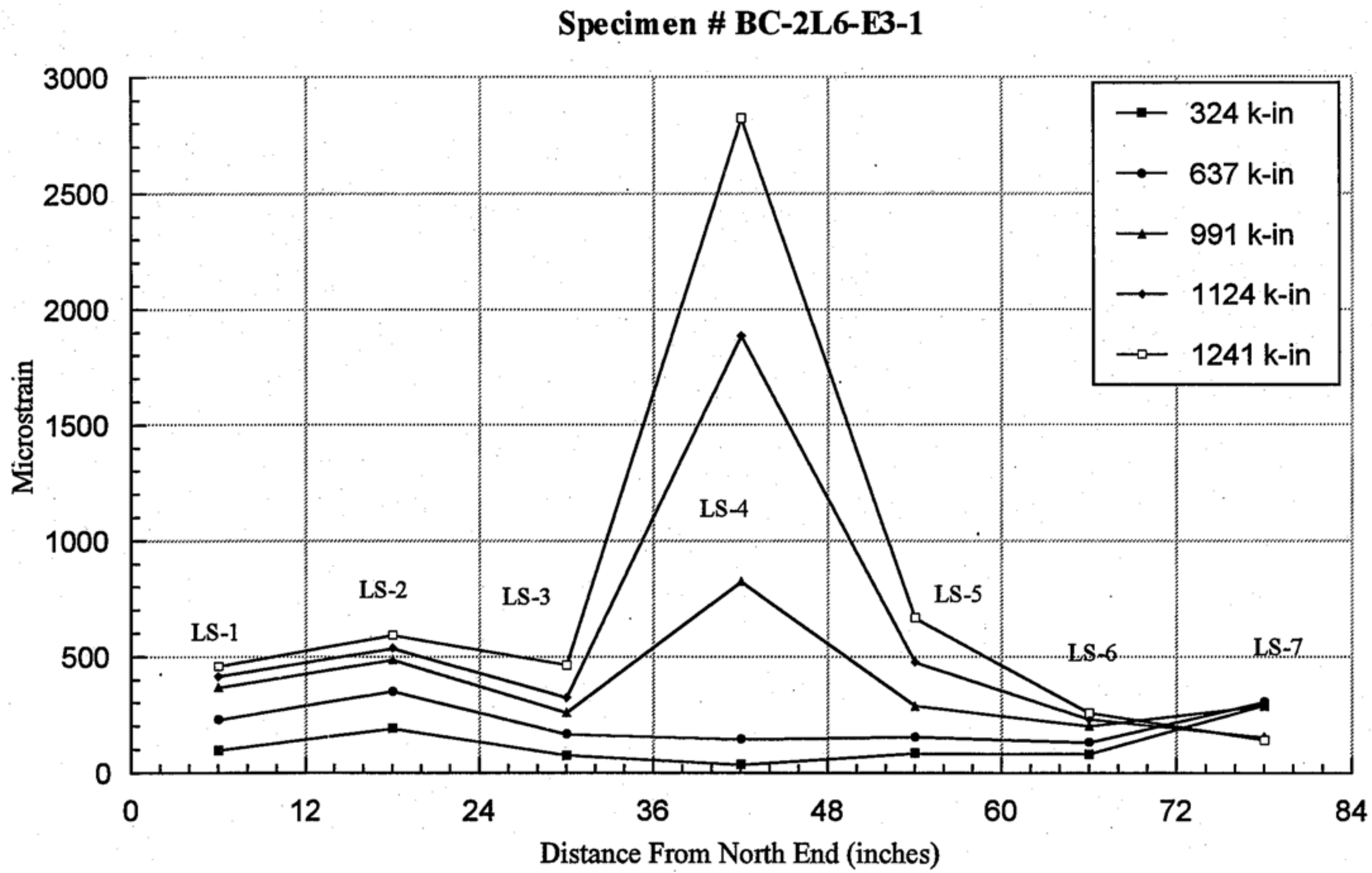

Fig. 3.8b - Longitudinal Compressive Strain Distribution Along Beam Length

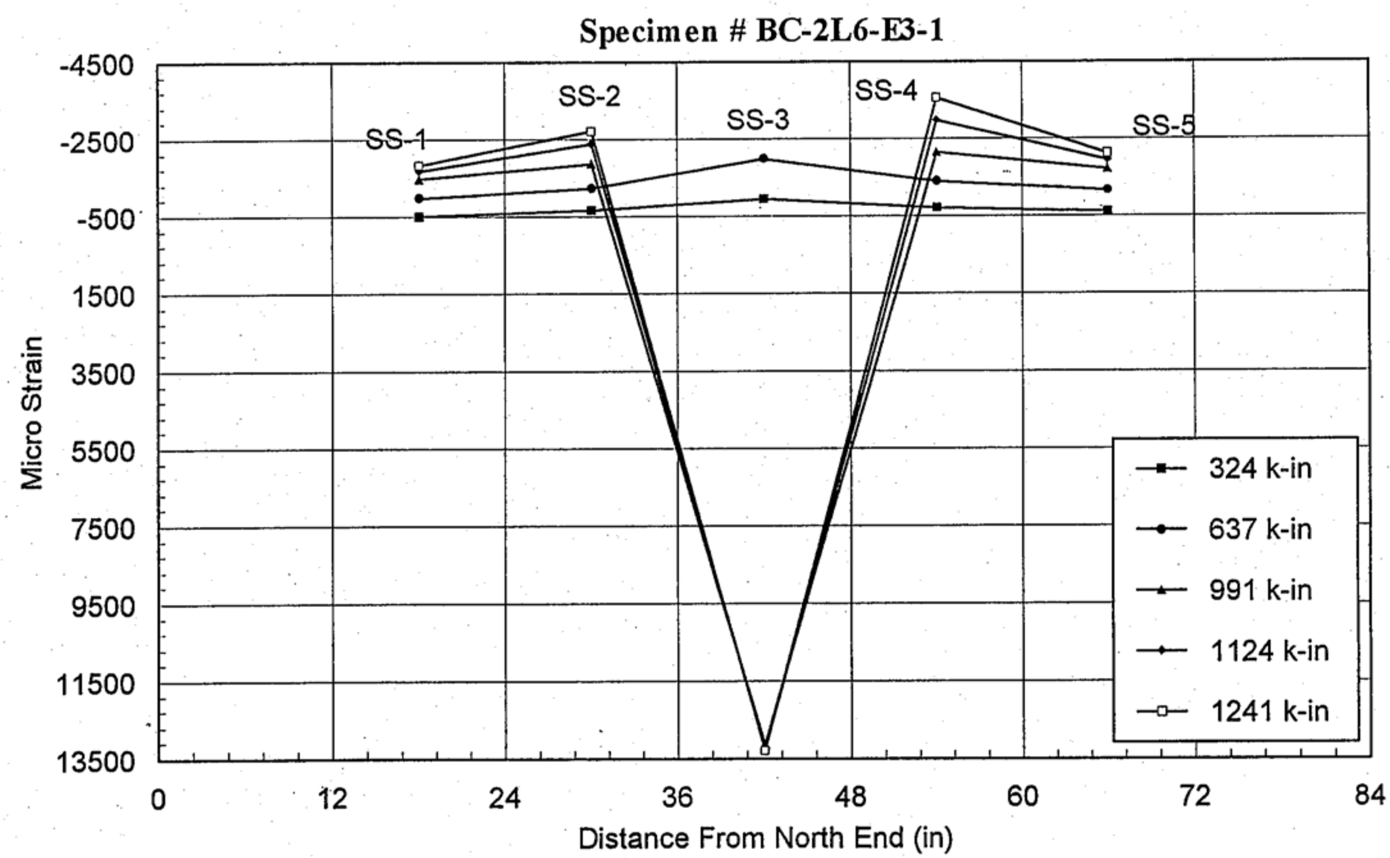

Fig.3.8c - Longitudinal Tension Strain Distribution Along Beam Length

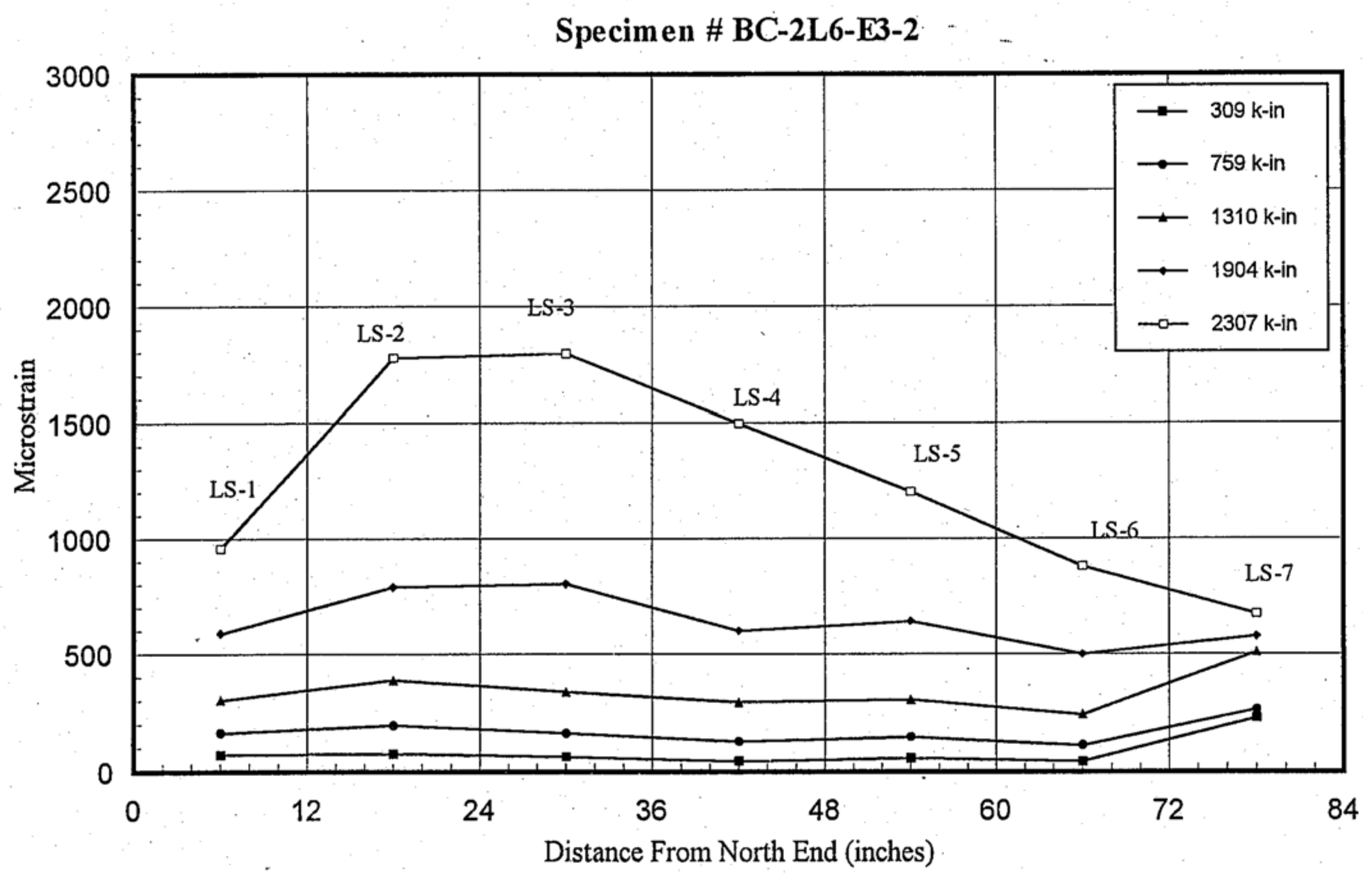

Fig. 3.8c - Longitudinal Compressive Strain Distribution Along Beam Length

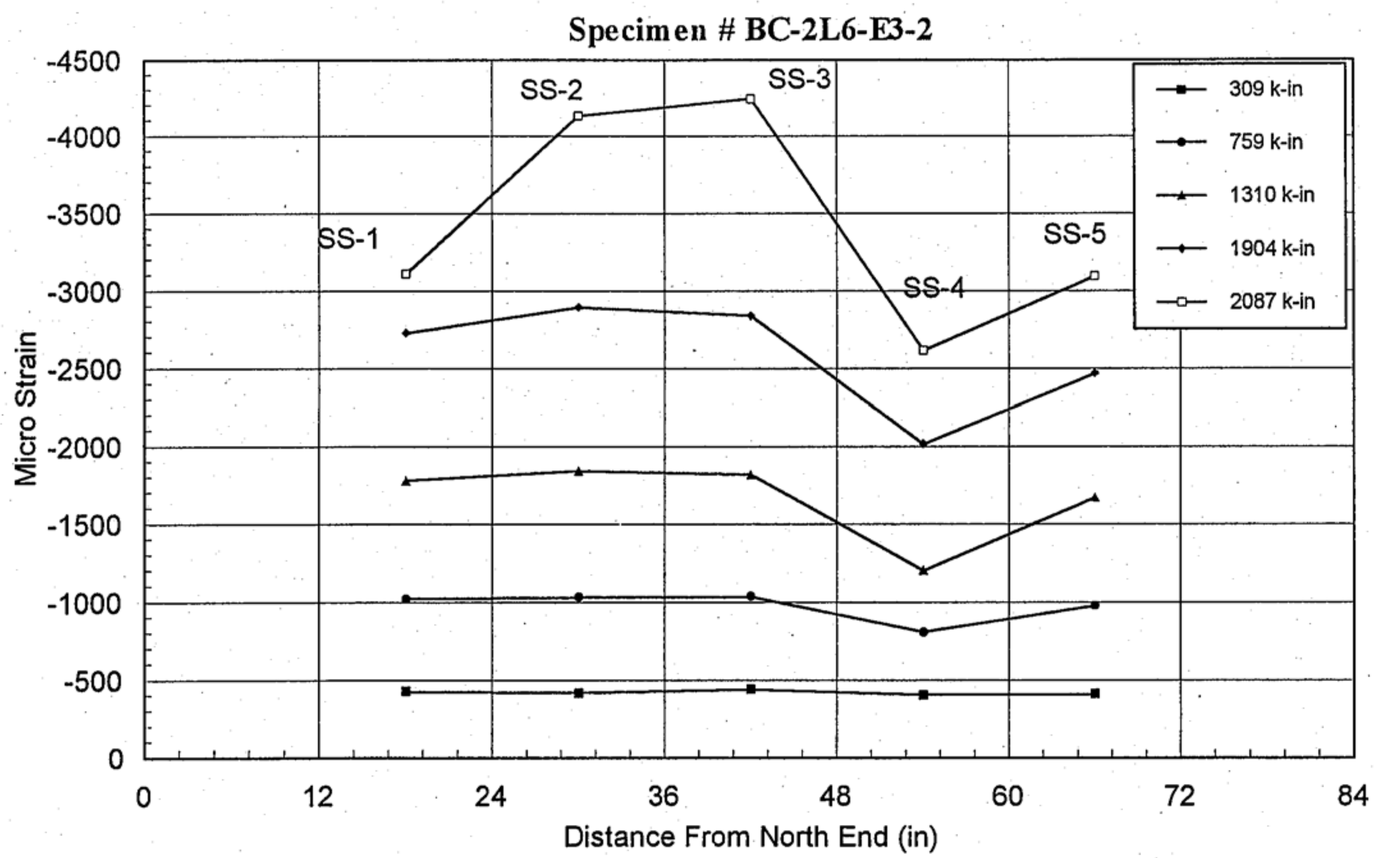

Fig. 3.9a - Moment vs. Transvers Strain At Midspan

Specimen # BC-0L6-E3

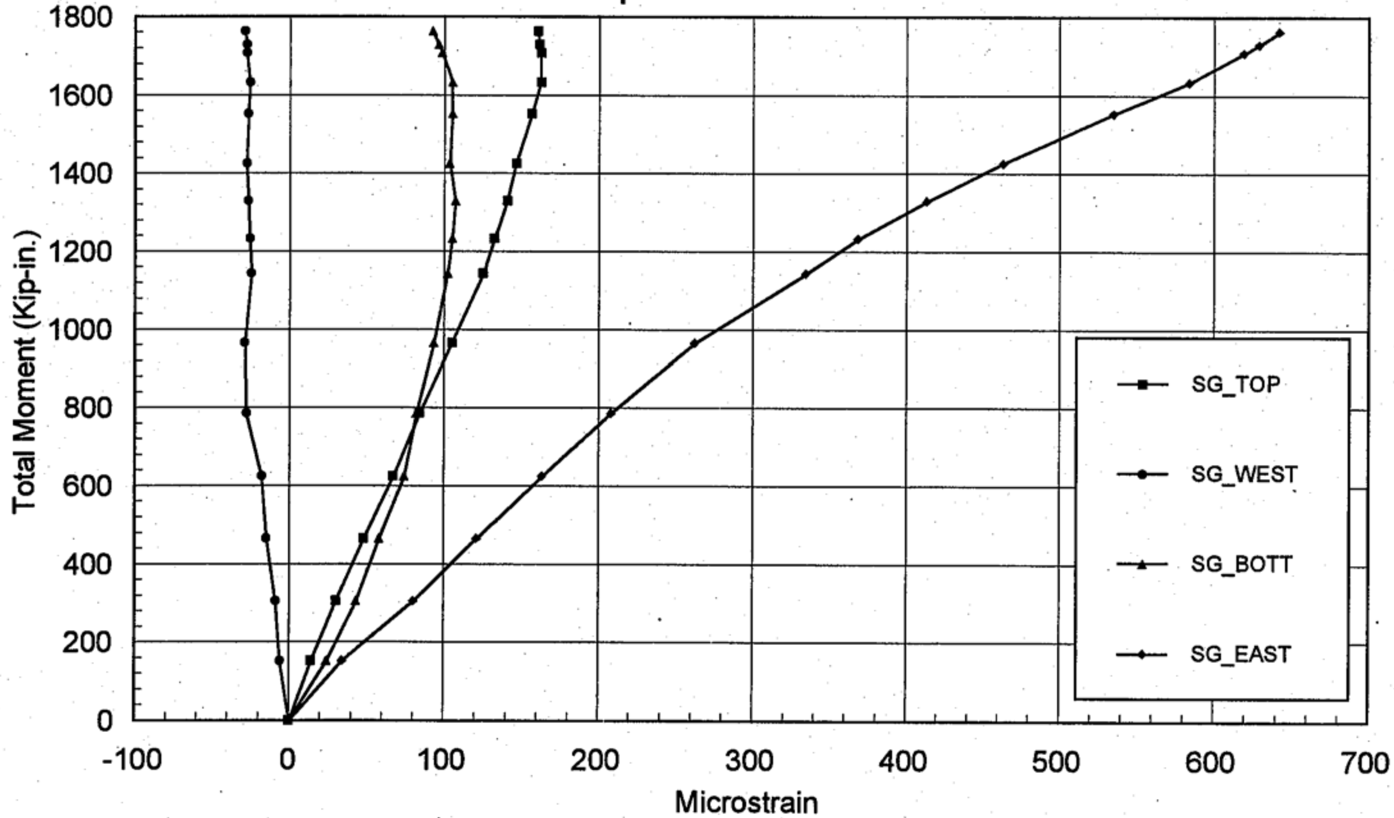

Fig. 3.9b - Moment vs. Transverse Strain At Midspan

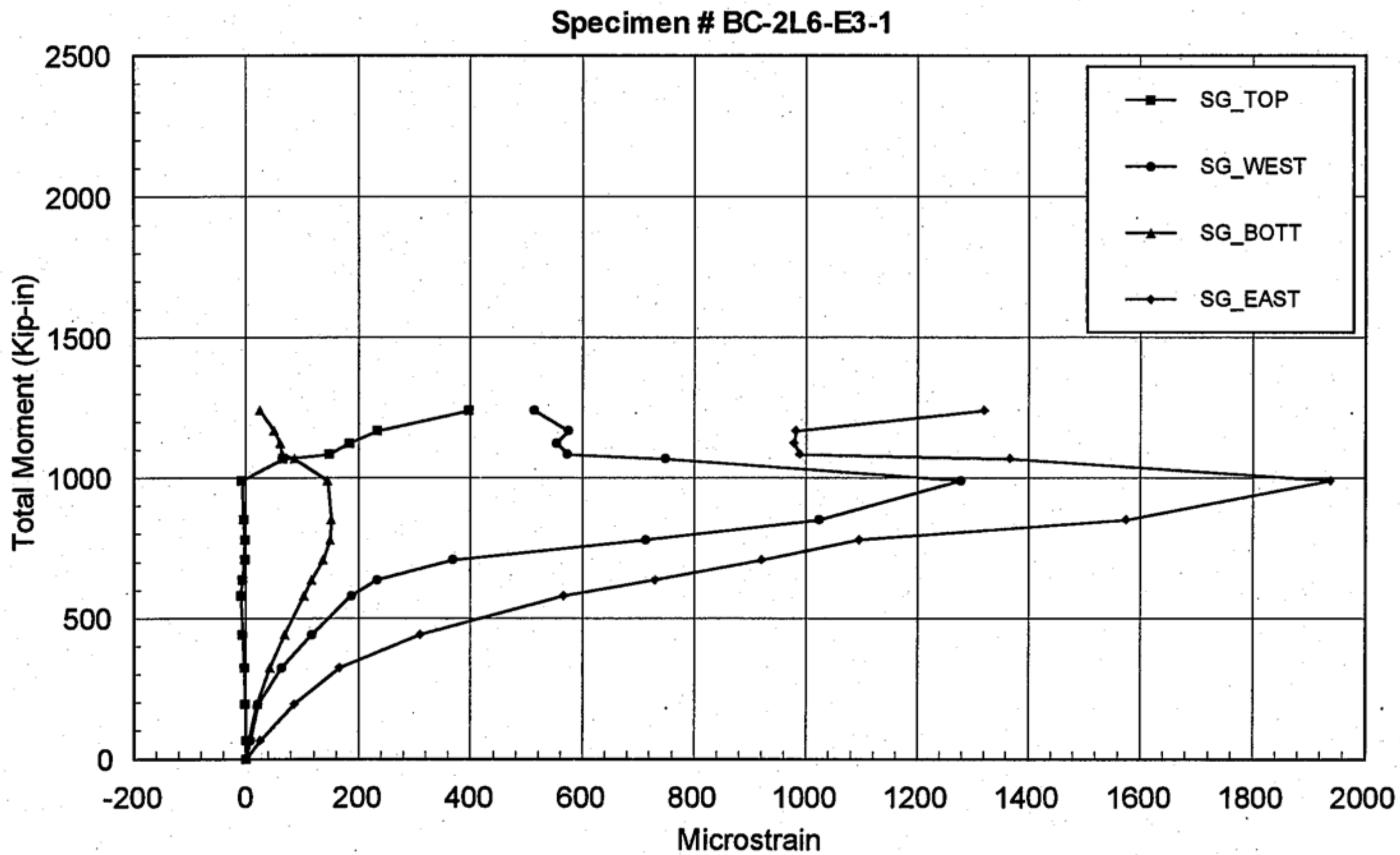

Fig. 3.9c - Moment vs. Transverse Strain At Midspan

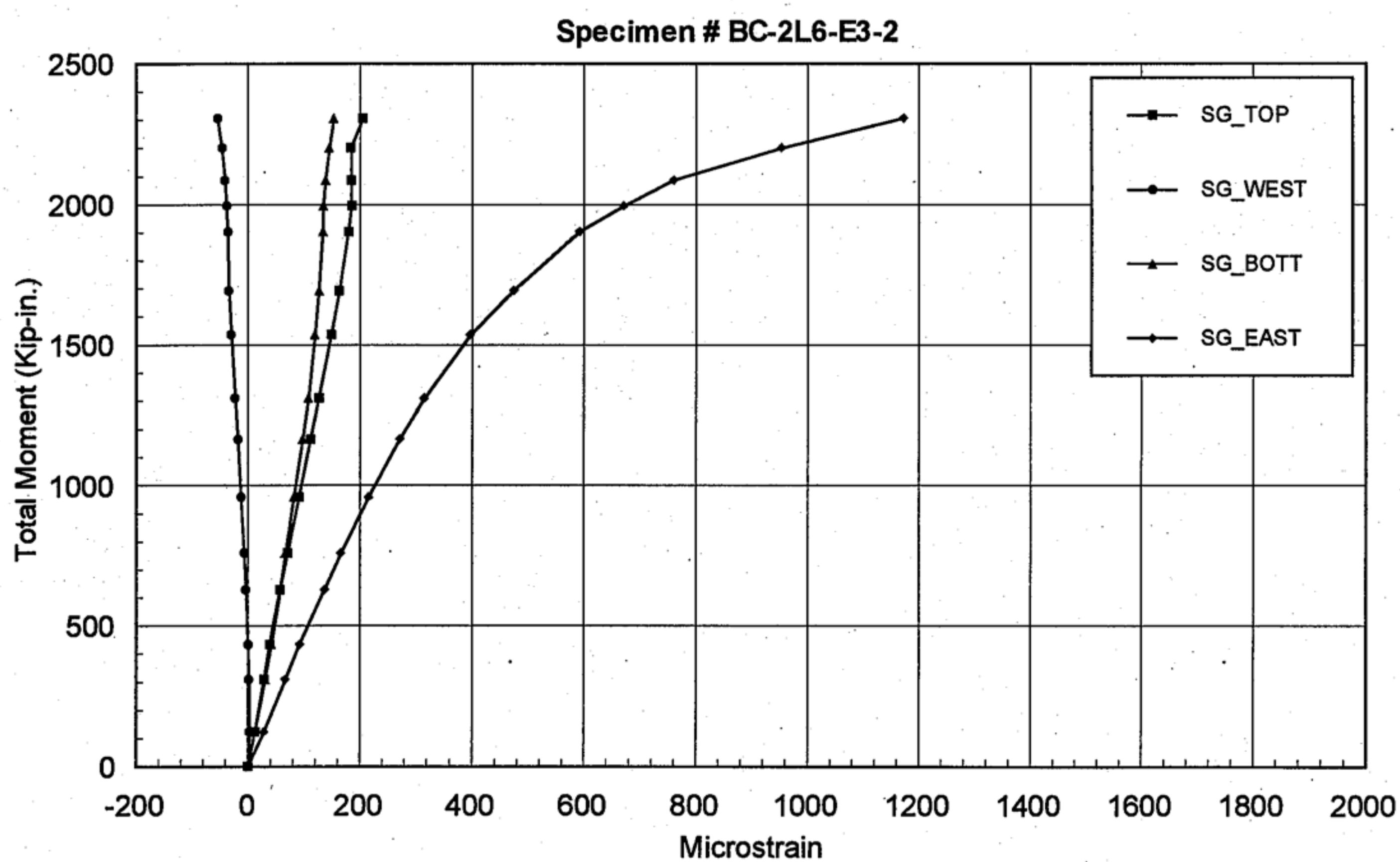

Fig 3.10a - Applied Moment vs. Center line Deflection

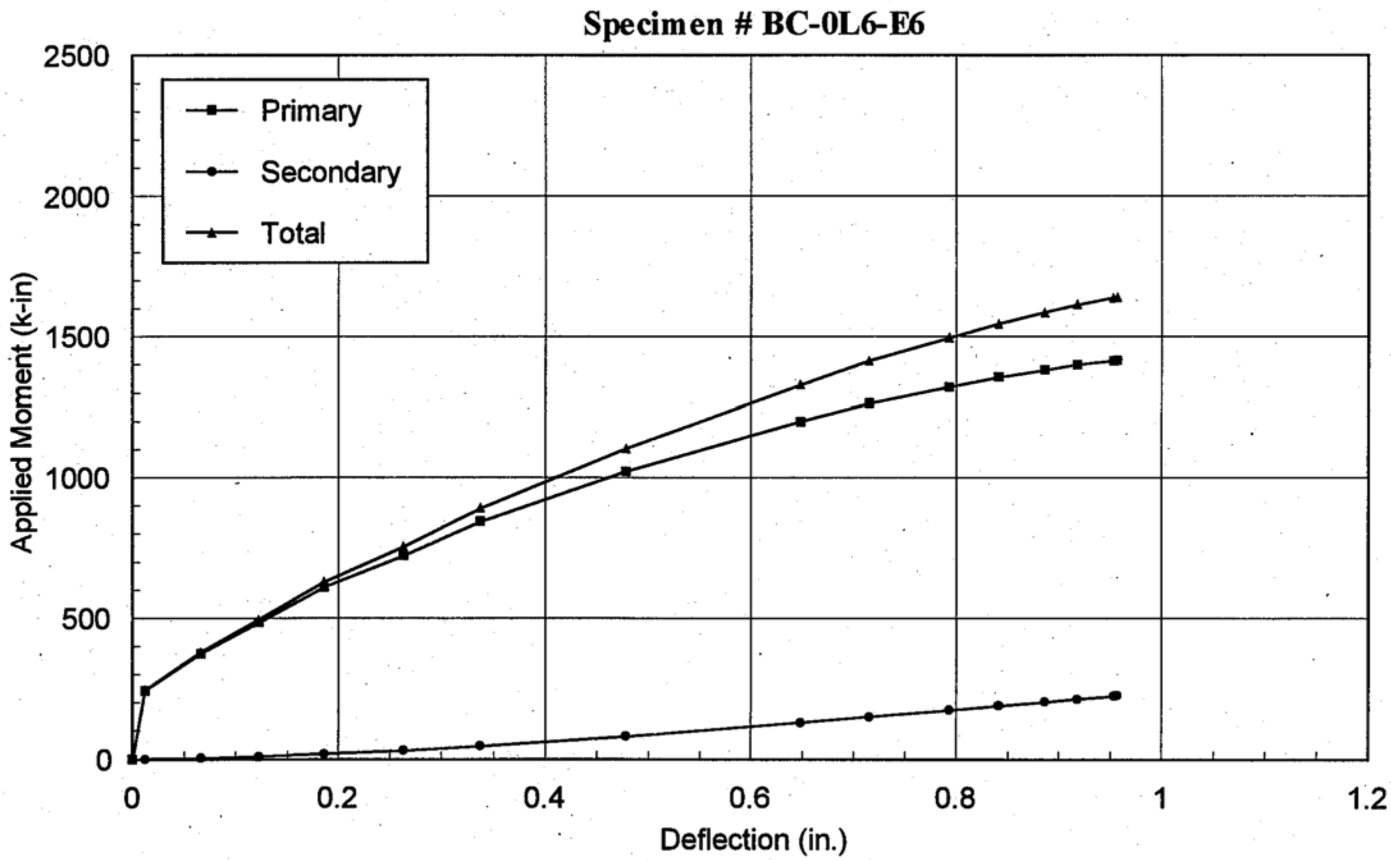

Fig 3.10b - Applied Moment vs. Center line Deflection

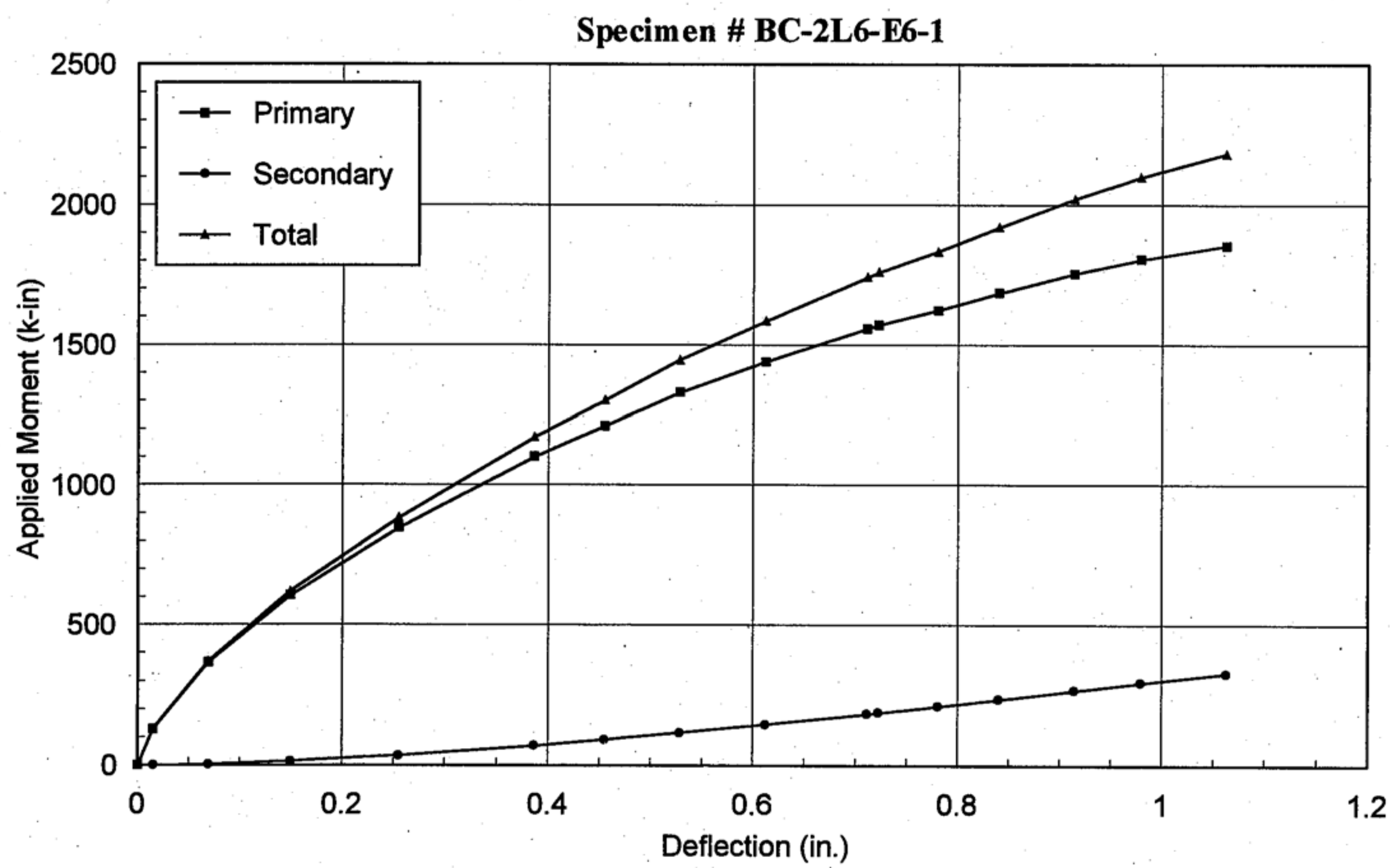

Fig. 3.10c - Applied Moment vs. Center line Deflectiont

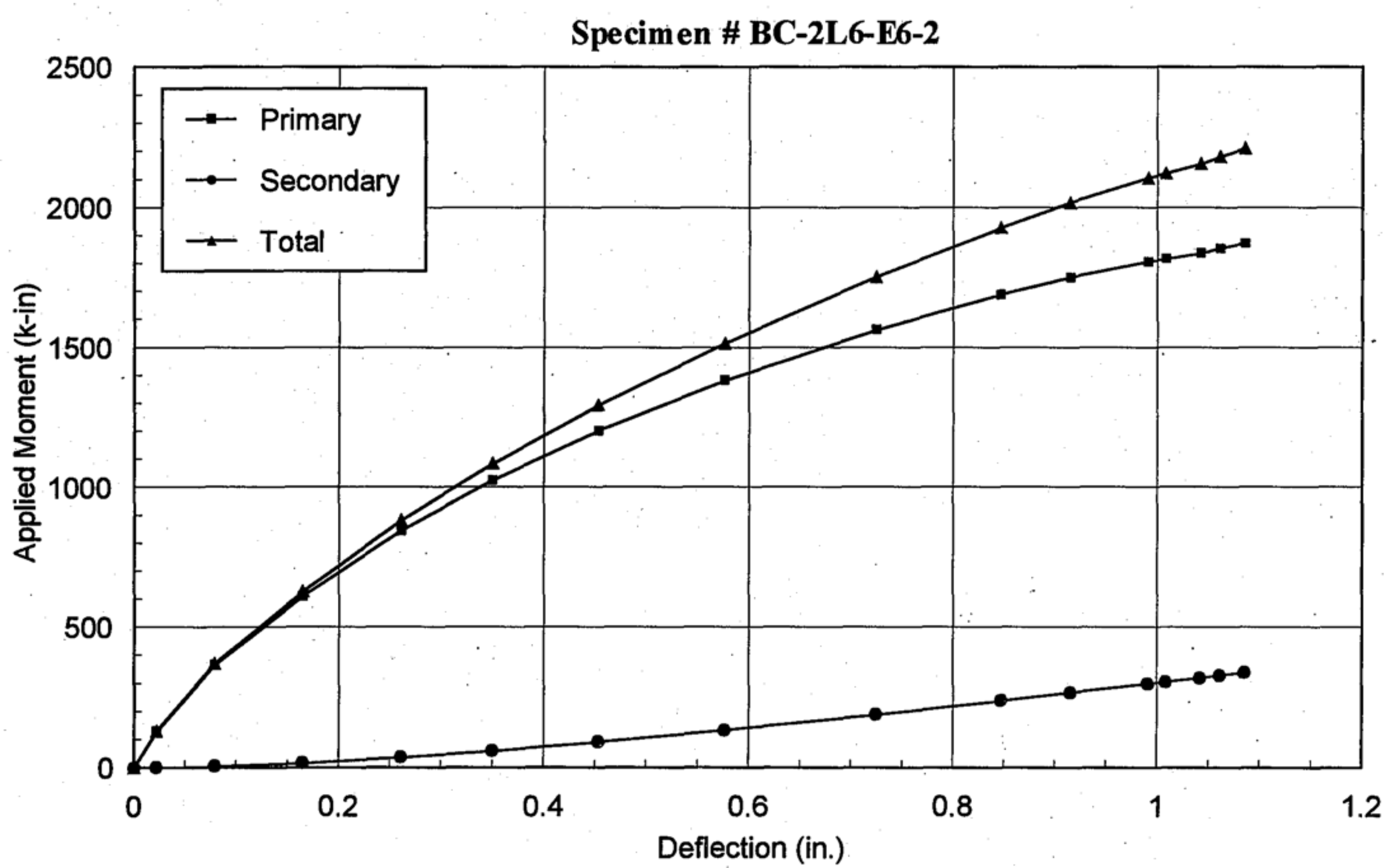

Fig. 3.11a - Centerline Strain Distribution

Specimen # BC-0L6-E6

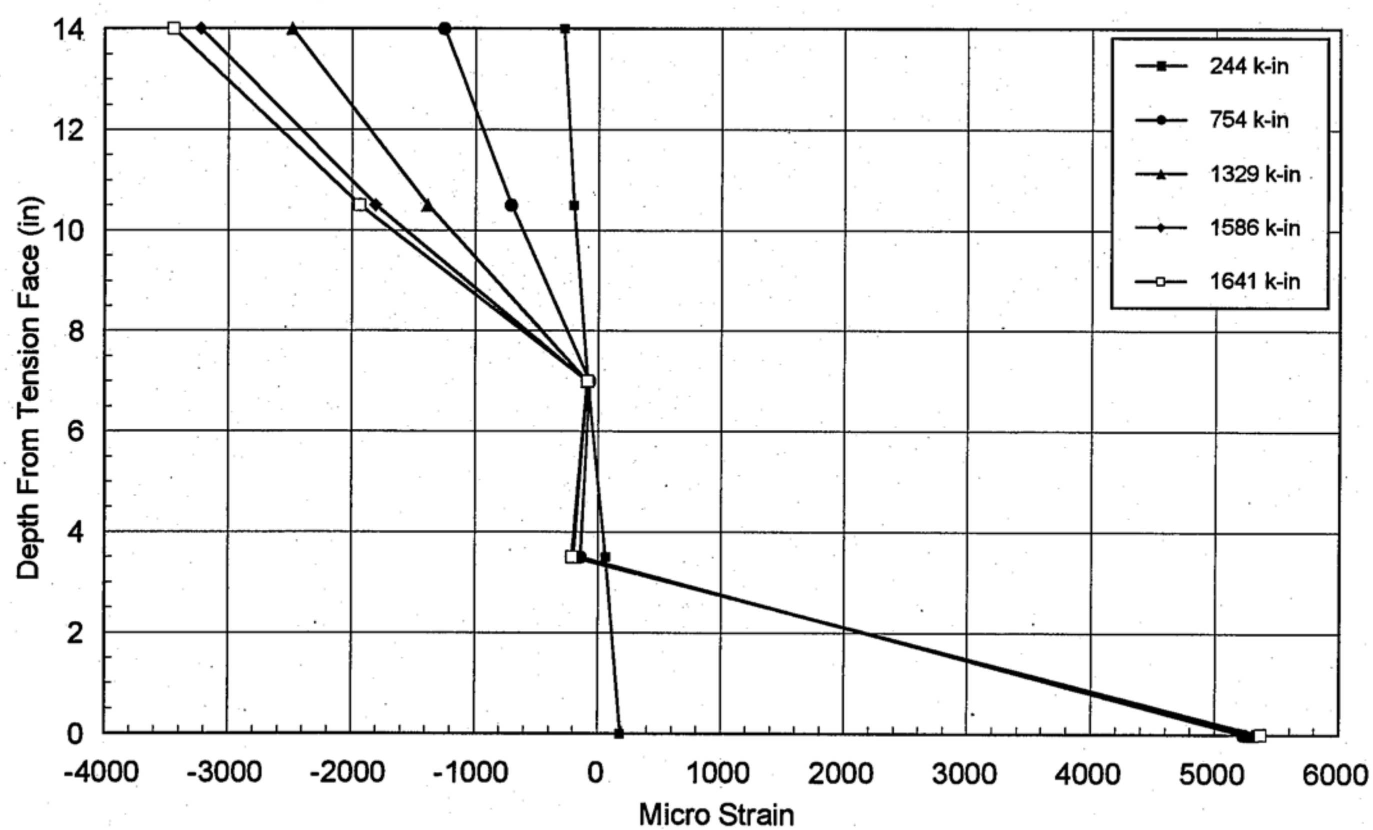

Fig. 3.11b - Centerline Strain Distribution

Specimen # BC-2L6-E6-1

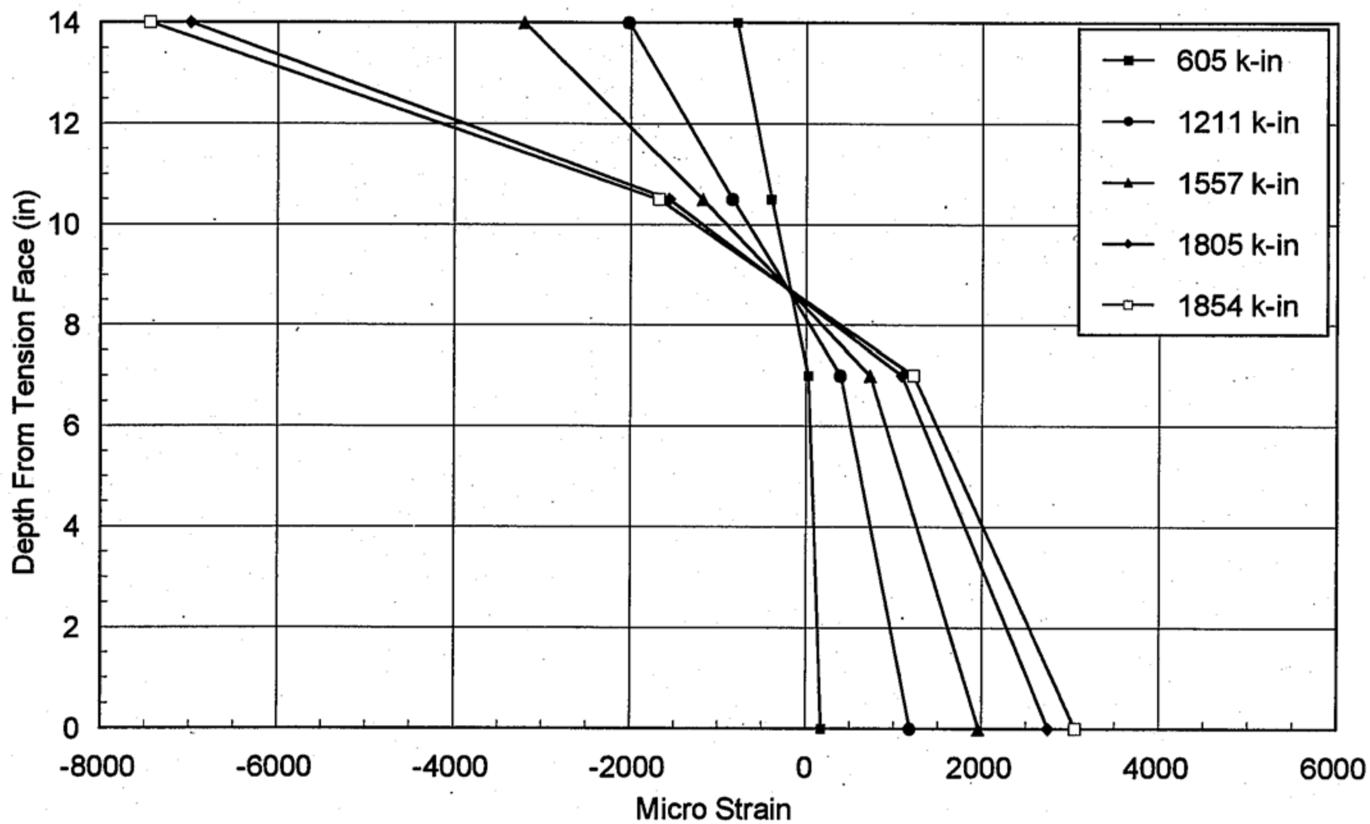

Fig. 3.11c - Centerline Strain Distribution

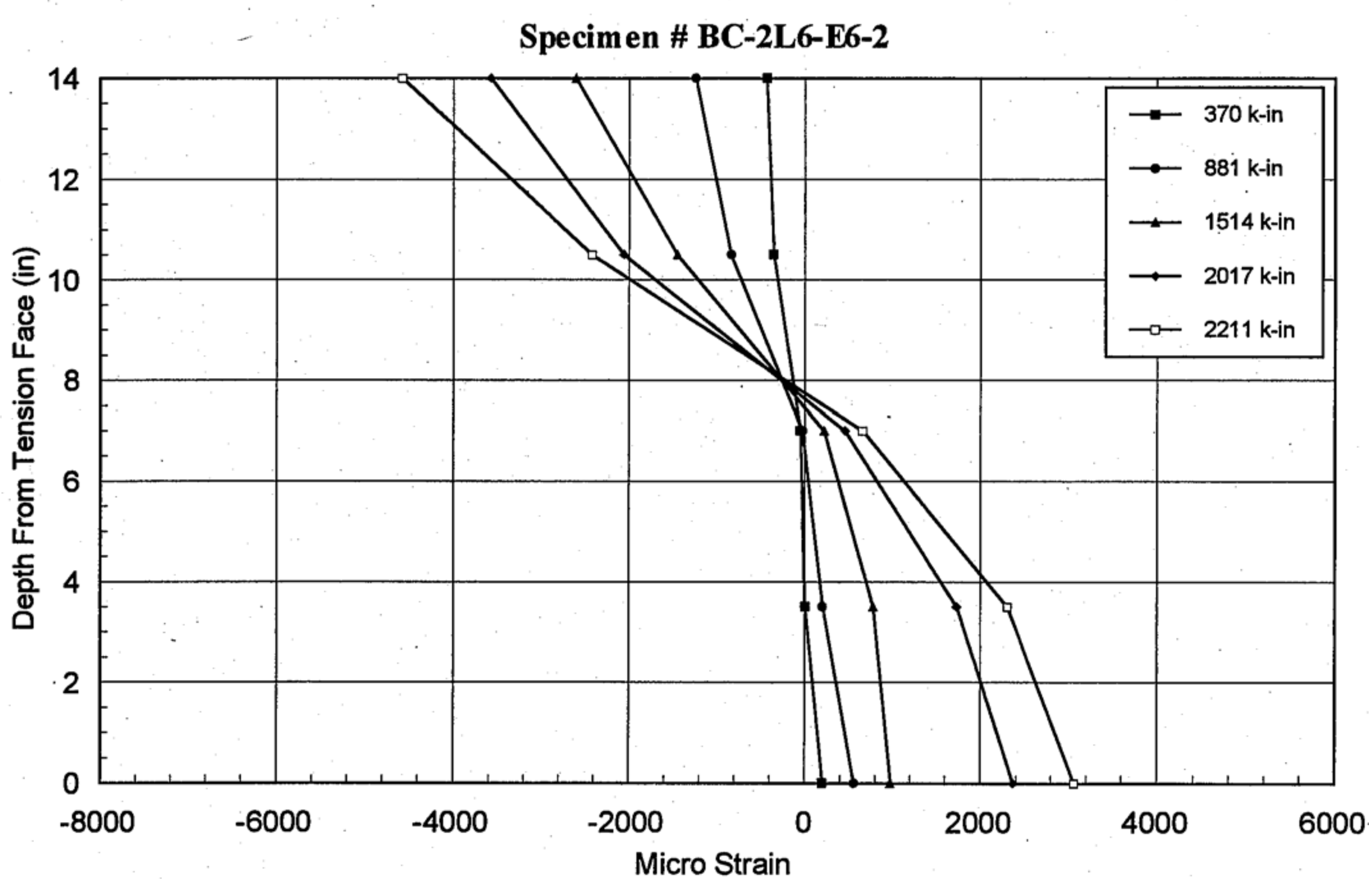

Fig. 3.12a - Longitudinal Tension Strain Distribution Along Beam Length

Specimen # BC-0L6-E6

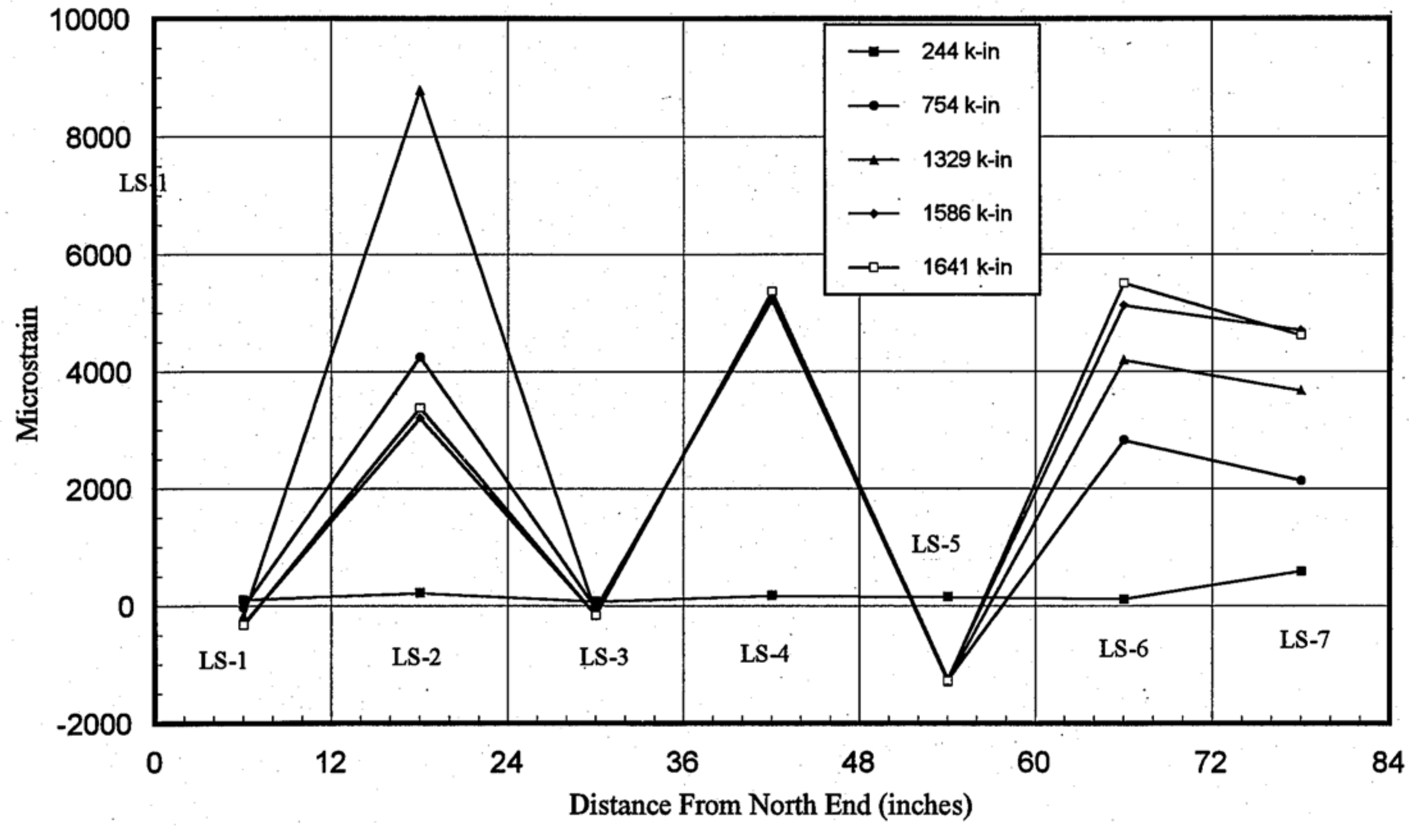

Fig. 3.12a - Longitudinal Compressive Strain Distribution Along Beam Length

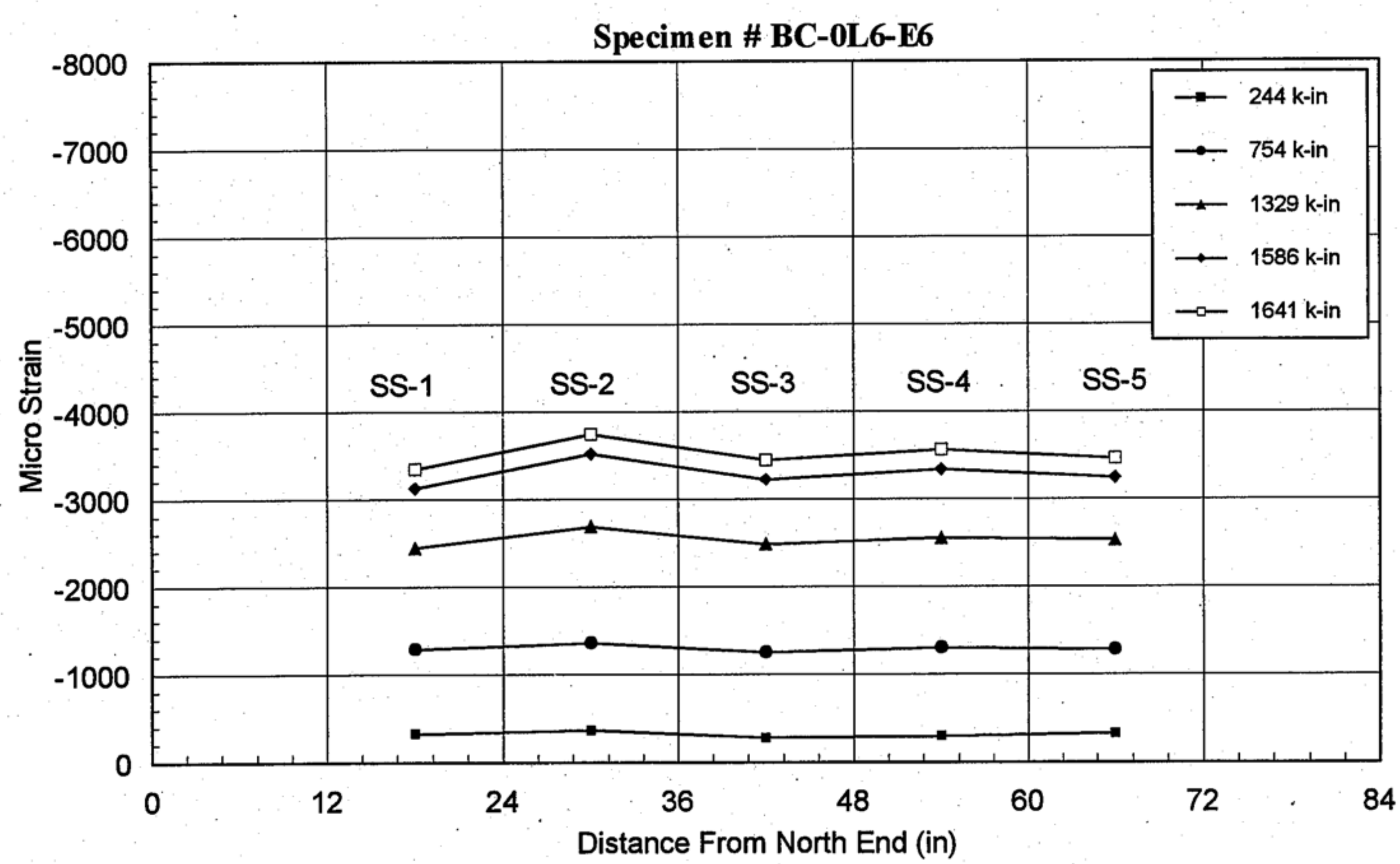

Fig. 3.12b - Longitudinal Tension Strain Distribution Along Beam Length

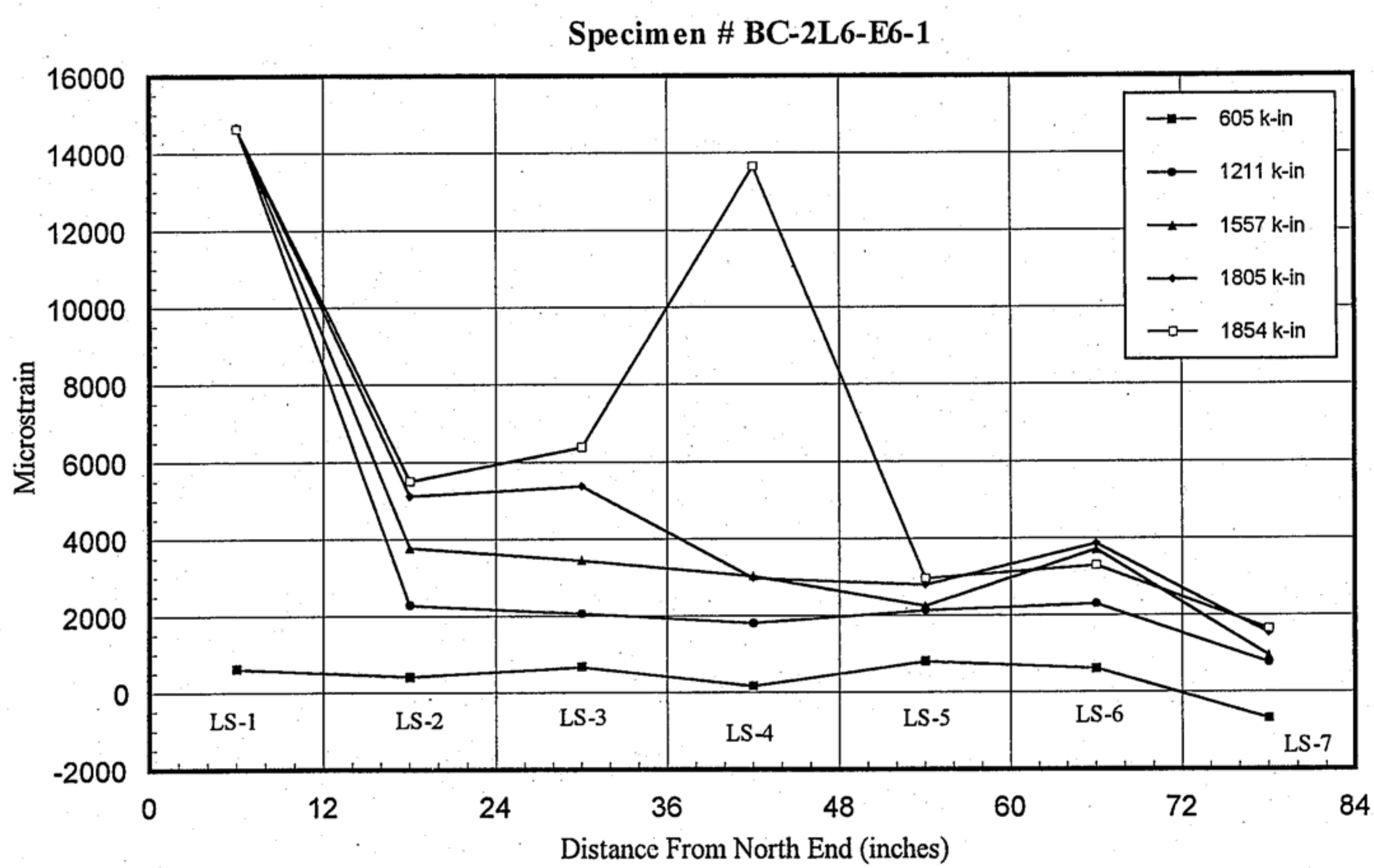

Fig. 3.12b - Longitudinal Compressive Strain Distribution Along Beam Length

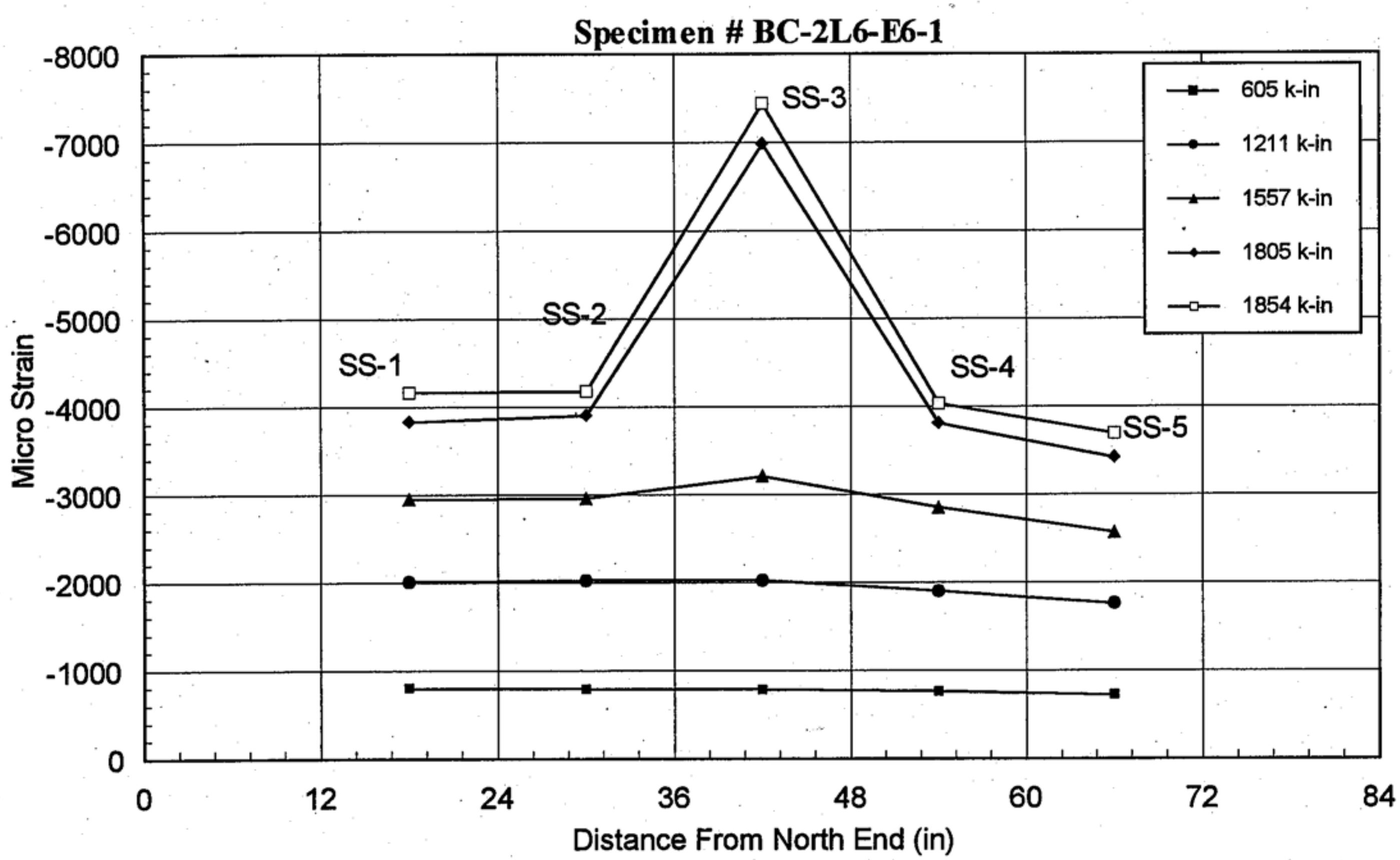

Fig. 3.12c - Longitudinal Tension Strain Distribution Along Beam Length

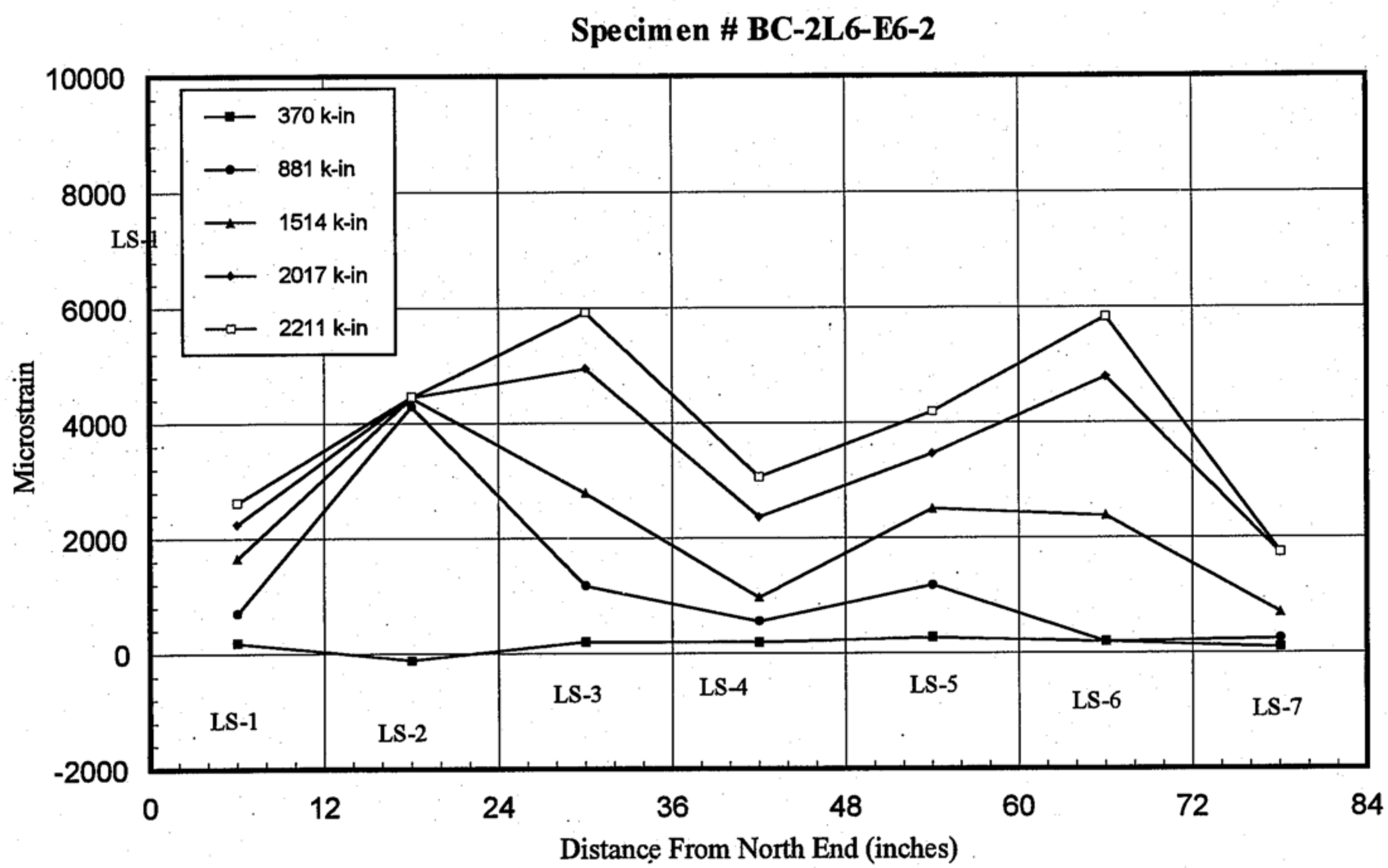

Fig. 3.12c - Longitudinal Compressive Strain Distribution Along Beam Length

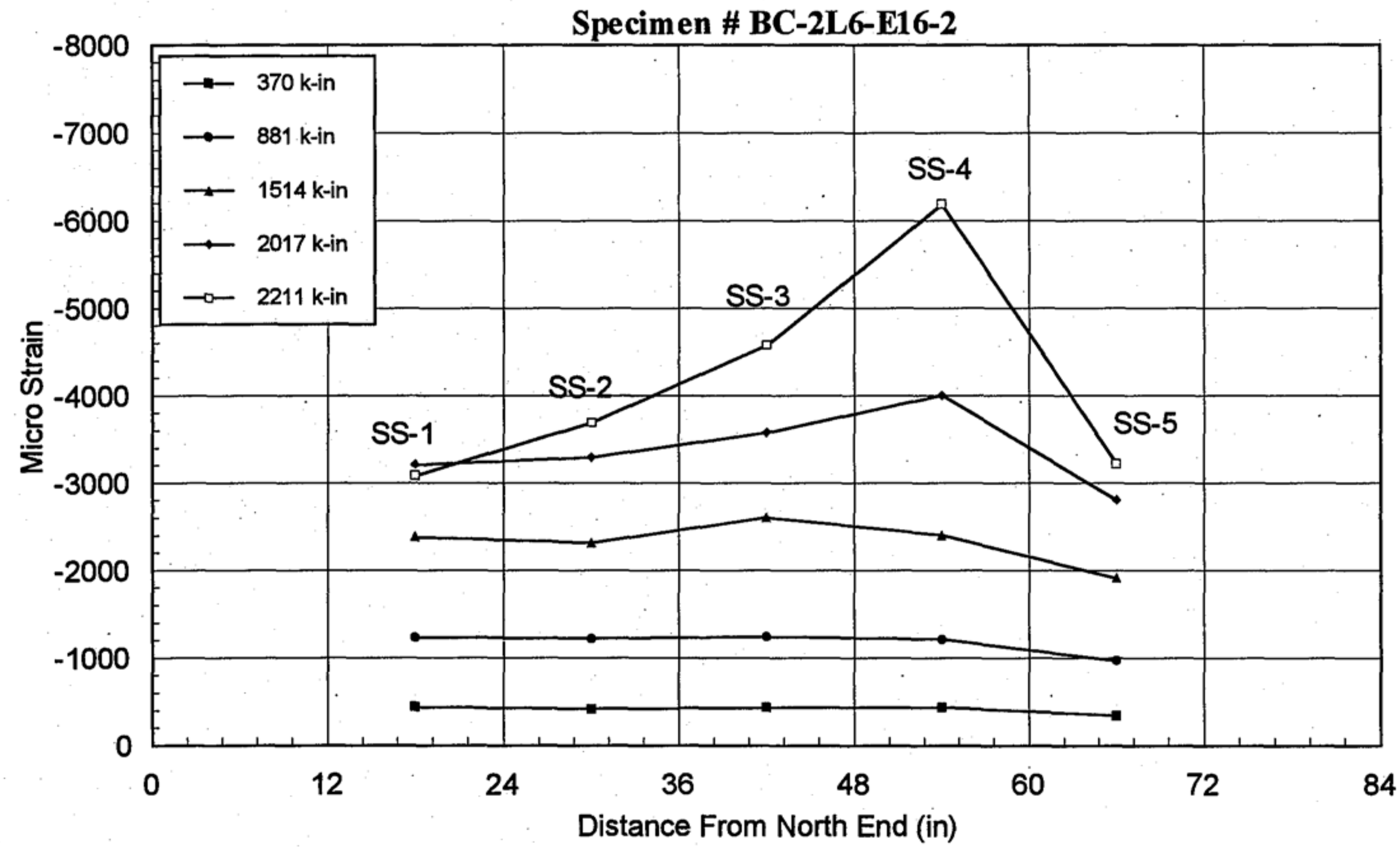

Fig. 3.13a - Moment vs. Transverse Strain At Midspan

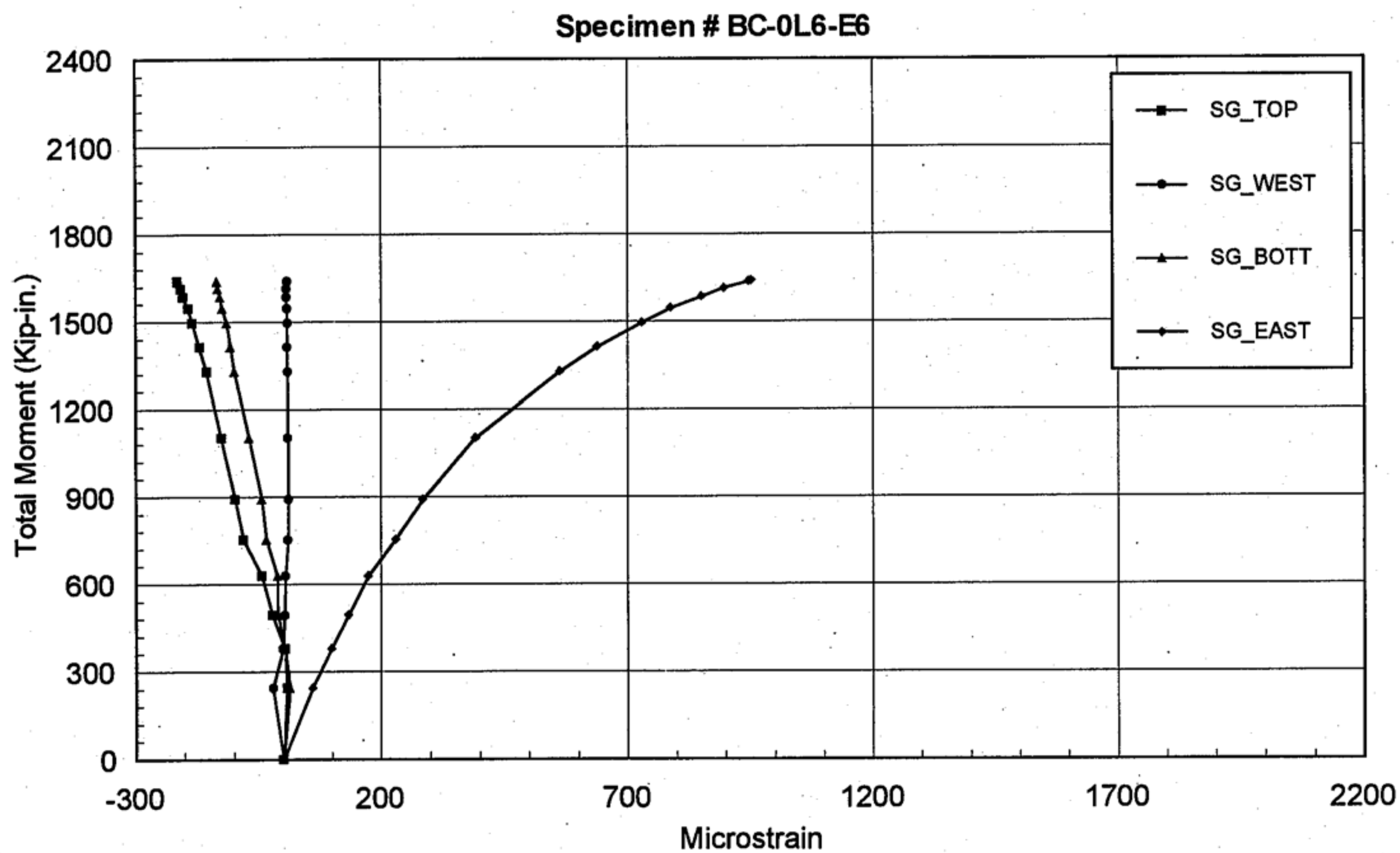

Fig. 3.13b - Moment vs. Transverse StrainAt Midspan

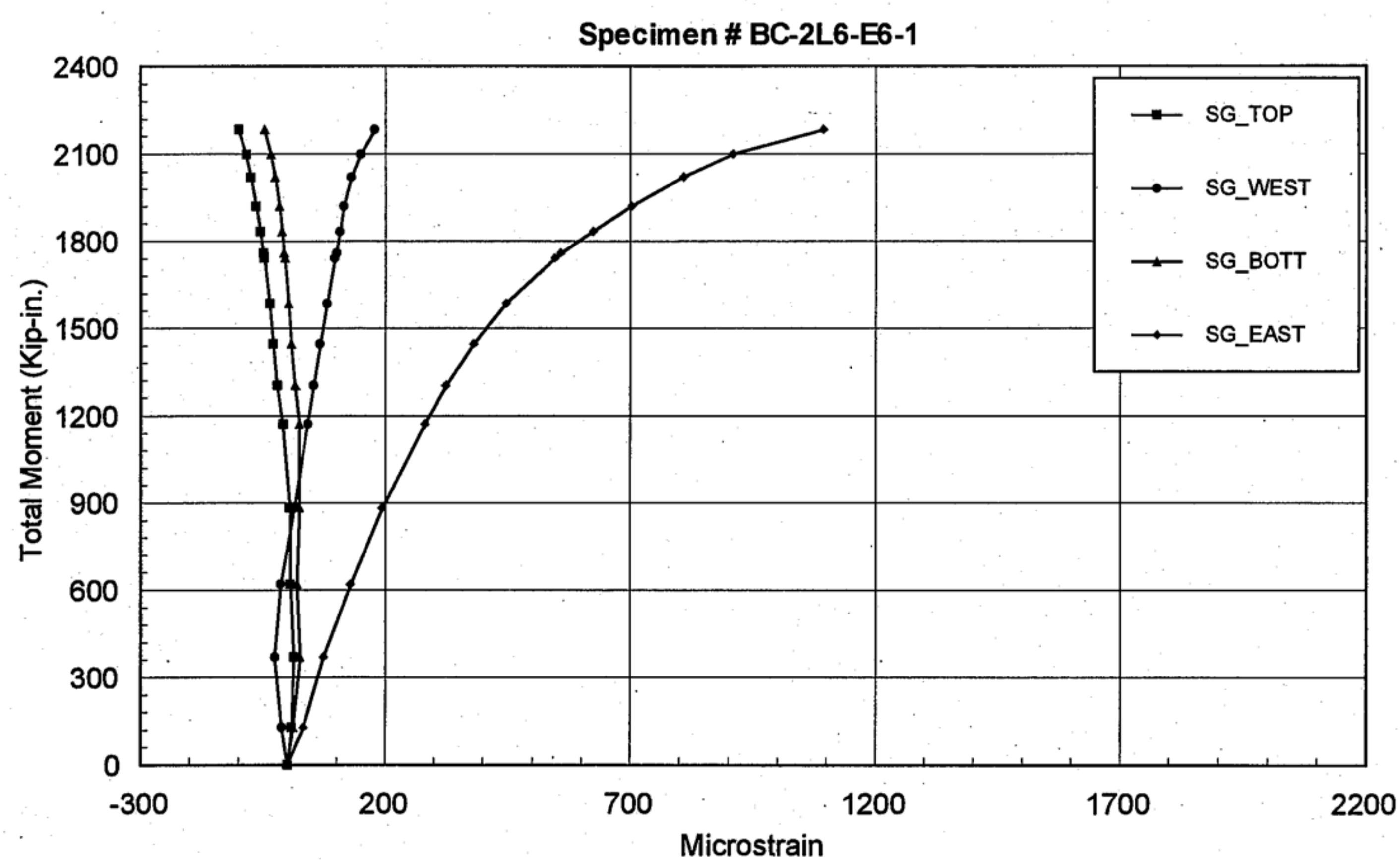

Fig. 3.13c - Moment vs. Transverse Strain At Midspan

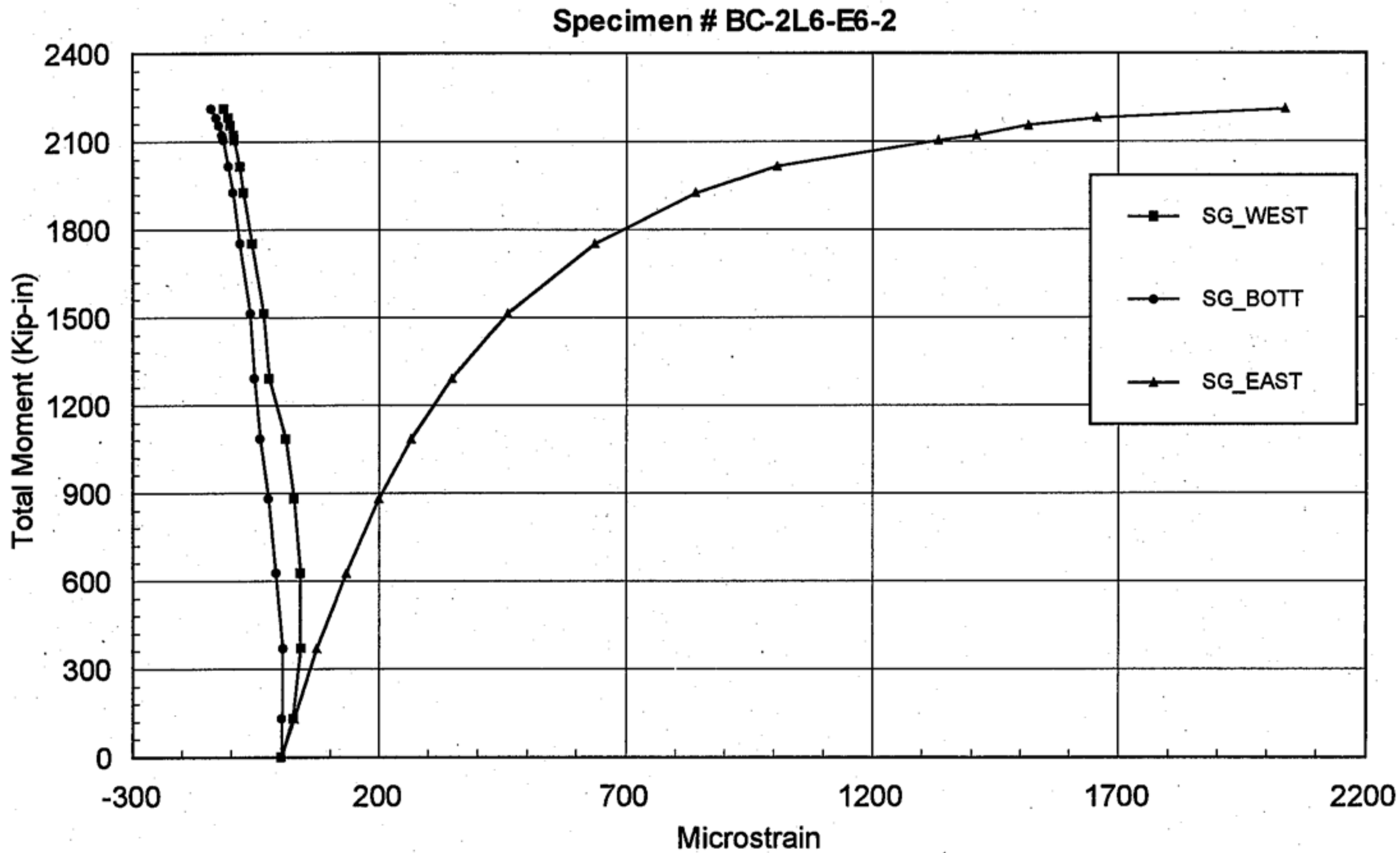

Fig 3.14a - Applied Moment vs. Center line Deflection

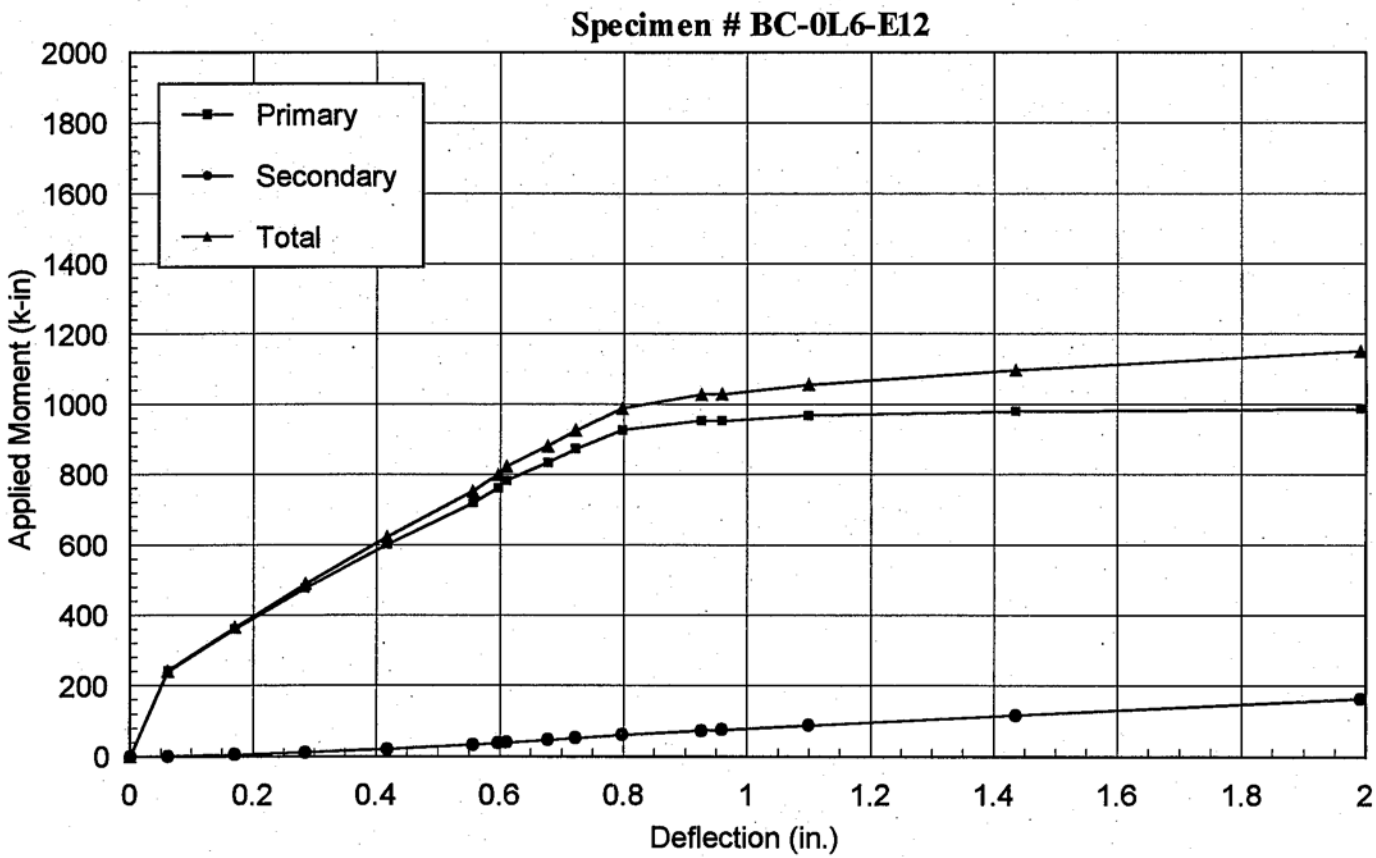

(Fig 3.14b) Applied Moment vs. Deflection At Center line

Specimen # BC-2L6-E12-1

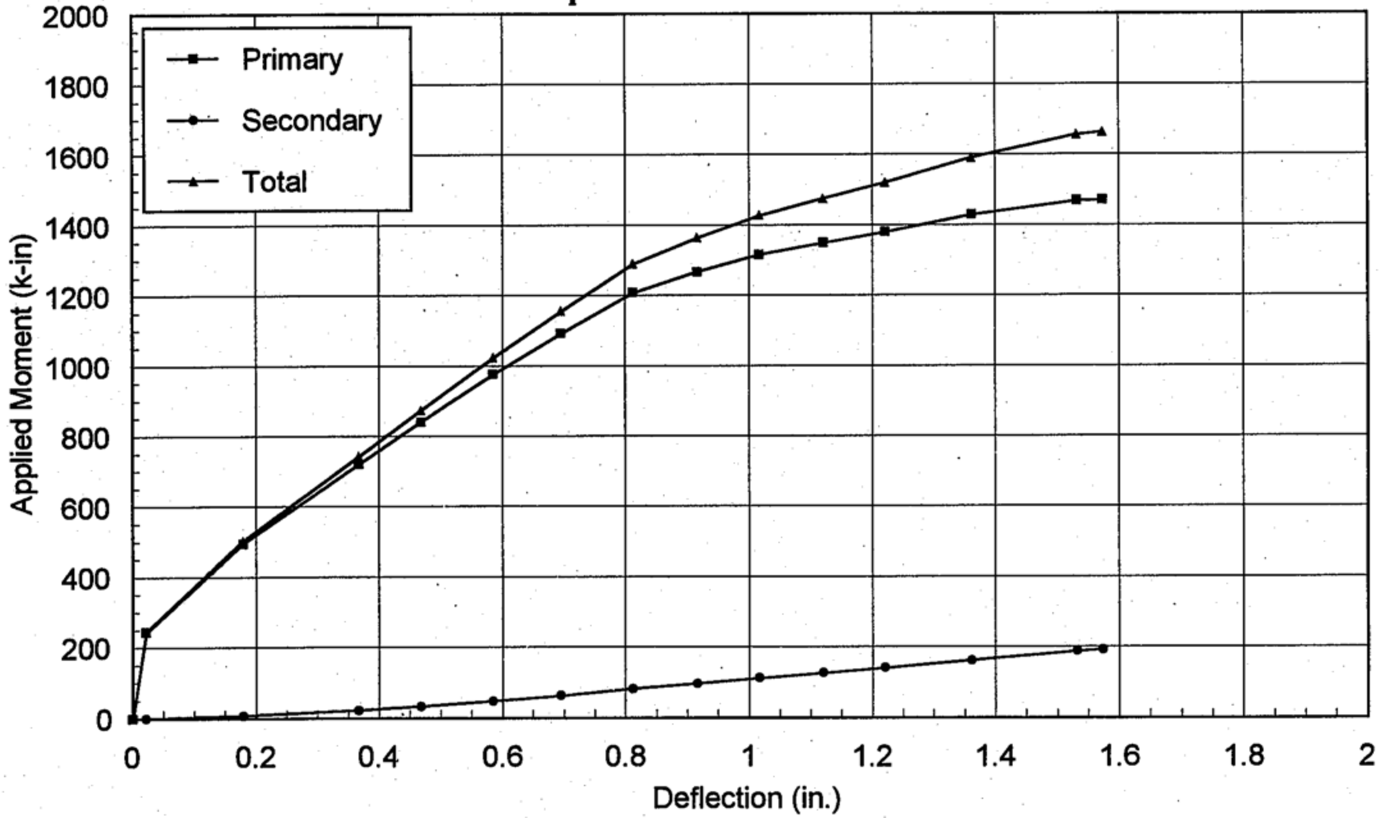

Fig 3.14c - Applied Moment vs. Center line Deflection

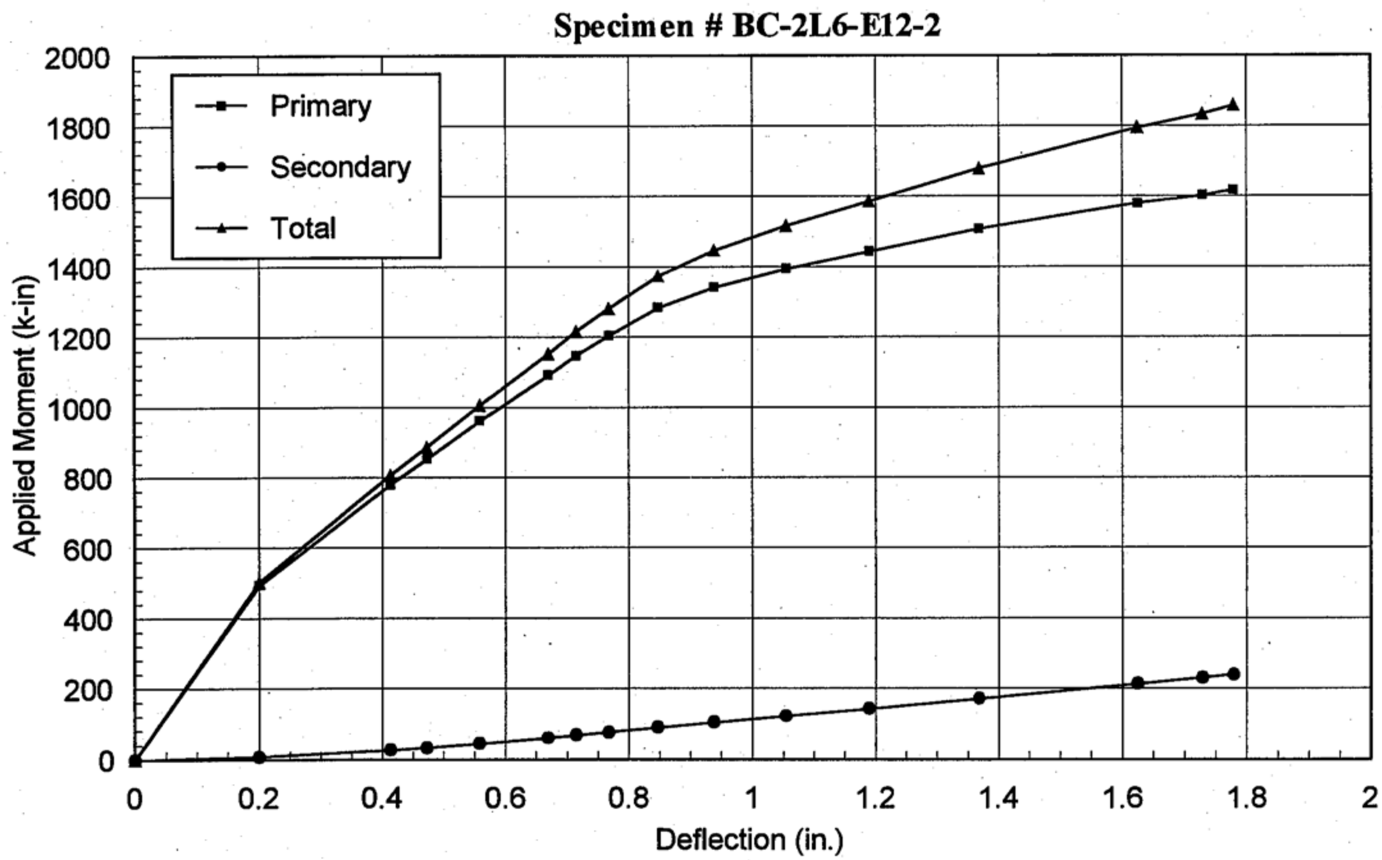

Fig. 3.15a - Centerline Strain Distribution

Specimen # BC-0L6-E12

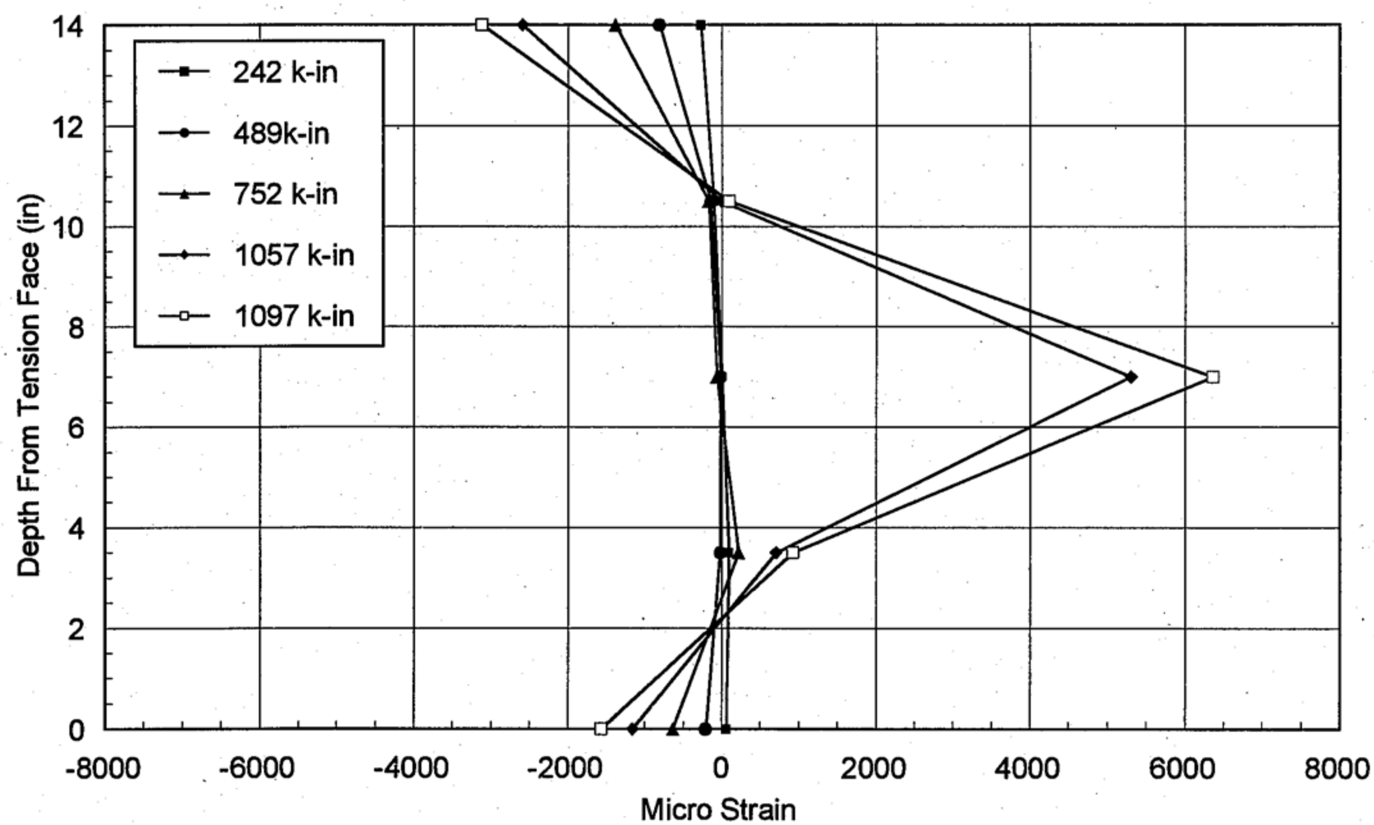

(Fig. 3.15b) Centerline Strain Distribution

Specimen # BC-2L6-E12-1

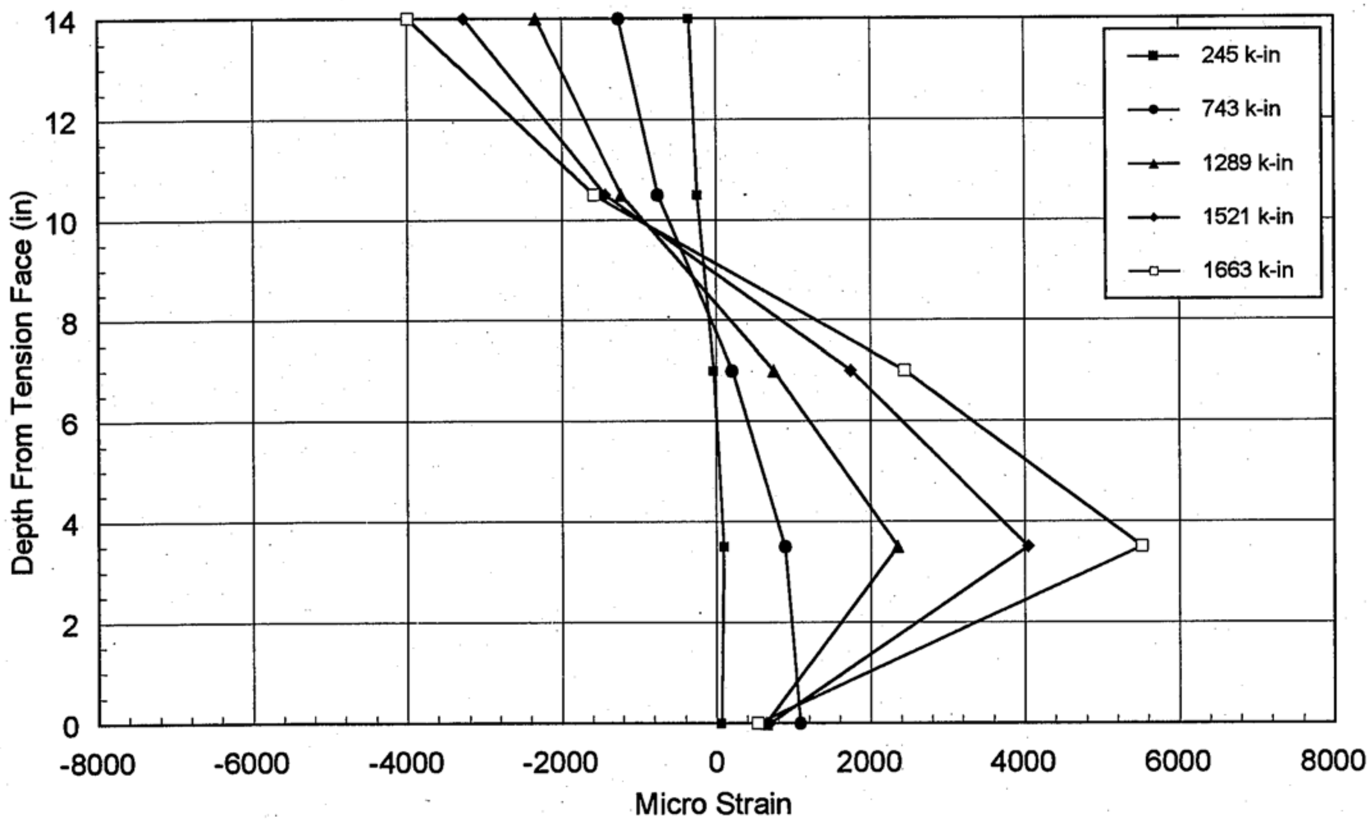

Fig. 3.15c - Centerline Strain Distribution

Specimen # BC-2L6-E12-2

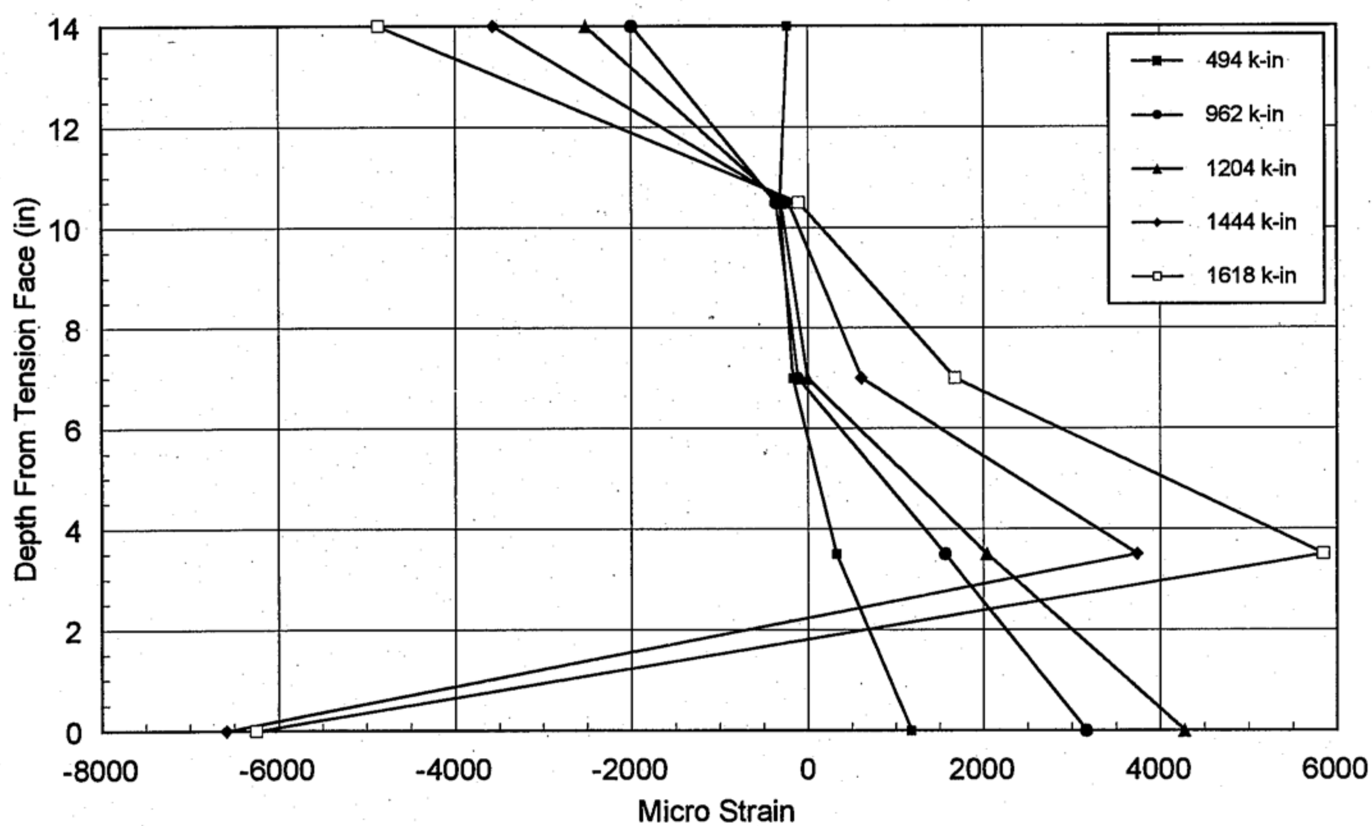

Fig. 3.16a - Longitudinal Tension Strain Distribution Along Beam Length

Specimen # BC-0L6-E12

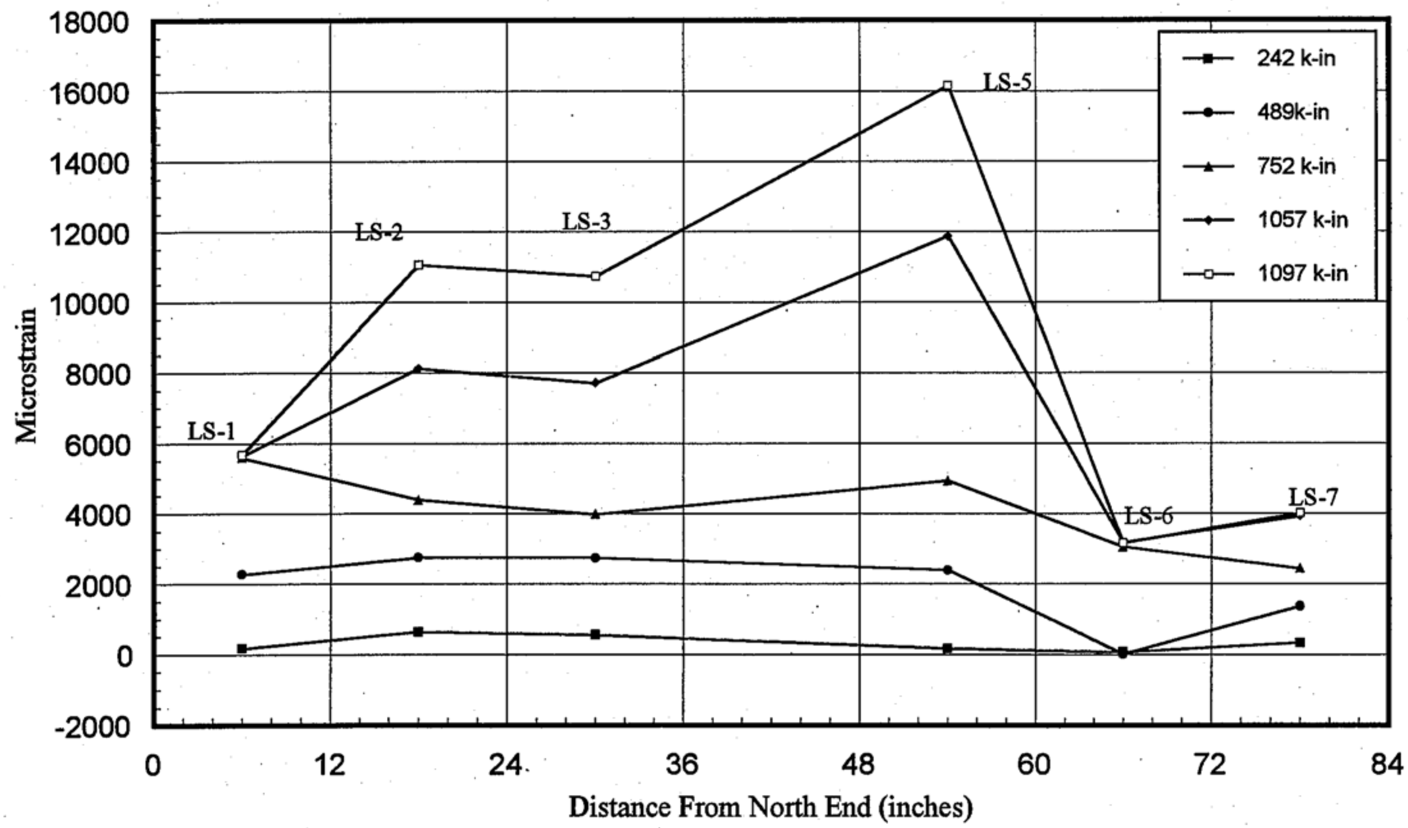

Fig. 3.16a - Longitudinal Compressive Strain Distribution Along Beam Length

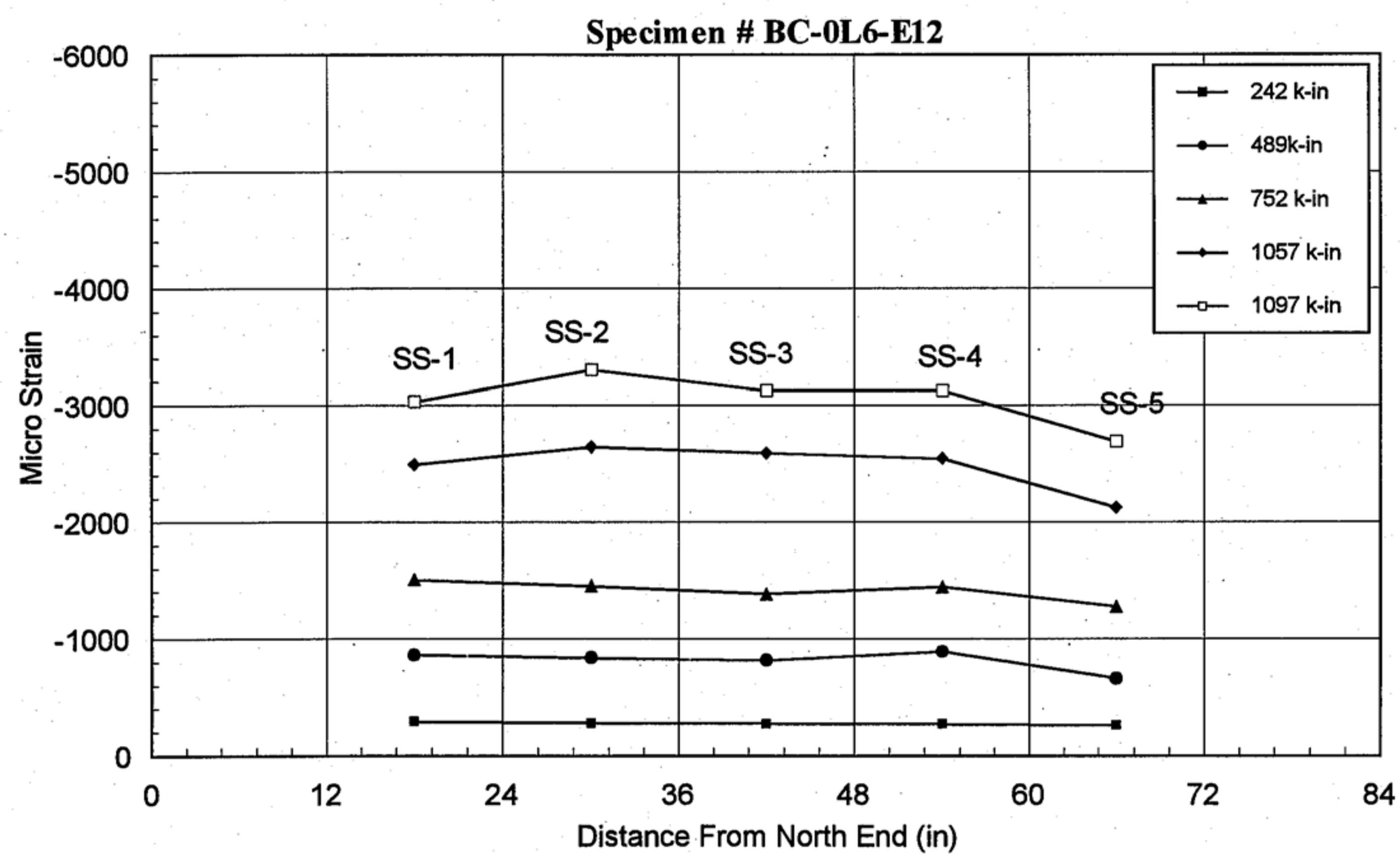

Fig. 3.16b - Longitudinal Tension Strain Distribution Along Beam Length

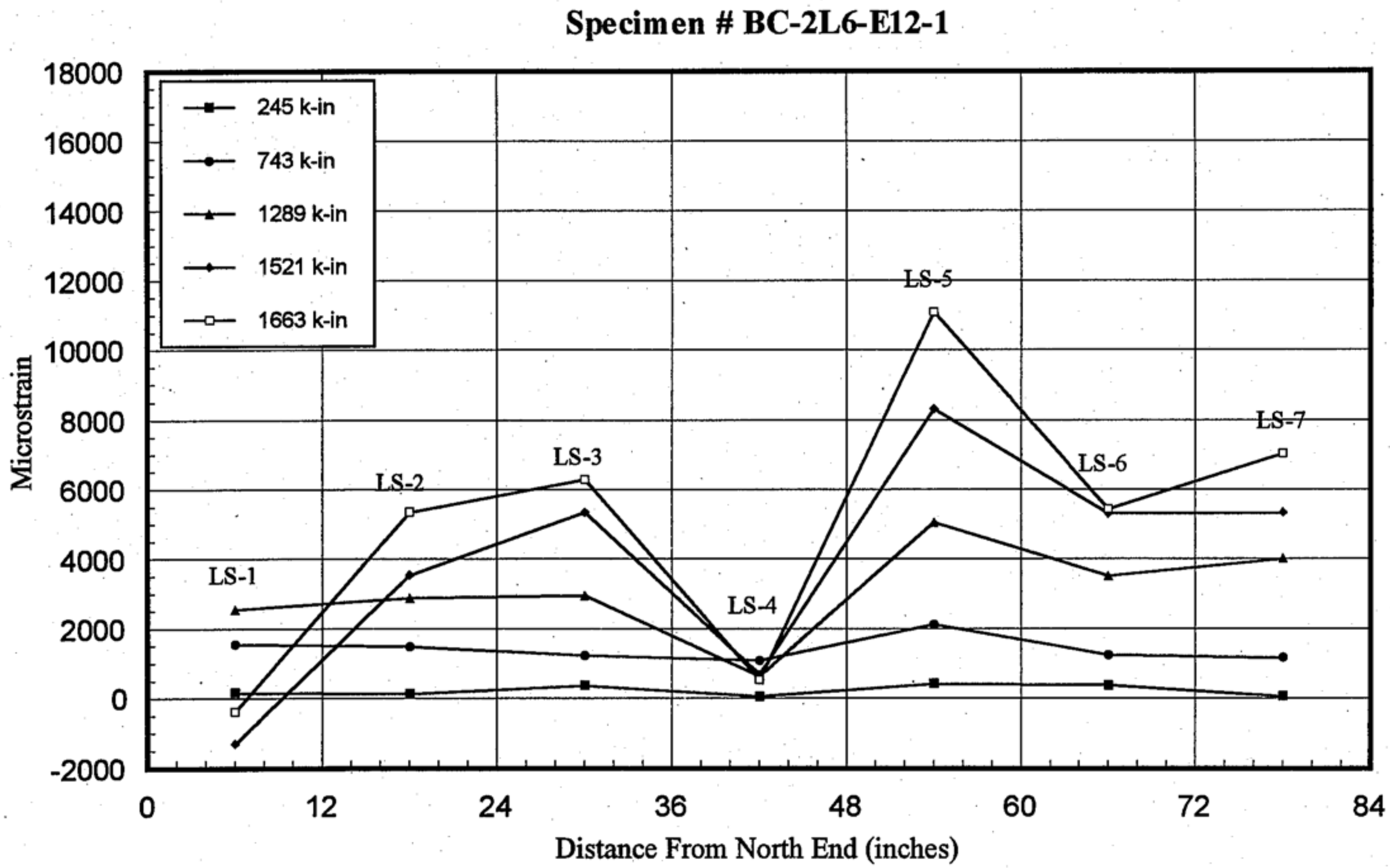

Fig. 3.16b - Longitudinal Compressive Strain Distribution Along Beam Length

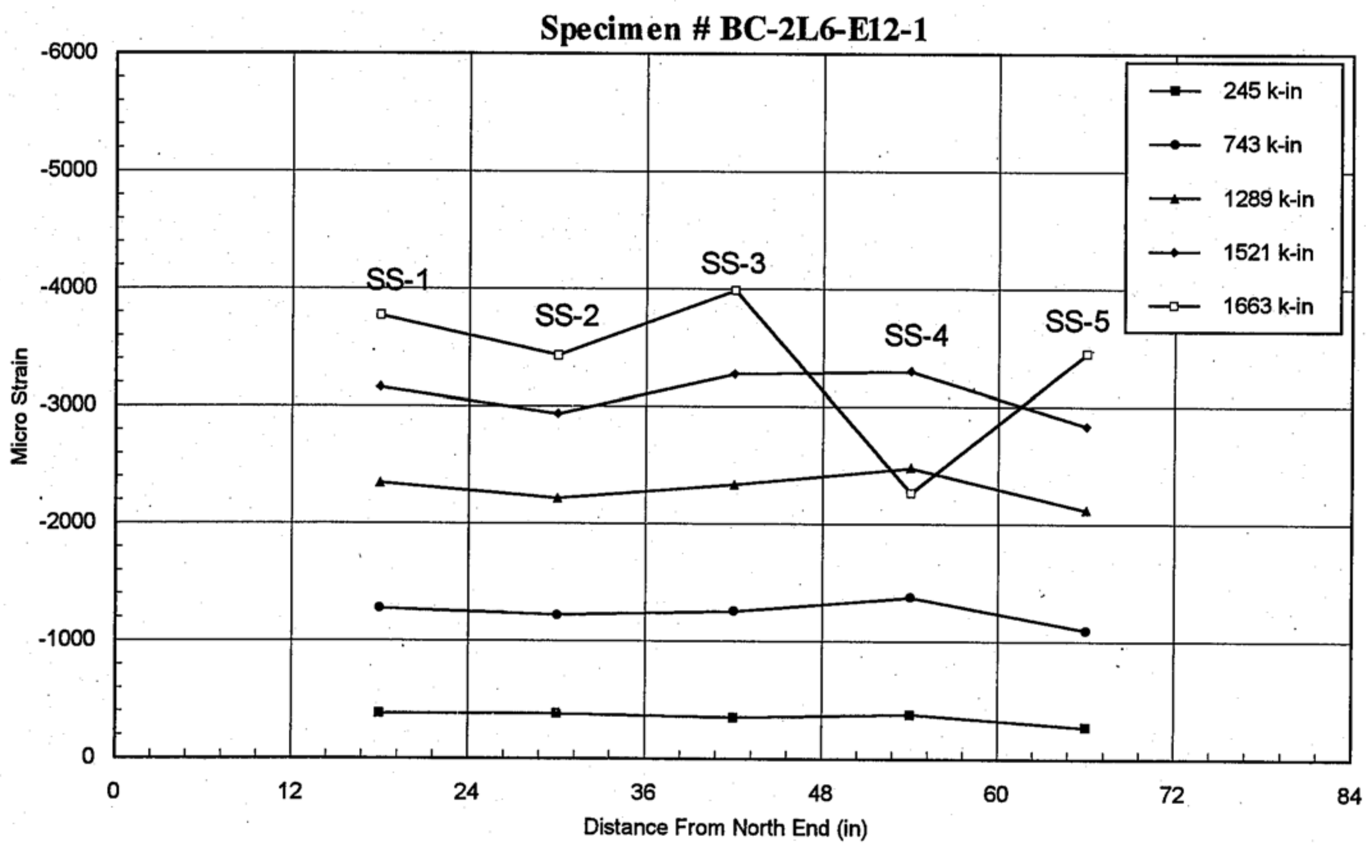

(Fig. 3.16c) Longitudinal Tension Strain Distribution Along Beam Length

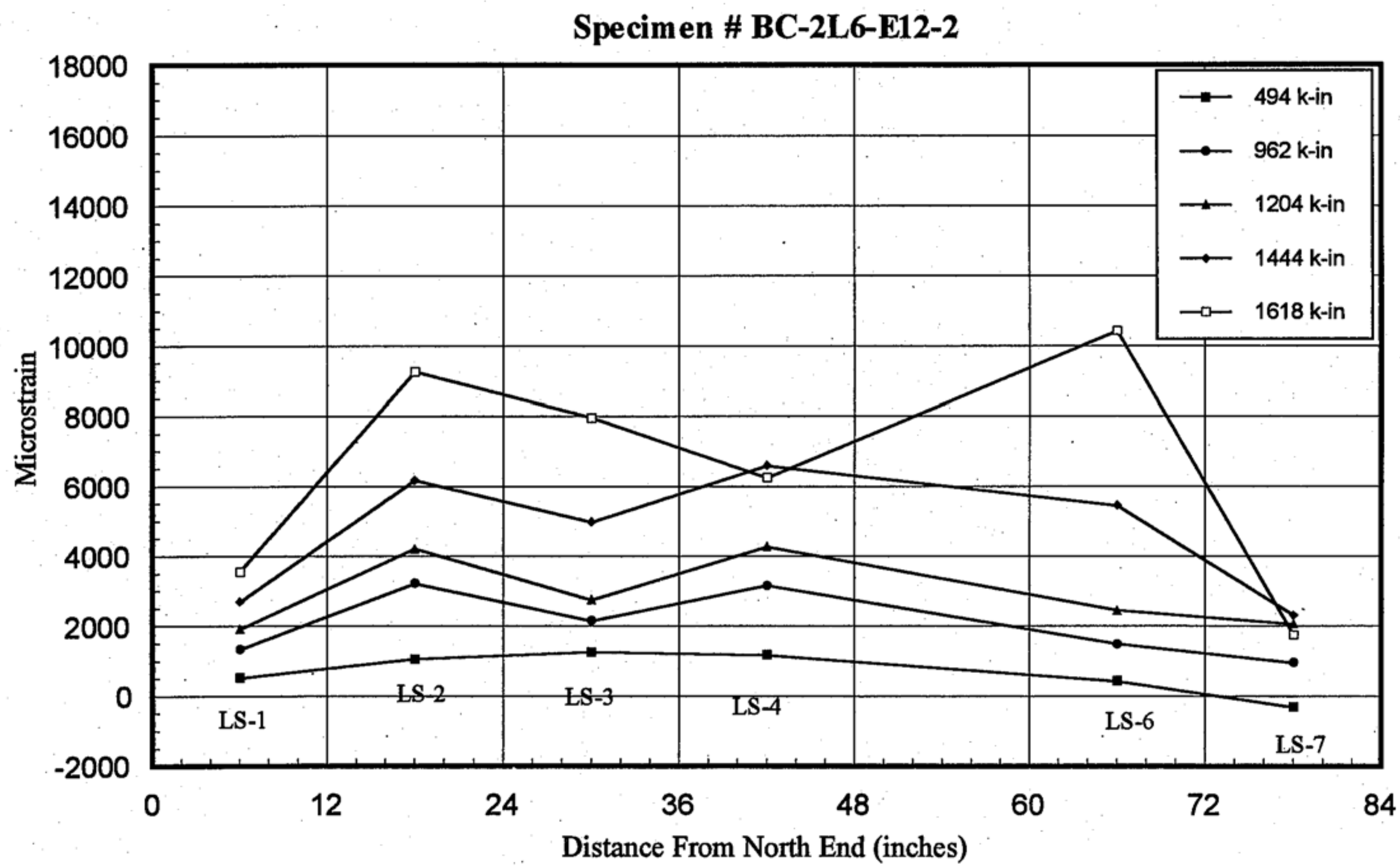

Fig. 3.16c - Longitudinal Compressive Strain Distribution Along Beam Length

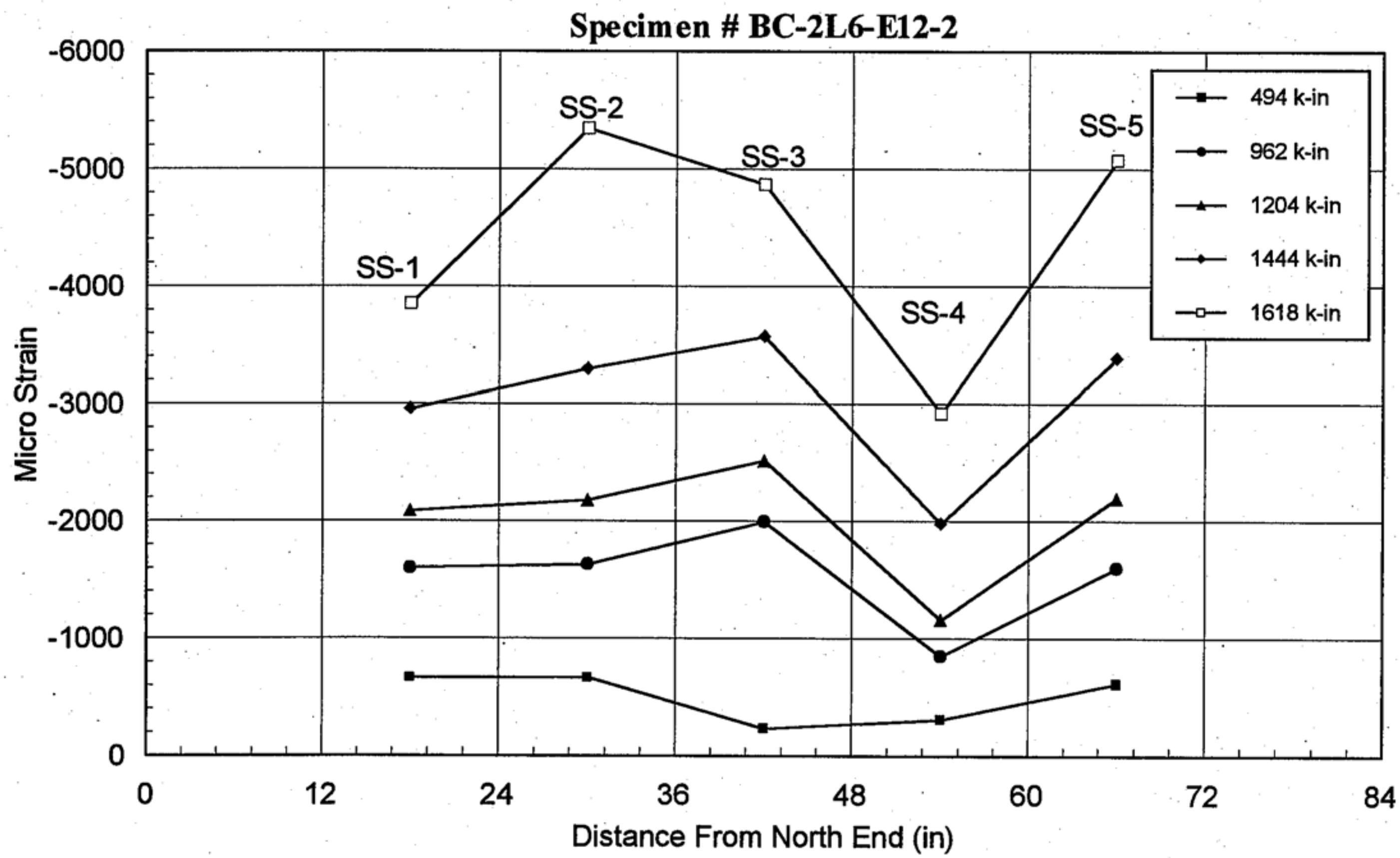

Fig. 3.17a - Moment vs. Transverse StrainAt Midspan

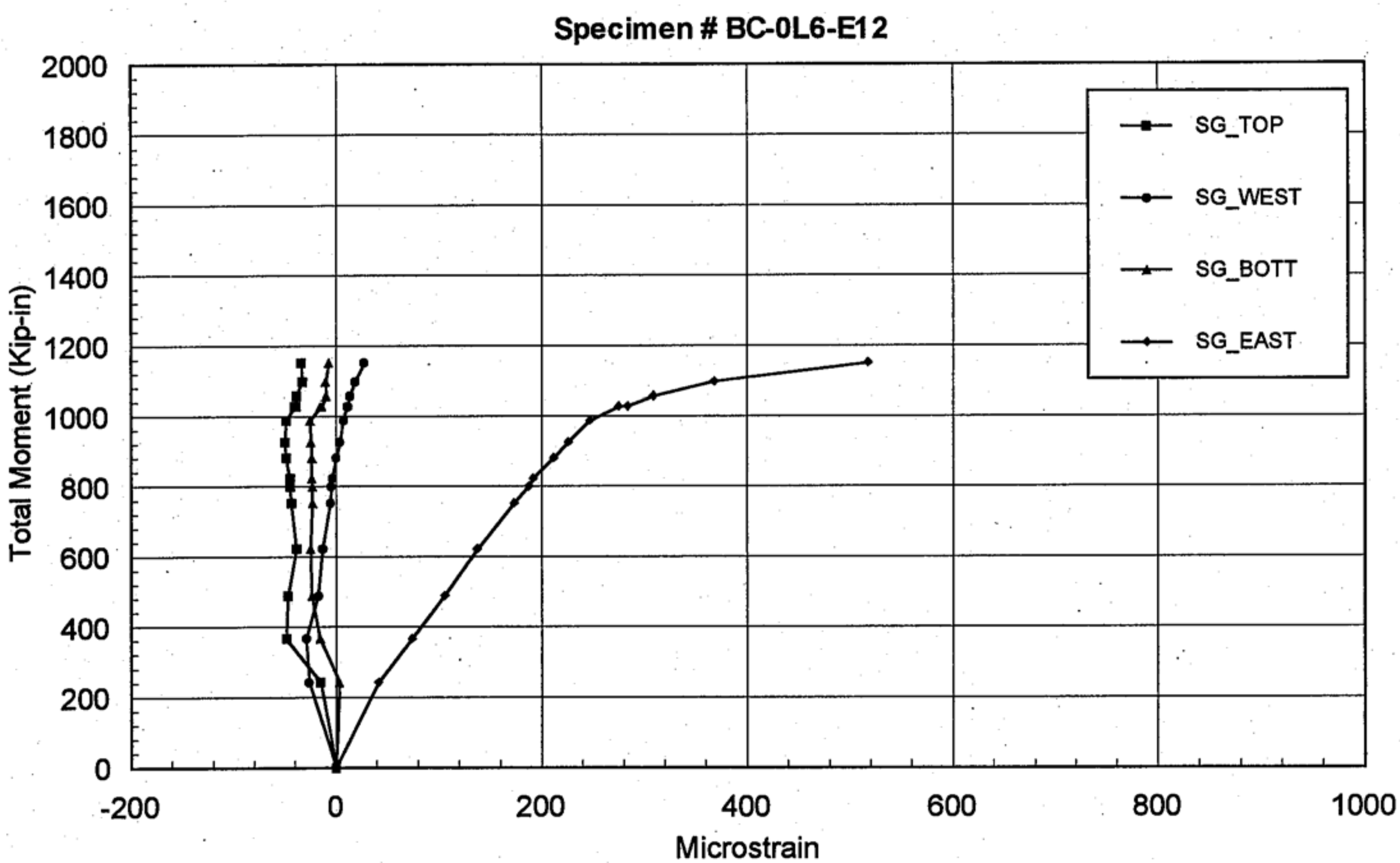

Fig. 3.17b - Moment vs. Transvers Strain At Midspan

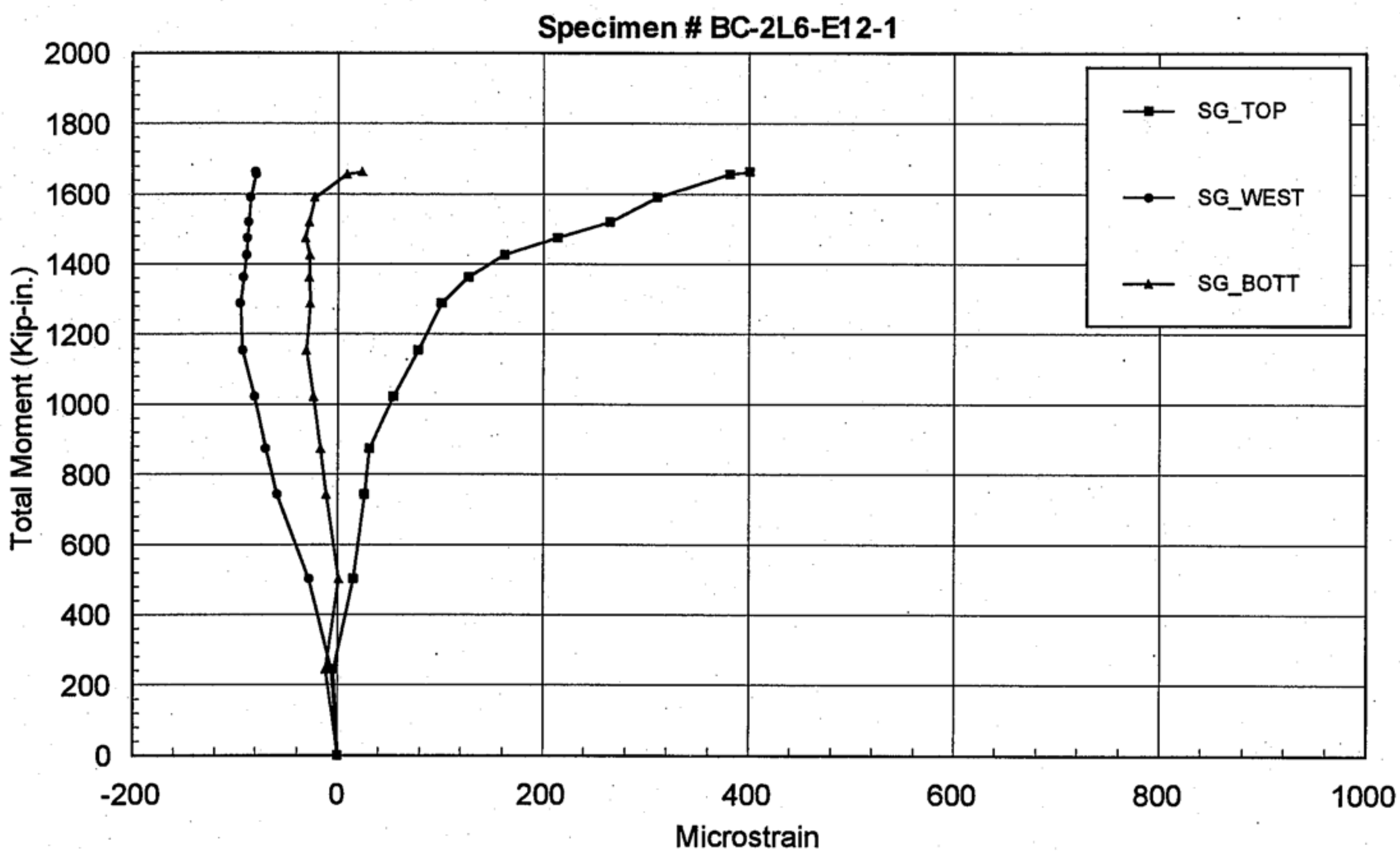

Fig. 3.17c - Moment vs. Transverse Strain At Midspan

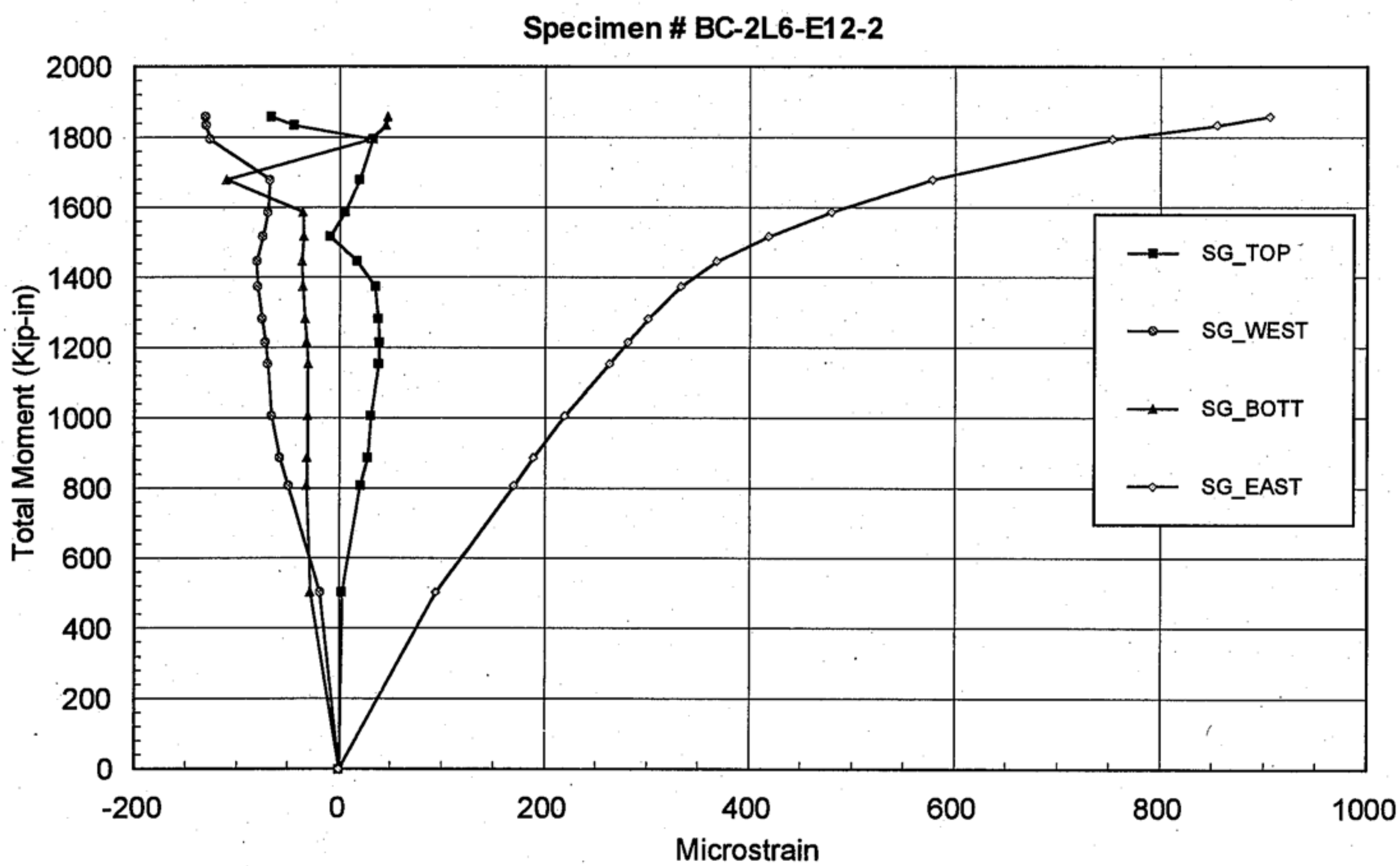

Fig 3.18a - Applied Moment vs. Center line Deflection

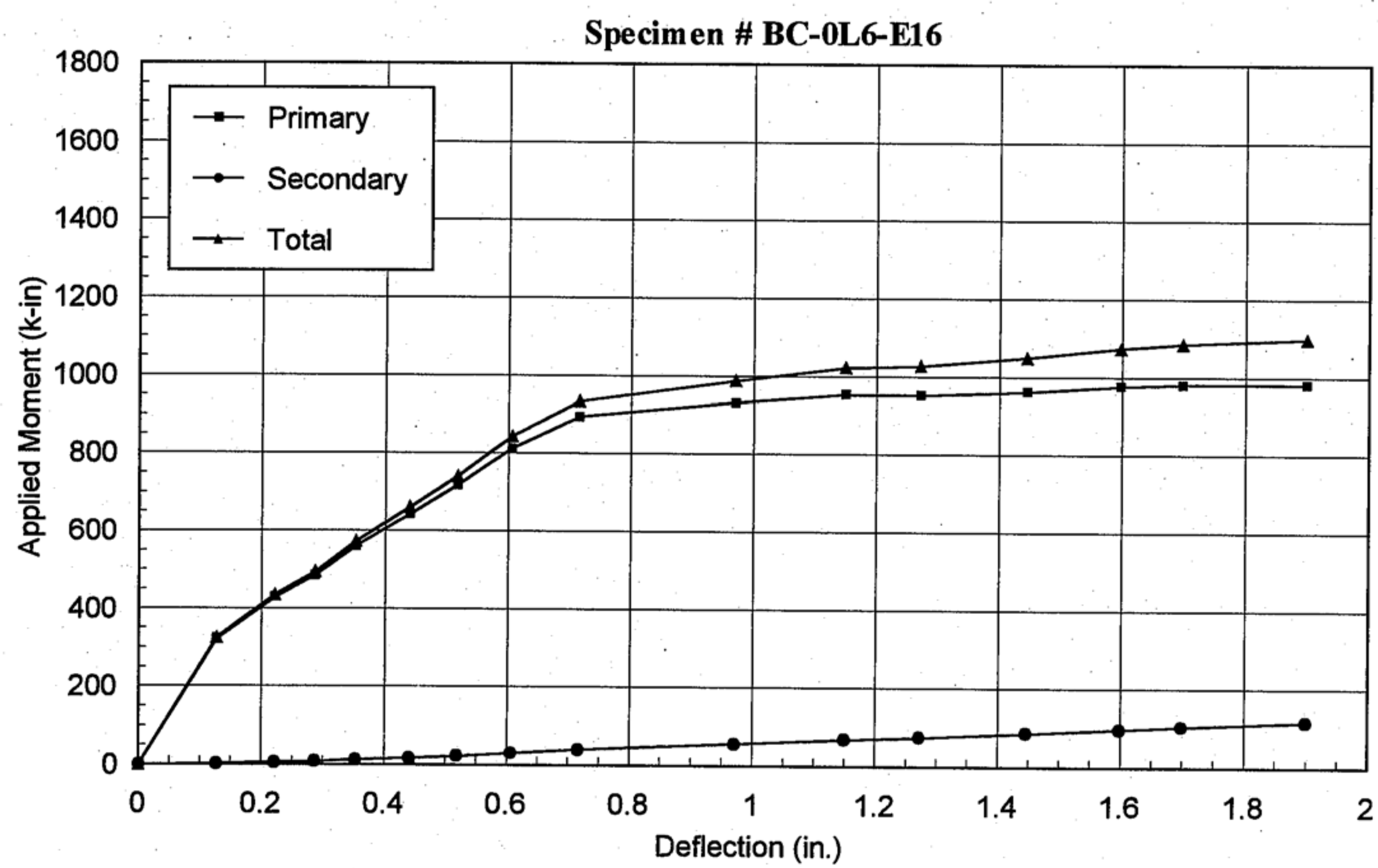

Fig 3.18b - Applied Moment vs. Center line Deflection

Specimen # BC-2L6-E16-1

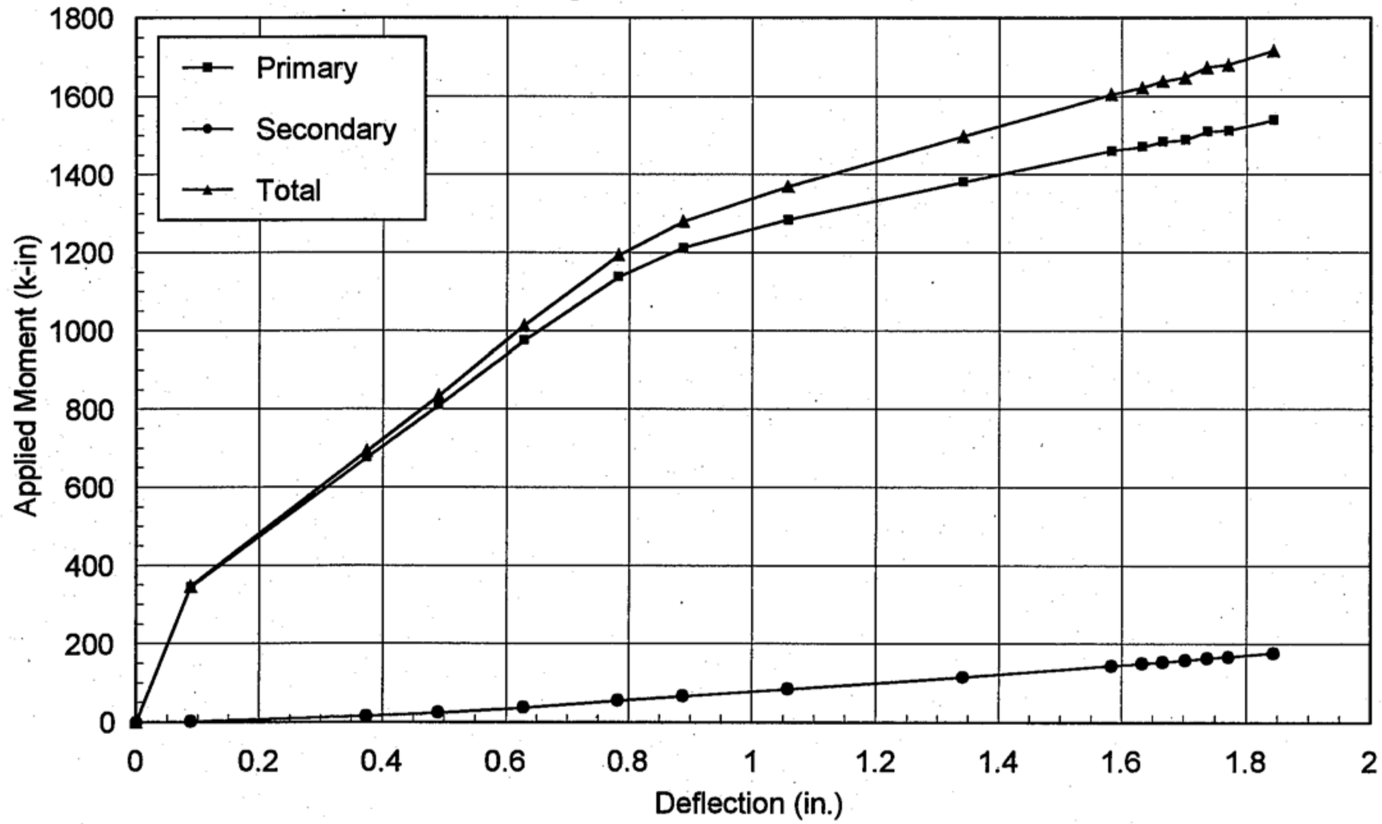

Fig 3.18c - Moment vs. Center line Deflection

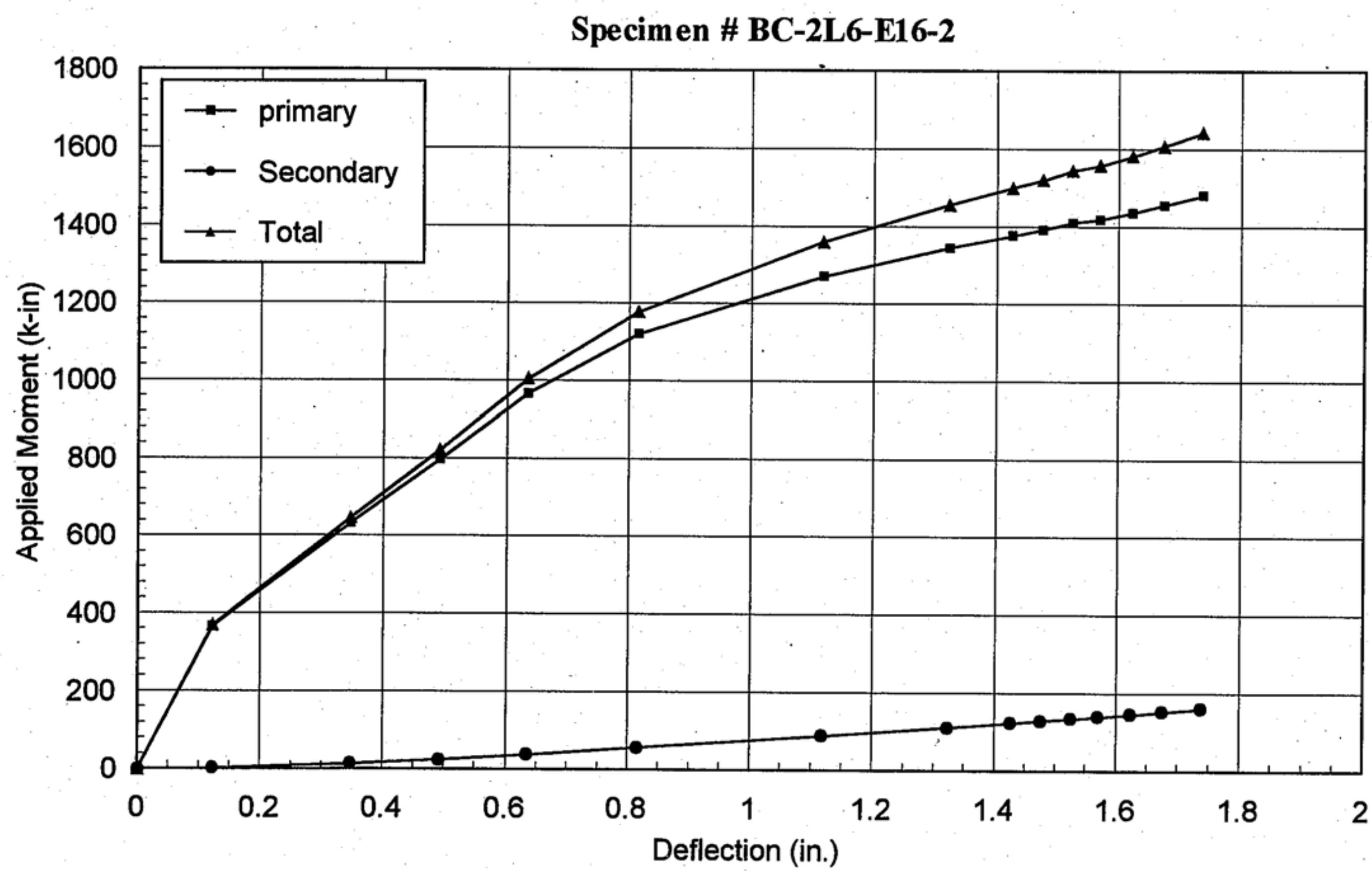

Fig. 3.19a - Centerline Strain Distribution

Specimen # BC-0L6-E16

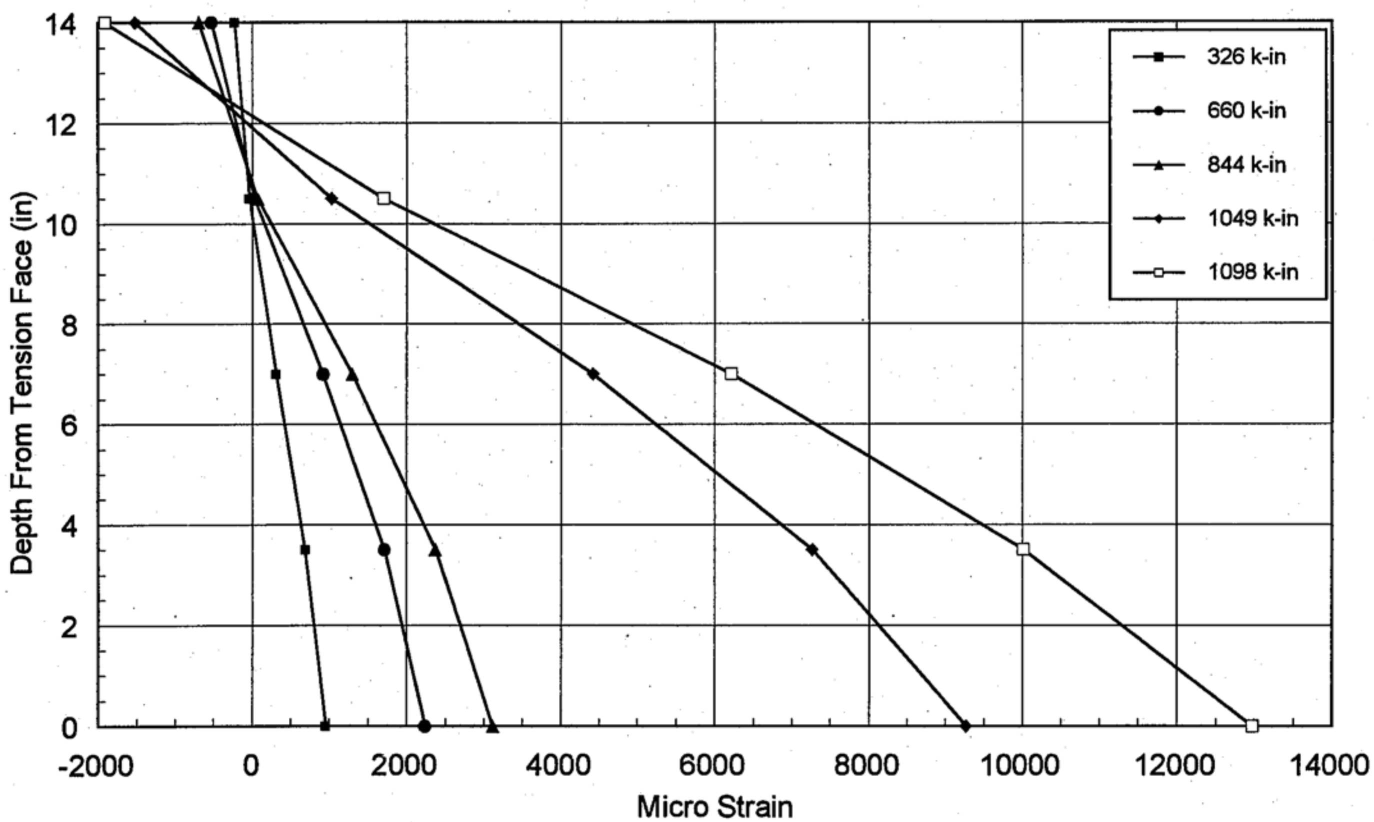

Fig. 3.18b - Centerline Strain Distribution

Specimen # BC-2L6-E16-1

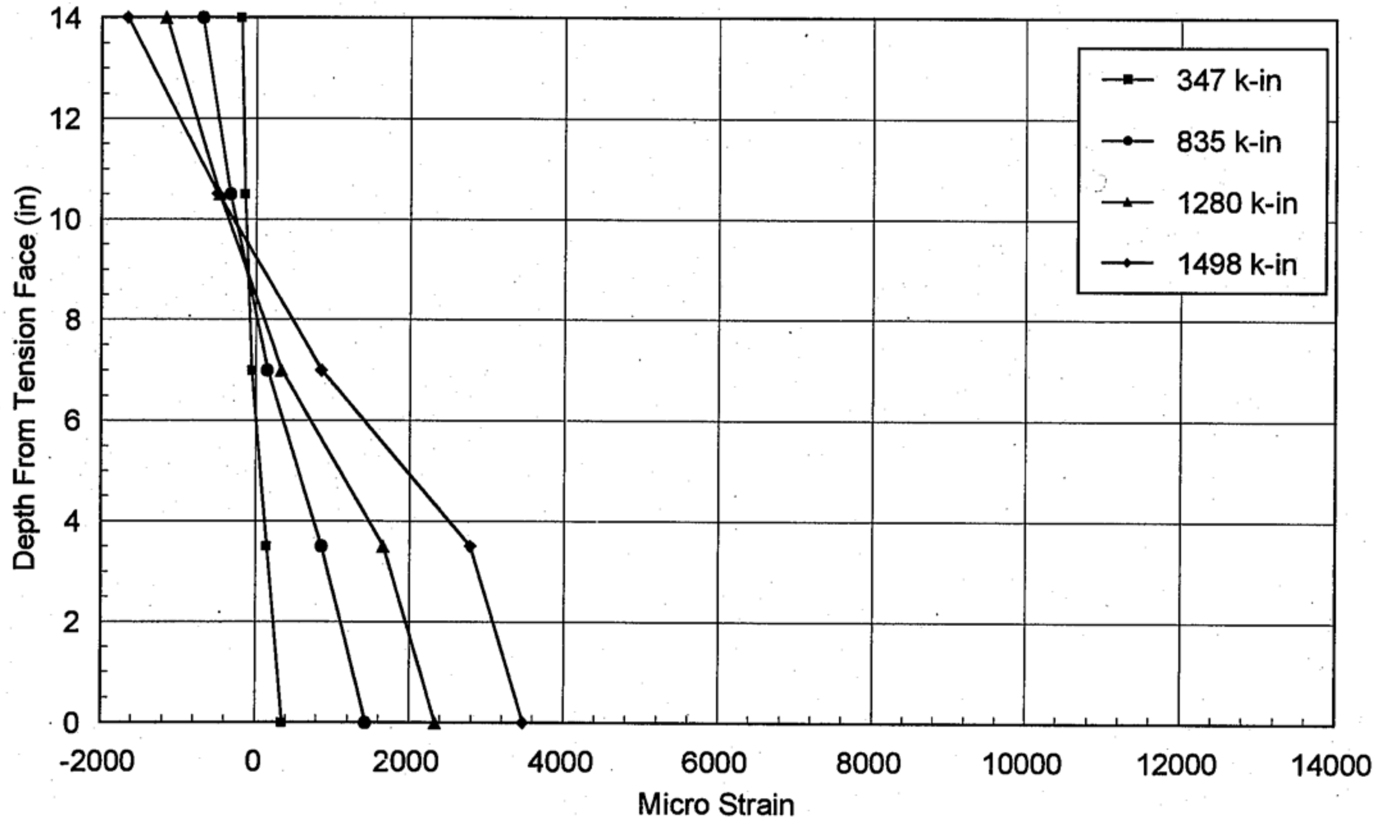

Fig. 3.19c - Centerline Strain Distribution

Specimen # BC-2L6-E16-2

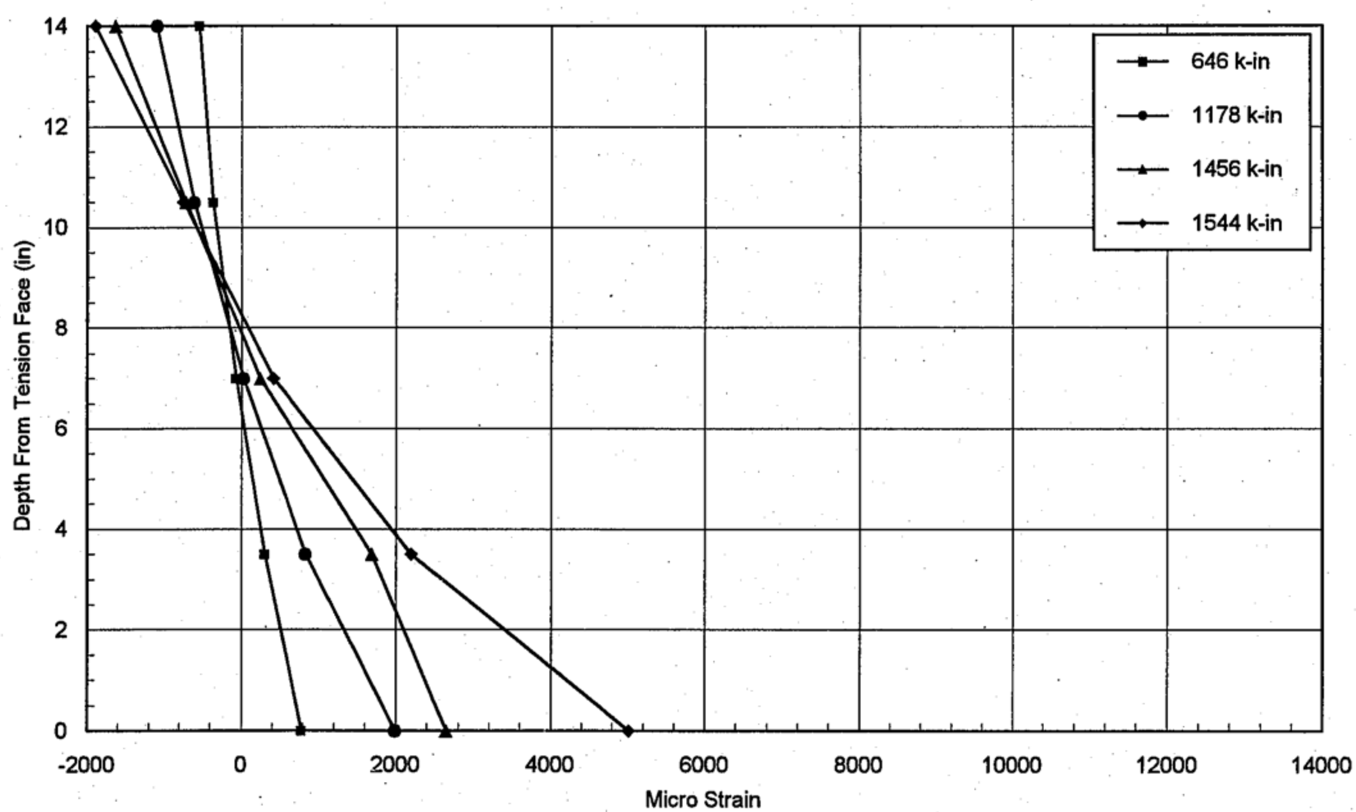

Fig. 3.20a - Longitudinal Tension Strain Distribution Along Beam Length

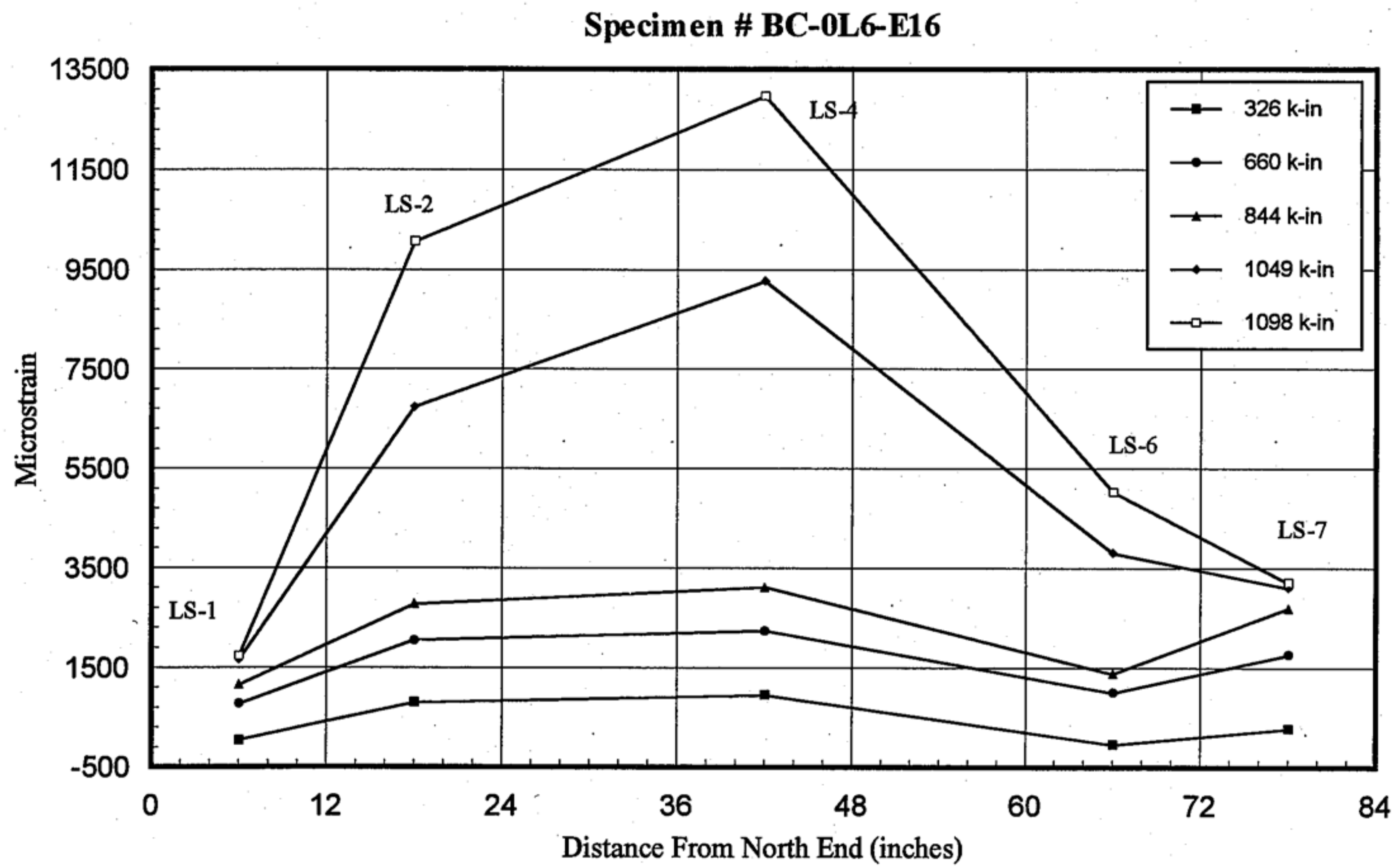

Fig. 3.20a - Longitudinal Compressive Strain Distribution Along Beam Length

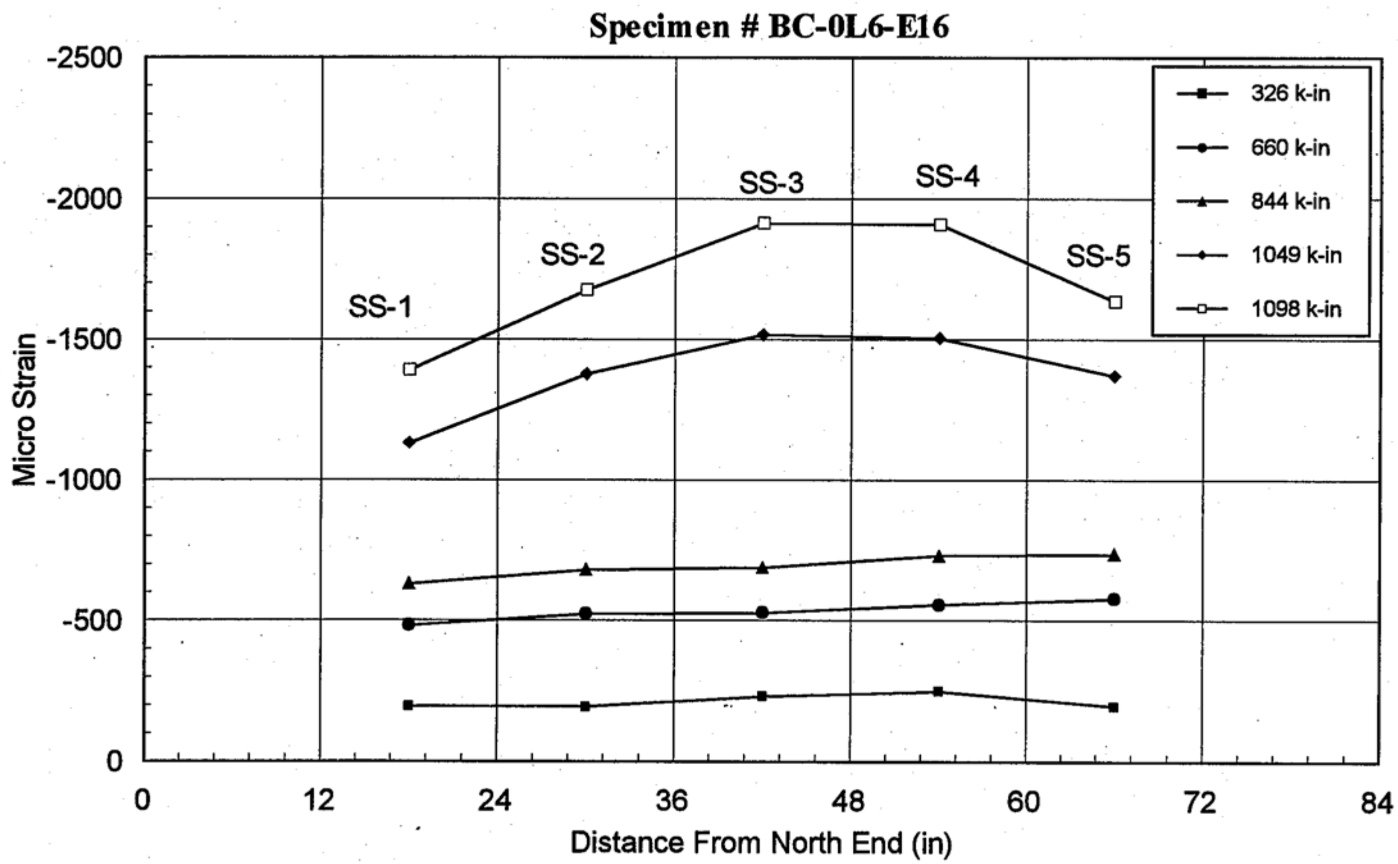

Fig. 3.20b - Longitudinal Tension Strain Distribution Along Beam Length

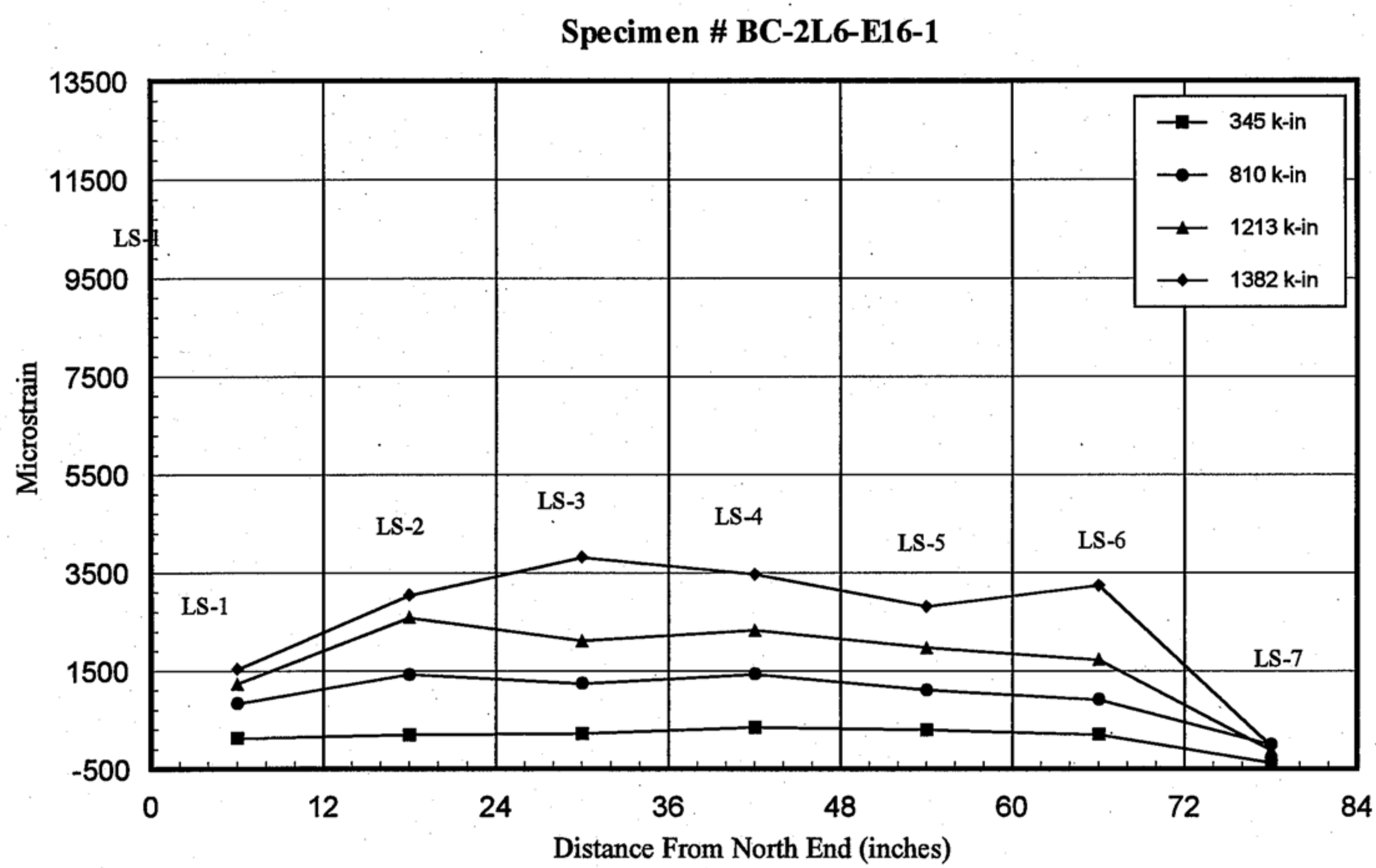

Fig. 3.20b - Longitudinal Compressive Strain Distribution Along Beam Length

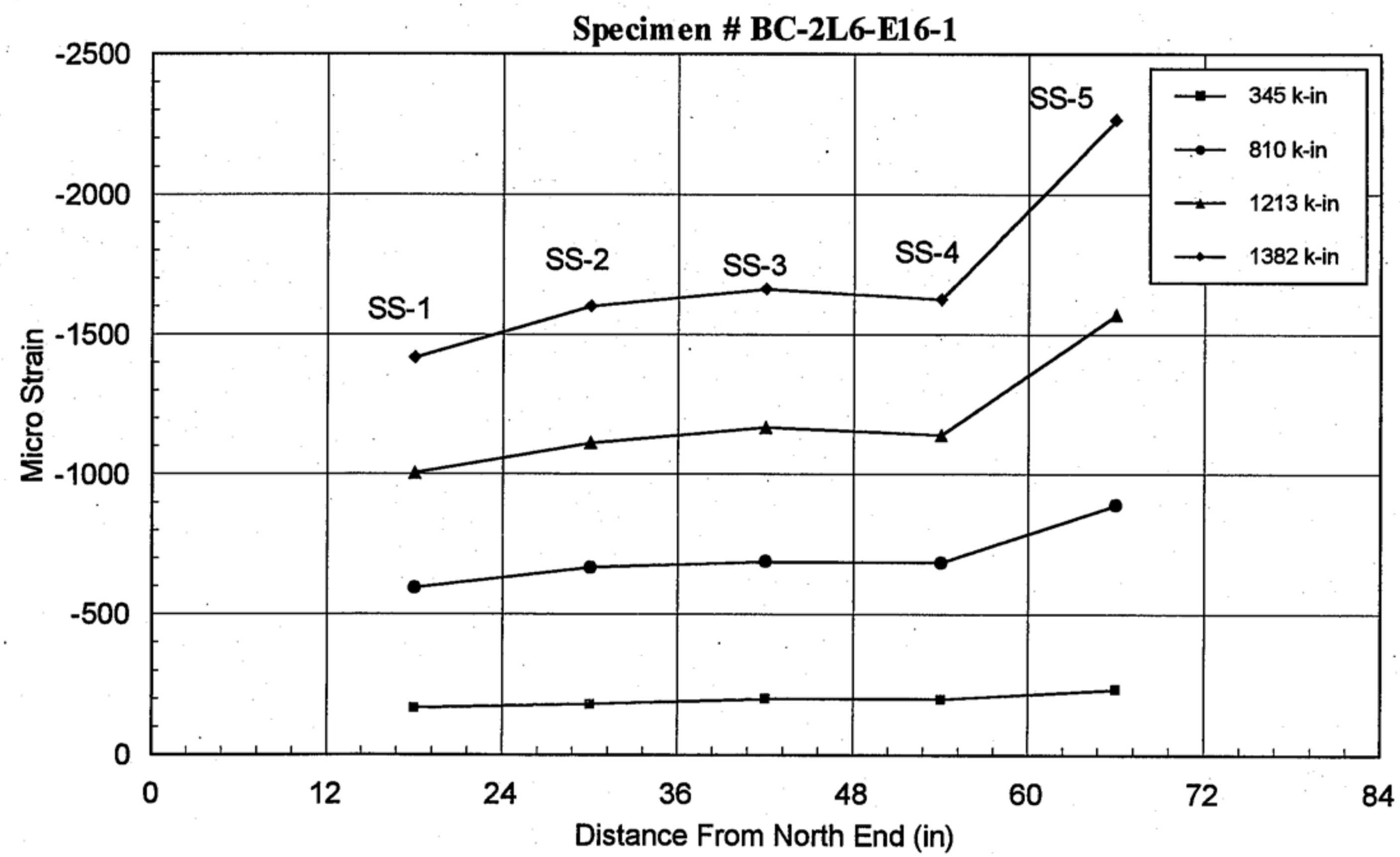

Fig. 3.20c - Longitudinal Tension Strain Distribution Along Beam Length

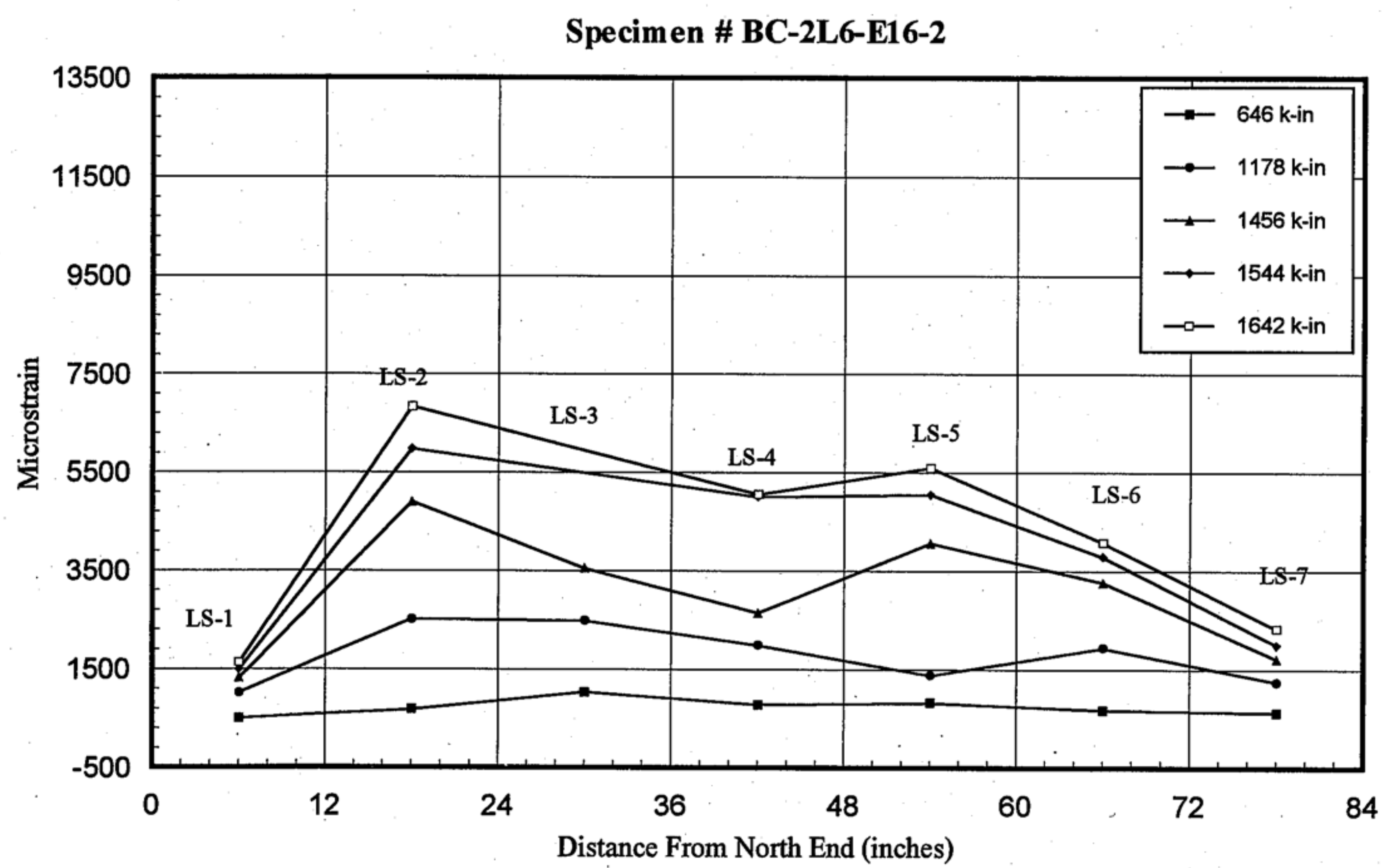

Fig. 3.20c - Longitudinal Compressive Strain Distribution Along Beam Length

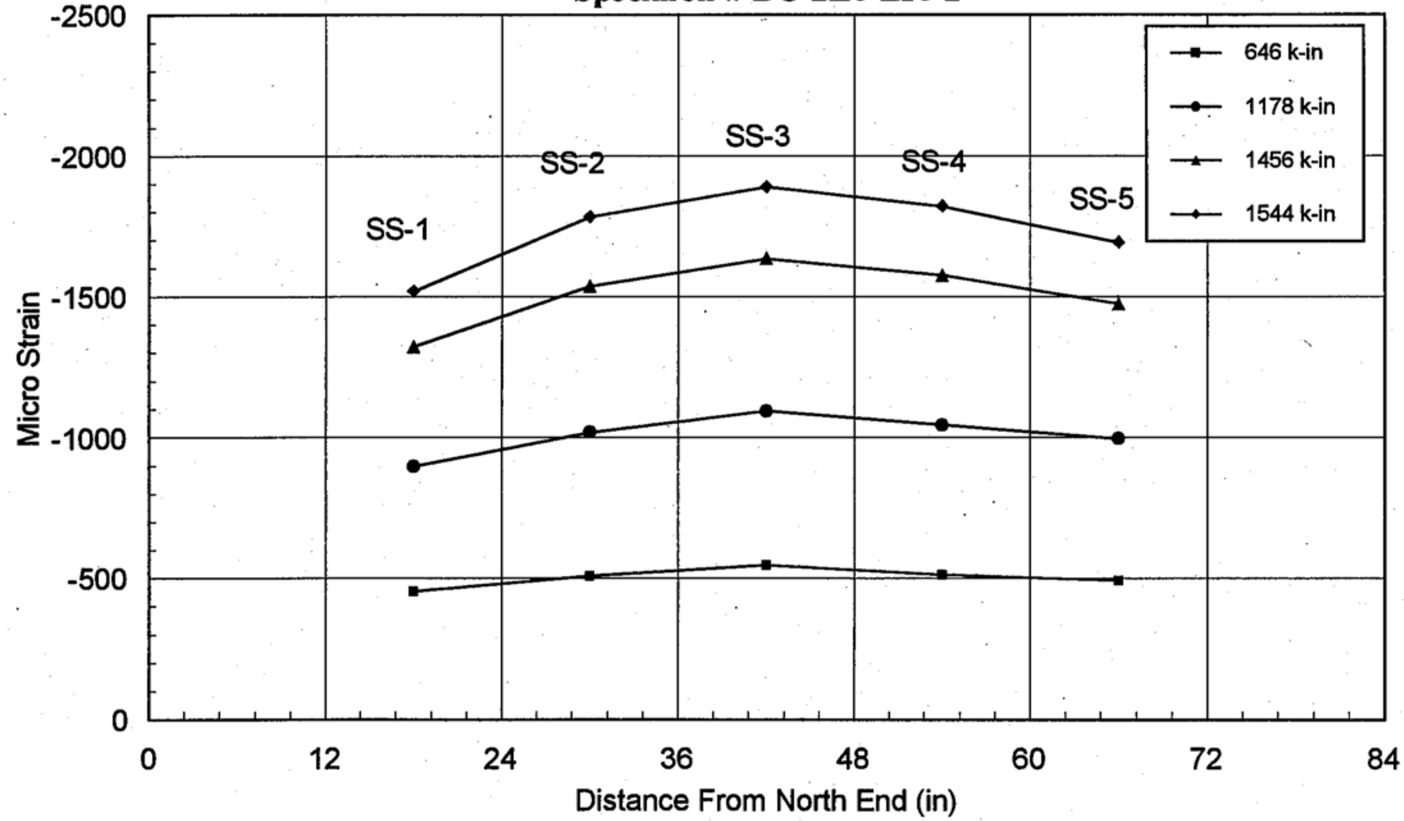

Fig. 3.21a - Moment vs. Transverse Strain At Midspan

Specimen # BC-0L6-E16

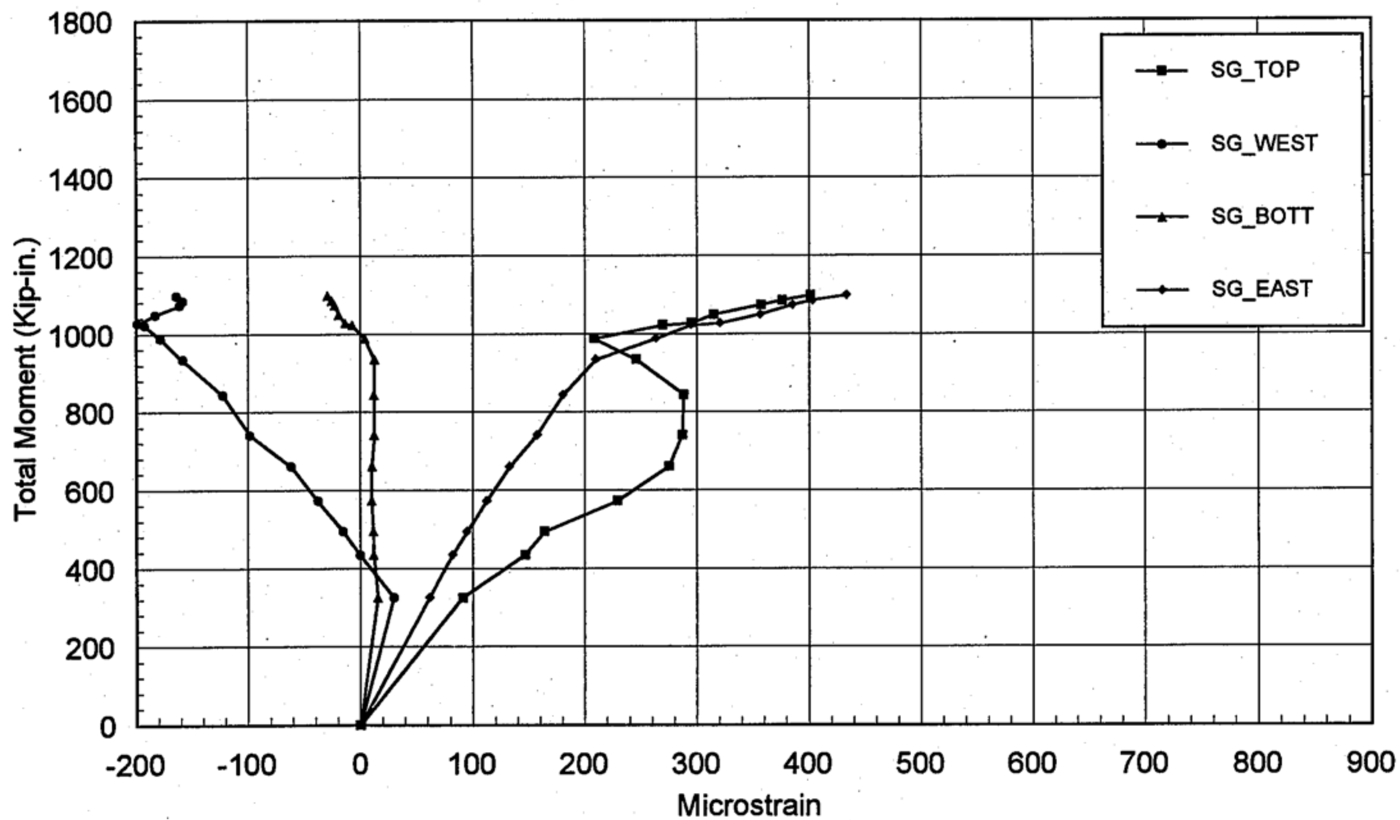

Fig. 3.21b - Moment vs. Transverse Strain At Midspan

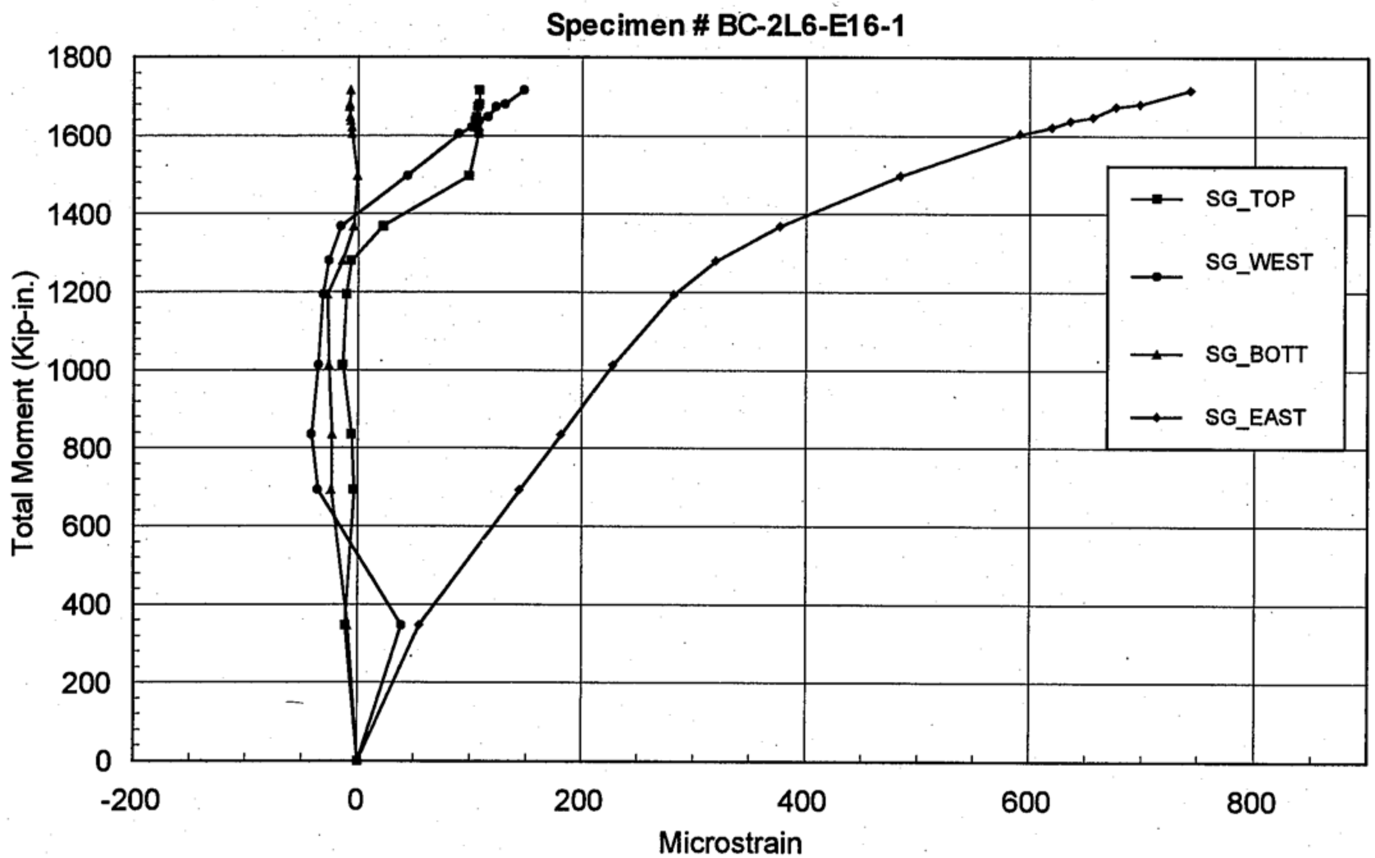

Fig.3.21c - Moment vs. Transverse Strain At midspan

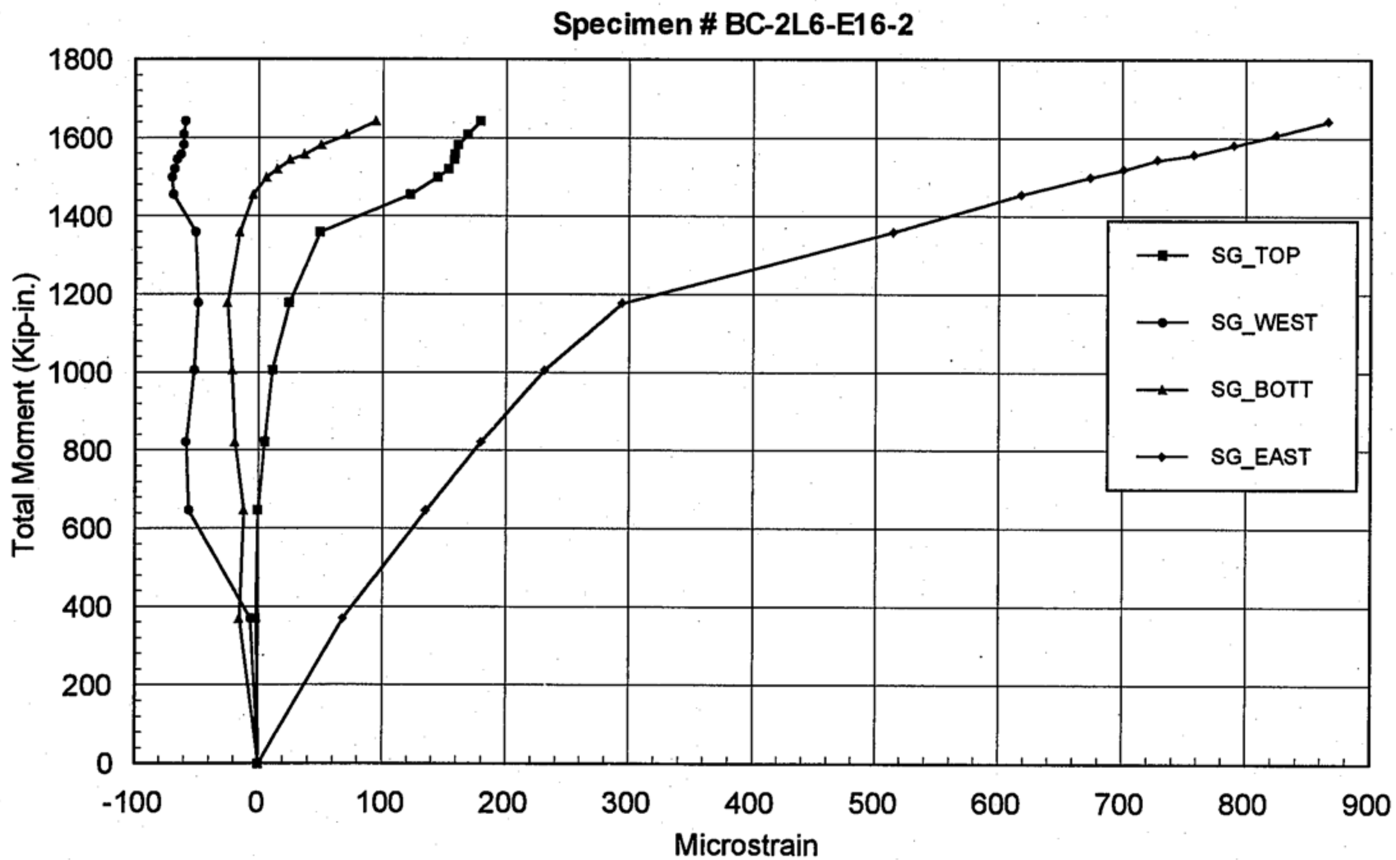

Fig. 3.22a - Applied Moment vs. Mid-Span Deflection

Specimen # BC-0L6-FL (No Corbels)

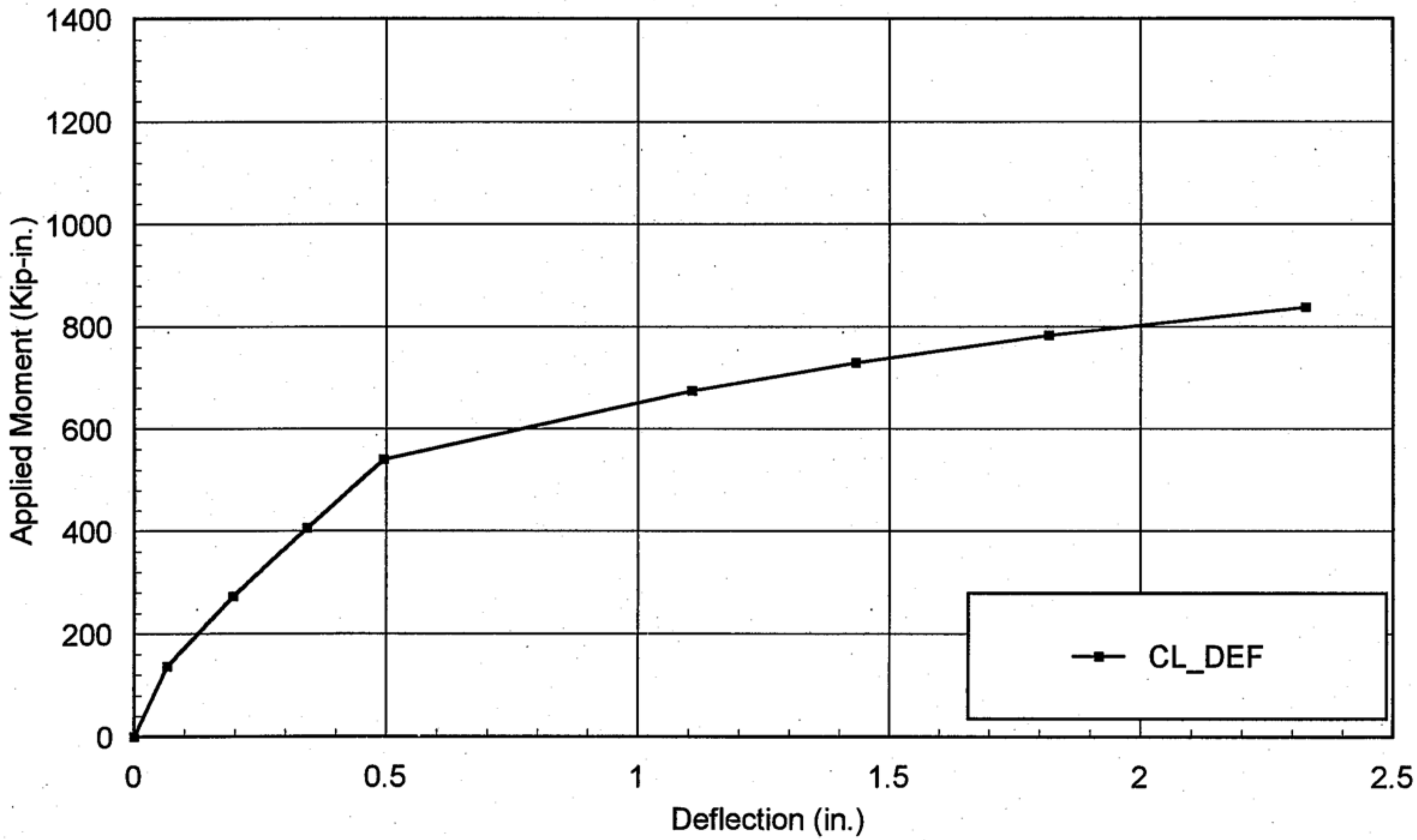

Fig. 3.22b - Moment vs Mid-Span Deflection

Specimen # BC-2L6-FL-1 (No Corbels)

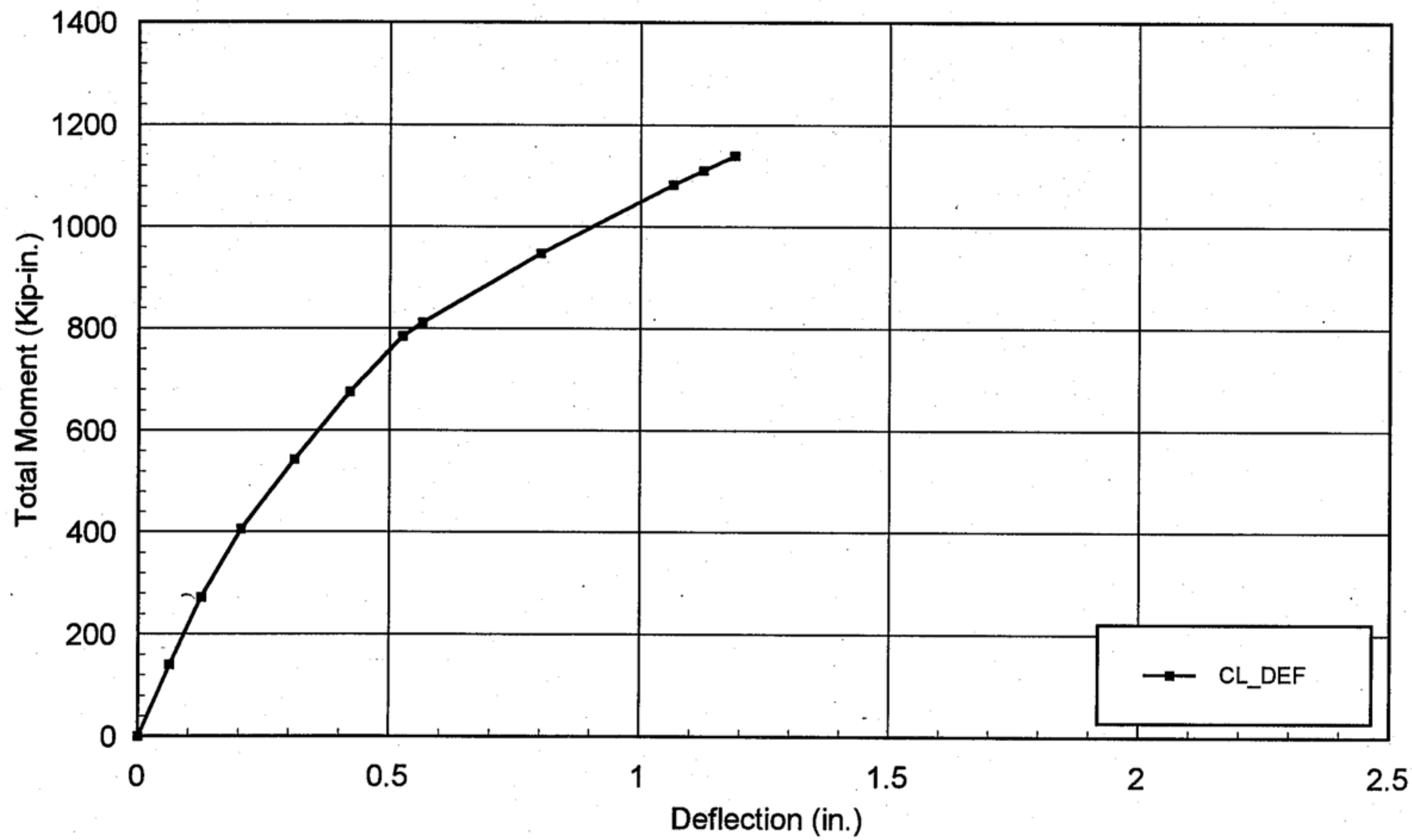

Fig. 3.22c - Moment vsS. Mid-Span Deflection

Specimen # BC-2L6-FL-2 (No Corbels)

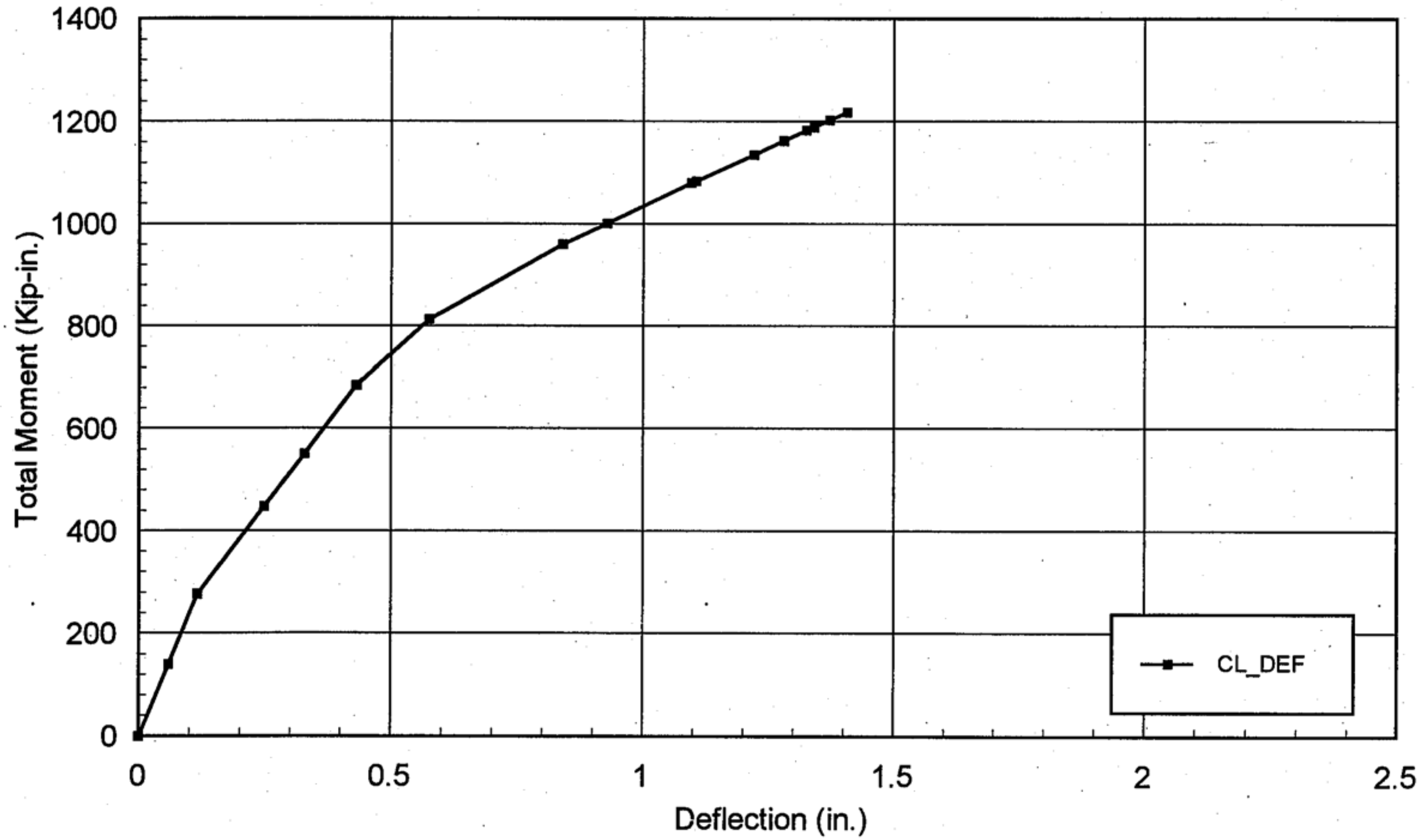

Fig. 3.22d - Moment vs. Mid-Span Deflection

Specimen # BC-2L6-FL-3 (No Corbels)

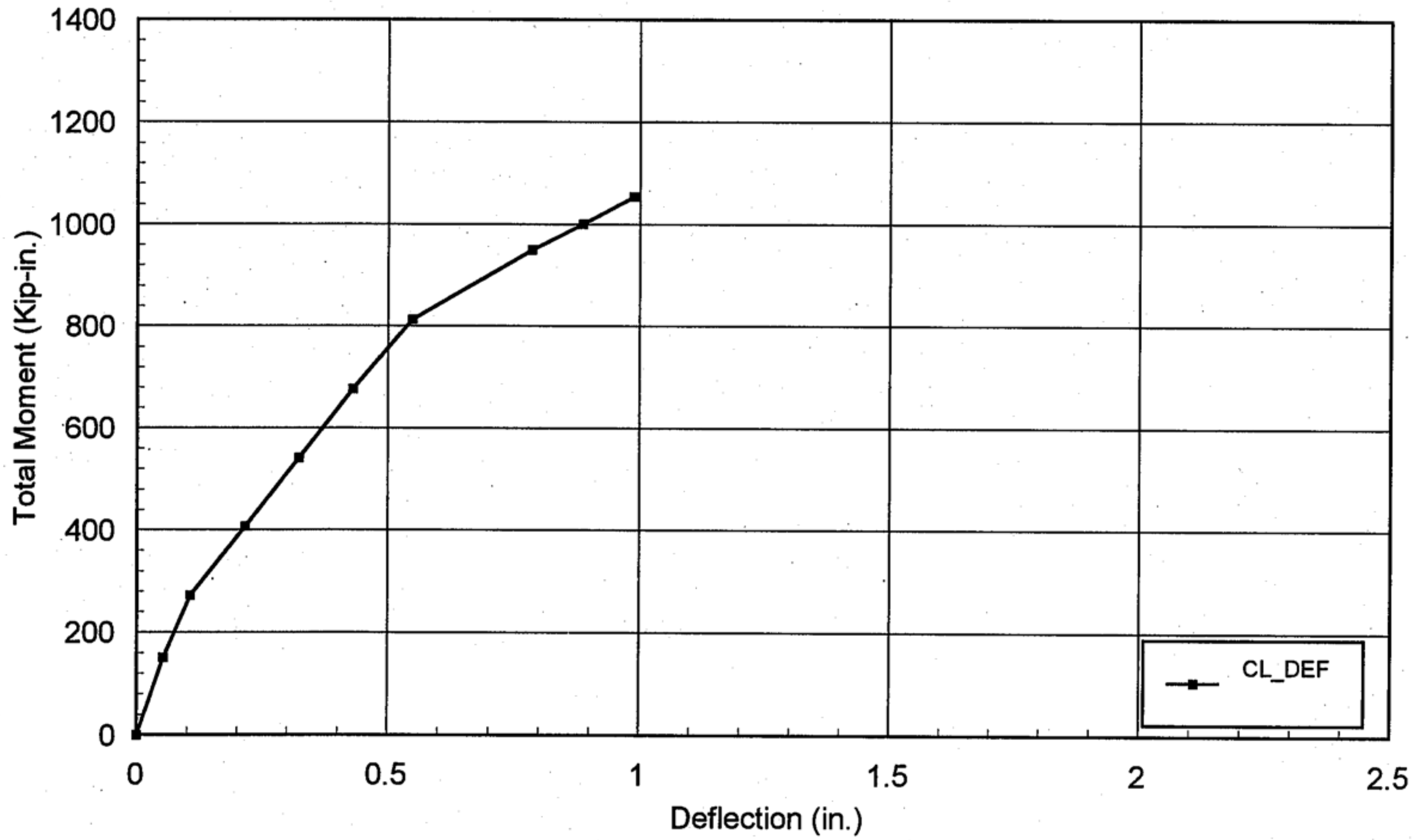

Fig. 3.23a - Center Line Strain Distribution

Specimen # BC-0L6-FL (No Corbels)

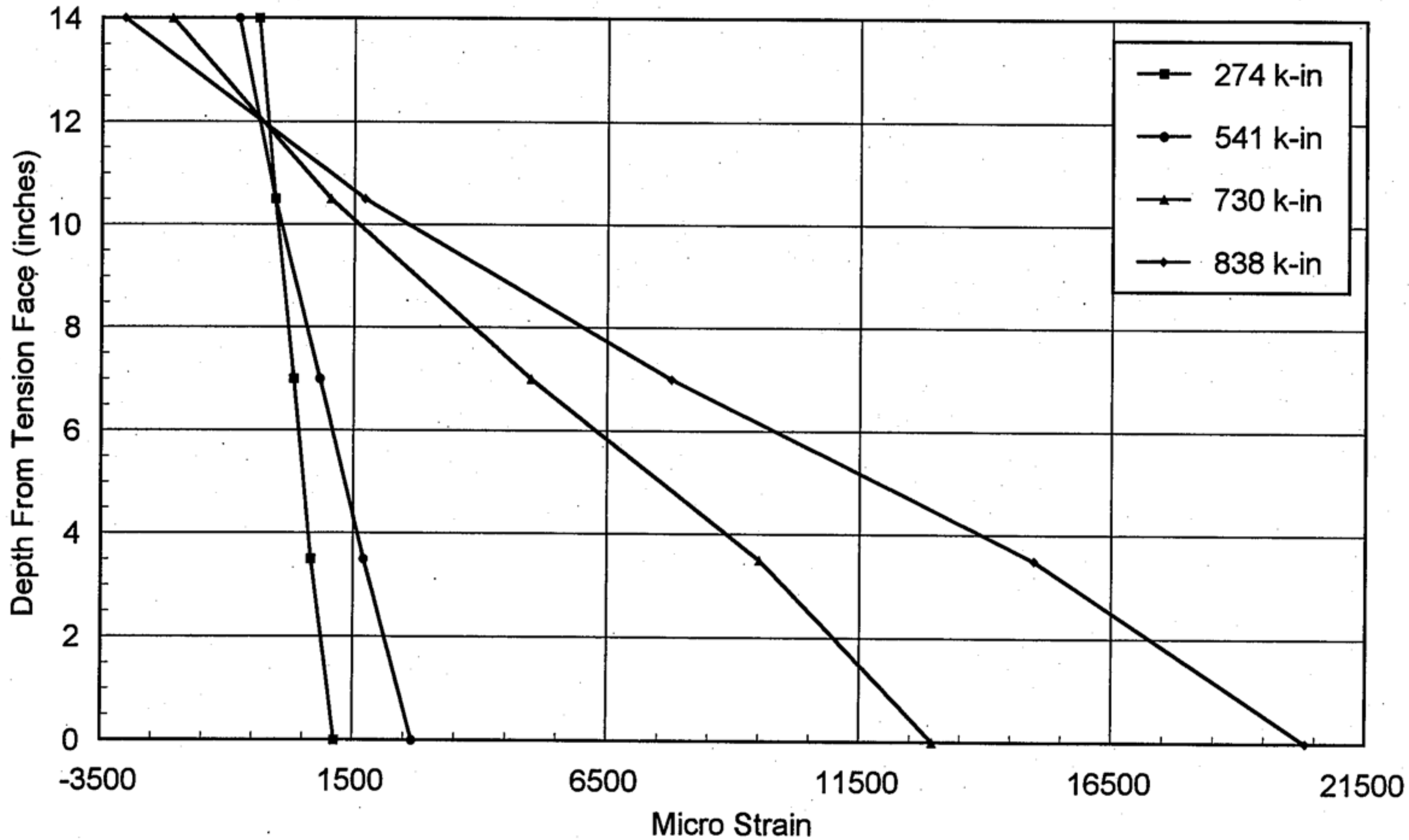

Effective confinement ratio: ke

$$k_e = \frac{A_e}{A_{cc}} \qquad \text{(eq. 11)}$$

where A_e and A_{ce} are respectively the confined and concrete core area, given

by: $A = t_x{}^* t_y - ((wx^2 + wy^2)/3) - A_s$ (eq. 12) A_{ce}

$= A_c$ - $A_\$$ (eq. 13)

with $w_x = t_x$ - 2r and $w_y = t_y$ - 2r. The area section area ratios of the composite

wraps $p_{j,x}$ and $P_{j,y}$ are given by:

$$P_{j,x} = 2 * \frac{t_j}{t_x} \qquad \text{(eq.14)}$$

$$P_{j,y} = 2 * \frac{t_j}{t_y} \qquad \text{(eq. 15)}$$

where ti is the total effective thickness of the wrap.

The average jacket stress (at the *axial* load peak): f_j

f_j = $E_j * \epsilon_{j,experimental}$ (eq. 16)

where E_j and $\epsilon_{jExperimental}$ are the modulus of elasticity of the dry composite wrap and the average experimental transverse strain.

a.2) Interaction Diagram

- Nominal concentric load capacity: P_n

$P_{,,}$= 0.85*f_{cc}*(A_g-A_{st})+A_{st}*f_y (eq.17)

where f. is the compression strength of wrapped concrete, the other variables were defined for the unconfined model (Appendix B 1). Note that when P_n is maximal, the bending moment (M.) is equal to 0.

- Balanced failure point (based *on*and $\epsilon_c = \epsilon_{cu}$ and $\epsilon_{FRP} = \epsilon_{FRP}$, ultimate) is calculated *as* follows:

$$c = c_b = \frac{\varepsilon_{cu} * h}{\varepsilon_{FRP} + \varepsilon_{cu}} \qquad \text{(eq. 18)}$$

$a = \beta_1 * c$ (eq. 3)

$$\varepsilon'_s = \frac{\varepsilon_{cu} * (c - d)}{c} \quad \text{(eq 4)}$$

$C_b = 0.85 * .f_{cc} * a * b$ (eq. 19)

where C_b is the compressive force taken by concrete.

Tar bottom = $E_{FRP} * \epsilon_{FRP} * \epsilon_{FRP} * b$ (eq. 20)

$$T_{FRP} \text{ distributed} = E_{FRP} * \left(\frac{\varepsilon_{FRP} + 0}{2} \right) * t_{FRP} * I_d * 2sides \quad \text{(eq. 21)}$$

$l_d = h\text{-}c\text{-}r$

(eq. 22) where TF'' bottom is the tension force generated by the composite at the bottom face of the column. Tmp distributed is the average tension force generated by the composite on the sides of the column and Id is the tension zone depth.

$Fs = E_s * \epsilon_s * A_s$ (eq. 23)

$F's = E_s * \epsilon'_s * A'_s$ (eq. 24)

$$M_{ab} = C_B * (Y - a/2) + F_s^*(y\text{-}d) + F*(d\text{-}y) + T_{FRP}\ bott.*y + T_{FRP}\ distr*(la*2/3\text{-}(y\text{-}c)) \quad \text{(eq. 25)}$$

$P_{nb} = (C_B + f s) - (fs + f_F, bolt. + f_F, distr.)$ (eq. 26)

- <u>Point corresponding two yielding of steel (E, = E$_y$) is calculated as follows:</u>

$$c = c_y = \frac{\varepsilon_{cu} * h}{\varepsilon_{FRP} +} \qquad \text{(eq. 27)}$$

where c_y stands for neutral axis depth corresponding to $\epsilon_s = \epsilon_y$. Having obtained c, the equation (8) to (26) can be followed to find P_n and M_n values.

- <u>Other points:</u>

Similarly, other points either controlled by compression ($c > c_b$) or by flexure ($c < c_b$) can be determined (see flow chart bellow).

b) Flow chart for interaction diagram generation

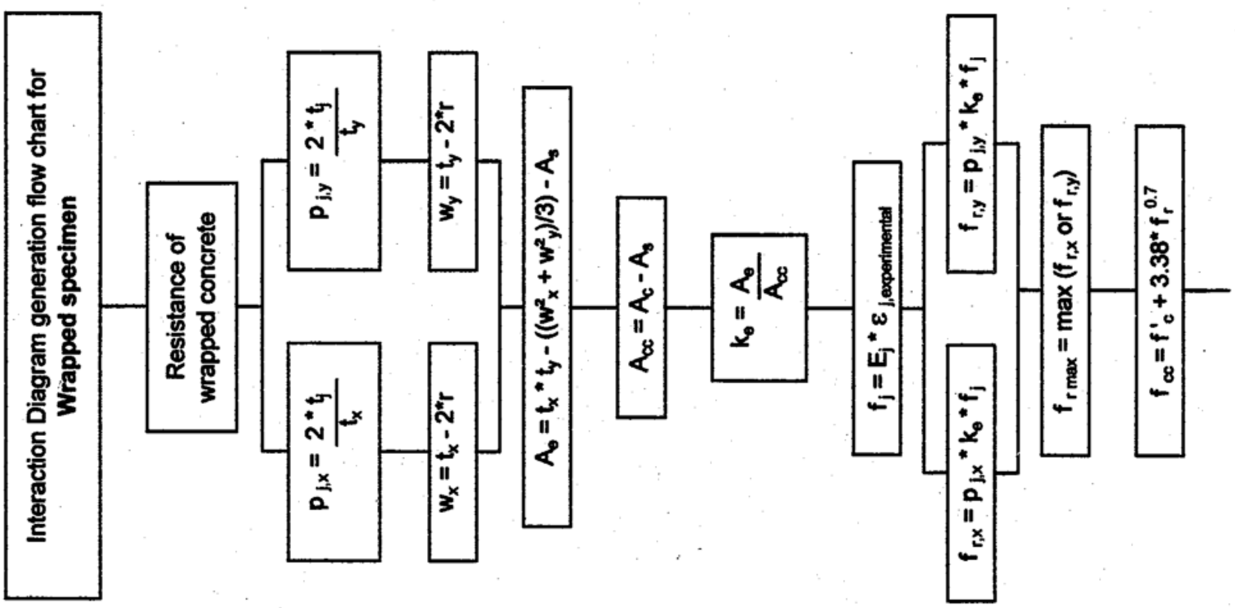

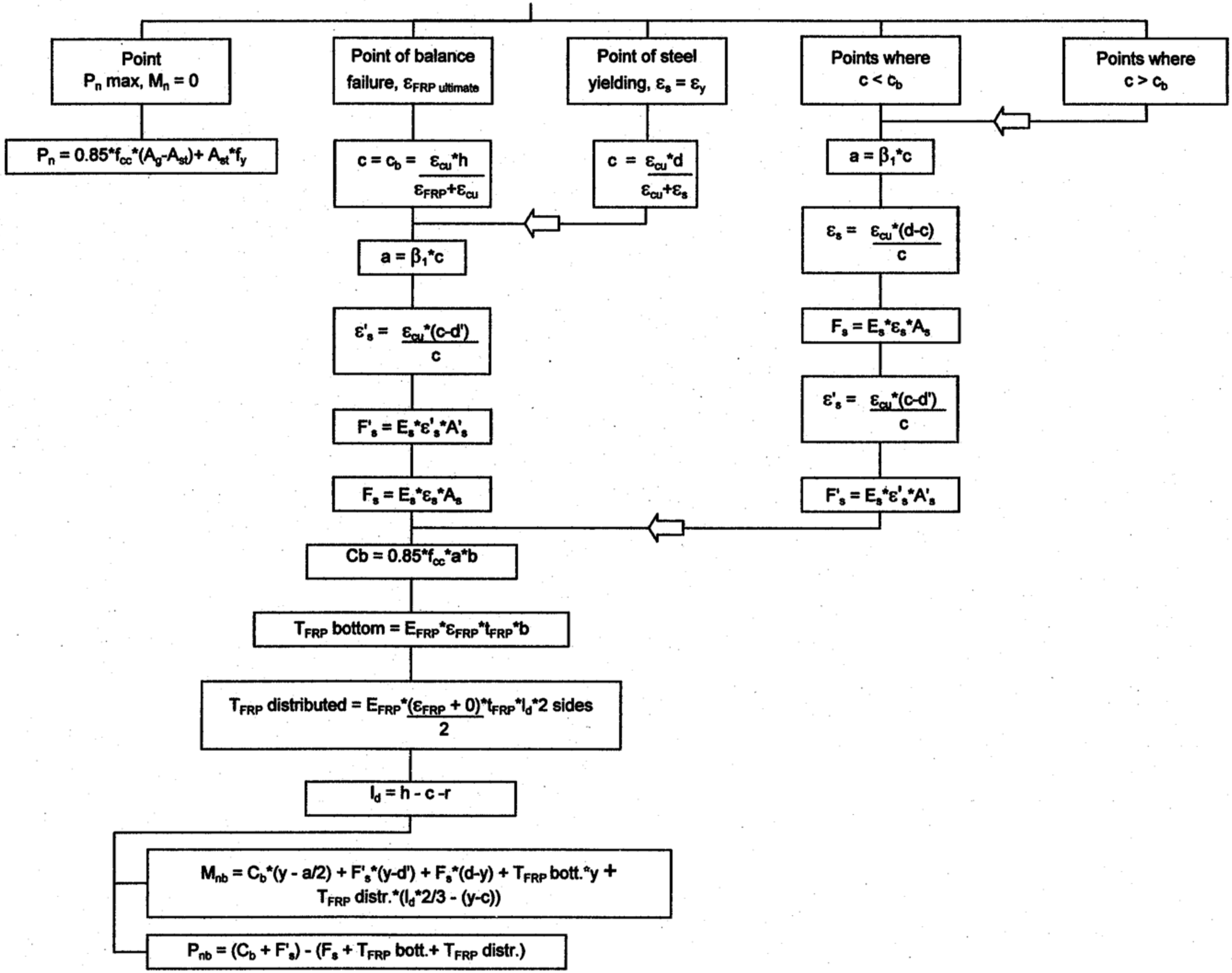
Point
P_n max, M_n = 0
P_n = 0.85*f_cc*(A_g-A_st)+ A_st*f_y
Point of balance
failure, ε_FRP ultimate
c = c_b = ε_cu*h / (ε_FRP+ε_cu)
a = β_1*c
ε'_s = ε_cu*(c-d') / c
F'_s = E_s*ε'_s*A'_s
F_s = E_s*ε_s*A_s
Point of steel
yielding, ε_s = ε_y
c = ε_cu*d / (ε_cu+ε_s)
Points where
c < c_b
a = β_1*c
ε_s = ε_cu*(d-c) / c
F_s = E_s*ε_s*A_s
ε'_s = ε_cu*(c-d') / c
F'_s = E_s*ε'_s*A'_s
Points where
c > c_b
Cb = 0.85*f_cc*a*b
T_FRP bottom = E_FRP*ε_FRP*t_FRP*b
T_FRP distributed = E_FRP*(ε_FRP + 0)/2*t_FRP*l_d*2 sides
l_d = h - c -r
M_nb = C_b*(y - a/2) + F'_s*(y-d') + F_s*(d-y) + T_FRP bott.*y +
T_FRP distr.*(l_d*2/3 - (y-c))
P_nb = (C_b + F'_s) - (F_s + T_FRP bott.+ T_FRP distr.)

c) Interaction Diagrams

<u>Wrapped specimen (2 layers) : f'c = 8.8 ksi</u>

f'c (ksi) =	8.80	E_{FRP} (ksi) =	33 500	As (in²) =	0.880	b (in) =	8.0
f_{cc} (ksi) =	9.49	ε_{FRP} =	0.012	A's (in²) =	0.880	h (in) =	14.0
ε_{cu} =	0.00300	$\varepsilon_{j\,FRP}$ (trans) =	0.003	Ast (in²) =	1.760	y (in) = h/2 =	7.0
fy (kip) =	60.0	A_{FRP}/yarn (in²) =	0.00070	Ag (in²) =	112	d (in) =	12.0
Ey (ksi) =	30 000	yarns/in =	6.5	β_1 =	0.85	d' (in) =	2.0
εy =	0.00200	nb. of layers =	2			r (in) =	1.0
		t_{FRP} tot (in/in) =	0.0091				

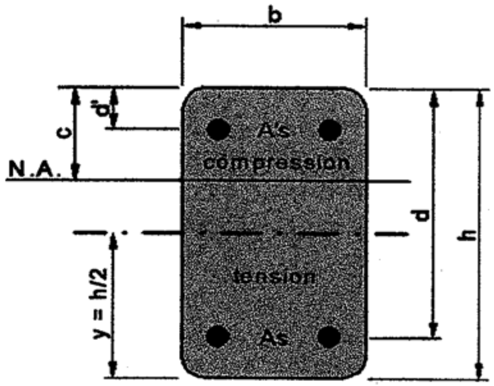

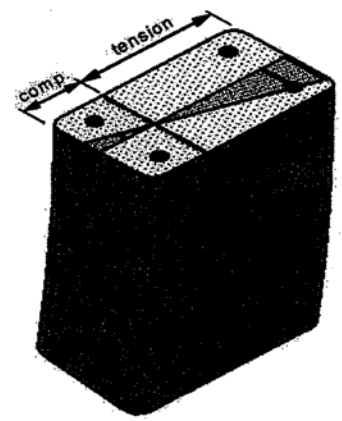

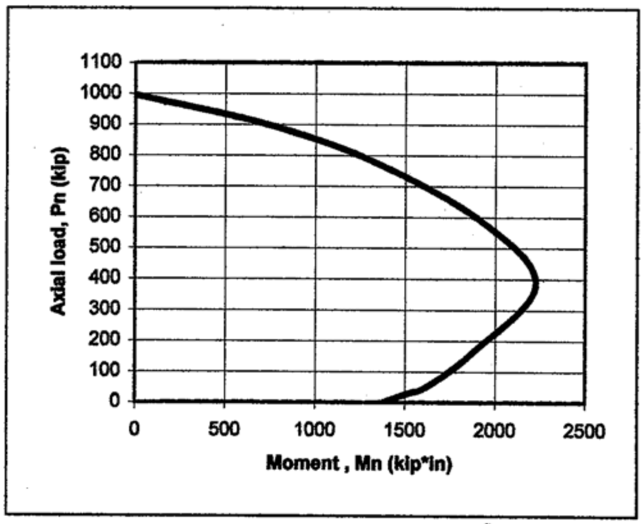

Results wrapped specimen

c (in)	P_n (kip)	M_n (kip*in)	e_n (in)
2.2	0.1	1372.8	10204.0
2.5	27.5	1505.5	54.7
2.80	52.8	1623.2	30.7
4.0	165.6	1878.1	5.8
7.20	383.2	2225.5	11.3
10.0	586.7	1925.1	3.3
13.0	779.7	1321.6	1.7
15.0	901.1	724.5	0.0
∞	995.2	0.0	-

<u>Resistance of wrapped concrete</u>

Section area ratio :

$p_{j,x}$ = $2 * \frac{t_j}{t_x}$

$p_{j,x}$ = 0.23%

$p_{j,y}$ = $2 * \frac{t_j}{t_y}$

$p_{j,y}$ = 0.13%

w_x = $t_x - 2*r$

w_x (in) = 6.0

w_y = $t_y - 2*r$

w_y (in) = 12.0

A_e = $t_x*t_y - ((w_x^2+w_y^2)/3) - A_s$

A_e (in²) = 50.24

A_{cc} = $A_c - A_s$

A_{cc} (in²) = 110.24

k_e = $\frac{A_e}{A_{cc}}$ = 0.46

f_j (ksi) = $E_j * \varepsilon_{j,experimental}$ = 100.5

$f_{r,x}$ = $p_{j,x} * k_e * f_j$

$f_{r,x}$ (ksi) = 0.104

$f_{r,y}$ = $p_{j,y} * k_e * f_j$

$f_{r,y}$ (ksi) = 0.060

$f_{r\,max}$ (ksi) = **0.104**

f_{cc} = $f'_c + 3.38 * f_r^{0.7}$

f_{cc} (ksi) = **9.49**

<u>Point no.1 of diagram : maximum axial load, moment = 0</u>

Pn max = $0.85 * f_{cc} * (A_g - A_{st}) + A_{st} * f_y$

P_n max (kip) = **995.2**

M_n (kip*in) = **0**

Point no.2 of diagram : balance failure ($\varepsilon_{FRP} = \varepsilon_{FRP\ ultimate}$)

c_b = $\dfrac{\varepsilon_{cu} * h}{\varepsilon_{FRP} + \varepsilon_{cu}}$

c_b (in) = 2.80

a = $\beta_1 * c$

a (in) = 2.38

ε's = $\dfrac{\varepsilon_{cu} * (c - d')}{c}$

ε's =	0.00086	<	0.00200	

F's (kip) = 25.7

Fs (kip) = 60.0

C_B (ksi) = $0.85 * f_{cc} * a * b$ — C_B (kip) = 153.7

T_{FRP} bottom (ksi) = $E_{FRP} * \varepsilon_{FRP} * t_{FRP} * b$ — T_{FRP} bott. (kip) = 29.3

T_{FRP} distributed (ksi) = $E_{FRP} * \left(\dfrac{\varepsilon_{FRP} + 0}{2}\right) * t_{FRP} * l_d * 2\ \ sides$ — T_{FRP} dist. (kip) = 37.3

l_d (in) = h - c - r = 10.20

M_{nb} = $C_B * (y - \frac{a}{2}) + f'_s * (y - d') + f_s * (d - y) + f_{FRP}\ bott. * y + f_{FRP}\ distr. * (l_d * \frac{2}{3} - (y - c))$

M_{nb} (kip*in) = 1623.2

P_{nb} (kip) = $(C_B + f'_s) - (f_s + f_{FRP}\ bott. + f_{FRP}\ distr.)$

P_{nb} (kip) = 52.8

Point no.3, εs = εy (yielding of steel)

c = $\dfrac{\varepsilon_{cu} * d}{(\varepsilon_{cu} + \varepsilon_s)}$

c (in) = 7.20

a = $\beta_1 * c$

a (in) = 6.12

ε's = $\frac{\varepsilon_{cu} * (c - d')}{c}$

ε's = 0.00217 > 0.00200

$F'_s = E_s * \varepsilon'_s * A'_s$ — F's (kip) = **60.0**

$F_s = E_s * \varepsilon_s * A_s$ — Fs (kip) = **60.0**

C_B (ksi) = $0.85 * f_{cc} * a * b$ — C_B (kip) = **395.1**

ε_{FRP} = $\frac{\varepsilon_{cu} * (h - c)}{c}$ = 0.00283

T_{FRP} bottom (ksi) = $E_{FRP} * \varepsilon_{FRP} * t_{FRP} * b$ — T_{FRP} **bott. (kip) =** **6.9**

T_{FRP} distributed (ksi) = $E_{FRP} * \left(\frac{\varepsilon_{FRP} + 0}{2}\right) * t_{FRP} * l_d * 2 \ sides$ — T_{FRP} **dist. (kip) =** **5.0**

l_d (in) = h - c - r = 5.80

M_n = $C_B * (y - \frac{a}{2}) + f'_s * (y - d') + f_s * (d - y) + f_{FRP} \ bott. * y + f_{FRP} \ distr. * (l_d * \frac{2}{3} - (y - c))$

M_n (kip*in) = **2225.5**

P_n (kip) = $(C_B + f'_s) - (f_s + f_{FRP} \ bott. + f_{FRP} \ distr.)$

P_n (kip) = **383.2**

<u>Point no.4, 5 of diagram : c < c_b (flexure failure)</u>

To create adequatly the graph, please enter c values in increasing order for point 4 and 5

<u>Point no.4</u>

c (in) = **2.2** — **OK : possible value of c** — n.b. : c_b (in) = 2.80

a = $\beta_1 * c$

a (in) = 1.87

ε_c = 0.00300

ε_s = $\frac{\varepsilon_{cu} * (d - c)}{c}$

ε_s = 0.01336 > 0.00200

$F_s = E_s * \varepsilon_s * A_s$ | Fs (kip) = **60.0**

$\varepsilon's = \dfrac{\varepsilon_{cu} * (c - d')}{c}$

$\varepsilon's =$ 0.00027 < 0.00200

$F'_s = E_s * \varepsilon'_s * A'_s$ | F's (kip) = **8.2**

$\varepsilon_{FRP} =$ 0.012 | T_{FRP} **bott. (kip) = 29.3**

T_{FRP} distributed (ksi) = $E_{FRP} * \left(\dfrac{\varepsilon_{FRP} + 0}{2}\right) * t_{FRP} * l_d * 2 \;\; sides$ | T_{FRP} **dist. (kip) = 39.5**

l_d (in) = h - c - r = 10.80

C_B (ksi) = $0.85 * f_{cc} * a * b$ | C_B **(kip) = 120.7**

$M_n = C_B * (y - \frac{a}{2}) + f'_s * (y - d') + f_s * (d - y) + f_{FRP}\ bott. * y + f_{FRP}\ distr. * (l_d * \frac{2}{3} - (y - c))$

M_n (kip*in) = **1372.8**

P_n (kip) = $(C_B + f'_s) - (f_s + f_{FRP}\ bott. + f_{FRP}\ distr.)$

P_n (kip) = **0.1**

Point no.6, 7, 8 and 9 of diagram : c > c_b (compression failure)

To create adequatly the graph, please enter c values in increasing order for point 6,7 and 8
The value of c can be greater than "h", but the value of "a" is limited to "h"

Point no.6 : before yielding of As (εs < εy)

c (in) = **4.0** **OK : possible value of c**

a = $\beta_1 * c$

a (in) = **3.4** **< h** **OK : possible value of a**
a (in) = **3.4**

ε_c = 0.00300

$\varepsilon_s < \varepsilon_y$

$\varepsilon_s = \dfrac{\varepsilon_{cu} * (d-c)}{c}$

ε_s = 0.00600 > ey

ε_s = **0.00200**

$F_s = E_s * \varepsilon_s * A_s$ — **Fs (kip) = 60.0**

$\varepsilon'_s = \dfrac{\varepsilon_{cu} * (c-d')}{c}$

ε'_s = 0.00150 < 0.00200

$F'_s = E_s * \varepsilon'_s * A'_s$ — **F's (kip) = 45.0**

$\varepsilon_{FRP} = \dfrac{\varepsilon_{cu} * (h-c)}{c}$

ε_{FRP} = 0.00750 **> 0 : OK**

ε_{FRP} = **0.00750** — **T_{FRP} bott. (kip) = 18.3**

T_{FRP} distributed (ksi) = $E_{FRP} * \left(\dfrac{\varepsilon_{FRP}+0}{2}\right) * t_{FRP} * l_d * 2$ *sides* — **T_{FRP} dist. (kip) = 20.6**

l_d (in) = h - c - r = 9.00

C_B (ksi) = $0.85 * f_{cc} * a * b$ — **C_B (kip) = 219.5**

$M_n = C_B * (y - \frac{a}{2}) + f'_s * (y - d') + f_s * (d - y) + f_{FRP}\ bott. * y + f_{FRP}\ distr. * (l_d * \frac{2}{3} - (y - c))$

M_n (kip*in) = **1878.1**

P_n (kip) = $(C_B + f'_s) - (f_s + f_{FRP}\ bott. + f_{FRP}\ distr.)$

Note that this formula may be not accurate enough for Mn value close to 0

P_n (kip) = **165.6**

Fig. 3.23b - Center Line Strain Distribution

Specimen # BC-2L6-FL-1 (No Corbels)

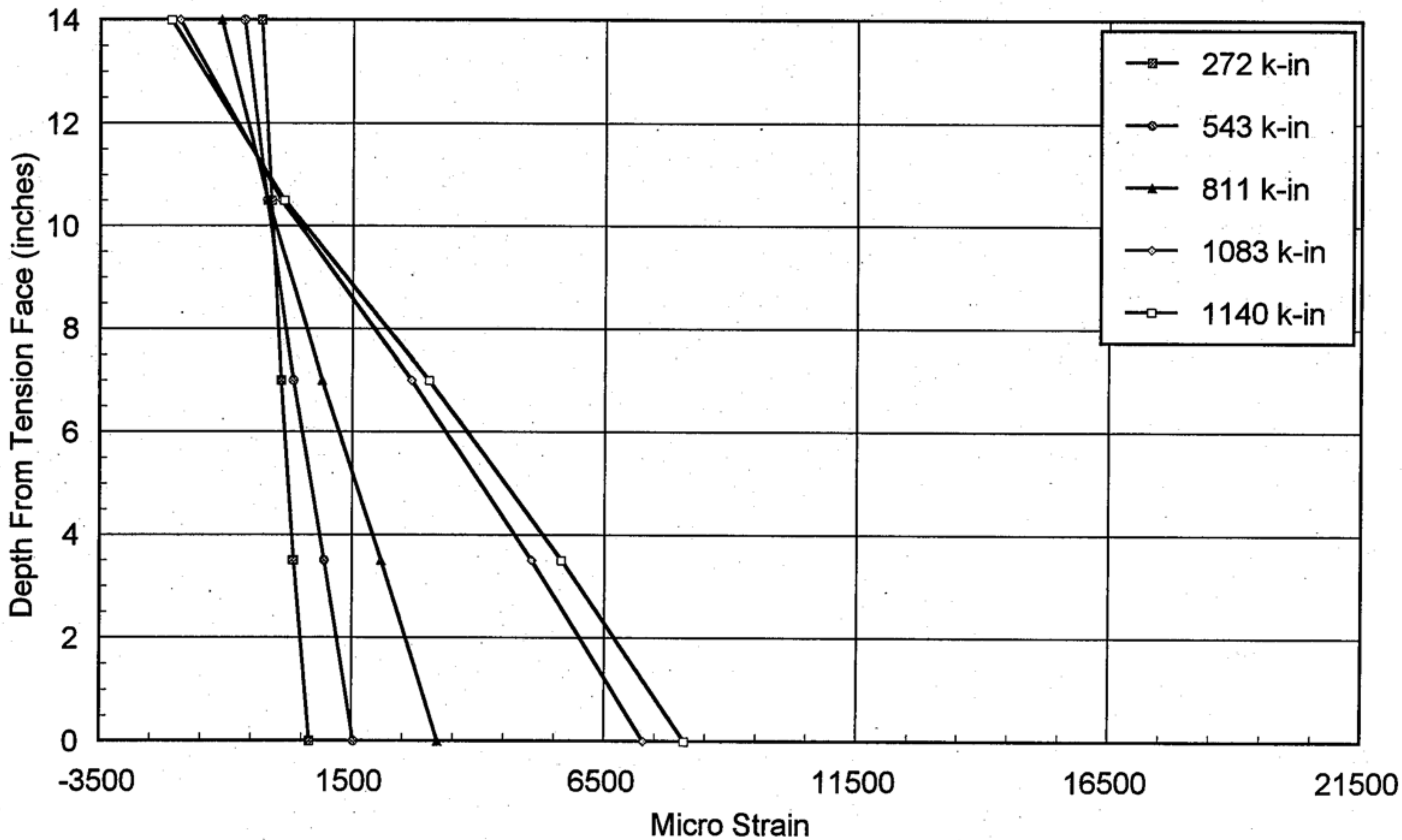

Fig. 3.23c - Center Line Strain Distribution

Specimen # BC-2L6-FL-2 (No Corbels)

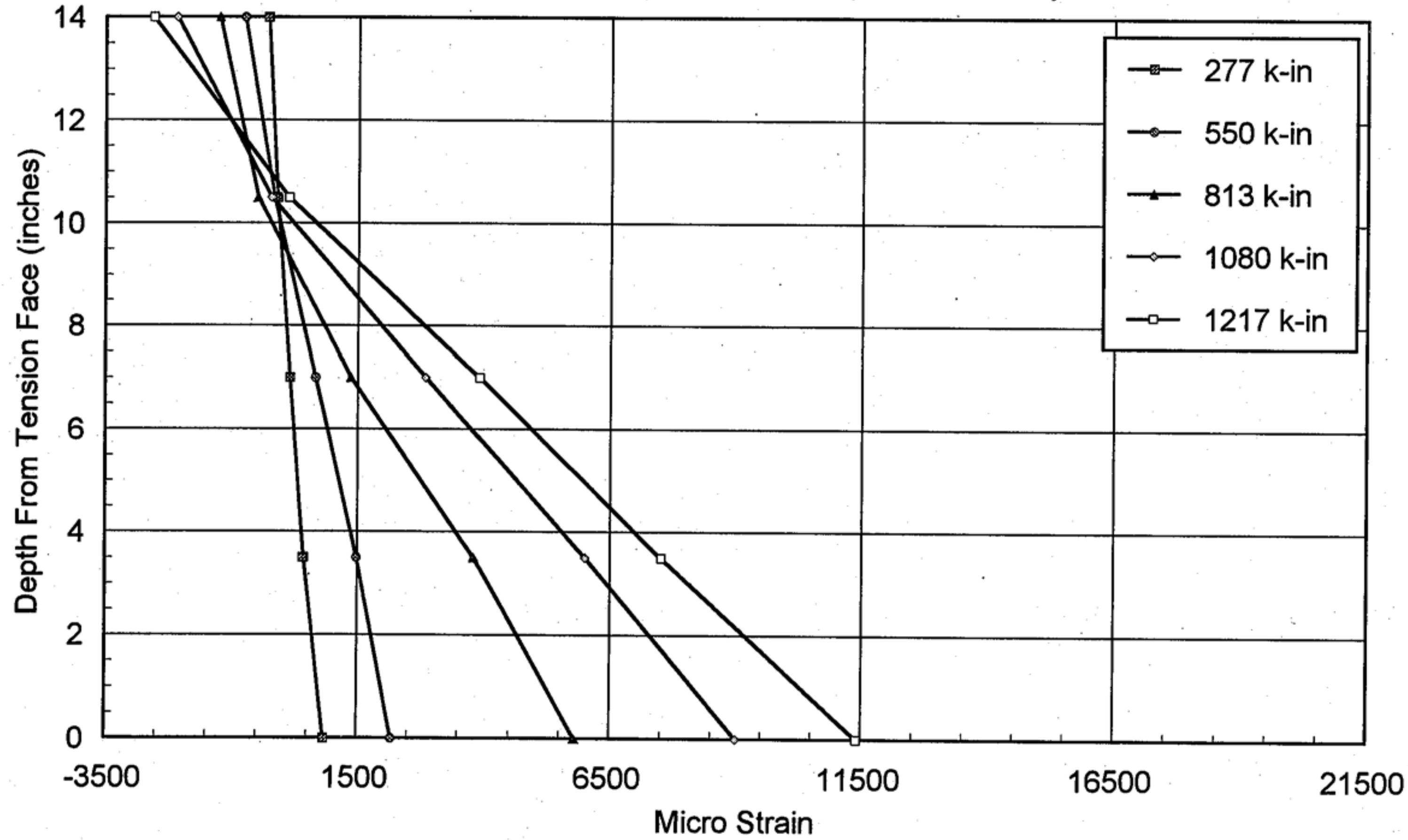

Fig. 3.23d - Center Line Strain Distribution

Specimen # BC-2L6-FL-3 (No Corbels)

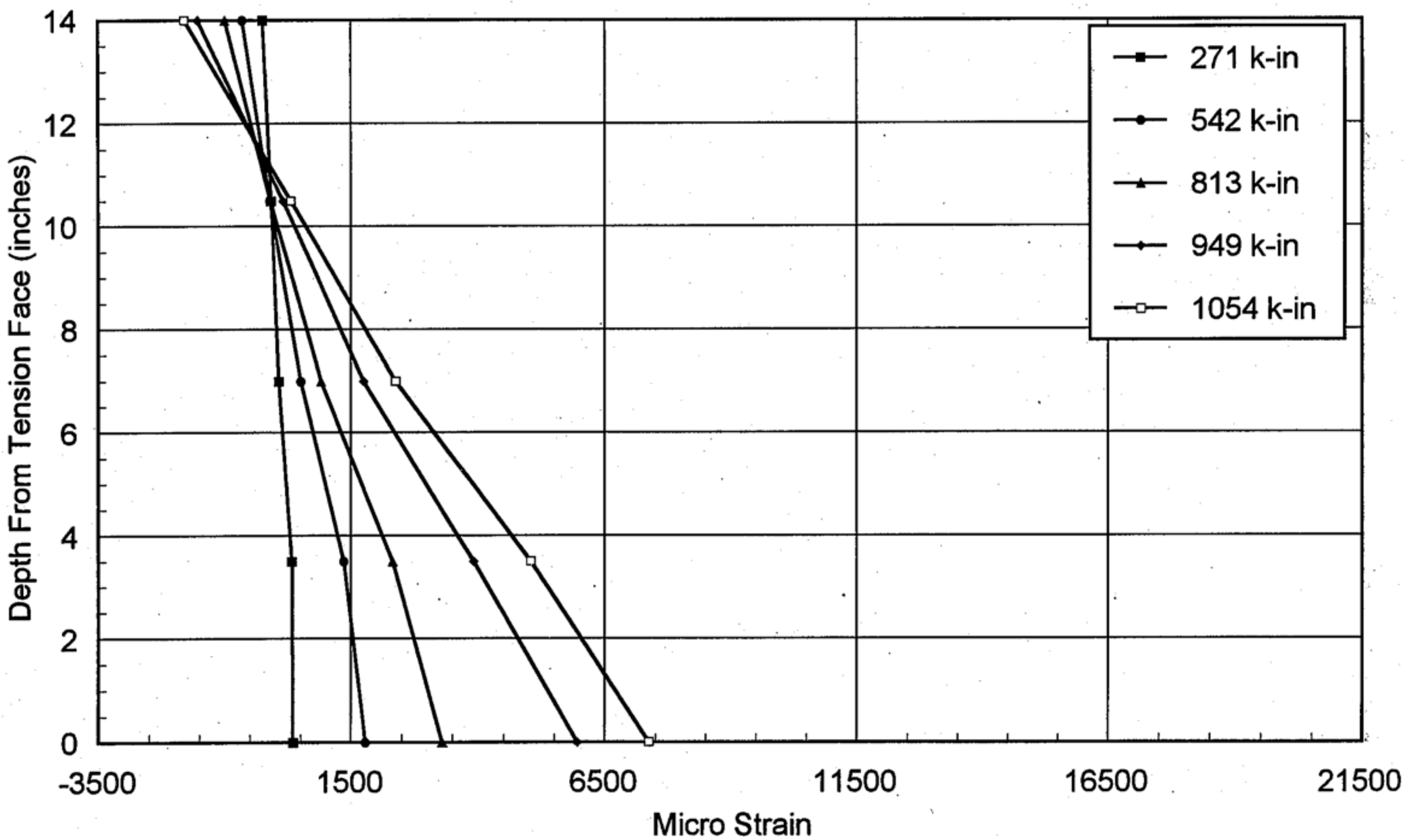

Fig. 3.24a - Moment VS. Strain At Midspan

Specimen # BC-0L6-FL (No Corbels)

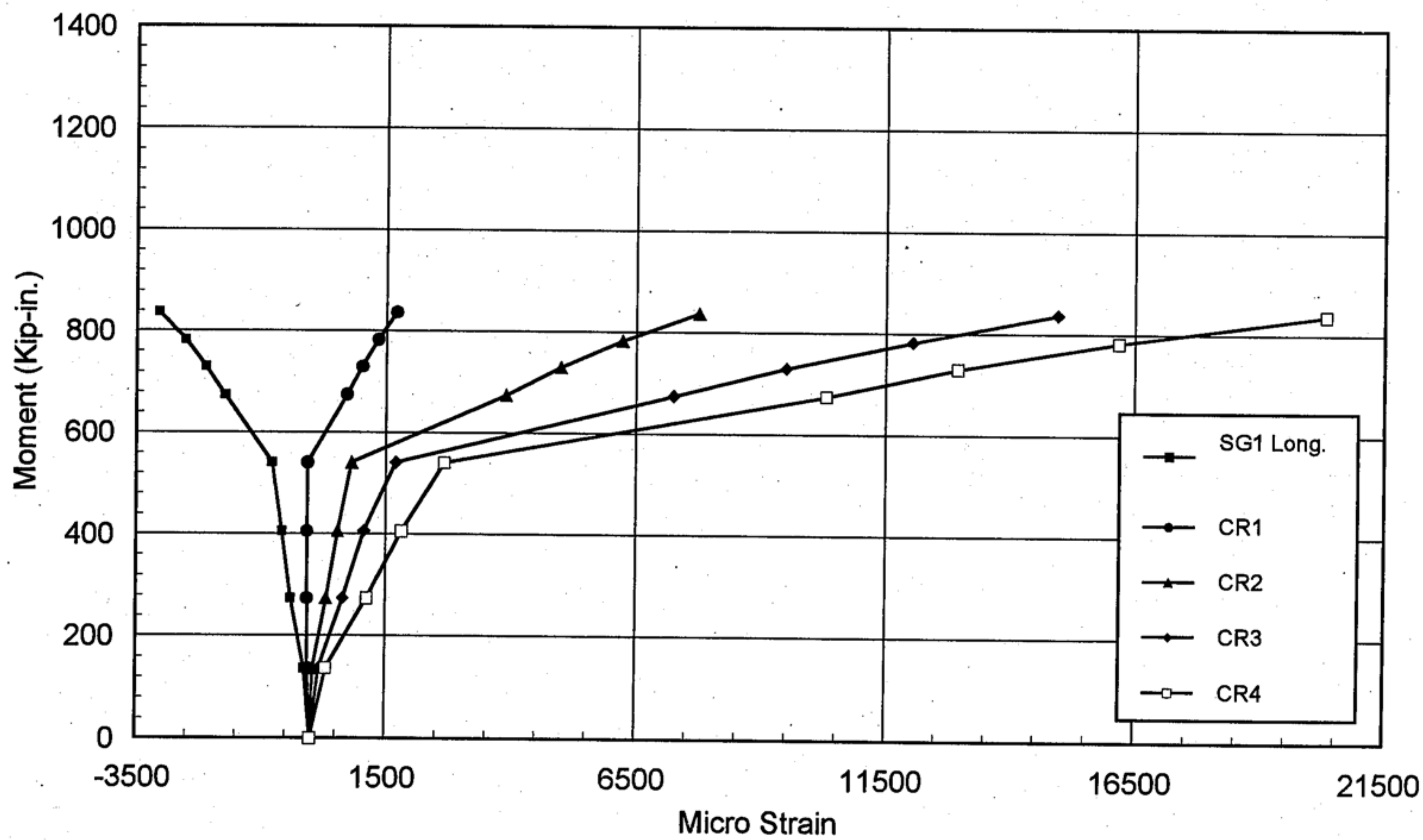

Fig. 3.24b - Momen tvs. Strain At Midspan

Specimen # BC-2L6-FL-1 (No Corbels)

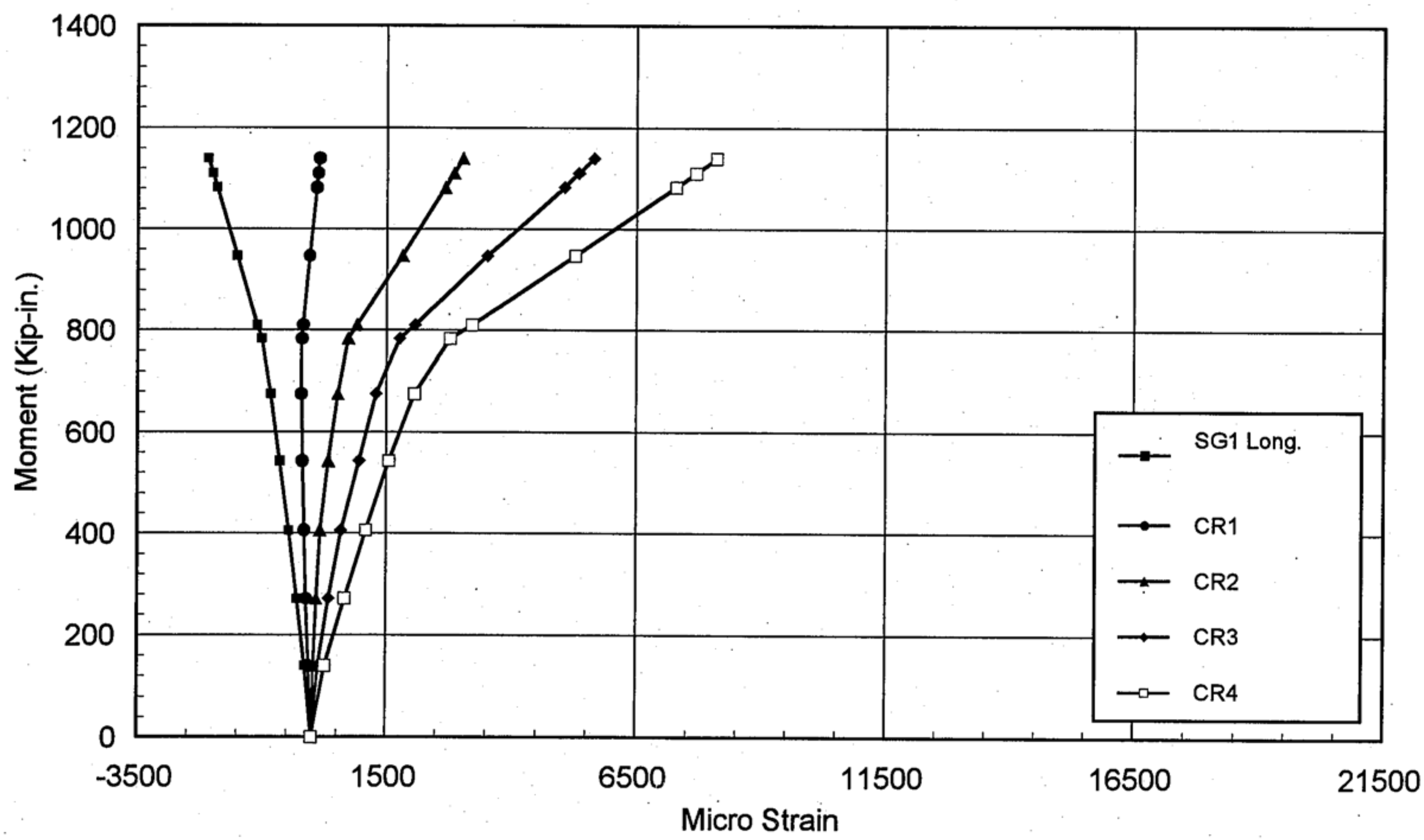

Fig. 3.24c - Moment vs. Strain At Midspan

Specimen # BC-2L6-FL-2 (No Corbels)

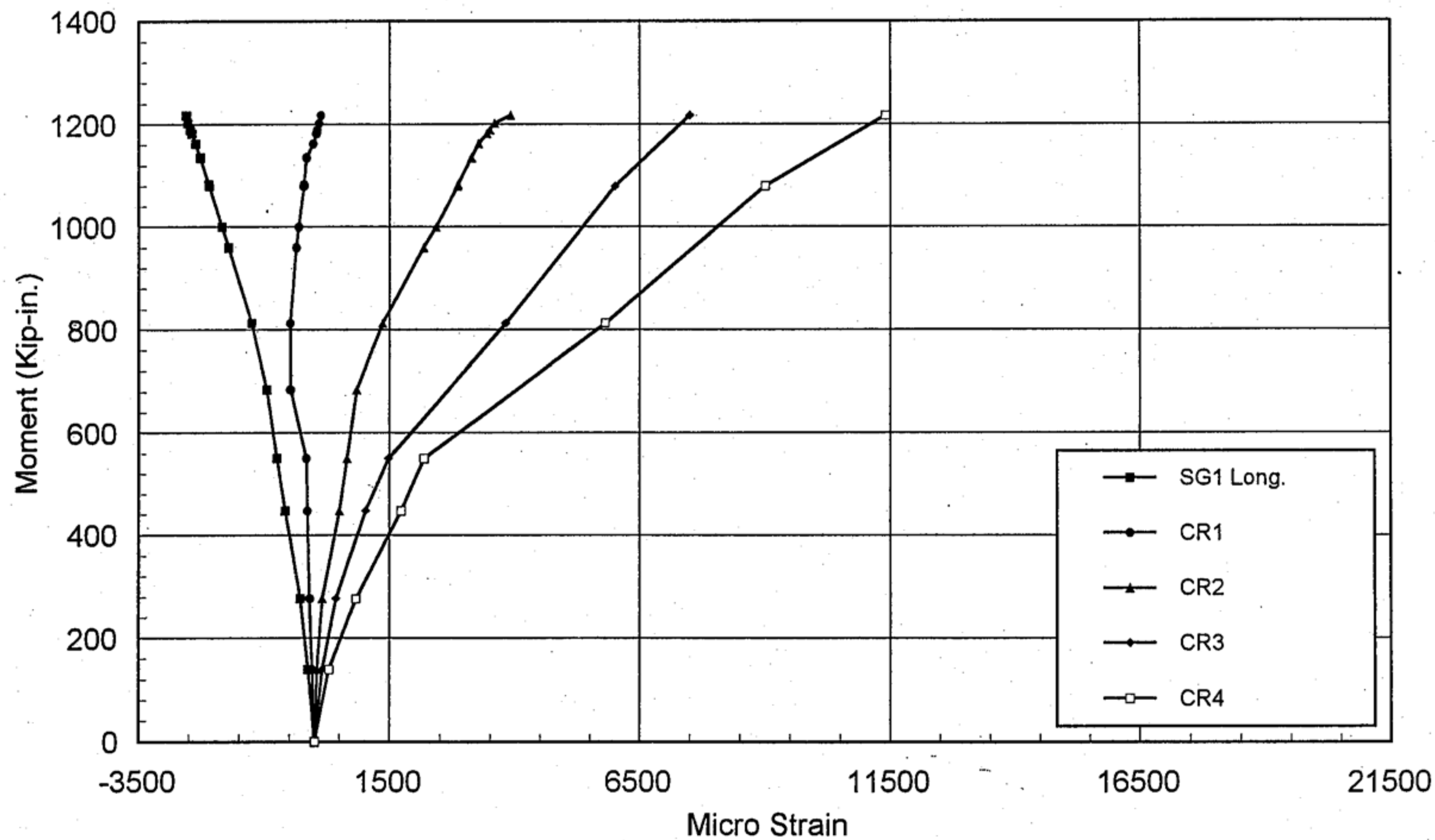

Fig. 3.24d - Moment vs. Strain At Midspan

Specimen # BC-2L6-FL-3 (No Corbels)

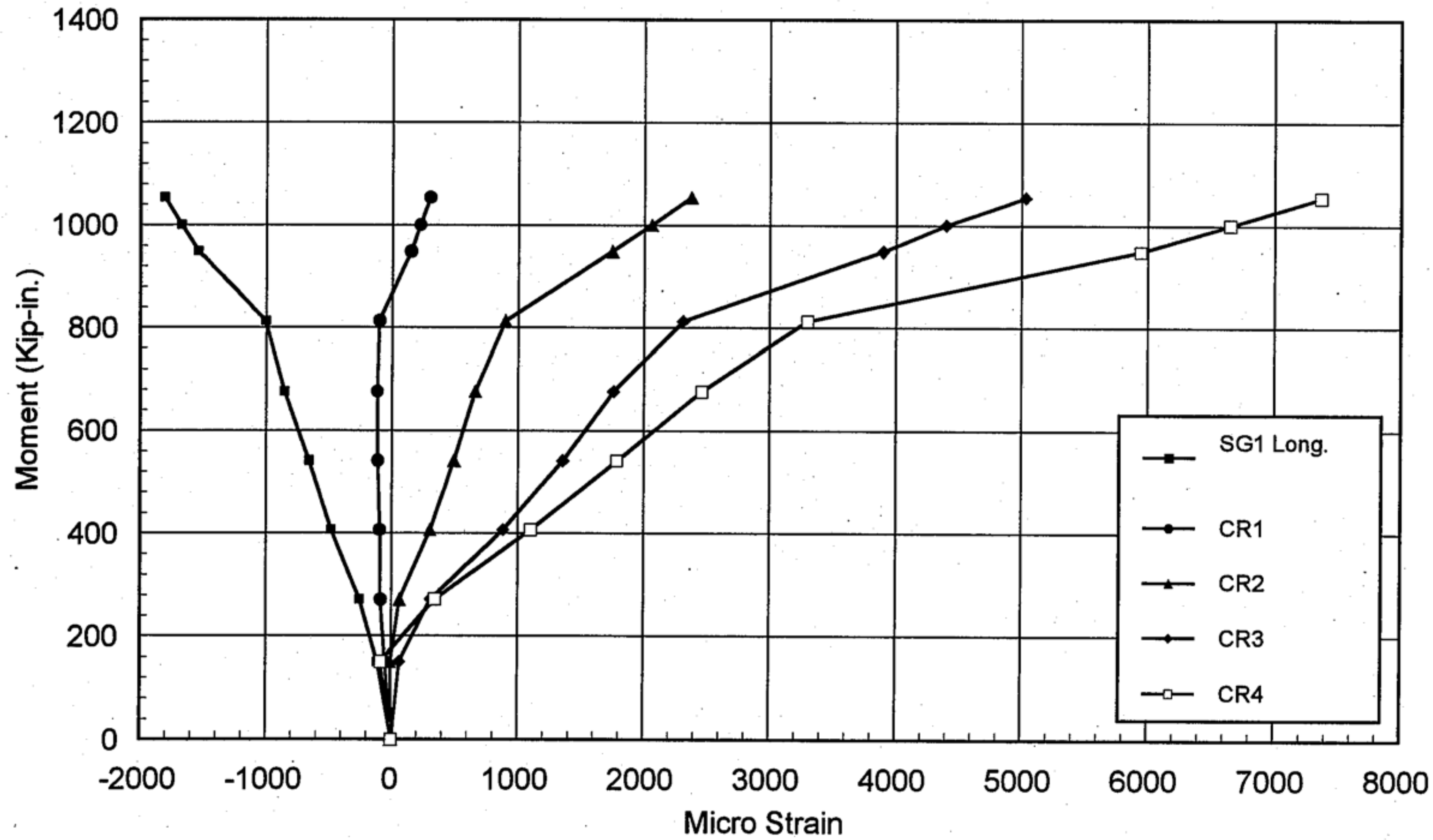

Fig. 3.25a - Moment vs.Transverse Strain At Midspan

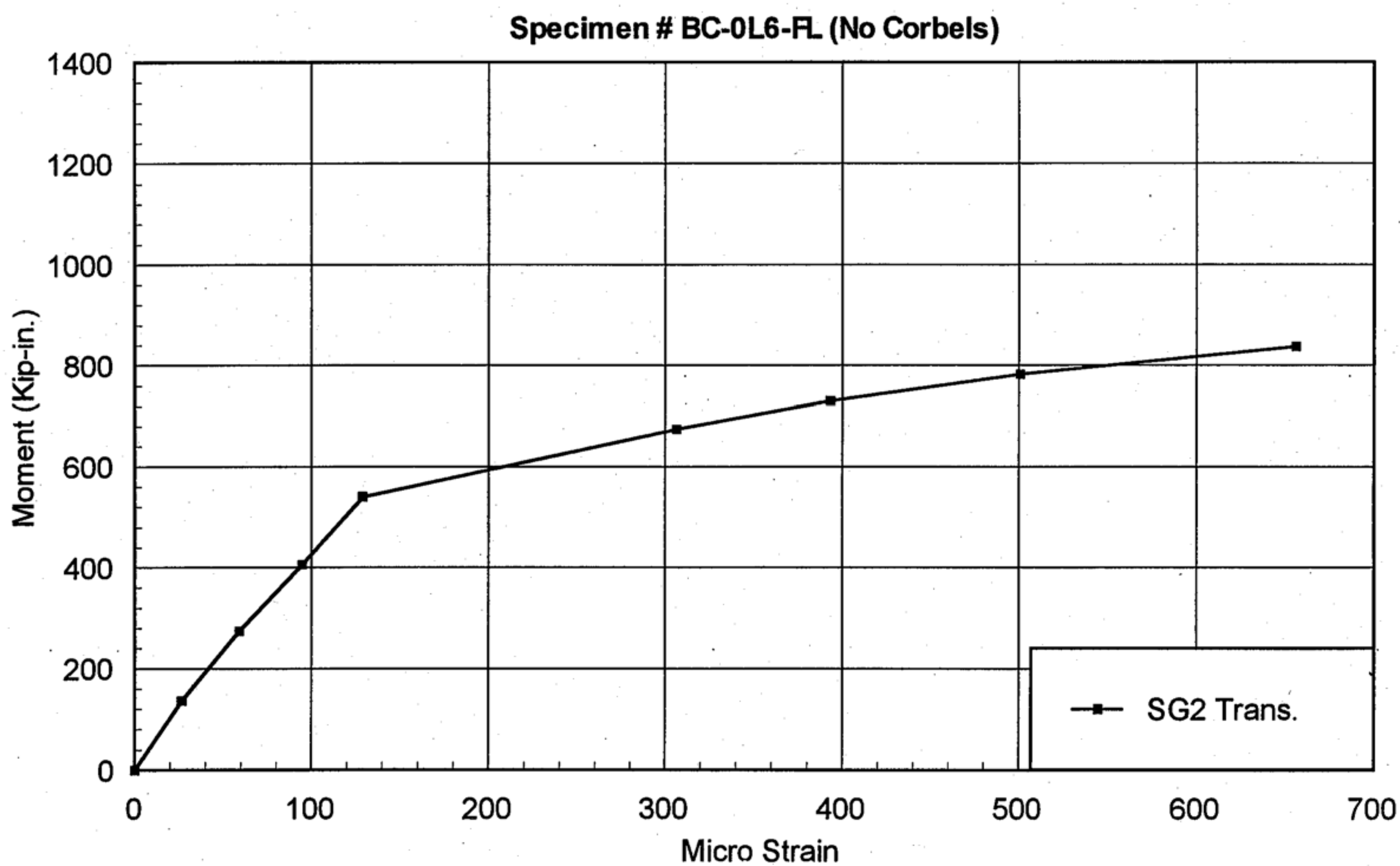

Fig. 3.25b - Moment vs. Transverse Strain At Midspan

Specimen # BC-2L6-FL-1 (No Corbels)

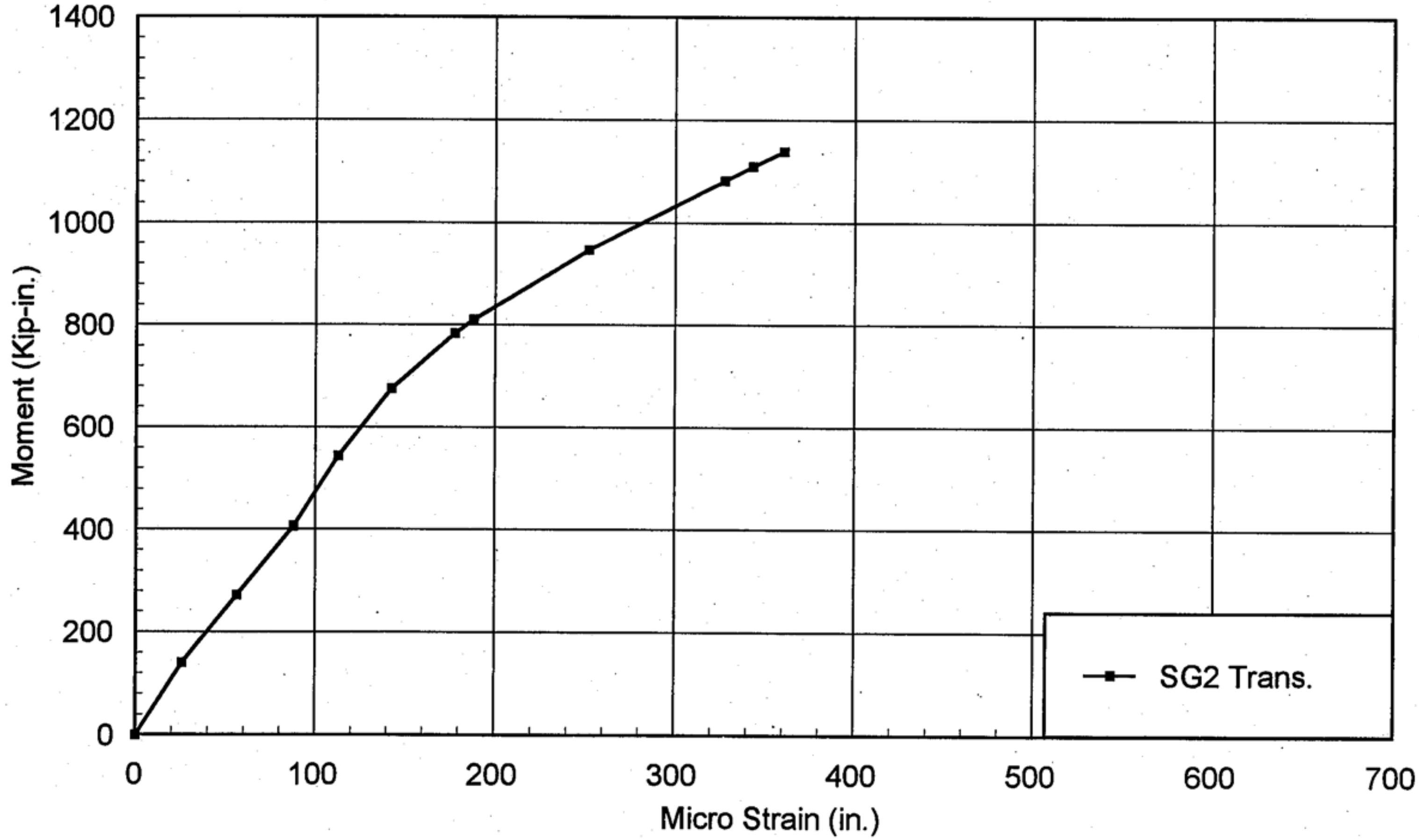

Fig. 3.25c - Moment vs.Transverse StrainAt Midspan

Specimen # BC-2L6-FL-2 (No Corbels)

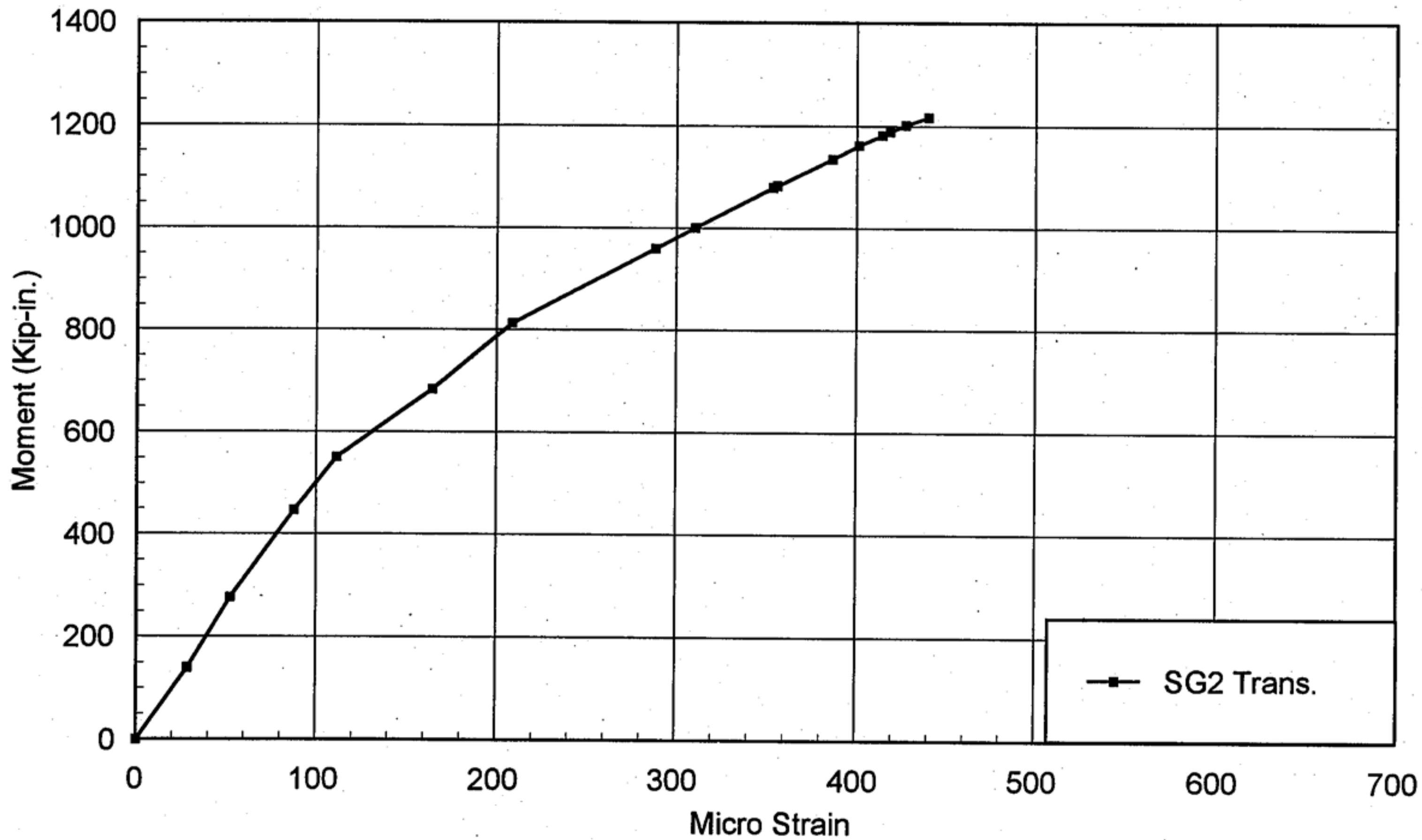

Fig. 3.25d - Moment vs. Transverse Strain At Midspan

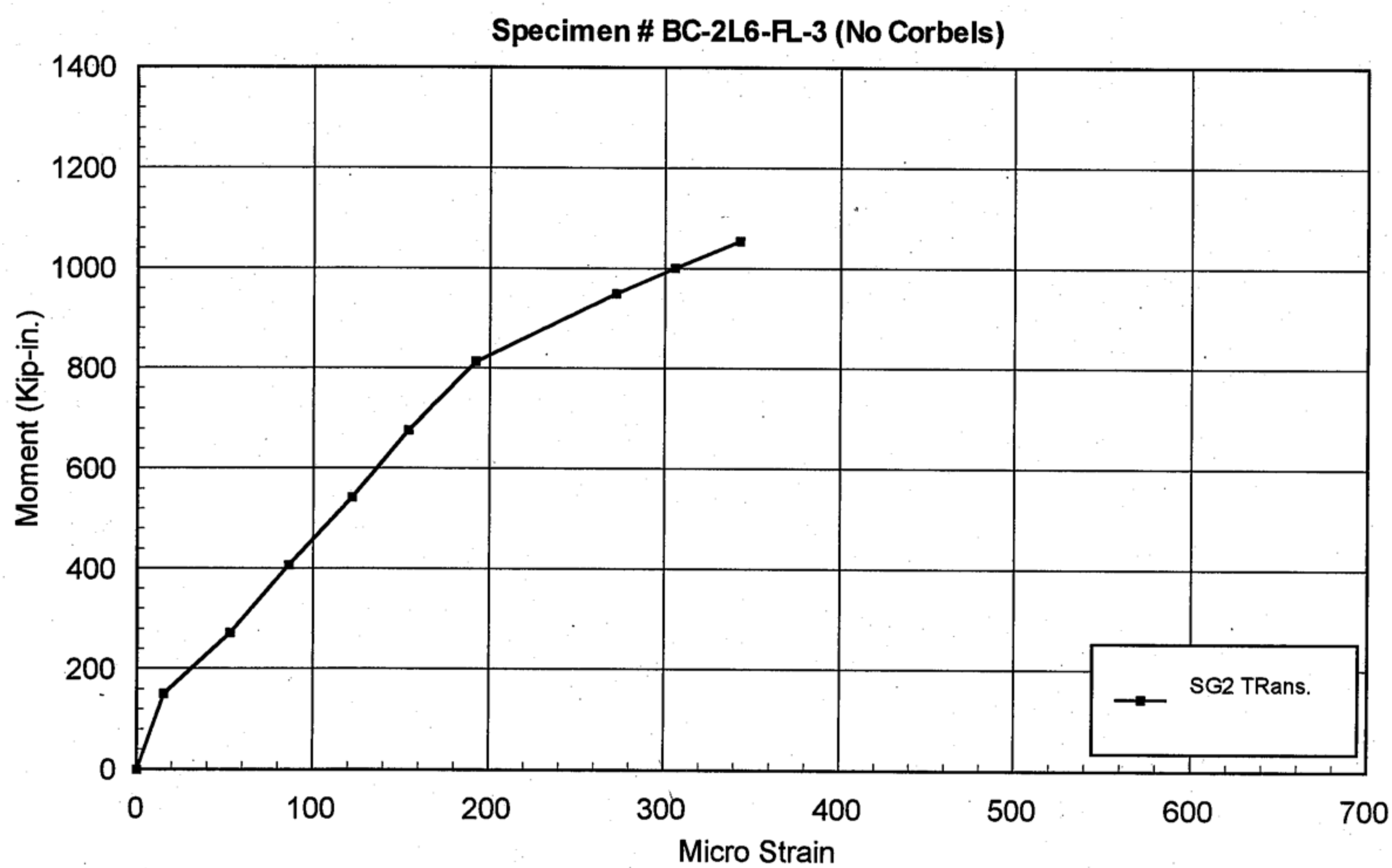

Fig. 4.1(a) – Typical failure mode for wrapped specimens subjected to high axial loading in addition to flexure

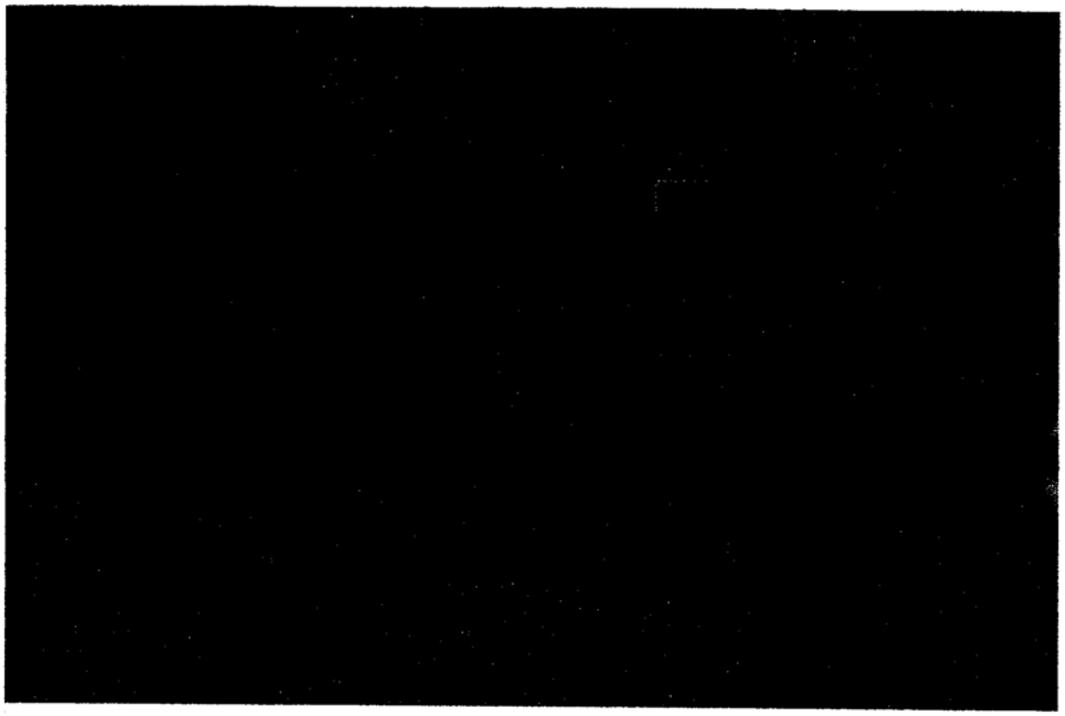

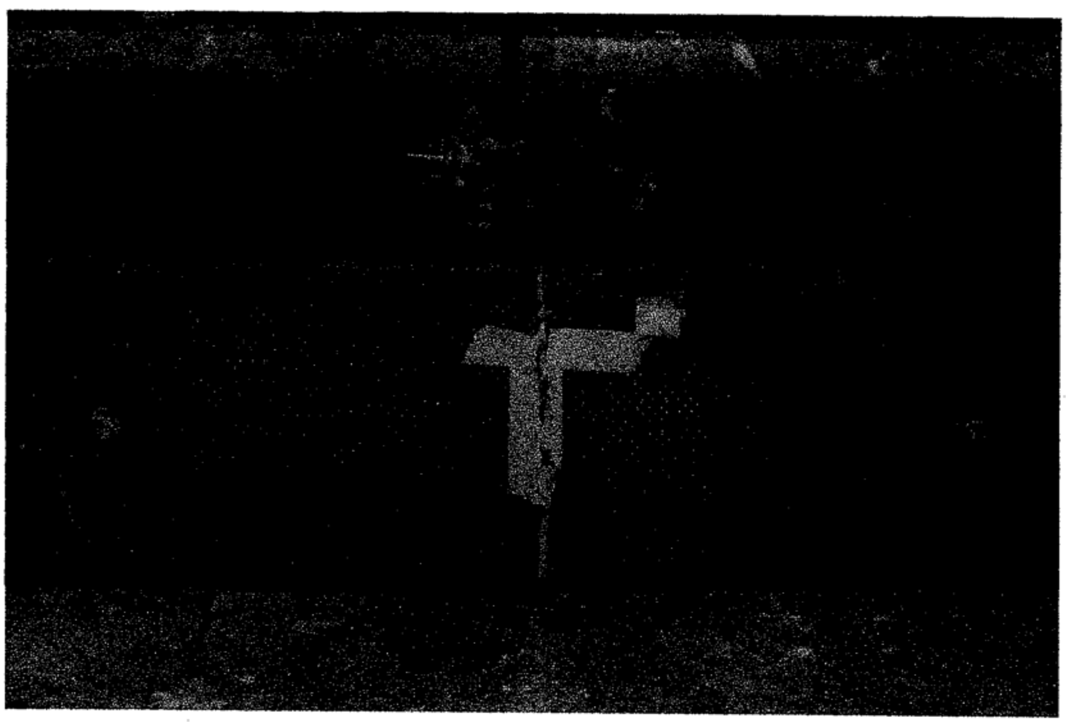

Fig. 4.1(b) – Typical failure mode for wrapped specimens controlled by flexure

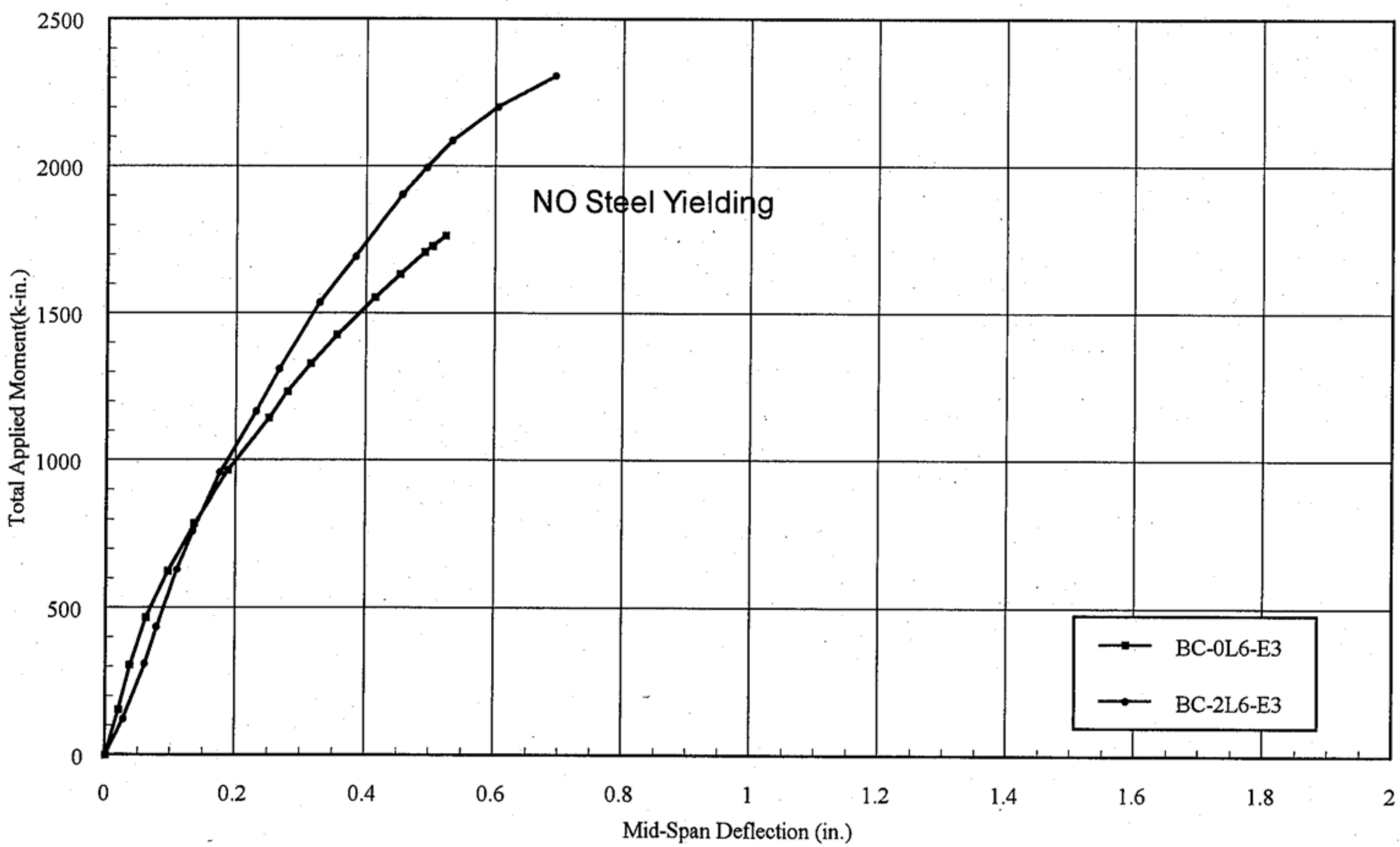

Fig. 4.2 - Total Applied Moment Versus Mid-Span Deflection
(a) Eccentricity=3"

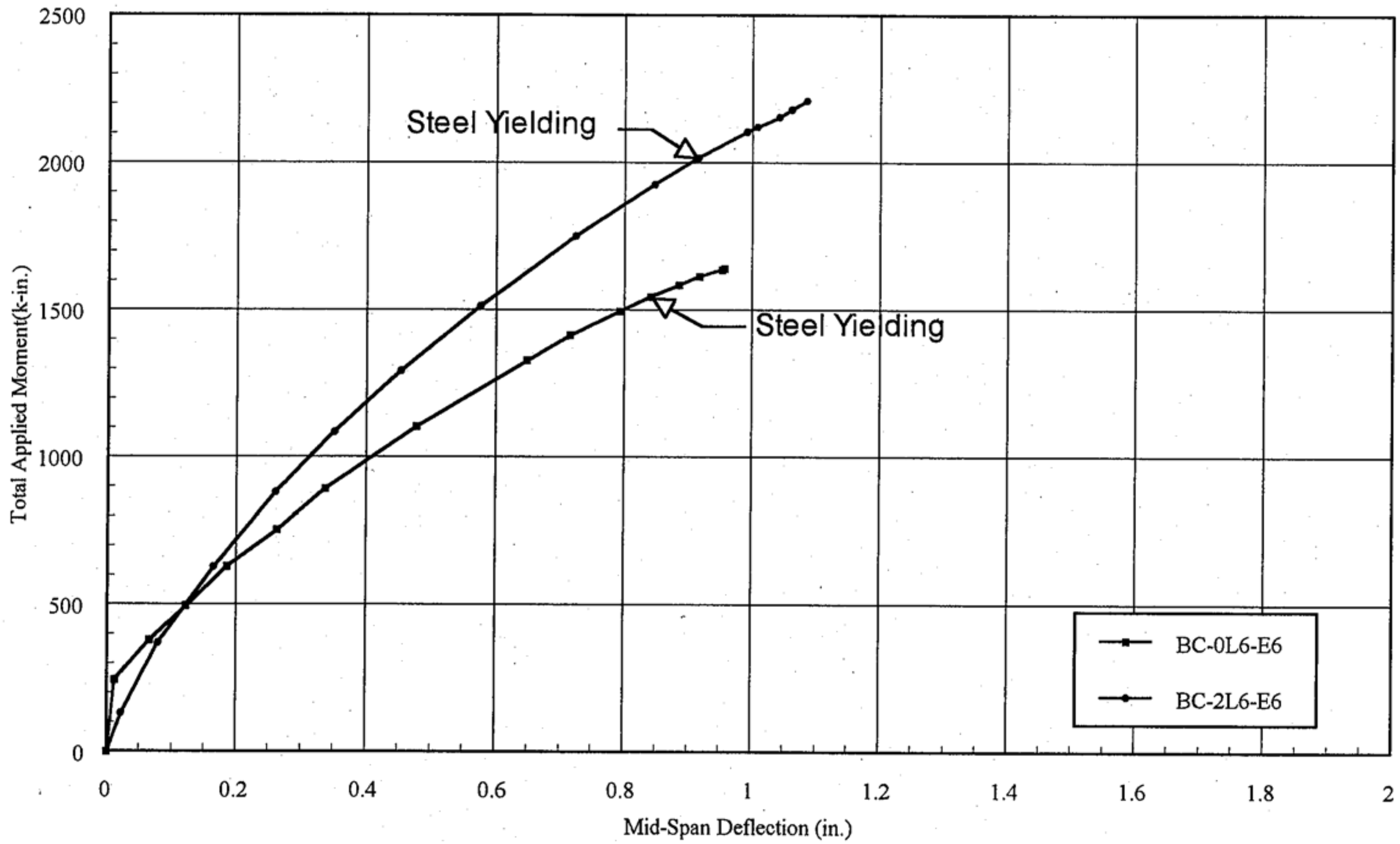

Fig. 4.2 - Total Applied Moment Versus Mid-Span Deflection
(b) Eccentricity=6"

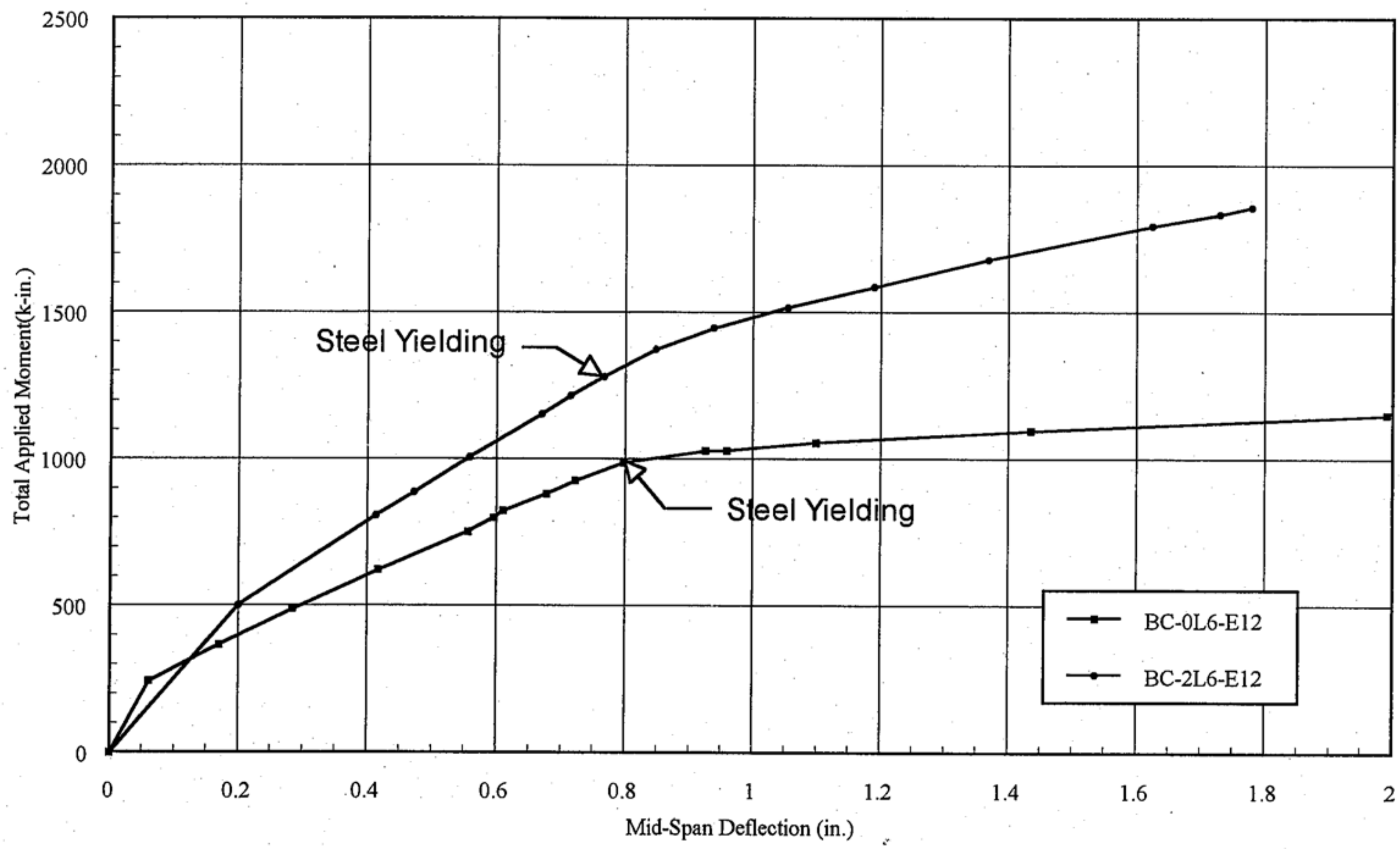

Fig. 4.2 - Total Applied Moment Versus Mid-Span Deflection
(c) Eccentricity=12"

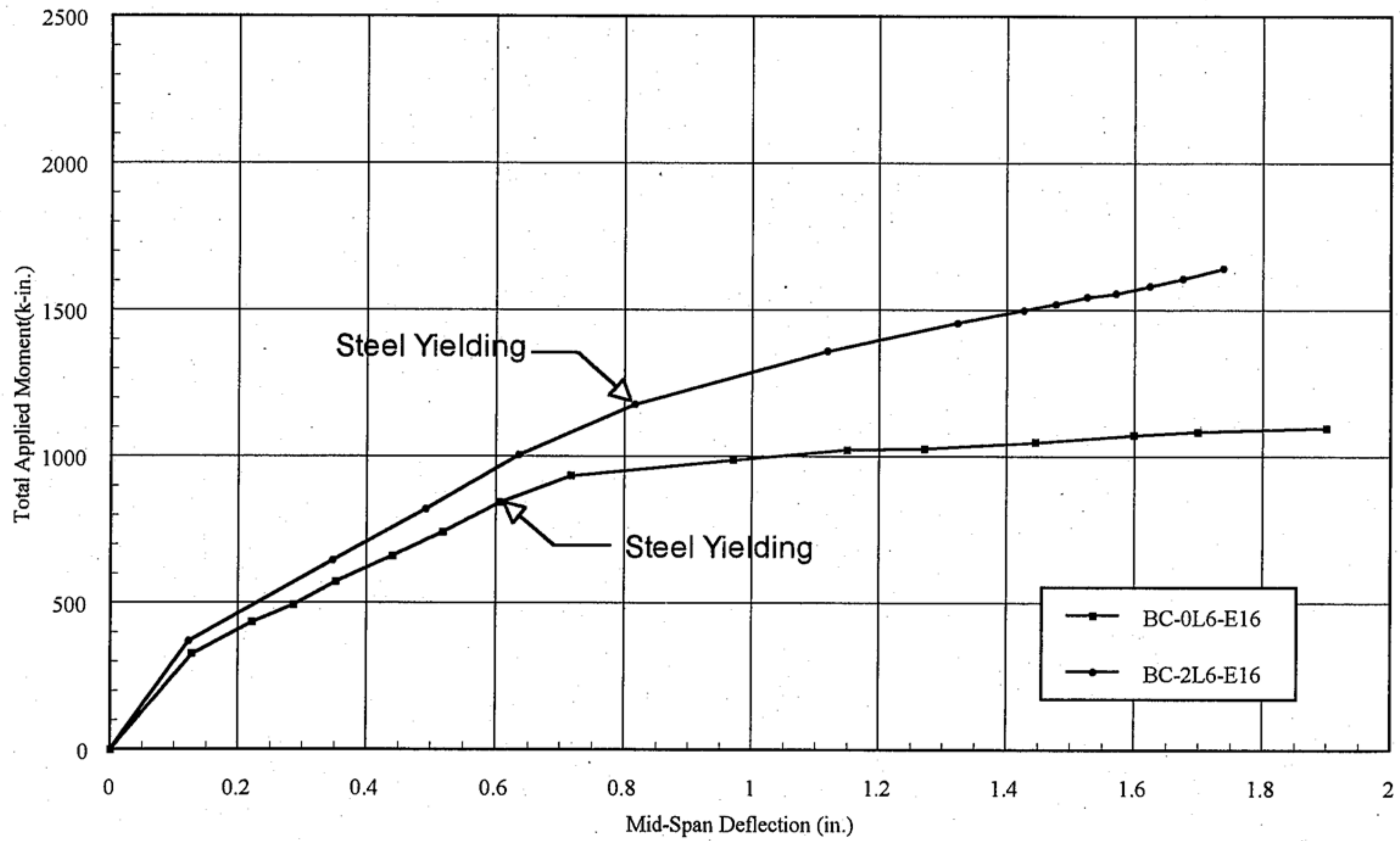

Fig. 4.2 - Total Applied Moment Versus Mid-Span Deflection
(d) Eccentricity=16"

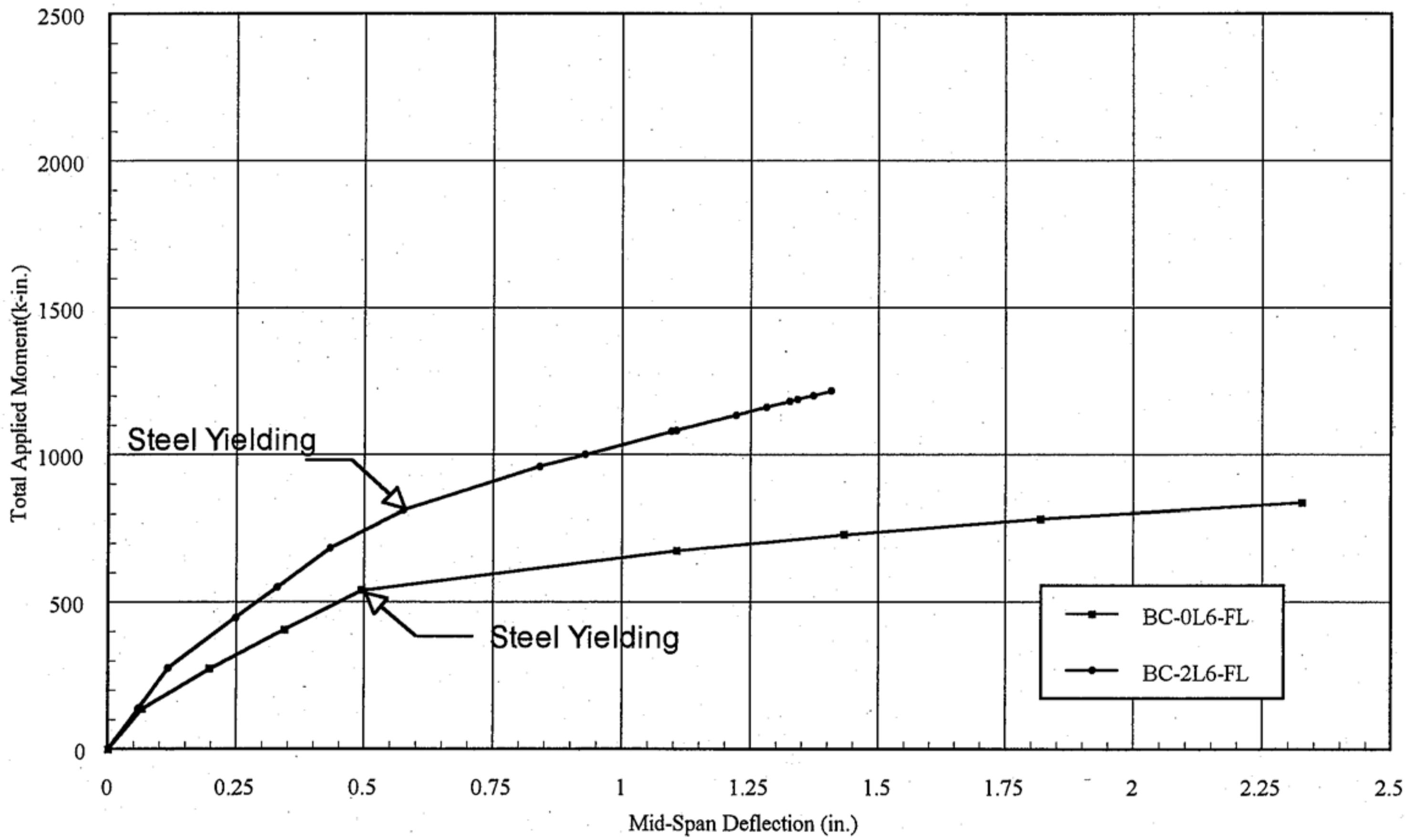

Fig. 4.2 - Total Applied Moment Versus Mid-Span Deflection
(e) Pure Bending

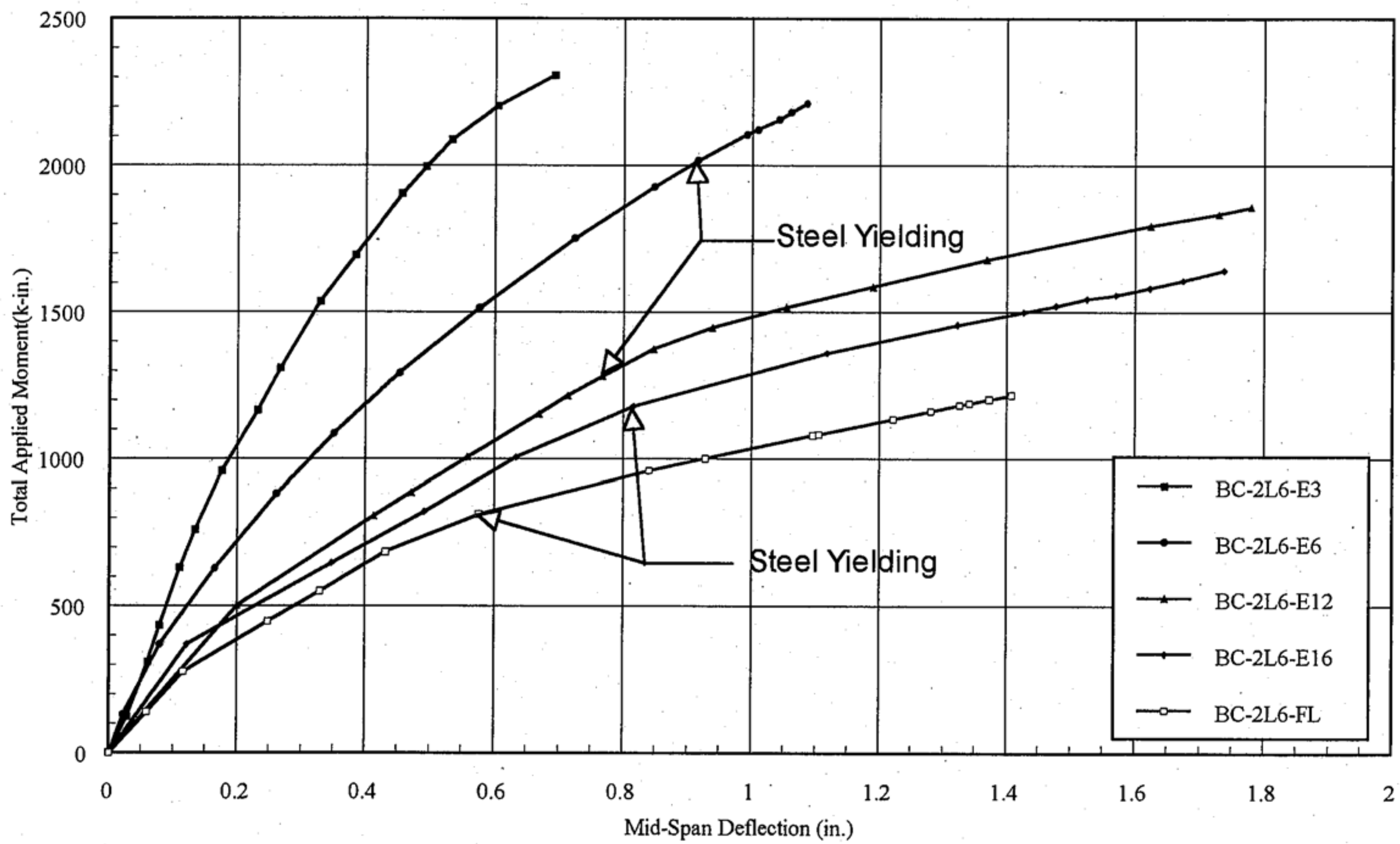

Fig. 4.3 - Effect of Eccentricity on Moment-Deflection Curves of Wrapped Columns

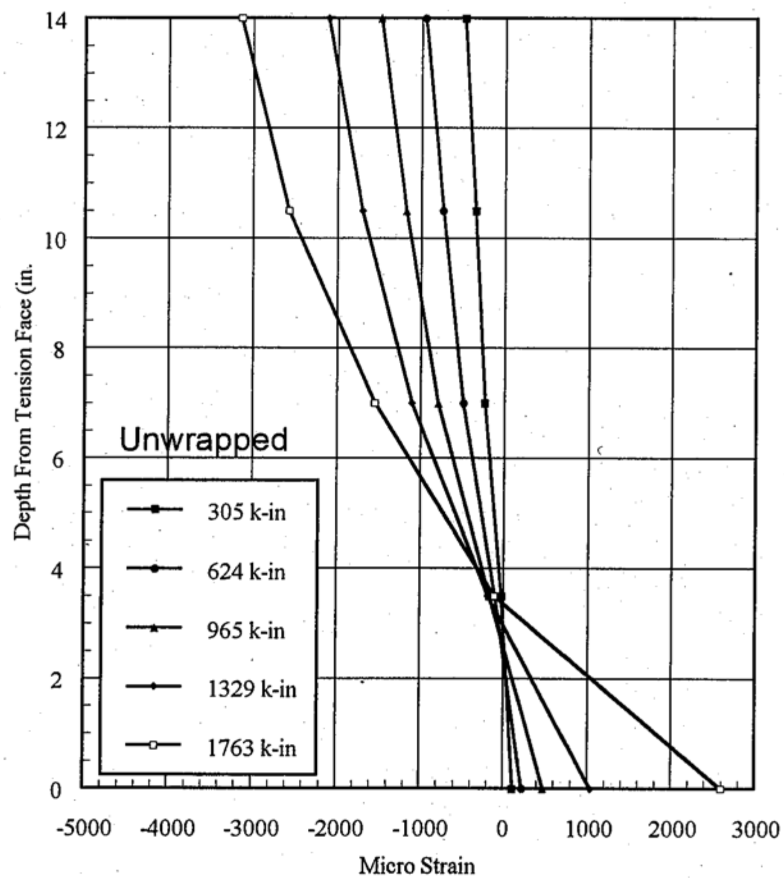

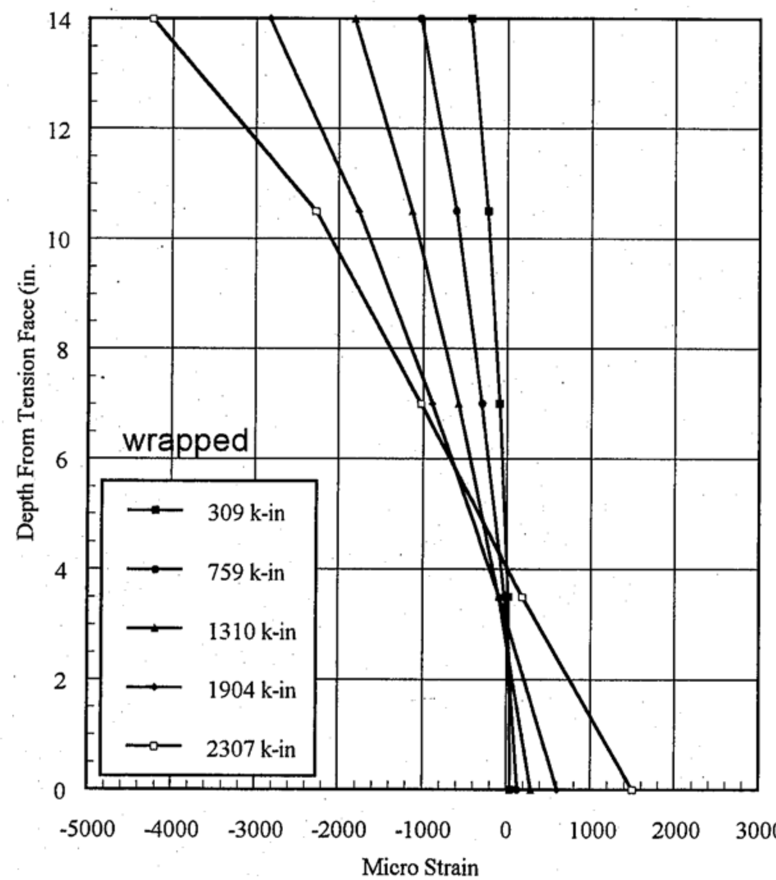

Fig. 4.4 - Longitudinal Strain Distribution At Mid - Span
(a) Eccentricity=3"

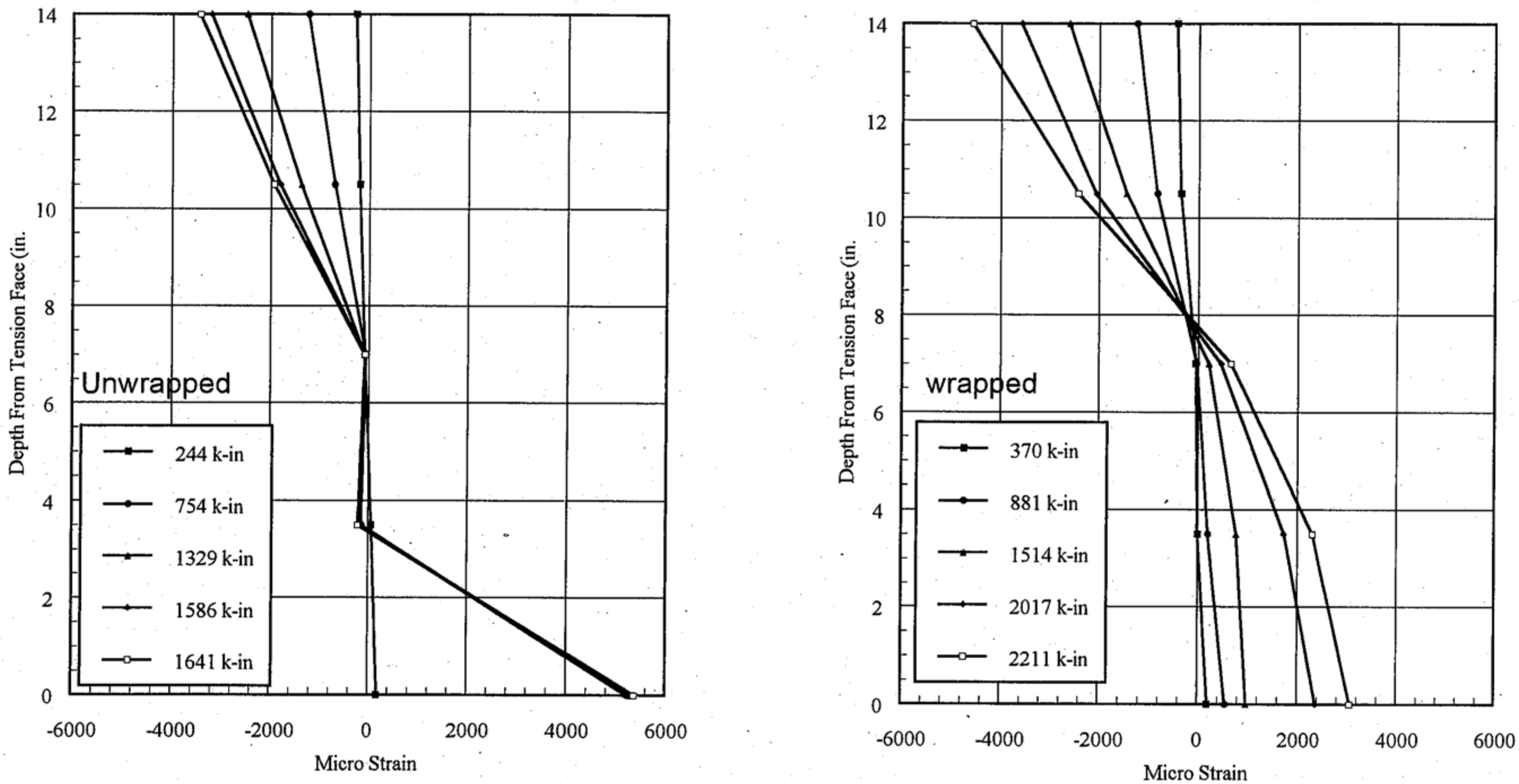

Fig. 4.4 - Longitudinal Strain Distribution At Mid - Span
(b) Eccentricity=6"

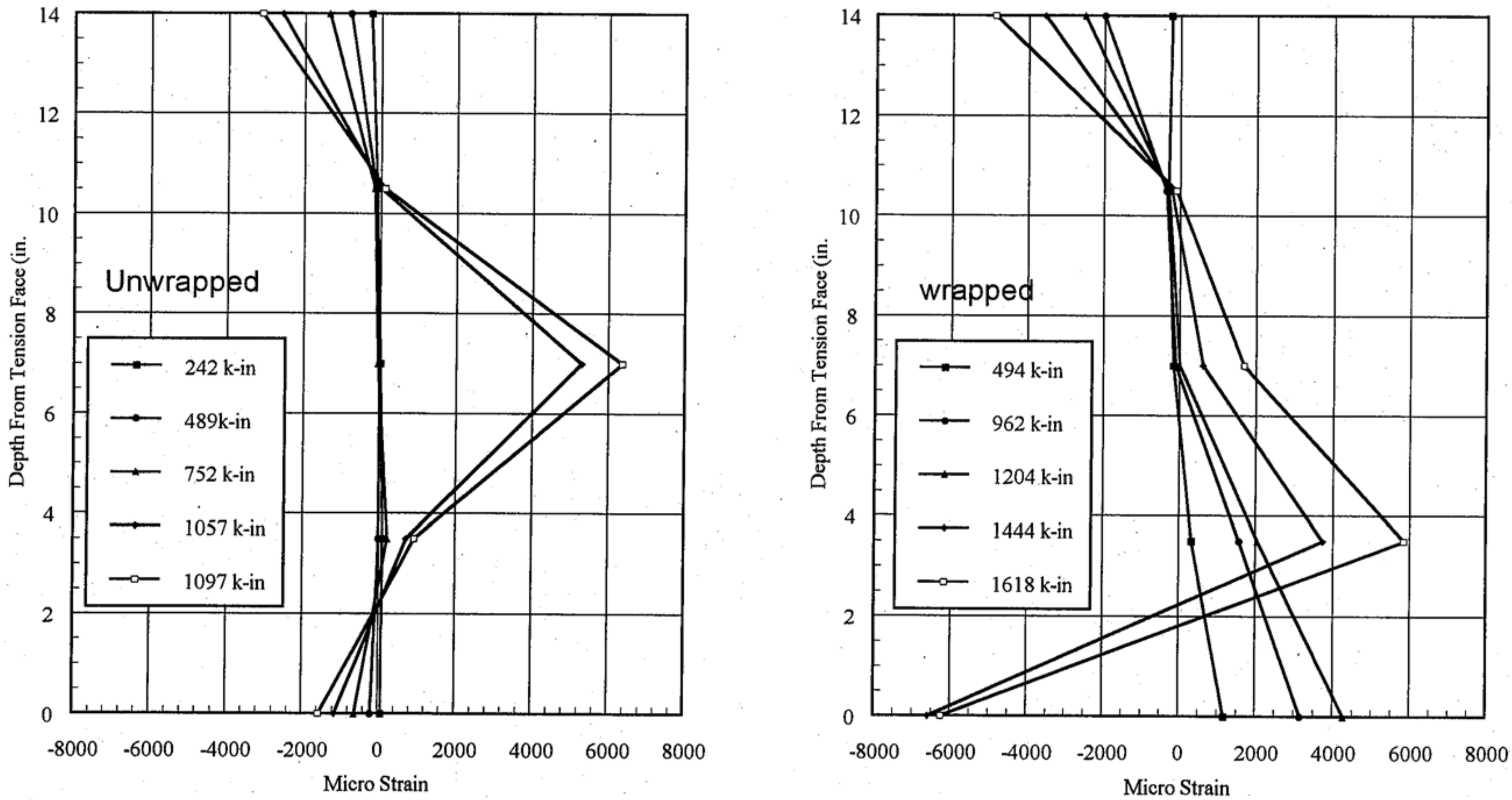

Fig. 4.4 - Longitudinal Strain Distribution At Mid - Span
(c) Eccentricity=12"

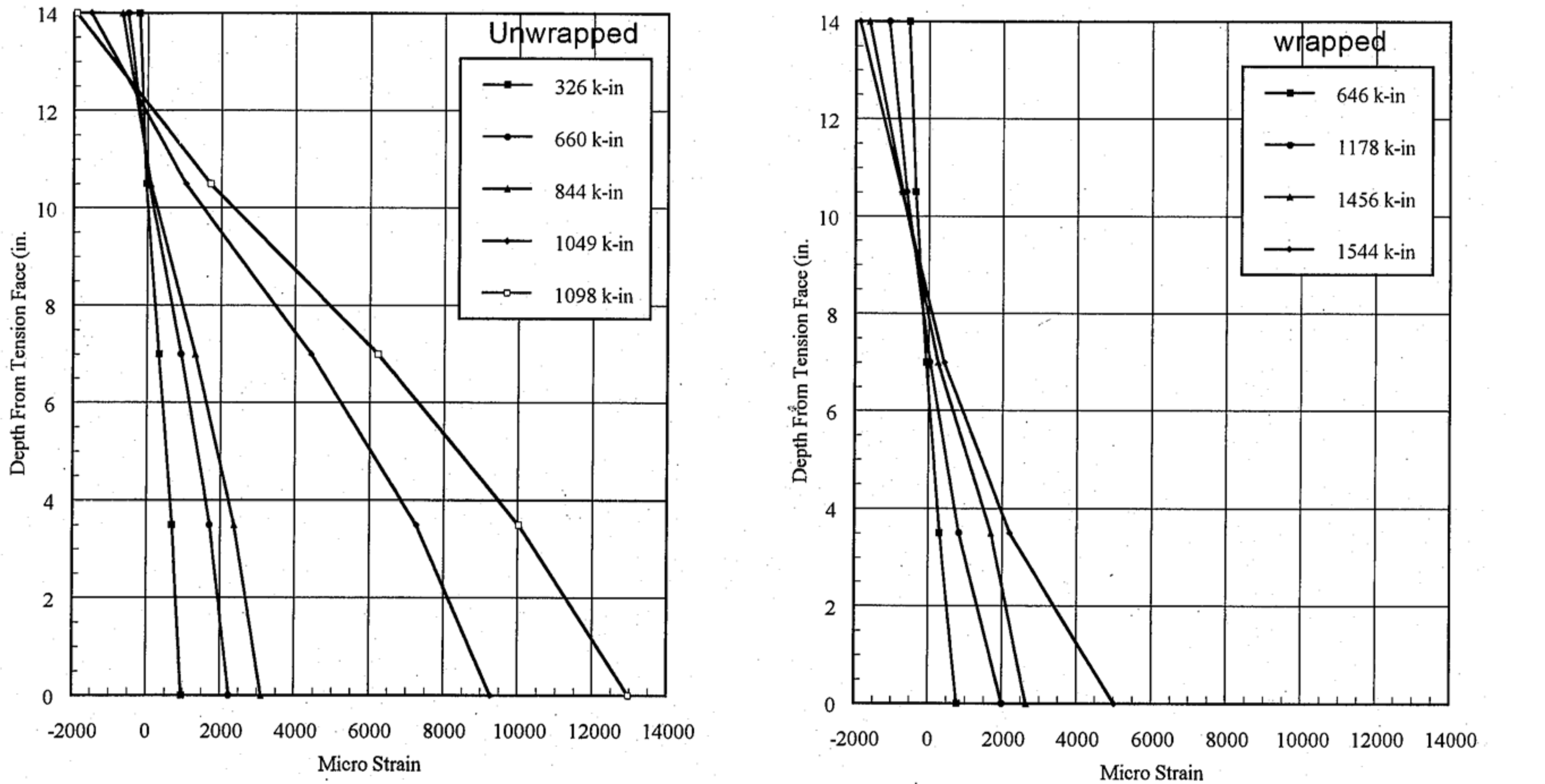

Fig. 4.4 - Longitudinal Strain Distribution At Mid - Span
(d) Eccentricity=16"

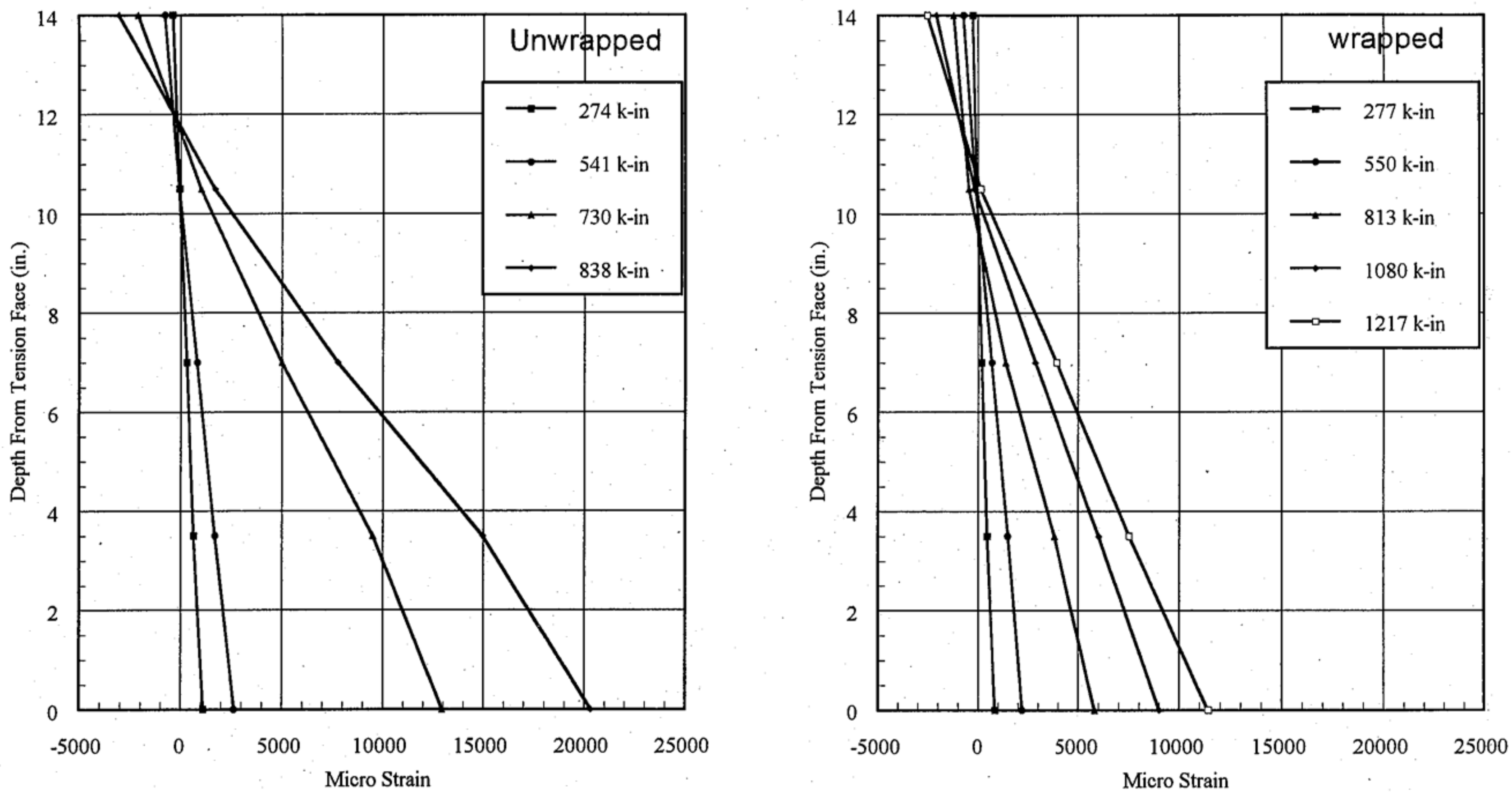

Fig. 4.4 - Longitudinal Strain Distribution At Mid - Span
(e) Pure Bending

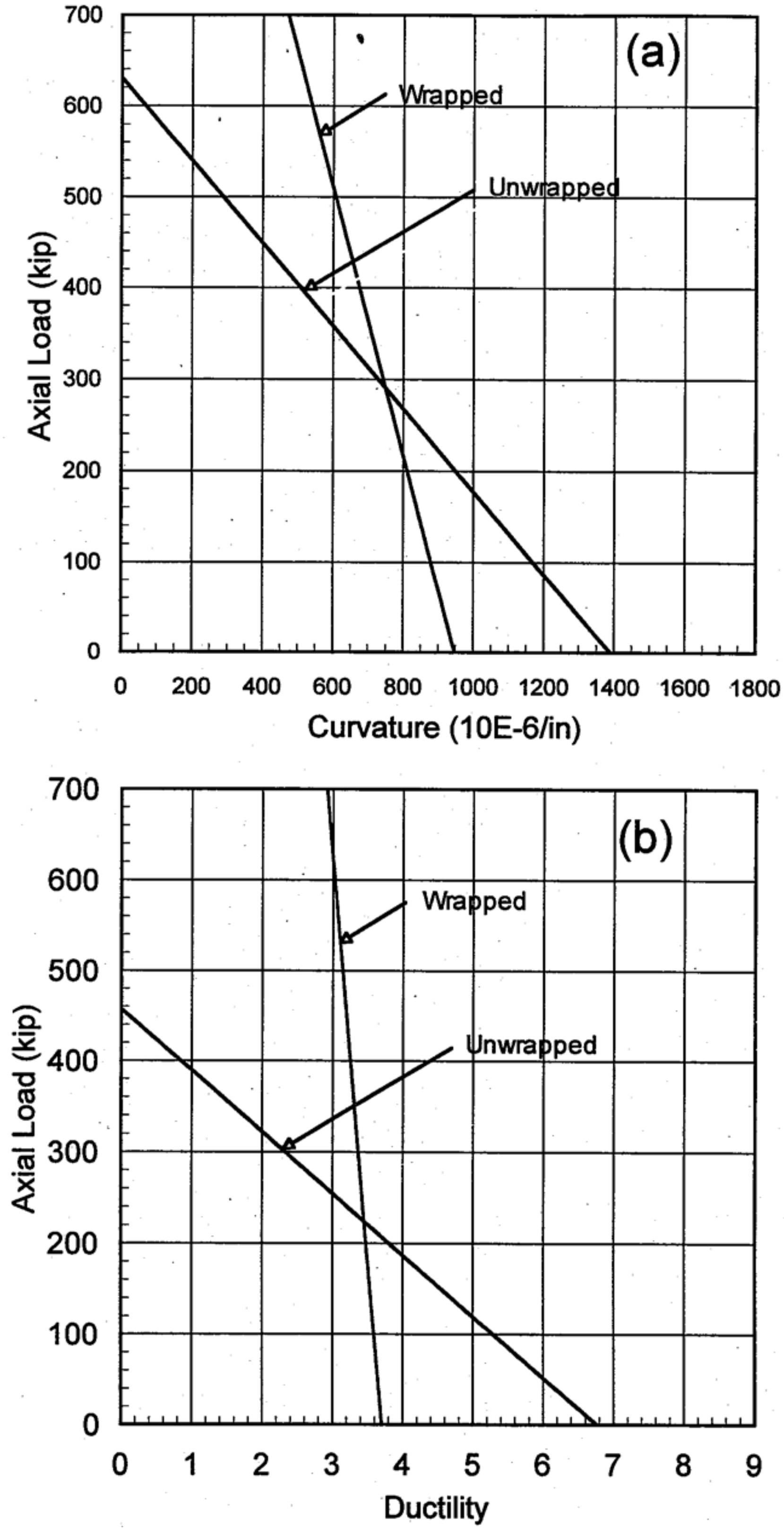

Fig. 4.5 - Axial Load verses curvature (a) and Ductility (b)

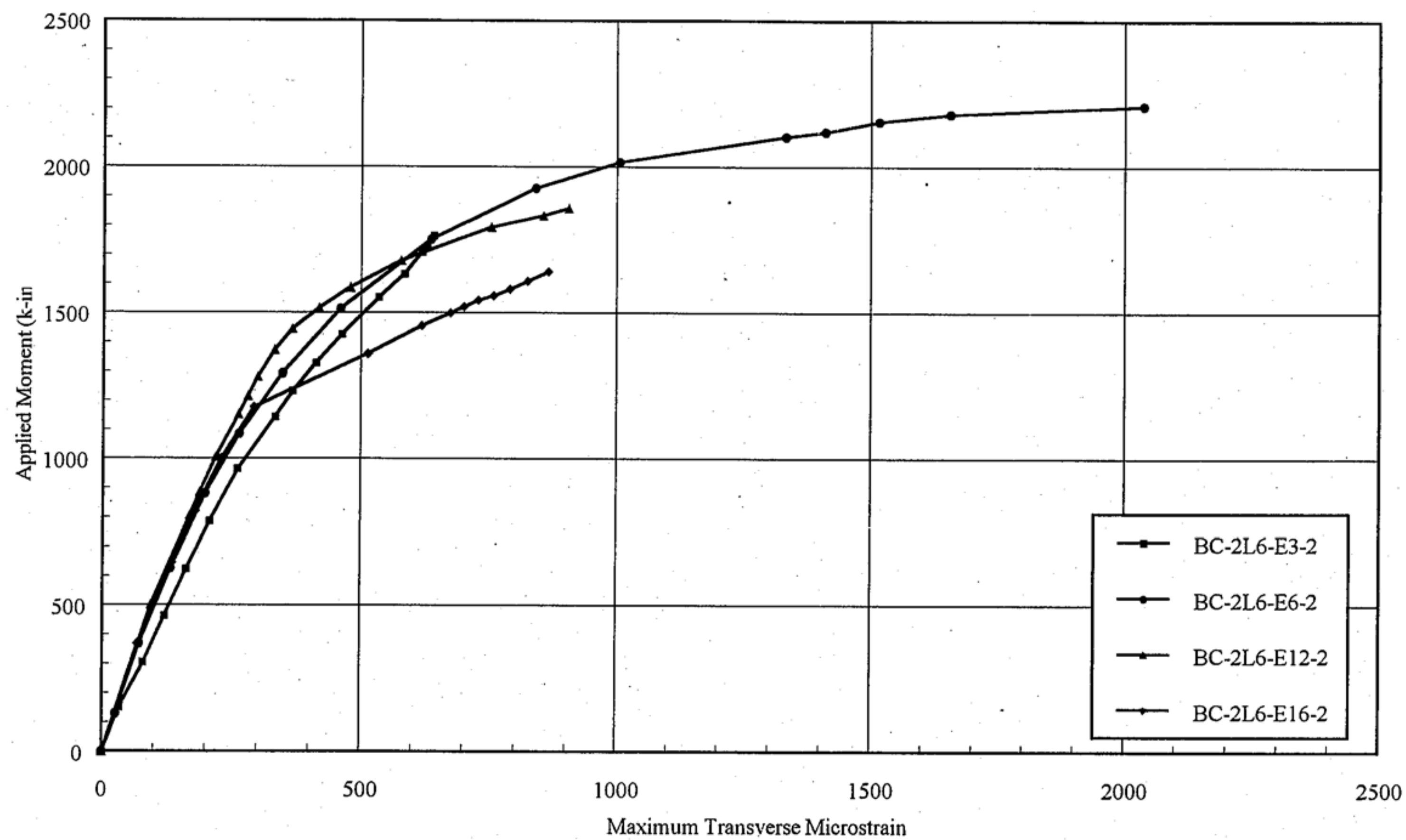

Fig. 4.6 - Applied Moment verses Mid-Span Transverse Stain

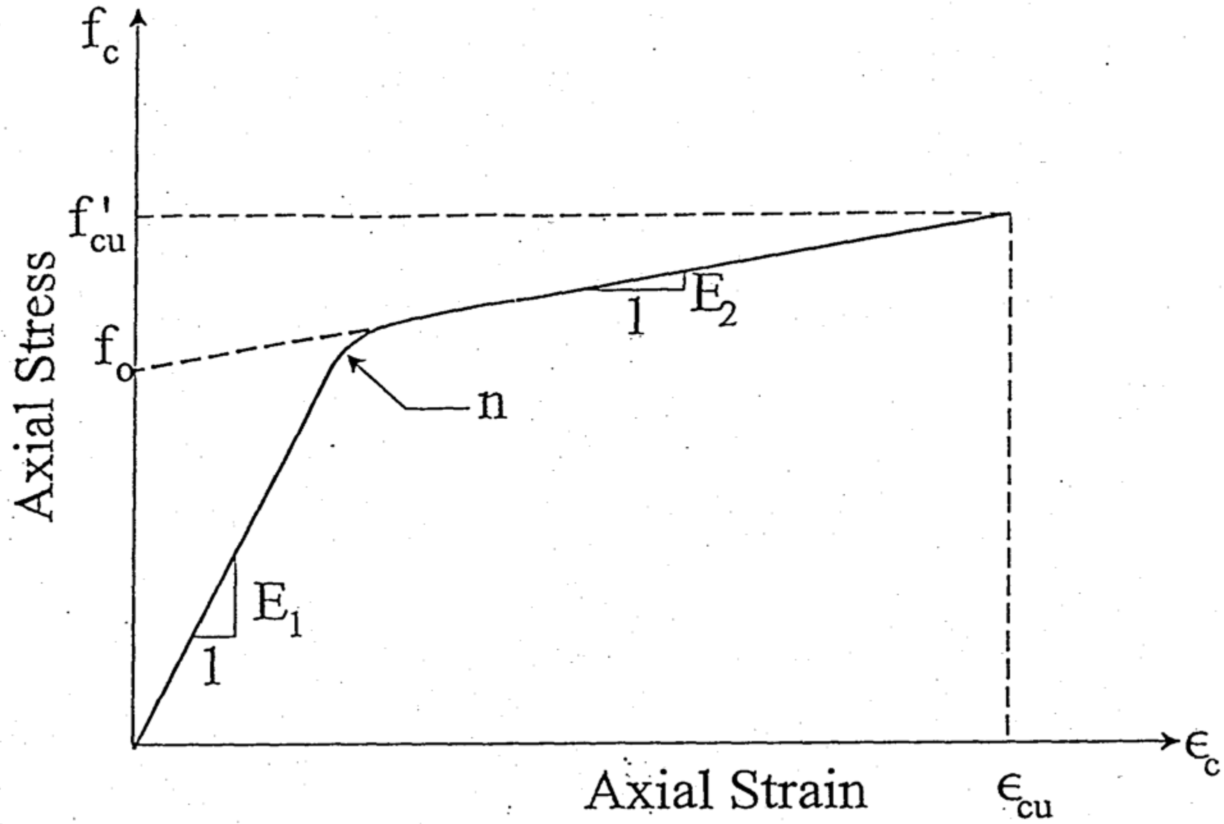

Fig. 4.7 Parameters of the Confinement Model for Wrapped Circular Columns

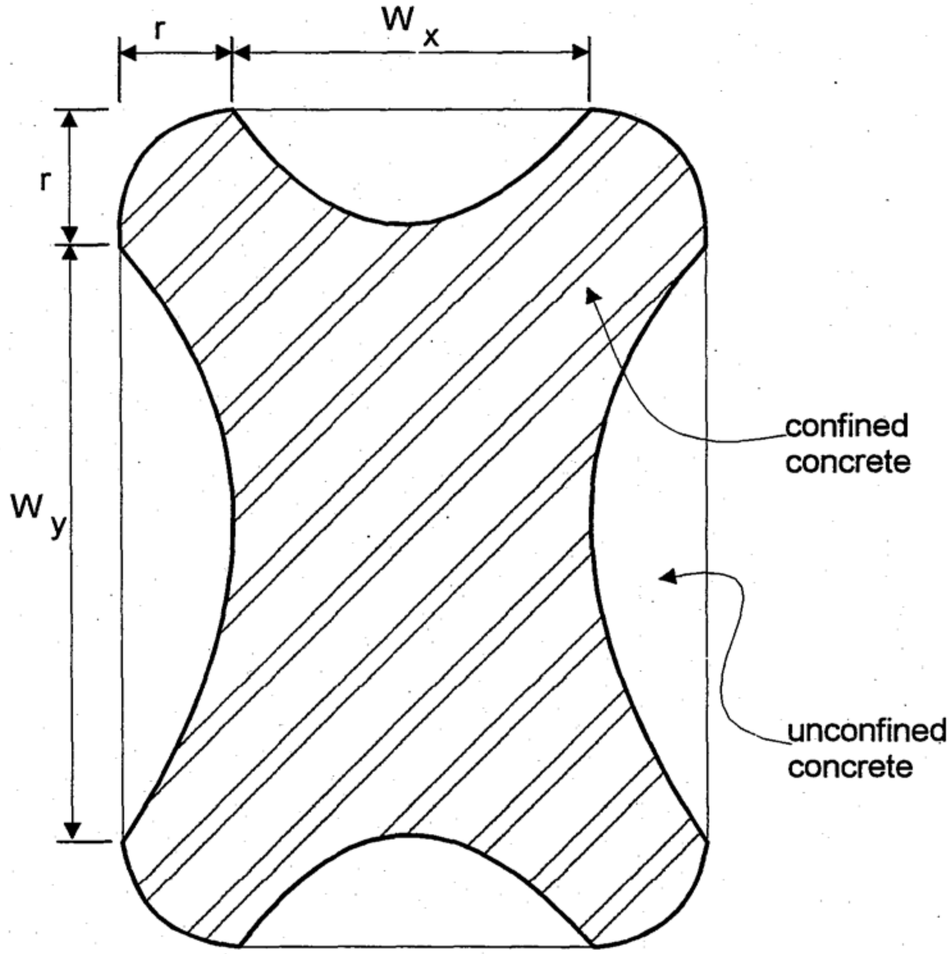

Fig. 4.8 Effective Wrap Confinement of a Rectangular Section

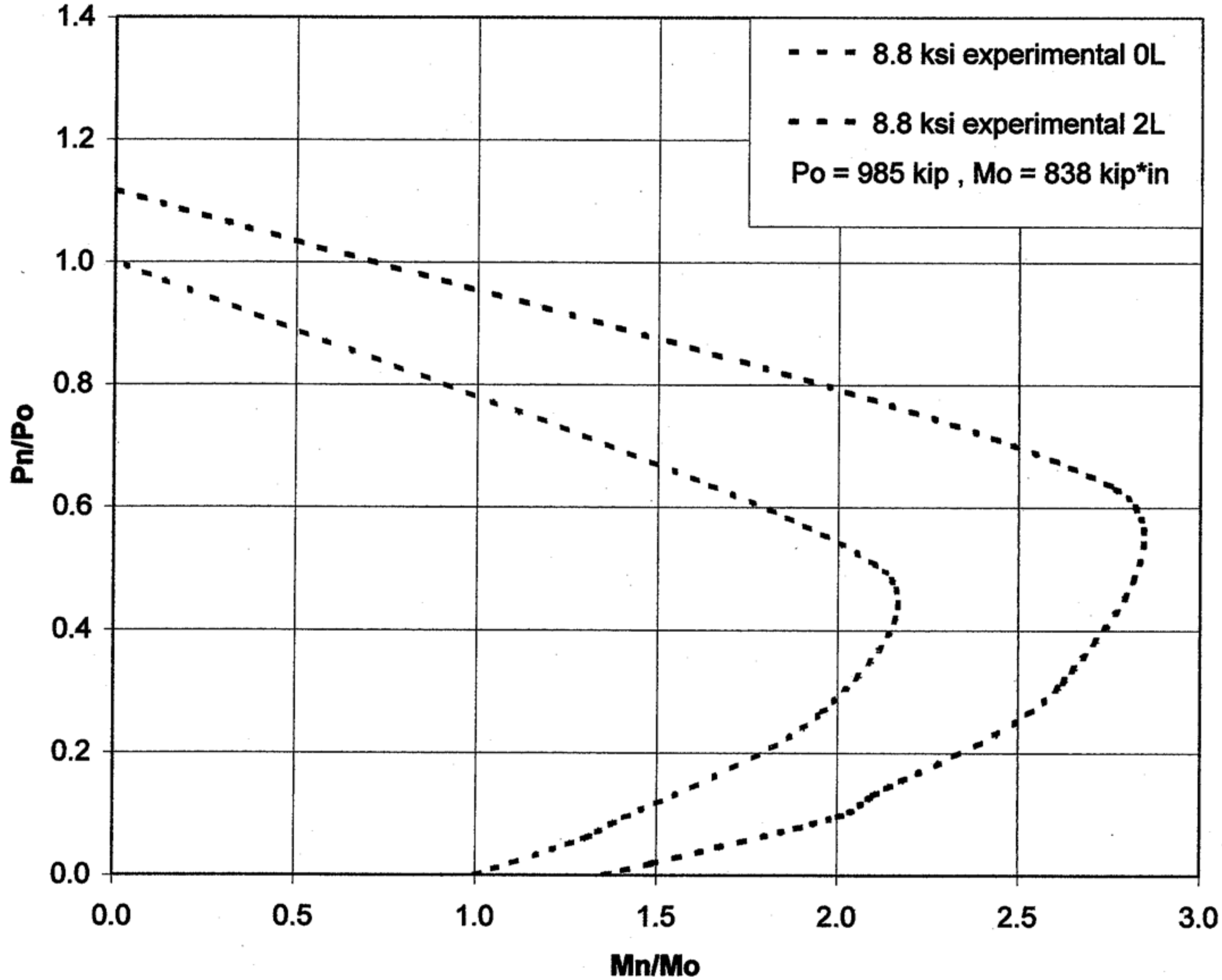

Fig. 4.9 – Experimental Interaction Diagram for HSC (8.8 ksi) Unwrapped (0L) versus Wrapped (2L)

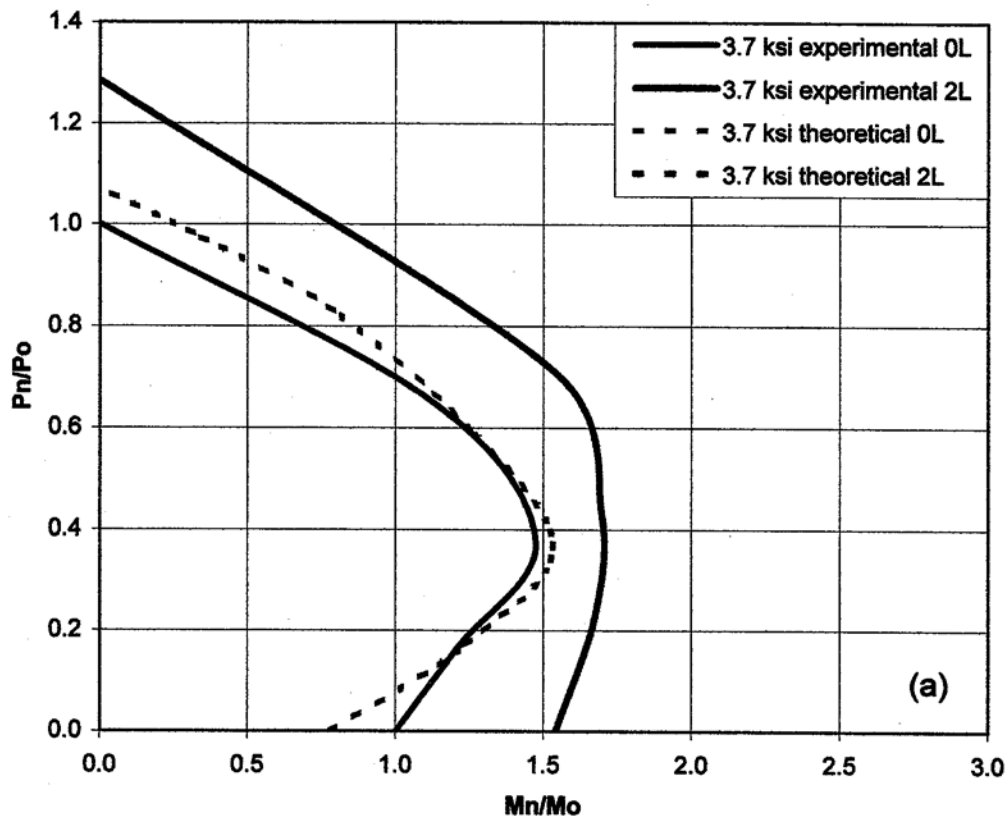

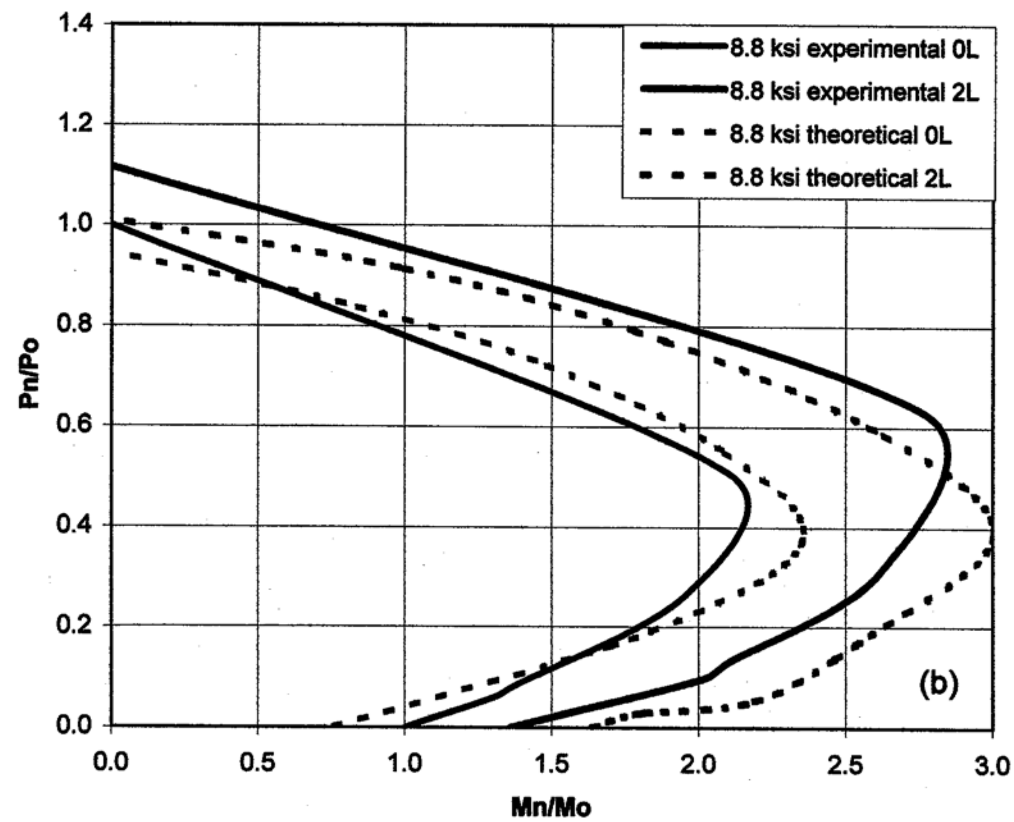

Fig. 4.10 – Interaction Diagrams for (a) NSC (3.7 ksi) and (b) HSC (8.8 ksi) – Theoretical versus Experimental (Unwrapped, 0L and Wrapped, 2L)

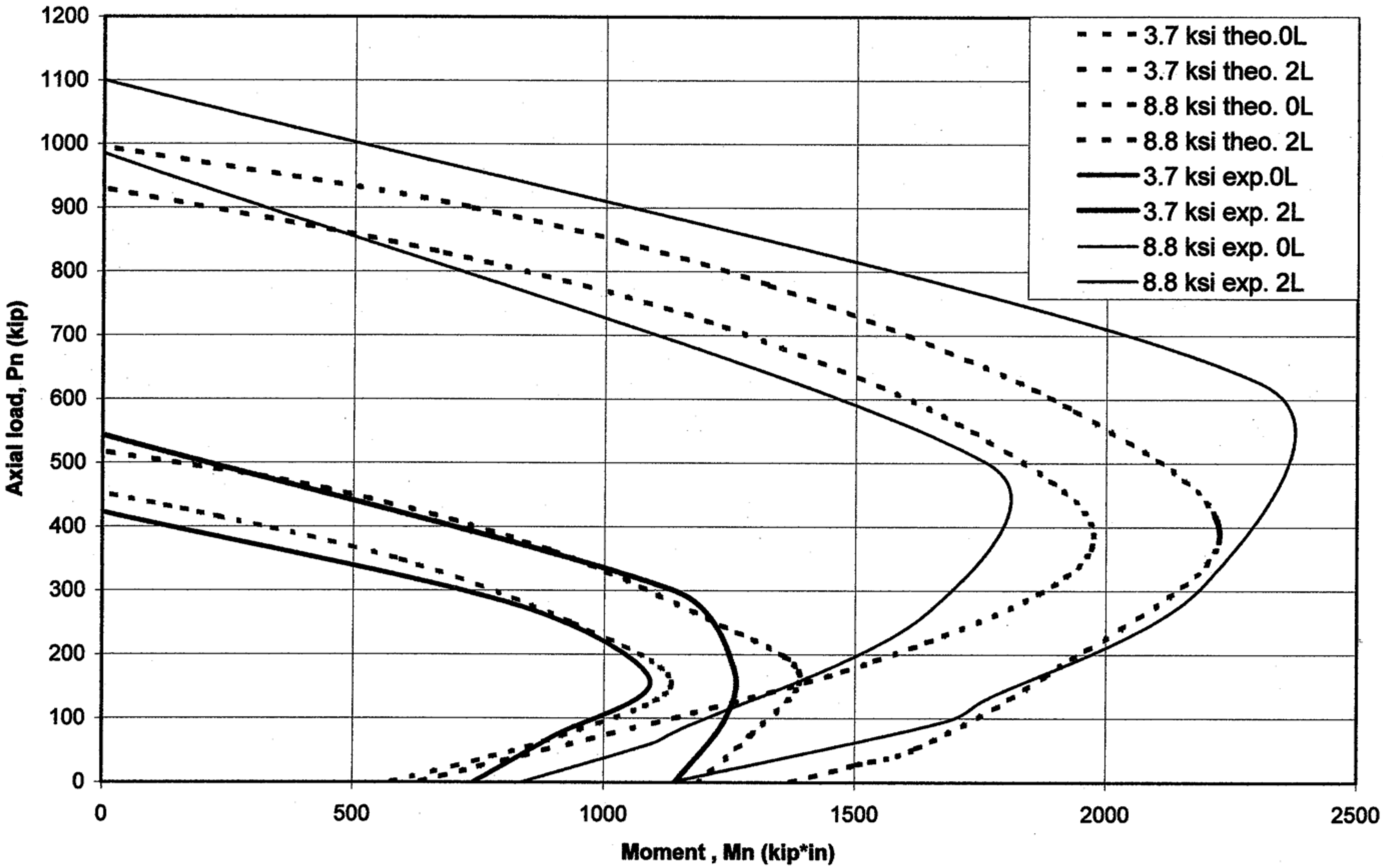

Fig. 4.11 – Summary of Interaction Diagram obtained for both NSC and HSC

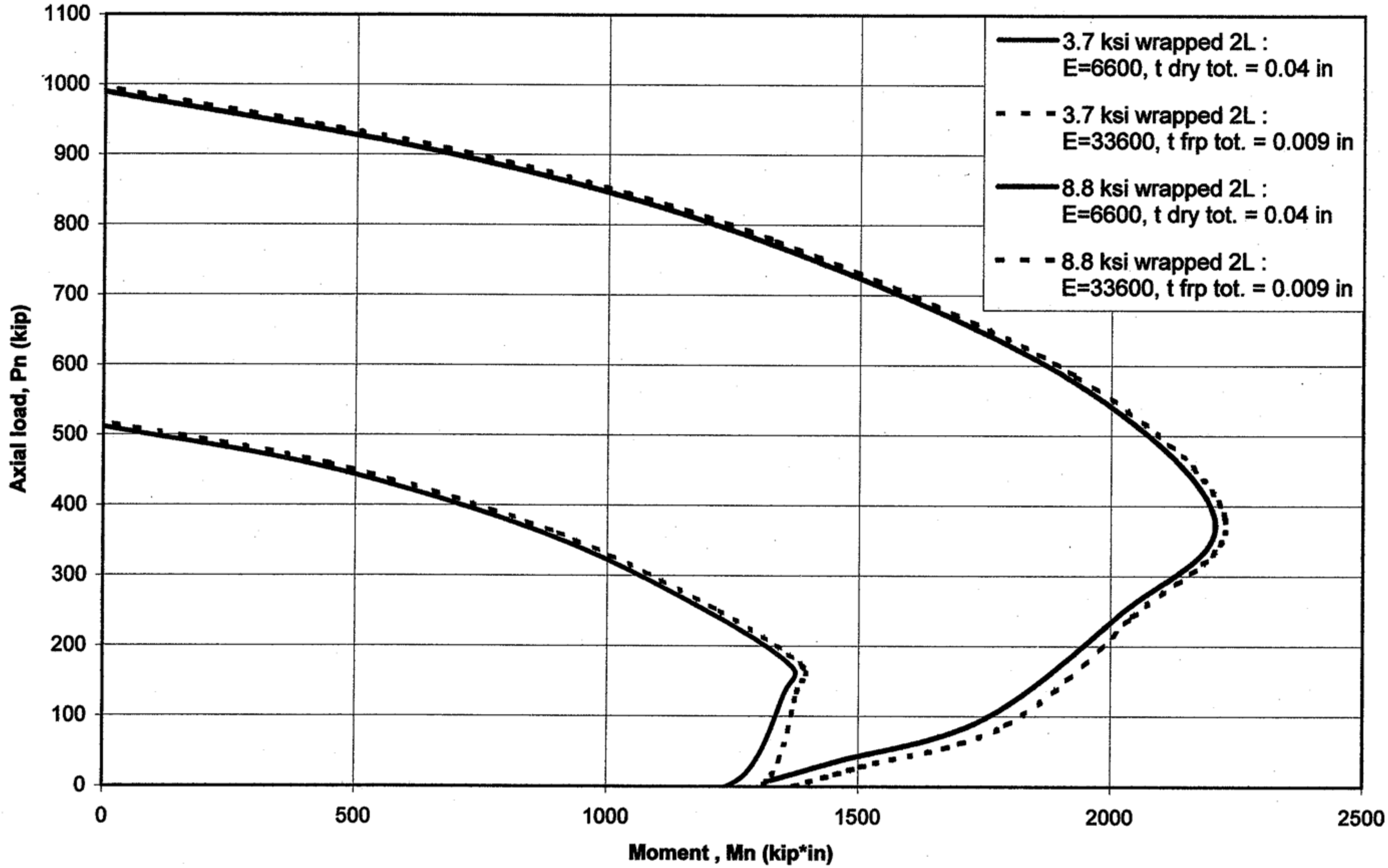

Fig. 4.12 –Interaction Diagrams for Wrapped Specimen (2L) - Method using dry composite characteristics versus Method using CFRP characteristics

APPENDIX A

- CONCRETE MIX DESIGN PROPERTIES OF

CARBON FIBERS - PROPERTIES OF EPOXY

Appendix. A1

FLORIDA ROCK INDUSTRIES, INC.

MATERIALS TESTING LABORATORY
1005 Kissimmee Street / P.O. Box 2251
Tallahassee, Florida 32304
(904) 576-4141

ACCREDITED CONCRETE TESTING LABORATORY — CONCRETE MATERIALS ENGINEERING COUNCIL — CMEC

CONCRETE MIX DESIGN

CLASS OF CONCRETE: **6000 PSI Pea Rock** MIX NO.: **4-7513**

PROJECT:
ARCHITECT:
ENGINEER:
CONTRACTOR:

DATE: **01-19-99**
REPORT NO.: **1**

MATERIALS

CEMENT:	**Portland Type I/II**	**ASTM C150 Florida Crushed Stone, Co.**
CEMENTITIOUS MATERIAL:		
FINE AGGREGATE:	**Silica Sand**	**ASTM C 33 Roberts Sand Company**
COARSE AGGREGATE I:	**#7 Pea Gravel**	**ASTM C 33 Martin Marietta Aggregates**
COARSE AGGREGATE II:		
AIR-ENTRAINING AGENT:	**Entrapped Air**	
CHEMICAL ADMIXTURE:	**MBL-80**	**ASTM C494 Master Builders, Inc.**

TESTS ON AGGREGATES

FINE AGGREGATE	Specific Gravity	Unit Weight	Colorimetric Test	GRADATION (% PASSING U.S. SIEVE) 3/8"	#4	#8	#16	#30	#50	#100	#200	F.M.
I	2.63	105	lighter than std.		100	97	84	54	19	3	----	2.43

COARSE AGGREGATE	Specific Gravity	Unit Weight	L.A. Abrasion	GRADATION (% PASSING U.S. SIEVE) 2"	1 1/2"	1"	3/4"	1/2"	3/8"	#4	#8	#16	F.M.
I	2.64	104	n/a				100	95	56	6	3	1	6.34
II													

MIX DESIGN FOR **6000** PSI CONCRETE AT **28** DAYS

Cement Content*: **7.5 cwt/cu. yd.**	Slump: **4.0 +/- 1.0** in.	Fine Agg. Volume: **43.2** %
Water/Cement (by weight)*: **0.4**	Air: **1.5 % Entrapped** %	Unit Weight: **148.3** PCF

* Based on total cementitious material.

MATERIALS	QUANTITIES (SSD BASIS)	VOLUME (CU. FT.)
Portland Type I/II	750	3.82
Silica Sand	1274	7.76
#7 Pea Gravel	1680	10.20
Water	300	4.81
Entrapped Air	---	.41
MBL-80, oz.	56.0	------
		27.00

REMARKS:

Contractor assumes responsibility for ordering and placing mixes by Mix No. as approved by Architect/Engineer.

The concrete supplier can be responsible for concrete strength only if field sampling, specimen molding, curing and testing are done by qualified personnel (ACI Certification or equal) and conform with applicable ASTM Standards (C31, C39, C94, C1077). The concrete supplier is entitled to a copy of all concrete test reports (ASTM C94) for the documentation of control standards required by ACI 301 and ACI 318.

PRODUCT INFORMATION

TECHNICAL FORMATION

THORNEL® Carbon Fiber T-300 12K

1. Description

THORNEL Carbon Fiber T-300 12K is a continuous length, high-strength, high-modulus fiber consisting of 12,000 filaments in a one-ply construction. The fiber surface has been treated to increase the interlaminar shear strength in a resin matrix composite.

2. Typical Properties and Characteristics

Property	U.S. Customary Units	Value	S.I. Units	Value
Tensile Strength	$lb/in^2 \times 10^3$	530	GPa	3.65
Tensile Modulus	$lb/in^2 \times 10^6$	33.5	GPa	231
Density	lb/in^3	0.064	Mg/m^3	1.76
Filament Diameter	μ	7	μm	7
Elongation at Break	%	1.4	%	1.4
Elastic Recovery	%	100	%	100
Carbon Assay	%	92	%	92
Surface Area	m^2/g	0.45	m^2/g	0.45
Longitudinal Thermal Conductivity	BTU-ft/hr(ft^2)(°F)	5	W/m K	8.5
Electrical Resistivity	Ohm-cm $\times 10^{-4}$	18	μohm-m	18
Longitudinal CTE at 70°F (21°C)	PPM/°F	−0.3	PPM/K	−0.5

3. Typical Strand Properties

Property	U.S. Customary Units	Value	S.I. Units	Value
Yield	yd/lb	627	m/g	1.26
Denier	g/9000m	7130	g/9000m	7130
Twist	tpi	0	tpm	0
Filaments/Strand	—	12000	—	12000
Fiber Area in Yarn Cross Section	$in^2 \times 10^{-5}$	70	mm^2	0.452

EPOXY

PR2032 Laminating Resin

LAMINATING SYSTEMS FOR COMPOSITE PARTS

DESCRIPTION

PR2032 is a medium viscosity, unfilled, light amber laminating resin that is designed for structural production applications. When used with the three hardeners listed here, the combinations provide excellent wet-out of fiberglass, carbon and aramid fibers. Special additives have been incorporated into these products to promote chemical adhesion to fabrics made with these fibers. Typical applications include aircraft and sail plane skins and structural components, auto bodies, radomes and prototype parts.

Hardeners PH3660 and PH3665 are the standard production hardeners for fabricating composite parts. PH3660has a one hour working time, and PH3665 has been developed to provide a longer working time for larger and/or more complicated laminates when needed. Both of these hardeners will cure completely at room temperature without additional heat. PH3630 is a faster setting hardener for smaller laminates which also works very well for patching and repairs. PH3630 has a similar viscosity to PH3660 and PH3665, so handling will be the same, except for the faster cure.

These products can be considered low toxicity materials that have minimum hazard potential when used properly and in a clean and responsible manner. PR2032 does not contain any hazardous diluents or extenders. Hardeners PH3630, PH3660and PH3665 do not contain methylene dianiline (MDA), or other potentially harmful aniline derivatives. Neither the resin or the hardeners will crystallize in normal shipping and storage conditions, including refrigerated storage. Both components have excellent moisture resistance, for minimal problems in high humidity environments.

PRODUCT SPECIFICATIONS

	PR2032	PH3660	Test method
Color	Lt. Amber	Amber	Visual
Viscosity	1,650 cps	190-200 cps	ASTM D2393
Specific Gravity	1.15	0.96	ASTM D1475
Pot Life, 4 fl. oz. mass	---	1 hour	ASTM D2471
Mix ratio, By Weight By Volume	---	100:27 3 to 1	Manufacturer

HANDLING & CURING

PH3660 and PH3665 are the hardeners typically used to fabricate larger composite parts. PH3660has a one hour working time, and can be used for all sizes of parts using the contact layup method of fabrication. If the vacuum bagging technique is being used, PH3660 should only be used for smaller parts. Hardener

PH3665 has a longer working time that is useful for vacuum bagging larger parts before the resin has gelled. Hardener PH3630 is intended for smaller laminates, fast re- pairs, or additions to a primary structure.

With hardener PH3630, plan to allow the laminate to cure 18 to 24 hours, at a minimum of 72 F before removing the structure from the mold. With hardeners PH3660 and P-H3665, allow at least24 hours before demolding to prevent distortion. This can be accelerated by applying heat after the resin has gelled. Be careful using heat guns and lamps, as they tend to concentrate heat, producing localized hot spots which can damage the epoxy. These systems can be cured at ambient temperatures, or given an elevated temperature cure. The higher the curing temperature is, the higher the resulting service temperature. With a higher temperature cure, a safe service temperature well over 200 F can be obtained.

TECHNICAL DATA

	PR2032/PH3660	Test Method
Mix Ratio, By Weight By Volume	100:27 3 to 1	Manufacturer
Color	Light Amber	Visual
Mixed Viscosity, centipoise, @ 77°F	900-950 cps	ASTM D2393
Pot Life, 4 fluid ounces mass	1 hour	ASTM D2471
Cured Hardness, Shore D	88D	ASTM D2240
Specific Gravity, gms. /cc	1.11	ASTM D1475
Density lb./cu.in. lb./gallon	0.0401 9.26	ASTM D792
Specific Volume, cu. in. /lb.	25	ASTM D792
Tensile Strength, psi (1)	45,170 psi	ASTM D638
Elongation (1)	1.96%	ASTM D638
Tensile Modulus, psi (1)	2.62×10^6 psi	ASTM D638
Flexural Strength, psi (1)	62,285 psi	ASTM D790
Flexural Modulus, psi (1)	2.56×10^6 psi	ASTM D790
Glass Transition Temperature (Tg)	196°F	TMA
Coefficient of Thermal Expansion Range: 100°F – 150°F	4.3×10^{-5} in./in./°F	ASTM D696

(1) Properties derived with 10 ply laminate, hand lay-up, Style 181 glass fabric, 55% glass content.

SAFETY and HANDLING

These products are designed to offer the user high performance products with minimum hazard potential when properly used. **Generally, these resins and hardeners will present no handling problems if users exercise care to protect the skin and eyes, and, if good ventilation is provided in the work areas.** However, all epoxy resins and hardeners can be irritating to the skin, and prolonged contact may result in sensitization; and breathing of mist or vapors may cause allergenic respiratory reaction, especially in highly sensitive individuals. As such, avoid contact with eyes and skin, and avoid breathing vapors.

Wear protective rubber apron, clothing, gloves, face shield or other items as required to prevent contact with the skin. In case of skin contact, immediately wash with soap and water, followed by a rinse of the area with vinegar, and then a further wash with soap and water. The vinegar will neutralize the hardener and lessen the chances of long term effects. Use goggles, a face shield, safety glasses or other items as required to prevent contact with the eyes. If material gets into the eyes, immediately flush with water for at least 15 minutes and call a physician.

Generally, keep the area as clean and uncluttered as possible, and clean up any minor spills immediately to prevent accidental skin contact at a later time. Keep tools clean and properly stored. Dispose of trash and empty containers in the proper receptacle.
Do not use any of these types of products until Material Safety Data Sheets have been read and understood,

APPENDIX B

Interaction diagrams for unwrapped and wrapped beam-columns

B.1 Unwrapped beam-column specimen

a) Equations b) Flow chart c) Excel spreadsheet

B.2 Wrapped beam-column specimen

d) Equations

e) Flow chart

f) Excel spreadsheet

B.1 Unwrapped beam-column specimen

a) Equations

a.1) Nominal concentric load capacity: P_n

$$P_n = 0.85 * f'_c * (A_g - A_{st}) + A_{st} * f_y \quad \text{(eq. 1)}$$

where f'_c is the compression strength of concrete, A_g is the total gross area of concrete section, A_{st} is the total steel area ($A_{st} = A_s + A'_s$), and f_y is the yield stress of steel reinforcement. Note that when P_n is maximal, the bending moment (M_n) is equal to 0.

a.2) Balanced failure point ($\varepsilon_c = \varepsilon_{cu}$ and $\varepsilon_s = \varepsilon_y$) is calculated as follows:

$$c = c_b = \frac{\varepsilon_{cu} * d}{\varepsilon_{cu} + \varepsilon_y} \quad \text{(eq. 2)}$$

$$a = \beta_1 * c \quad \text{(eq. 3)}$$

$$\varepsilon'_s = \frac{\varepsilon_{cu} * (c - d')}{c} \quad \text{(eq. 4)}$$

$$f'_s = E_s * \varepsilon'_s \quad \text{(eq. 5)}$$

Note that ε'_s should not be greater than ε_y.

a.3) Interaction diagram generation:

$$M_{nb} = 0.85 * f'_c * b * a * (y - \frac{a}{2}) + A'_s * f'_s * (y - d') + A_s * f_y * (d - y) \quad \text{(eq. 6)}$$

$$P_{nb} = 0.85 * f'_c * b * a + A'_s * f'_s - A_s * f_y \quad \text{(eq. 7)}$$

Similarly, other points either controlled by compression ($c > c_b$) or by flexure ($c < c_b$) can be determined (see flow chart below).

b) Flow chart for interaction diagram generation

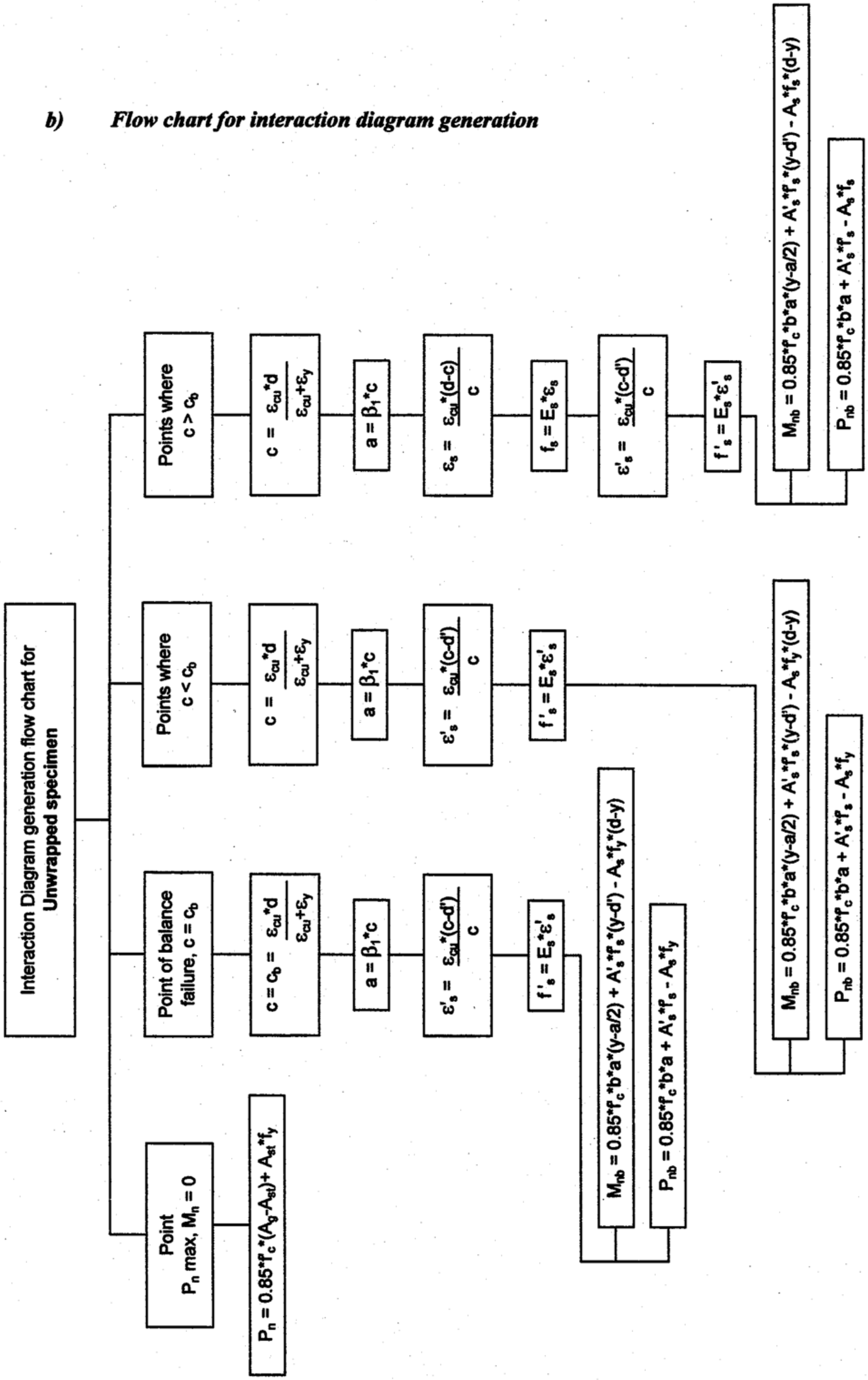

c) *Interaction Diagrams*

Non wrapped specimen : f'c = 8.8 ksi

f'c (ksi) =	8.8	As (in^2) =	0.880	b (in) =	8.0
ε_{cu} =	0.00300	A's (in^2) =	0.880	h (in) =	14.0
fy (ksi) =	60.0	Ast (in^2) =	1.760	y (in) = h/2 =	7.0
Ey (ksi) =	30000	Ag (in^2) =	112	d (in) =	12.0
εy =	0.00200	β_1 =	0.85	d' (in) =	2.0

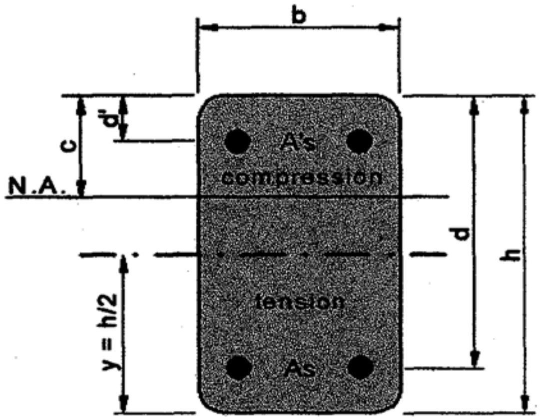

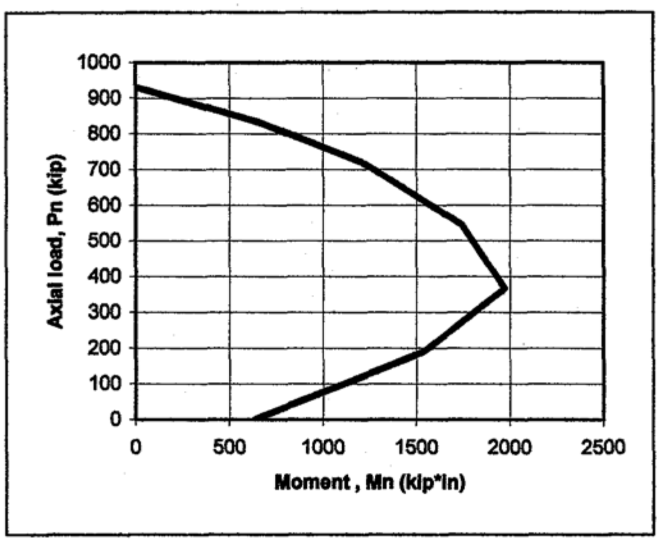

Results non wrapped specimen

c (in)	P_n (kip)	M_n (kip*in)
1.53	**0.7**	**636.5**
4	**190.3**	**1540.3**
7.20	**366.2**	**1970.9**
10.0	**545.6**	**1742.0**
13.0	**720.1**	**1208.9**
15.0	**831.6**	**661.7**
∞	**930.2**	**0.0**

Point no.1 of diagram : maximum axial load, moment = 0

Pn max = $0.85 * f'_c * (A_g - A_{st}) + A_{st} * f_y$

P_n max (kip) = **930.2**

M_n (kip*in) = **0**

Point no.2 of diagram : balance failure, moment maximum

c_b = $\dfrac{\varepsilon_{cu} * d}{\varepsilon_{cu} + \varepsilon_y}$

c_b (in) = 7.20

a = $\beta_1 * c$

a (in) = 6.12

ε's = $\dfrac{\varepsilon_{cu} * (c - d')}{c}$

ε's = 0.00217 > 0.00200

f's = $E_s * \varepsilon'_s$

f's (ksi) = 60.0

M_{nb} = $0.85 * f'_c * b * a * (y - \frac{a}{2}) + A'_s * f'_s * (y - d') + A_s * f_y * (d - y)$

M_{nb} (kip*in) = **1970.9**

P_{nb} (kip) = $0.85 * f'_c * b * a + A'_s * f'_s - A_s * f_y$

P_{nb} (kip) = **366.2**

Point no.3, 4 of diagram : $c < c_b$ (flexure failure) n.b. : c_b (in) = **7.20**

To create adequatly the graph, please enter c values in increasing order for point 3 and 4

Point no.3

c (in) = **1.53** **OK : possible value of c**

a = $\beta_1 * c$

a (in) = 1.30

ε_c = 0.00300

$\varepsilon_s > \varepsilon_y$

ε_y = 0.00200

$f_s = f_y$

$\varepsilon's = \dfrac{\varepsilon_{cu} * (c - d')}{c}$

ε's = -0.00092

f's (ksi) = -27.6

$$M_n = 0.85 * f'_c * b * a * (y - \frac{a}{2}) + A'_s * f'_s * (y - d') + A_s * f_y * (d - y)$$

M_n (kip*in) = **636.5**

$$P_n \text{ (kip)} = 0.85 * f'_c * b * a + A'_s * f'_s - A_s * f_y$$

P_n (kip) = **0.7**

Point no.5, 6, 7 of diagram : $c > c_b$ (compression failure)

To create adequatly the graph, please enter c values in increasing order for point 5,6 and 7
The value of c can be greater than "h", but the value of "a" is limited to "h"

Point no.5

c (in) = **10.0** **OK : possible value of c**

a = $\beta_1 * c$

a (in) = 8.5 **< h** **OK : possible value of a**
a (in) = **8.5**

ε_c = 0.00300

$\varepsilon_s < \varepsilon_y$

$$\varepsilon_s = \frac{\varepsilon_{cu} * (d - c)}{c}$$

ε_s = 0.00060 **> 0 As act as tension reinforcement**

fs (ksi) = 18.0

$$\varepsilon's = \frac{\varepsilon_{cu} * (c - d')}{c}$$

$\varepsilon's$ = 0.00240 **>** 0.00200

f's (ksi) = 60.0

$$M_n = 0.85 * f'_c * b * a * (y - \frac{a}{2}) + A'_s * f'_s * (y - d') + A_s * f_s * (d - y)$$

M_n (kip*in) = **1742.0**

$$P_n \text{ (kip)} = 0.85 * f'_c * b * a + A'_s * f's - A_s * f_s$$

Note that this formula may be not accurate enough for Mn value close to 0

P_n (kip) = **545.6**

B.2 Wrapped beam-column specimen

a) *Equations*

a.1) Compressive strength of confined concrete: f_{cc}

$$f_{cc} = f'_c + 3.38 * f_r^{0.7} \quad \text{(eq. 8)}$$

where f'_c is the compressive strength of unconfined concrete and f_r is the confinement pressure of the jacket.

The confining pressure is calculated by using an effective confinement ratio based on the shape of the section, the figure below shows the confined concrete and the unconfined concrete for a rectangular column.

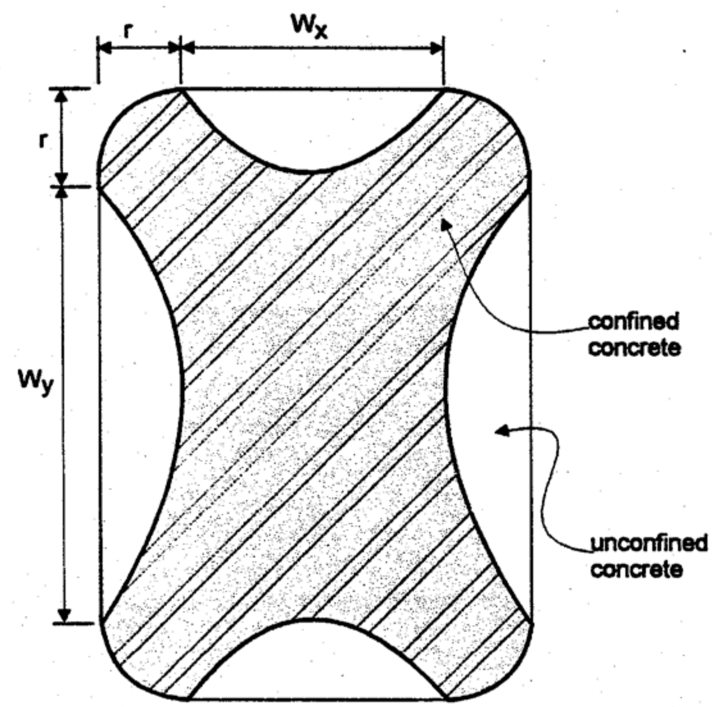

Lateral confining stresses induced by the jacket in the x and y directions:

$$f_{r,x} = p_{j,x} * k_e * f_j \quad \text{(eq. 9)}$$

$$f_{r,y} = p_{j,y} * k_e * f_j \quad \text{(eq. 10)}$$

where k_e is the effective confinement ratio given by equation (10).